

Decoding functional heterogeneity in immune cells

Citation for published version (APA):

Subedi, N. (2022). *Decoding functional heterogeneity in immune cells: New avenues for immunotherapy*. [Phd Thesis 1 (Research TU/e / Graduation TU/e), Biomedical Engineering]. Eindhoven University of Technology.

Document status and date:

Published: 03/06/2022

Document Version:

Publisher's PDF, also known as Version of Record (includes final page, issue and volume numbers)

Please check the document version of this publication:

- A submitted manuscript is the version of the article upon submission and before peer-review. There can be important differences between the submitted version and the official published version of record. People interested in the research are advised to contact the author for the final version of the publication, or visit the DOI to the publisher's website.
- The final author version and the galley proof are versions of the publication after peer review.
- The final published version features the final layout of the paper including the volume, issue and page numbers.

[Link to publication](#)

General rights

Copyright and moral rights for the publications made accessible in the public portal are retained by the authors and/or other copyright owners and it is a condition of accessing publications that users recognise and abide by the legal requirements associated with these rights.

- Users may download and print one copy of any publication from the public portal for the purpose of private study or research.
- You may not further distribute the material or use it for any profit-making activity or commercial gain
- You may freely distribute the URL identifying the publication in the public portal.

If the publication is distributed under the terms of Article 25fa of the Dutch Copyright Act, indicated by the "Taverne" license above, please follow below link for the End User Agreement:

www.tue.nl/taverne

Take down policy

If you believe that this document breaches copyright please contact us at:

openaccess@tue.nl

providing details and we will investigate your claim.

Decoding functional heterogeneity in immune cells

New avenues for immunotherapy

PROEFSCHRIFT

ter verkrijging van de graad van doctor aan de
Technische Universiteit Eindhoven, op gezag van de rector magnificus
prof.dr.ir. F.P.T. Baaijens, voor een commissie aangewezen door het College
voor Promoties, in het openbaar te verdedigen op vrijdag 3 juni 2022 om 13:30
uur

door

Nikita Subedi
geboren te Lalitpur, Nepal

Dit proefschrift is goedgekeurd door de promotoren en de samenstelling van de promotiecommissie is als volgt:

Voorzitter:	prof.dr. M. Merkx
Promotor:	prof.dr. C.V.C. Bouten
Copromotor:	dr. J. Tel.
Promotiecommissie leden:	prof.dr. C.M. Sahlgren prof.dr.ir. T.F.A. de Greef dr. H.D. Dolstra (Radboudmc, Radboud Institute for Molecular Sciences) dr. S.N. Nierkens (UMC Utrecht, Center for Translational Immunology)

*Het onderzoek of ontwerp dat in dit proefschrift wordt beschreven is
uitgevoerd in overeenstemming met de TU/e Gedragscode
Wetenschapsbeoefening*

Decoding functional heterogeneity in immune cells
New avenues for immunotherapy

Nikita Subedi

A catalogue record is available from the Eindhoven University of Technology Library.

ISBN/EAN: 978-94-6419-514-9

Copyright © 2022 by N.Subedi

All rights are reserved. No part of this book may be reproduced, stored in a database or retrieval system, or published in any form or in any way, electronically, mechanically, by print, by photo print, microfilm or any other means without prior written permission by the author.

Cover design by Nikita Subedi

Printed by GLIDEPRINT

TABLE OF CONTENTS

Summary.....7-12

Chapter 1.....15-54

General Introduction

Part 1: Droplet based microfluidics

Chapter 2.....57-77

A pipette-tip based method for seeding cells to droplet microfluidic platforms

Chapter 3.....79-106

An automated real-time microfluidic platform to probe single NK cell heterogeneity and cytotoxicity on-chip

Part 2: Decoding functional heterogeneity in immune cells

Chapter 4.....109-138

Single cell profiling reveals functional heterogeneity and serial killing in human peripheral and ex vivo-generated CD34⁺ progenitor derived natural killer cells

Chapter 5.....141-185

Single-cell analysis reveals that stochasticity and paracrine signaling control interferon-alpha production by plasmacytoid dendritic cells

Chapter 6.....187-202

Potent crosstalk between a single plasmacytoid dendritic cell and a natural killer cell through IFN α dependent manner

Chapter 7.....205-213

Discussion: new avenues for cellular immunotherapy

Appendix

Publication List.....214

Curriculum Vitae.....215

Acknowledgements.....216-219

SUMMARY

Cellular heterogeneity is a fundamental property of the immune system that enables it to recognize myriads of antigens for tissue maintenance, surveillance, repair, and defense against pathogens or cellular stress. Even though this plasticity has allowed robust immunological response on average, the cell-to-cell variation observed at different levels (at donor, tissue, cellular and subcellular levels) has made it difficult to design effective immunotherapeutic strategies. Therefore, understanding cellular heterogeneity in immune cell populations aid in the development of superior cell-based immunotherapies to treat infection, inflammation, and cancer (Chapter 1). Innovation in microsystems and microfluidics facilitated the integration of numerous complex interactions within the immune system to identify the existing cellular variance. However, the major shortcoming remains integrating an efficient cell pairing with real-time monitoring of the interaction in a high throughput manner. Droplet-based microfluidics integrated with microscopy facilitate compartmentalization of immune cells to understand cellular behavior and allow real-time monitoring at high throughput. In this thesis, we aimed to successfully integrate droplet-based microfluidic technology for investigating the underlying heterogeneity in human plasmacytoid dendritic cells (pDCs) and Natural Killer (NK) cells, ultimately improving cell-based immunotherapeutic strategies.

Droplet-based microfluidics is a well-established platform for single-cell encapsulation, however, when used with primary cells, efficient cellular distribution is often missed due to cell loss. To circumvent this problem, we devised a tip-loading approach (Chapter 2) that allowed us to match Poisson distribution in droplets and prevent the loss of rare cells from sedimentation and clumping. By further adjusting the cell concentration, we enabled a 1:1 pairing of effector immune cells with target cells. We used a glass-based observation chamber that allows immobilization of droplets, thus enabling tracking of over 60,000 droplets in real-time (Chapter 3). This enhanced the overall throughput of the analysis and provided a large data sample to monitor heterogeneous behavior within the immune cell population.

The NK cells and the pDCs are two important innate immune cells that display multiple functions ranging from cytotoxicity, immunoregulation, adaptive and tolerance ability. We used the droplet-based adaptation to investigate the functional heterogeneity within these

cells by monitoring the dynamics of their interaction with different target cells. By assessing NK cells (PB and Umbilical cord) interaction with the tumor cell, we showed that the NK cell compartment is composed of cells with different cytotoxic strengths and efficacy. Including paramagnetic nanoparticle-based immunoassay in droplets facilitated studying the association between the secretion and the cytotoxic function in NK cells (Chapter 4). Single-cell activation of pDCs in droplets showed that stimulation induces functional diversification of pDCs, and the IFN-I pathway is controlled by stochastic gene regulation. We also showed that the environmental signals further amplified this phenomenon rather than subsets-based division of labor (Chapter 5).

We paired NK cells together with pDCs inside the droplets to monitor their crosstalk at the individual level. In this study, we monitored the amount of IFN- γ and IFN- α secreted by NK cells and pDCs respectively to show that activation of pDCs can enhance NK cell activation (Chapter 6). This preliminary study is an example of the futuristic approach toward implementing single-cell tools into the understanding of cellular coordination in the immune system.

In this way, we showed a successful integration of droplet-based microfluidics to probe functional heterogeneity in immune cells. Finally, we discussed different solutions derived from single-cell studies to improve or develop more efficient cell-based immunotherapy approaches (Chapter 7).

SAMENVATTING

Cellulaire heterogeniteit is een fundamentele eigenschap van het immuunsysteem die het in staat stelt om talloze antigenen te herkennen voor weefselonderhoud, surveillance, reparatie en verdediging tegen pathogenen of cellulaire stress. Hoewel deze plasticiteit zorgt voor een robuuste immunologische respons, maakt de cel-tot-cel variatie die op verschillende niveaus (donor-, weefsel-, cellulair en sub-cellulair niveau) wordt waargenomen, het moeilijk om effectief immuno-therapeutische strategieën te ontwerpen. Daarom helpt het begrijpen van cellulaire heterogeniteit in immuun cel populaties bij de ontwikkeling van verbeterde cel-gebaseerde immuuntherapieën voor de behandeling van infecties, ontstekingen en kanker (Hoofdstuk 1). Innovatie in microsystemen en microfluidica hebben onderzoek mogelijk gemaakt naar vele complexe interacties binnen het immuunsysteem. De belangrijkste tekortkoming blijft echter het integreren van een efficiënte cel-cel paring waarbij cel interactie direct kan worden gemonitord voor grote hoeveelheden cellen. Microfluidische technieken die cellen vangen in druppels, gecombineerd met microscopie, vergemakkelijken de compartimentering van immuuncellen om cellulair gedrag te begrijpen en over de tijd te monitoren op een “high-throughput” manier. In dit proefschrift, beoogde we om op druppels gebaseerde microfluidische technologie toe te passen voor het onderzoeken van de onderliggende heterogeniteit in menselijke plasmacytoïde dendritische cellen (pDC's) en NK-cellen, met het uiteindelijke doel om cel-gebaseerde immuno-therapeutische strategieën te verbeteren.

“Droplet-based microfluidics” is een gevestigd platform voor het compartimenteren van individuele cellen, maar bij gebruik met primaire cellen wordt efficiënte cellulaire distributie vaak gemist vanwege cel verlies. Om dit probleem te omzeilen, hebben we een “tip-loading” aanpak bedacht (Hoofdstuk 2), waarmee we de Poisson-verdeling in druppels konden matchen en het verlies van zeldzame cellen door sedimentatie en klontering konden voorkomen. Door de cel concentratie verder aan te passen, hebben we een 1:1-koppeling van effector-immuuncellen met doel-cellen mogelijk gemaakt. We gebruikten een glazen observatiekamer die immobilisatie van druppeltjes faciliteerde, waardoor het mogelijk werd om meer dan 60.000 druppeltjes over de tijd te volgen (Hoofdstuk 3). Dit verbeterde de algehele doorvoer van de analyse en leverde een grote dataset op om heterogeen gedrag binnen de immuuncel populatie te volgen.

“Natural Killer” cellen en de plasmacytoïde dendritische cellen zijn twee belangrijke cellen binnen het aangeboren immuunsysteem, die meerdere functies vervullen, variërend van cytotoxiciteit, immuun-regulatie, adaptief en tolerantie. We gebruikten de op druppels gebaseerde aanpassing om de functionele heterogeniteit binnen deze cellen te onderzoeken en de dynamiek van hun interactie met verschillende doelcellen te volgen. Door de interactie tussen NK-cellen (PB en navelstreng) en de tumorcel te monitoren, hebben we aangetoond dat de NK-cel populatie is samengesteld uit cellen met verschillende cytotoxische sterktes en werkzaamheden. Integratie van een op paramagnetische nano-deeltjes gebaseerde immunoassay vergemakkelijkte het bestuderen van de associatie tussen secretie en cytotoxische functie in NK-cellen (Hoofdstuk 4). Activatie van enkele pDC's in druppeltjes toonde aan dat stimulatie zorgt voor functionele diversificatie van pDC's, en dat type I IFN signalering wordt gecontroleerd door stochastische genregulatie. Daarnaast toonden we aan dat omgevingssignalen dit fenomeen verder versterkten in plaats van op subsets gebaseerde taakverdeling (Hoofdstuk 5).

Om cellulaire interacties per cel te onderzoeken hebben we individuele NK-cellen en pDC's samen in druppeltjes gevangen. In deze studie hebben we de hoeveelheid IFN γ en IFN α gevolgd die wordt uitgescheiden door respectievelijk NK-cellen en pDC's om aan te tonen dat stimulatie van pDC's de activatie van NK-cellen kan verbeteren. Deze studie is een voorbeeld van de futuristische aanpak van het implementeren van hulpmiddelen voor het begrijpen van cellulaire coördinatie in het immuunsysteem op het niveau van één enkele cel.

Middels deze methodes demonstreerde we een succesvolle toepassing van op druppeltjes gebaseerde microfluidica om functionele heterogeniteit in immuun cellen te onderzoeken. Ten slotte hebben we verscheidenen toepassingen besproken gebaseerd op “single-cell” studies die gebruikt kunnen worden voor het ontwikkelen en verbeteren van efficiëntere cel-gebaseerde immunotherapieën (Hoofdstuk 7).

सारांश

सेलुलर विषमता प्रतिरक्षा प्रणालीको एक मौलिक गुण हो जसले यसलाई ऊतक मर्मत, निगरानी, मर्मत, र रोगजनक वा सेलुलर तनाव विरुद्ध रक्षाको लागि असंख्य एन्टिजेनहरू पहिचान गर्न सक्षम बनाउँछ। यद्यपि यो प्लास्टिसिटीले औसतमा बलियो immunological प्रतिक्रियालाई अनुमति दिएको छ, विभिन्न स्तरहरूमा (दाता, तन्तु, सेलुलर र सबसेलुलर स्तरमा) अवलोकन गरिएको सेल-देखि-सेल भिन्नताले प्रभावकारी immunotherapeutic रणनीतिहरू डिजाइन गर्न गाह्रो बनाएको छ। तसर्थ, प्रतिरक्षा सेलको सेलुलर विषमता बुझ्दा संक्रमण, सूजन र क्यान्सरको उपचार गर्न उच्च सेल-आधारित इम्युनोथेरापीहरूको विकासमा मद्दत गर्दछ (अध्याय १)। माइक्रो-प्रणाली र Microfluidics आविष्कारले प्रतिरक्षा प्रणाली भित्र धेरै जटिल अन्तरक्रियाहरूको एकीकरणलाई सहज बनायो। यद्यपि, प्रमुख कमजोरी उच्च थ्रुपुट तरिकामा अन्तरक्रियाको वास्तविक-समय निगरानीको साथ एक कुशल सेल जोडीलाई एकीकृत गर्न बाँकी छ। माइक्रोस्कोपीसँग एकीकृत Droplet based Microfluidics ले सेलुलर व्यवहार बुझ्न र उच्च थ्रुपुटमा वास्तविक-समय निगरानीलाई अनुमति दिन प्रतिरक्षा कोशिकाहरूको विभाजनलाई सुविधा दिन्छ। यस thesis मा हामीले मानव Plasmacytoid dendritic कोशिकाहरू (pDCs) र Natural Killer (NK) कोशिकाहरूमा अन्तर्निहित विषमताको अनुसन्धानको लागि Droplet-आधारित Microfluidic टेक्नोलोजीलाई सफलतापूर्वक एकीकृत गरेर, अन्ततः सेल-आधारित इम्युनोथेराप्युटिक रणनीतिहरू सुधार गर्न लक्ष्य राखेका छौं।

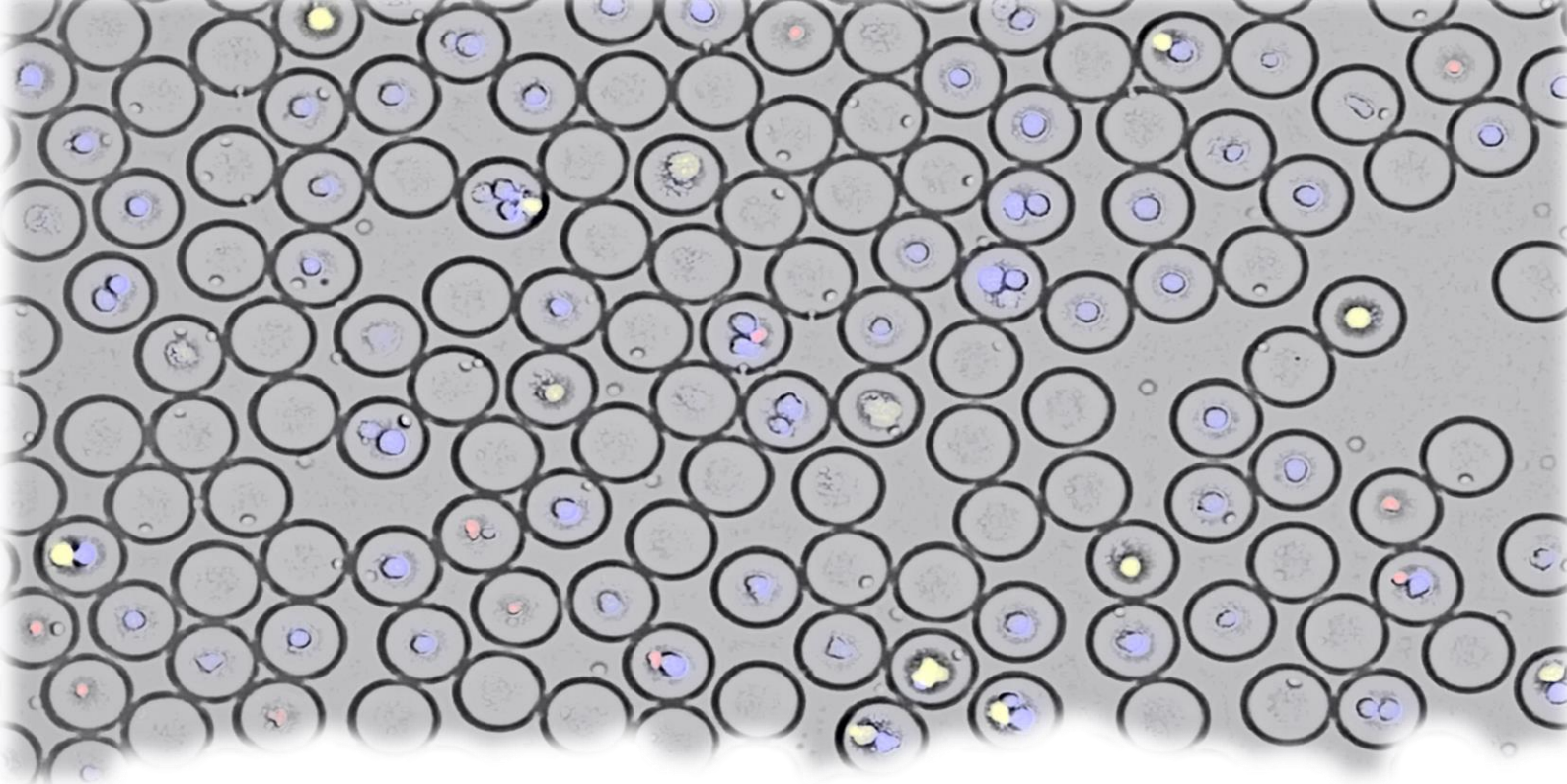
Droplet-आधारित Microfluidics एकल-सेल encapsulation को लागि एक राम्रो-स्थापित प्लेटफर्म हो, तथापि, प्राथमिक कक्षहरूमा प्रयोग गर्दा, कोशिकाको क्षतिको कारणले गर्दा प्रभावकारी सेलुलर वितरण प्रायः छुटेको छ। यस समस्यालाई रोक्नको लागि, हामीले Tip Loading दृष्टिकोण (अध्याय २) बनायौं जसले हामीलाई थोपाहरूमा Poisson वितरण मिलाउन र अवसादन र क्लम्पिङबाट दुर्लभ कोशिकाहरूको हानि रोक्न अनुमति दियो। सेल एकाग्रतालाई थप समायोजन गरेर, हामीले लक्षित कोशिकाहरूसँग प्रभावकारी प्रतिरक्षा कोशिकाहरूको १: १ जोडी सक्षम गर्यौं। हामीले अवलोकन कक्ष प्रयोग गर्नु जसले थोपाहरूको स्थिरतालाई अनुमति दिन्छ, यसरी वास्तविक समयमा ६०,००० भन्दा बढी थोपाहरूको ट्राकिङ सक्षम पाछ (अध्याय ३)। यसले विश्लेषणको समग्र थ्रुपुट बढायो र प्रतिरक्षा सेल जनसंख्या भित्र विषम व्यवहार अनुगमन गर्न ठूलो डेटा नमूना प्रदान गर्‍यो।

Natural Killer कोशिकाहरू र Plasmacytoid Dendritic कोशिकाहरू दुई महत्त्वपूर्ण जन्मजात प्रतिरक्षा कोशिकाहरू हुन् जसले cytotoxicity, immunoregulation, adaptive र सहनशीलतादेखि लिएर धेरै कार्यहरू प्रदर्शन गर्दछ। हामीले विभिन्न लक्ष्य कक्षहरूसँग तिनीहरूको अन्तरक्रियाको गतिशीलता अनुगमन गरेर यी कक्षहरू भित्र कार्यात्मक विषमताको अनुसन्धान गर्न ड्रपलेट-आधारित अनुकूलन प्रयोग गर्यौं। NK कोशिकाहरू (PB र Umbilical cord) को ट्युमर सेलसँगको अन्तरक्रियाको मूल्याङ्कन गरेर, हामीले NK कोशिकाहरू विभिन्न साइटोटोक्सिक शक्ति र प्रभावकारिता भएका कोशिकाहरू मिलेर बनेको देख्यौं। थोपाहरूमा Paramagnetic nanoparticle आधारित immunoassay सहित NK कोशिकाहरूमा स्राव र cytotoxic प्रकार्य बीचको सम्बन्धको अध्ययन गर्न सहज भयो (अध्याय ४)। थोपाहरूमा pDCs को एकल-कोशिका सक्रियताले देखायो कि उत्तेजनाले

(stimulation) pDCs को कार्यात्मक विविधीकरणलाई प्रेरित गर्दछ , र IFN-I मार्ग stochastic gene नियमन द्वारा नियन्त्रित छ। हामीले यो पनि देखायौं कि वातावरणीय संकेतहरूले यस घटनालाई श्रमको उप-समूहहरूमा आधारित विभाजनको सट्टा थप विस्तार गरेको छ (अध्याय ५)।

हामीले व्यक्तिगत स्तरमा तिनीहरूको crosstalk निगरानी गर्नका लागि थोपाहरू भित्र pDCs सँग NK कोषहरू जोड्यौं। यस अध्ययनमा, हामीले IFN γ र IFN α को मात्रा NK कोशिकाहरू र pDCs द्वारा गुप्त गरिएको क्रमशः अनुगमन गर्यौं कि pDCs को सक्रियताले NK सेल सक्रियता बढाउन सक्छ (अध्याय ६) । यो प्रारम्भिक अध्ययन प्रतिरक्षा प्रणालीमा सेलुलर समन्वयको समझमा एकल-कोशिका उपकरणहरू लागू गर्ने दिशामा भावि अध्ययन सम्भावनाहरूको एक उदाहरण हो।

यसरी, हामीले प्रतिरक्षा कोशिकाहरूमा कार्यात्मक विषमताको जाँच गर्न Droplet-आधारित Microfluidics को सफल उपयोग गरेर देखाएका छौं । अन्तमा, हामीले cell-आधारित इम्युनोथेरापी दृष्टिकोणहरू (अध्याय ७) सुधार गर्न वा विकास गर्न एकल-सेल अध्ययनहरूबाट व्युत्पन्न विभिन्न समाधानहरू छलफल गरेका छौं।



CHAPTER 1

GENERAL INTRODUCTION

This chapter has been partially adapted from following papers:

1. Understanding Natural killer cell biology from a single cell perspective

Nikita Subedi, Liesbeth Petronella Verhagen, Esmée Michelle Bosman, Ilse

van Roessel Jurjen Tel

Cellular Immunology,

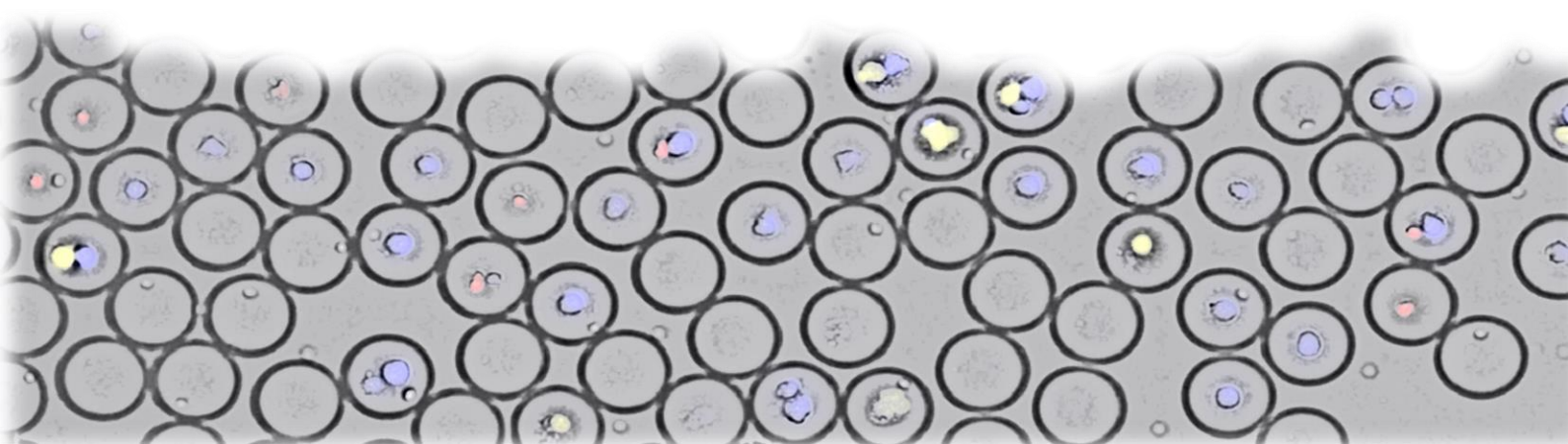
Published: March 3, 2022

2. Integrating Immunology and Microfluidics for Single Immune Cell Analysis

Nidhi Sinha, Nikita Subedi, Jurjen Tel

Frontiers in immunology, 9:2373

Published: October 16, 2018



Resolving cellular heterogeneity: Studying immune cells at single cell level

The human immune system recognizes myriads of environmental triggers and is highly flexible in generating a variety of signaling responses over time. Several types of cells collaborate with antibodies and cytokines to generate an appropriate immune response. The spatial organization and migration of cells within tissues, as well as the dynamic nature of cellular communication, enhances the complexity of our immune system and collectively mount the response. The nature and magnitude of an immune response are dependent on dynamic molecular and cellular interactions where well-orchestrated cellular communication is the key factor to maintain them. The question arises whether all immune cells fight all pathogens and tumors similarly to leverage this broad flexibility and diversity. Even though there are multiple subsets of immune cells, with each subset responding to specific stimuli, responses are often initiated by individual cells within each subset and communicated to other cells to establish a more complex, population level response[1]. Stochastic expression of genes (influenced by a cellular microenvironment) or pre-defined molecular drivers (as in case of B-cell and T-cell receptors) are driving factors behind heterogeneity in the human immune system[1]. Numerous studies over the last decades established that heterogeneity is a trademark of the human immune system[2,3]. Experiments performed at population level average out the behavior of individual cells[4]. Hence, bulk studies fail to provide a coherent understanding of the immune system by masking their phenotype, expressed genes, proteins or metabolites at single-cell level and cellular communication between single immune cells[4,5]. The advent of single-cell technologies and the subsequent possibility to study the behavior of individual immune cells uncovered several biological functions that were previously not detectable with bulk studies[6–8]. For instance, Shalek et al. demonstrated the importance of paracrine communication during immune response using single-cell analysis[9]. Single-cell analysis enabled the investigation of maturation, activation, and signaling pathways of individual immune cells triggered by various environmental factors as well as intercellular communication[10–12]. Additionally, this approach identified new immune cell subsets[13,14]. For instance, single cell transcriptomics, introduced a paradigm shift in the CD4+ T helper field and enabled the identification of multiple functionally distinct T helper cell subsets in addition to the well-established Th1 and Th2 subsets[15–18].

Single-cell technology requires isolation of individual cells from a population for multiple data extraction from each isolated cell in order to gain information on the genotype, phenotype, lineage, protein secretion, proliferation, activation, maturation, cytolytic activity and intercellular communication[19]. Single-cell analysis tools are currently investigated by various research groups worldwide and hold great promise in providing a comprehensive understanding of our immune system[20]. Following the isolation of individual immune cells, multiple experimental operations for DNA sequencing, RNA sequencing, and protein expression profiling can be implemented to map the lineage and identify subsets of immune cells[21–23].

1. Immune cell heterogeneity and its implication for immunotherapy

Harnessing the host's immune system to treat cancer was first conceptualized by William Coley, also known as the father of immunotherapy, who used live bacteria as an immune stimulant to treat cancer[24]. Immunotherapy relies on the abilities of our immune system to identify and eliminate malignancy during initial transformation via immune surveillance[25]. A successful immunotherapeutic approach exploits a well-coordinated interaction between immune cells and cancer cells in the tumor microenvironment (TME), however the complexity of these interactions kindled by the heterogeneity of immune cell subpopulations has become a real challenge.

Recent advances in immunotherapies range from stimulating effector mechanisms to counteracting inhibitory and suppressive mechanisms. Over the years, Natural Killer (NK) cells gained popularity for immunotherapy of cancer given their unique combination of potent anti-tumor effector functions and safety profile[26,27]. The capacity of NK cells to discriminate healthy from diseased cells creates the opportunity to safely use healthy NK cells in an allogeneic setting and to maximally benefit from their anti-tumor potential without risking the development of graft-versus-host pathology[28,29]. In vivo, NK cells interact with other immune cells, such as dendritic cells (DCs) or T cells, for an enhanced activation[30]. Plasmacytoid dendritic cells (pDCs), the major producer of type 1 interferons (IFN-I), play a significant role during in vivo NK cell development and recruitment[31]. Activated pDCs on their own have been shown to safely induce antigen specific T cell responses against melanoma patients[32]. NK cells receive an activation signal from pDCs in juxtacrine and paracrine manner for augmented cytotoxic and secretory functions[33]. Also, NK cells

maintain the activation of pDCs and support them in activating CTLs. In this way, a bidirectional talk between NK cells and pDCs provides a positive feedback activation for both the innate immune cell types. Even though the cross-talk between these immune subsets has been explored during viral infections, its implications in cancer immunotherapy are not well understood[34]. Since these cells play an important role in maintaining the balance between adaptive and innate immune responses and have potential anti-tumor functions, a deeper understanding of their interplay will add to the clinical outcomes of combinatorial cell therapy. Despite encouraging results from adaptive NK cell therapy, further investigations to improve the clinical efficacy are required. One of the key strategies would be to explore the interaction dynamics of NK cells with other accessory and target cells (infected or transformed cells). It is also important to consider the functional heterogeneity of NK cells in form of distinct subsets and activated stages. Since the function of these cells relies on the array of activating and inhibitory receptors, the nature of the response they generate is highly variable and depends on the dynamics of cellular interaction with their target cells. The heterogeneity within the pDCs population upon diversification has also been observed. The emerging notion about functional heterogeneity of both NK cells and pDCs is likely to augment potential applications of dendritic and NK cell-targeting therapies in combination or separately.

In the forthcoming sections, a comprehensive overview of phenotypical and functional heterogeneity in the NK cell population along with a brief overview on heterogeneity in pDCs is provided. Subsequently, information regarding emerging single cell technologies is also discussed.

2. Natural Killer Cells (NK cells)

In the early seventies, a subset of innate immune lymphocytes capable of inducing spontaneous yet selective cytotoxicity against cancer cells without pre-exposure was recognized and coined as NK cells[35,36]. These cells play an important role in anti-viral immunity and immune surveillance by identifying and eliminating transformed or infected cells through distinct recognition mechanisms[37]. NK cells are large granular lymphocytes derived from CD34⁺ hematopoietic progenitor cells that originate in bone marrow, constitute around 10-15% of the total peripheral blood lymphocyte population and have been traditionally defined as CD3⁻ and CD56⁺ cells[38].

According to the developmental model proposed by Freud and Caligiuri, the maturation of NK cells involves six distinct stages, starting with the $\text{Lin}^- \text{CD34}^+ \text{CD133}^+ \text{CD244}^+$ hematopoietic stem cells that differentiate into towards CD45RA^+ lymphoid-primed multipotential progenitors in Stage 1, and into common lymphoid progenitors. Common lymphoid progenitors (CLPs) then form NK progenitor cells characterized by the loss of CD34 and expression of the surface marker LFA-1 leading to NK cell lineage commitment. Later these cells mature into the $\text{CD56}^{\text{bright}}$ NK cell subpopulation that subsequently differentiate into the CD56^{dim} NK cell subpopulation. At this stage there is the expression of CD16 and KIRs and finally NK cells differentiate into adaptive NK cells.

Even though the linear model of development gives fundamental information regarding the development of NK cells, several lines of evidence also suggest a more branched model whereby different precursor populations may independently develop into distinct subsets of mature NK cells. The contradictory developmental scheme for NK cells maturation is shown in Figure 1.

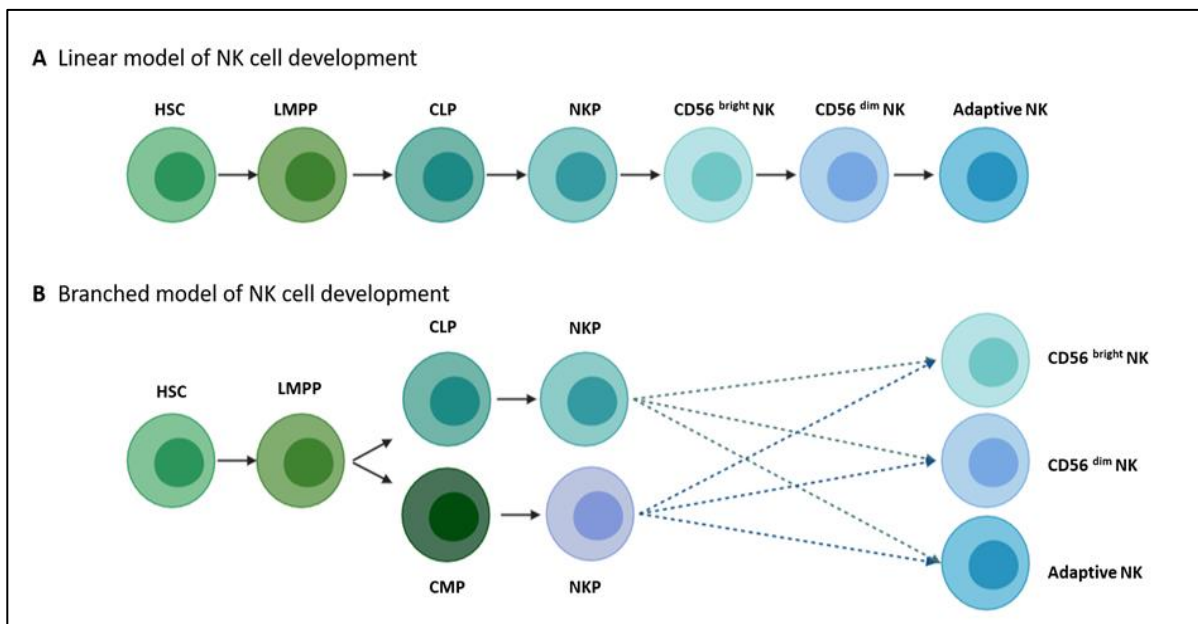


Figure 1. The linear and branched model of NK cell development and maturation: **A.** Linear model explains a direct route of NK cell development from hematopoietic stem cells to the NK cell progenitor sequentially developing into $\text{CD56}^{\text{bright}}$, dim and into adaptive NK cell. **B.** Branched model suggest that the hematopoietic stem cells differentiate into lymphoid-primed multipotent progenitors (LMPP), which then differentiate toward common lymphoid (CLP) or myeloid progenitors (CMP). These progenitors give rise to individual NK cell progenitors (NKP) into specific NK cell subsets. Figure adapted from Cichocki et.al. *Front. Immunol.*[7] . Figure created using BioRender (<https://biorender.com/>)

One of the examples of such illustration is the experiment that showed that NK cells derived from CMPs and granulocytic monocytic precursors (GMPs) isolated from cord blood could efficiently differentiate into NK cells when cultured in presence of supporting cytokines and stroma. This finding challenged the belief that all NK cells are exclusively derived from CLPs[39]. In addition, in healthy adults, PB CD56⁻ NK cells have been identified, which is an intermediate cell type progressing to CD56^{dim} NK cells, supporting the idea that different NK cell development pathways exist. Also, NK cells, which phenotypically resemble CD56^{dim} cells, have been identified however they lack inhibitory receptors such CD94/NKG2A and KIRs. It is currently unknown how these NK cells can originate from CD56^{bright} NK cells[40]. Existence of these different conflicting theories suggests that there is a need for a more definitive understanding in the field[39,41,42].

Resolving these issues requires an in-depth investigation of NK cell distribution, maturation, function, and transcriptional profiles across different anatomical sites and compartments. Advancing single-cell technologies like RNA sequencing has revealed several tissue-specific patterns related to the development and maturation of multiple lineages. Based on the evidence gathered from the study, Dogra et al. have proposed a model for anatomic control of NK cell development and function that shows site-specific segregation of NK cell maintenance and differentiation[43]. Several other single cell-based studies investigating NK cell development have been discussed in later sections.

3.1. NK cell surface receptors and regulation

NK cells have the intrinsic ability to identify “self” to distinguish healthy from target cells (e.g., virus-infected cells or tumor cells). The concept of “dynamic equilibrium” suggests that the stimulation of NK cells and their effector function depends on integrating signals from both activating and inhibitory receptors[44–46]. Virtually all cells express MHC-I molecules (HLA molecules), which function as ligands for inhibitory receptors on the NK cell surface, contributing to self-tolerance. NK inhibitory receptors broadly fall into two subcategories— C-type lectin-like inhibitory receptors (e.g. NKG2A) and killer-cell immunoglobulin-like receptors (KIRs)[47,48]. Apart from MHC class I molecules, other different “self-signals” detected by NK cells, as other inhibitory receptors (e.g., sialic acid binding Siglec receptors) can also regulate cellular activation[37]

In contrast to healthy cells, virus-infected cells or tumor cells lack or have reduced MHC class I expression to avoid antigen-dependent recognition and therefore also have reduced inhibitory signals for NK cells. Simultaneously, activating receptor ligands, such as the Fas death receptor and MHC-I chain-related proteins, are upregulated upon diseased conditions[49]. This causes NK cell activation, leading to target cell elimination through cytotoxicity or secretion of pro-inflammatory cytokines[50]. Different Activation NK cell receptors include KIR family receptors, type II C-type lectin-like molecule (NKG2D), NKG2C heterodimeric receptors, the nectin/nectin-like binding receptors DNAM-1/CD226 and CD2-like receptor- activating cytotoxic cell and Nkp46, Nkp30, and Nkp44 are the superfamily of natural cytotoxicity receptors (NCRs)[51]. These receptors act together with different adaptor proteins to initiate NK cell activation however, combined signaling via inhibitory and activation receptors determine the final functional output[51].

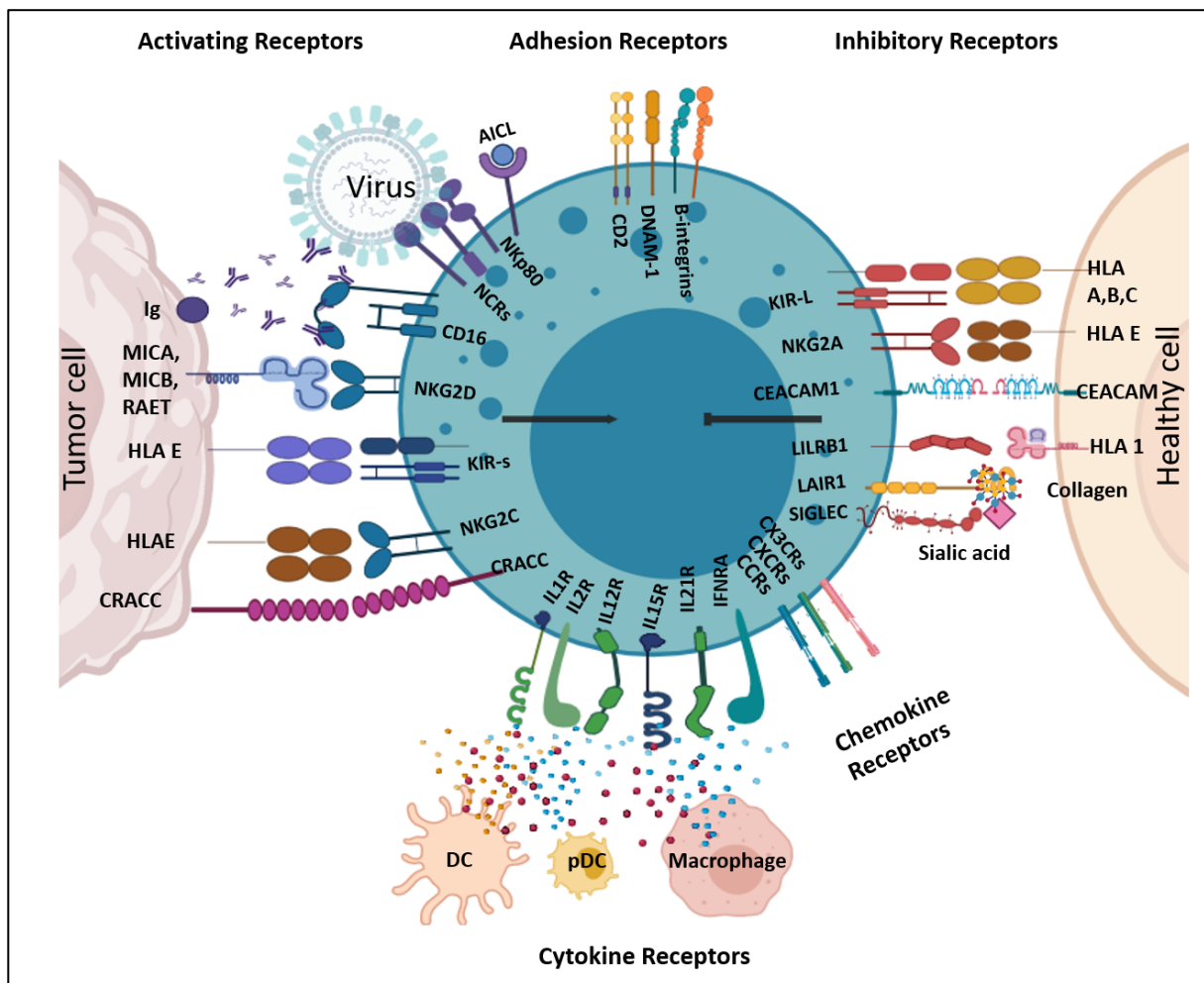


Figure 2. Regulation of NK cell via its surface receptors: Functional regulation of NK cells involves synergistic signaling via combination of different receptors expressed within their cell surface. Different

cell types provide ligands for these receptors that define whether the NK cell gets activated or not. Different activating and inhibitory receptors in human NK cells and their corresponding ligands along with other chemokines, adhesion receptors and cytokine receptors which are altogether show in the figure. Figure created using BioRender (<https://biorender.com/>)

Along with the above-mentioned receptors, NK cells also display surface expression of different cytokine receptors that play an integral role in NK cell regulation. NK cell maturation is dependent on the cytokine microenvironment generated by bidirectional crosstalk with other immune cells such as T cells, dendritic cells (DCs) and macrophages[37,52,53]. An array of different activation, regulatory as well as inhibitory receptors expressed on the NK cell surface and their involvement in regulating NK cells activity has been schematically presented in the Figure 2.

3.2. Heterogeneity within the NK cell compartment

The phenotypical variation within the NK cell population is marked by the combination and frequency of expressed surface receptors. Traditionally, the NK cell population is classified into two distinct subsets based on their level of CD56 expression: CD56^{bright}, and CD56^{dim} NK cells. The CD56^{bright} population is more immunomodulatory and known to be the precursor of the more cytotoxic CD56^{dim} population. The CD56^{dim} population constitutes the largest fraction of peripheral blood conventional NK (cNK) cells while the CD56^{bright} population is more dominantly present in tissues.

Even though this dichotomy is widely accepted, it fails to represent the complexity of NK cells at different maturation stages and cells residing at different anatomical locations. The recently discovered adaptive role of NK cells, along with tissue specific heterogeneity further enhances the complexity[54,55]. All these aspects do not fit the dichotomy dogma, and therefore studying NK cell diversity demands a fresh perspective. Here, heterogeneity within NK cells have been explained in terms of tissue of maturation and the functional attributions it displays (Figure 3A). However, these specific subgroups of cells are further influenced by the stage of maturation they are in and what combination of surface receptors they express. In the following sections the two main aspect of NK cell heterogeneity are discussed.

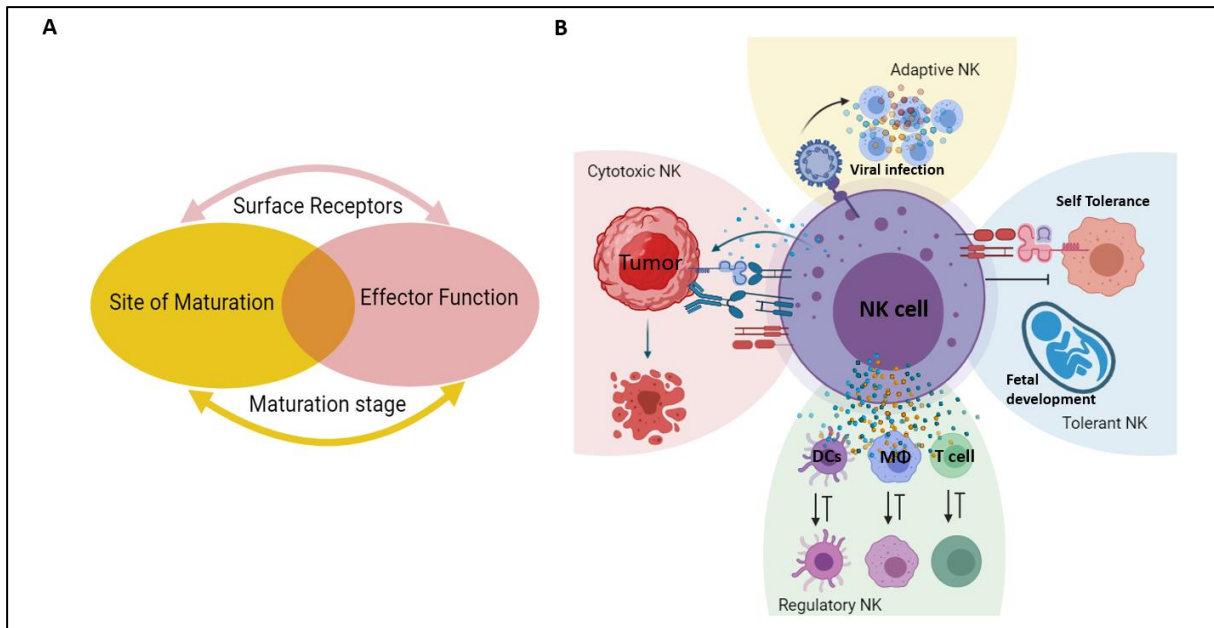


Figure 3. The NK cell heterogeneity beyond the dichotomy. A. The NK cell diversity can be categorically explained based on site of maturation and their functional ability. Both the groups can further be correlated via the surface receptors they express and the stage of maturation they are at. **B.** Based on different functions NK cell display, they can be cytotoxic, regulatory, tolerant, or adaptive in nature. Cytotoxic NK cell ($CD56^{dim} CD16^{bright}$ phenotype) display cell lysis as the major function while regulatory sub population ($CD56^{bright}$ phenotypes) are more adept in secreting cytokines such as $IFN-\gamma$ and $TNF-\alpha$. Regulatory NK cells function in modulating the functions of other immune cells such as DCs, macrophages and T cells. These cells help in quality assessment of DCs and T cells by lysing less mature cells. Tolerant NK cells are passive form of regulatory subsets that plays more important role in maintaining the tolerance to the self. Tolerant NK cells are also known for their ability to induce vascular remodeling to provide physiological support to the fetal development. Adaptive NK cell displays a different phenotypical as well as functional characteristic to other NK cells. These cells are found more in chronic viral infections and upon vaccination. Adaptive NK cells are responsible for generating memory NK cells however they show less cytotoxic and secretory ability. Figure created using BioRender (<https://biorender.com/>)

3.2.1. Tissue specific NK cell diversity

The ability of lymphocytes to migrate in interstitial tissues is essential for both innate and adaptive immune responses. NK cells play an important role in immune surveillance and instead of remaining confined to peripheral blood, they are widely distributed throughout the body. NK cells are found in healthy skin, gut, liver, lungs, and the uterus during pregnancy[56]

along with secondary lymphoid organs. Additionally, human NK cells were also identified in other tissues such as the kidney[57], joints[58], and breast[59] under pathophysiological conditions. Depending on the site and stage of the maturation, NK cells can display different surface markers and functions. cNK cells are mainly found in peripheral blood, migrate to a specific location to exert their effects, and can be further classified as either CD56^{bright}CD16⁻ or CD56^{dim}CD16⁺ cell types.

Specialized tissue resident NK (trNK) cells are identified in various tissues in the human body and contain a higher fraction of CD56^{bright} NK cells. Additionally, they express adhesion molecules, such as CD69, and chemokine receptors, including CCR5 and CXCR6 that preserve trNK cells in tissues and prevent them from entering the circulation. TrNK cells have several features comparable to CD56^{bright} cNK cells and are indirectly involved in inducing cytotoxicity. The trNK cells in the bone marrow, secondary lymphoid tissues and liver have an increased expression of the inhibitory receptor CD94/NKG2A and the receptor NKp46, but lower expression of CD94/NKG2C, KIRs and CD16[60]. Several functional and phenotypic similarities between trNK cells and CD56^{bright} cells suggest that trNK cells could be an immature cell type in transition to become cNK cells[61]. The topological organization of trNK cells within the microenvironment of different organs modulates their functional adaptations. The NK cells that localize in the blood, blood-rich sites such as BM, spleen, and lungs are largely CD56^{dim}CD16⁺ cells with cytotoxic capacity while NK cells are present only at low frequencies in lymphnodes, tonsils, and throughout the gastrointestinal tract where they are predominantly CD56^{bright} cells and show more regulatory functions. TrNK cells at those locations are mostly responsible for interaction with other cell types to maintain homeostasis and thus show more of regulatory function[61]. For example, NK cells at lymphnodes are responsible for T cell polarization, while uterine NK cells are mostly responsible for placental vascular remodeling[43]. Crinier et al. profiled the transcriptome of human spleen NK cells and compared them with peripheral blood NK cells. They identified four subsets of human spleen trNK cells of which two subsets lack any blood specific signatures and were therefore unique to spleen[62]. Moreover, three different NK cell subpopulations were discovered in human bone marrow. By pseudotime analysis, a subset of trNK cells (not found in blood) was found to be the precursor of both CD56^{dim}-like NK cells and CD56^{bright}-like NK cells[63]. These findings support the theory that NK cells enter the blood stream from the bone marrow and subsequently circulate to infiltrate multiple organs. In contrast, evidence also suggests that

some trNK cells belong to a distinct lineage of peripheral blood cNK cells. Research showed that those trNK cells can survive in situ for a considerable amount of time, do not translocate to the blood, require different transcription factors (such as Hobit and Tbet) for their development and are presumably terminally differentiated[60]. For instance, some NK cells have different functional roles compared to what has been shown earlier. Profiling tonsil NK cells demonstrated that the majority of tonsil NKs are composed of a CD56⁺CD16⁻ population that displays contrastingly higher NK activating and cytotoxic transcriptome[64]. These contrasting functional properties shown by the CD56^{bright} population suggest that trNKs possess an independent character that could have their own functional range.

Given their functional similarity and site of residence, ILC1s found in organs traditionally have been understood as trNK cells subtypes[65]. Despite sharing overlapping transcriptomic regions and a dependency towards IL-15 for proliferation and stability, the developmental pathways for both the cell types are rather different[66]. NK cell develops strictly from NK cell progenitors that are restricted to generate NK cells but none of the other ILC subsets. Apart from CD200R, no other reliable markers have been identified that distinguish murine NK cells with ILCs[67]. A recent study allowing multi-tissue single-cell analysis deconstructed the complex programs of mouse natural killer and type 1 innate lymphoid cells in tissues to identify unique transcriptional programs underlying both the cell types[68]. The study classified ILC1 as the Eomes⁻ tissue specific NK cells that expresses Zfp683[68]. Single cell-based applications as such could serve as the molecular guide in resolving the debate also in human immune cells.

3.2.2. Functional NK cell diversity

The NK cell phenotype and maturation state has been integrally conflated with effector function and used as the basis for classifying NK cells into distinct subsets (Figure 3B). The cells that have superior lytic abilities are known to be cytotoxic NK cells. They are phenotypically defined as CD56^{dim}CD16^{bright} subpopulation with larger expression of lytic granules, and KIRs and are thought to be more mature compared to other NK subsets[69]. The other less mature subsets display more regulatory functions via secretion of different cytokines. These subsets can be further subdivided as the regulatory and the tolerant population[70]. Both subsets are characterized by expression levels of CD56, NKG2A, CD2, CD62L and CCR7 molecules. However, these subsets vary in terms of functions as regulatory NK cells are more responsible

for modulating the immune responses from other immune cells and are functionally similar to the trNK cells[70]. The role of the regulatory NK cells has been quite evident in the maturation of dendritic cells, direct activation of adaptive immune cells and killing of immature DCs and overstimulated macrophages (Figure 3B). Tolerant NK cells on the other hand show dominant inhibitory characteristics and aid in fetal development during pregnancy as they are mostly found in decidual region[70] (Figure 3B).

Recently, it was discovered that a few percent of NK cells can develop immunological memory and differentiate into adaptive NK cells[54,71]. Adaptive NK cells were shown to proliferate and differentiate in reaction to a cytomegalovirus (CMV) infection upregulating HLA-E-specific activating receptor CD94/NKG2C[72]. Additionally, antigen-specific NK cell memory was also described in T and B cell deficient mice displaying hapten-specific contact hypersensitivity in skin cells after adoptive transfer of NK cells from a previously sensitized donor[73]. NK cells can undergo differentiation into memory-like effectors once exposed to various cytokines such as IL-12, IL-15, and IL-18[74]. In the peripheral blood of CMV⁺ individuals, adaptive NK cells were identified and described as CD56^{dim}CD16^{bright}, have reduced levels of the surface marker NKp30 and NKp46, and displaying a highly differentiated surface signature, namely, self-KIR⁺NKG2A⁻LILRB1⁺CD57⁺Siglec7⁻ [75][76]. Unlike cNK cells, Adaptive NK cells are poor responders to IL-12 and IL-18 and show reduced expression of the NCRs. However, upon activation via CD16 and NKG2C, they show rapid proliferation, immense secretion of IFN- γ and enhanced ADCC[77,78]. Furthermore, these specialized subsets have reduced expression of promyelocytic leukemia zinc finger while DNA methylation similar to cytotoxic T cells[75,79]. Adaptive NK cells upon continuous activation or chronic viral infection increase expression of check point inhibitors like LAG-3, PD1 thus rendering them into hypofunctional state[80]. All these features make Adaptive NK cells phenotypically as well as functionally different than cNK cells[60].

3.2.3. How does heterogeneity arise

As outlined in the sections, NK cells display a high level of diversity at single-cell level because of variegated expression of activating and inhibitory receptors, yet the developmental roots and functional consequences of this diversity remains unclear. The developmental model of NK cell origin explains that the diversity in the NK cell repertoire is the functional consequence of developmental stages during its maturation and is maintained by the expression of different

surface molecules. A given phenotype for a NK cell subset is the combination of these receptors expressed stochastically within the cells which might further determine its functional capabilities. Studying different developmental phases, it appears as if a group of NK cells starts from a common progenitor cell, however during different developmental stages, they drift from one another due to several intrinsic (genetic) or extrinsic factors (environmental) they are exposed to[60]. This concept for origination of heterogeneity has been shown in figure 4.

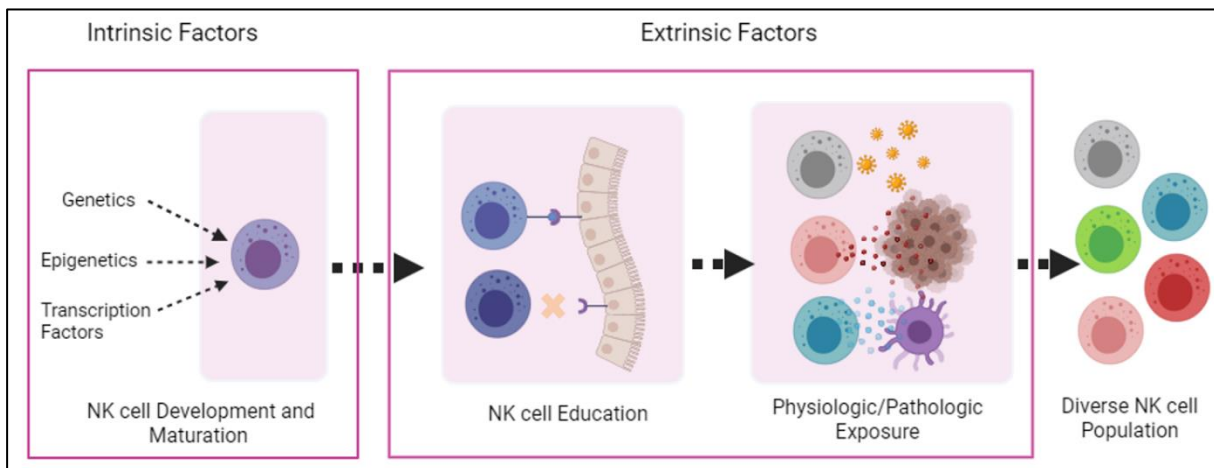


Figure 4. Origin of Heterogeneity: The NK cell diversity is acquired at different levels during the overall life cycle of NK cells. These variations are already acquired during the developmental phase of NK cells where different intrinsic factors such as genetics, epigenetics and transcription factors play an important role. Furthermore, upon maturation, NK cells go through an education process that prevents the cells from self-harm. However, there are also the population that do not match the HLA proteins upregulated by “self” cells thus making them more responsive towards acute viral infections. The third level of variation are induced due to different environmental exposure such as tissue specific cytokines, cross talk with other immune cells, tumor infiltration and encounter with infected cell types. Upon all these exposures, a repertoire of NK cells with different functional capabilities and preferences are generated thus resulting to unexpectedly wide diversity within the cell population. Figure created using BioRender (<https://biorender.com/>)

3.2.3.1. Intrinsic factors that govern NK cell heterogeneity

Host genetics and epigenetics have one of the important roles in determining the fate of the NK cell diversity and are composed together as one of the “intrinsic factors” in this review. In 1997, the study by Parham et al. showed that each individual expresses a different subset of KIR and suggested that the polymorphic allelic distribution could be one of the important factors regulating the NK cell diversity[81]. More recently, the variation in expression pattern KIRs was correlated with the host genetics[82]. By performing a multiparameter mass cytometry of 28 NK cell panels to phenotype peripheral blood NK cells from 5 sets of monozygotic twins and 12 unrelated adults they showed the existence of more than 100,000 possible NK cell phenotypes and no single phenotype accounted for more than 7% of total NK cells[82]. Receptor patterns and expression levels in identical twins, showed less variability compared to non-related individuals, marking genetics to be one of the determining factors for the observed heterogeneity. Furthermore, the genetic differences within an interracial and interethnic population also greatly influenced the stochastic expression of different cell surface receptors. Different functionally evolved NK cell subsets such as activated NK cells with adaptive memory-like functions are highly linked to epigenetic reprogramming including alterations in DNA methylation[75,83]. Wiencke et al. has provided a model for adaptive NK cell diversification whereby engagement of DAP12-coupled activating receptors results in epigenetic imprinting of the ZBTB16 locus, resulting in loss of promyelocytic leukemia zinc finger protein expression[83]. Promyelocytic leukemia zinc finger protein expression deficient NK cells also display stochastic hypermethylation of promoters encoding signaling proteins SYK, EAT-2, DAB2, and FcεRγ, resulting in the diversification of the adaptive NK cell repertoire. In addition to host genetics and epigenetics, another crucial intrinsic factor that governs cellular diversity is the involvement of different transcription factors[84–86]. Closer analysis of different organ-specific NK cell clusters showed discrete developmental stages at different points of differentiation. This study supported the notion that the developmental progression of NK cells goes from CD56^{bright} to CD56^{dim} NK cells and showed the existence of a “transitional” population with intermediate expression of CD56 or CD57 surface molecules that links the two phenotypes[87]. Similar developmental subsets consisting of mature, transitional, and terminal NK cell subsets were identified in murine bone marrow NK cells. Later it was identified that different developmental stages were regulated by different

transcription factors thus leading to heterogeneity[88,89]. It is widely appreciated that cNK cells differ from trNK by a different set of transcription factors during differentiation. For example, the development of liver-resident NK cells is dependent on the transcription factors Hobit and T-bet, whereas differentiation of cNK cells requires expression of the transcription factors Eomes and only moderately T-bet[90,91].

All these studies show how host intrinsic factors play an important role in modulating variation within NK cells. Even though host genetics determines the expression pattern of different KIRs together with selective transcription translation and post-translational modifications, external factors such as cytokine signaling, cell–cell interactions, epigenetic modifications and immunological experience further affects the gene expression at multiple levels generating multiple layers of heterogeneity within NK cell compartment.

3.2.3.2. Extrinsic factors that govern NK cell heterogeneity

NK cell development is equally affected by cues from the environment wherein they reside. Examples of such extrinsic factors include, NK cell education, the expression level of MHC-I molecules and, furthermore, different environmental cues such as cytokines, growth factors and pathogenic interactions, that shape the NK cell development process.

The expression pattern and the affinity of different KIRs identify self-molecules during maturation and play an important role in inducing the functional variation within the NK cell compartment. By the process of “education”, these cells can tune the functional ability of cells in an MHC-dependent or independent way[92,93]. Thus, generated educated population can identify self from foreign and have acquired more adept effector function while some with non-reactive or lacking expression of inhibitory receptors remain hypofunctional[94]. Around 10-20% less educated or uneducated cells, that might be considered potentially harmful co-exist together with functionally superior NK cells[95,96]. These uneducated NK cells have a high threshold for activation, thus maintaining the self-tolerance in the body[95,97]. They are also thought to play an important role during inflammatory microenvironments, like viral and bacterial infections and certain tumor invasions[98,99]. The state of education could be reversed by the cytokines, thus providing the possibility of changing the functional fate of the NK cells[100]. Thus educated, uneducated, non-binding and weakly-binding NK cells play their part in maintaining host immunity[99]. Apart from the host’s genetics, which can affect the stochastic expression of different inhibitory receptors on their surface, NK cell education also

depends on the expression of HLA molecules which varies among the population. Thus, in the process of developing functionally competent NK cells, a new level of diversity is generated within and between individuals.

NK cells can sense different chemokines that direct them towards the site of infection or adapt a certain functionality in response to cytokines being secreted. The role of cytokines, such as IL-15, in inducing intra-lineage plasticity to maintain phenotypical and functional diversity within NK cell repertoires has been recently identified[101]. IL-15 helps in controlling the cellular metabolism via activating the mammalian target of rapamycin (mTOR) and is essential for NK cell survival, development and proliferation[102]. The role of IL-15 has also been studied in maintaining the functional plasticity therefore providing the opportunity to tune different functional state within NK cell repertoire. Either way, the physiological as well as the pathological environment shapes the phenotype of NK cells in such a way that they are capable to serve a particular function. NK cells that have attained full maturation and education, leave the site of generation, and take up residence at the peripheral tissues. At the tissue level, these cells are exposed to different tissue specific cytokines, growth factors and pathogens. This difference in exposure can generate different phenotypical variants that are opted to fulfill specific tasks. For example, decidual NK cells found in the uterus have a distinct phenotype compared to peripheral blood NK cells. These cells share common features to CD56^{bright} cNK cells and secrete several chemokines like XCL1, CCL1 and angiogenic factors such as, vascular endothelial growth factor (VEGF), placental growth factor (PLGF), Ang1, and Ang2 that are involved in vascular remodeling and therefore promote the fundamental physiological process of pregnancy[103,104].

NK cell diversity expands with immune experience, which means that the more cells are exposed to environmental stimuli, the more there is diversification. At birth, NK cells have very low diversity but have high capacity for a range of responses. This variation enhances with age and over the course of a lifetime exposure, the NK repertoire diversifies, hence, becoming functionally specialized and unique to an individual. Even though the NK cell repertoire stabilizes over time, their adaptability to respond against novel antigens decreases [105]. The high NK cell diversity was identified to be significantly associated with 2.5 folds higher risk of HIV-1 acquisition[105].

The tumor microenvironment (TME) can steer and affect NK cell heterogeneity. This variation impairs the effectiveness of NK cells by limiting their capacity to infiltrate tumors, thus

dampening the cytolytic function of tumor-infiltrating NK cells. Additionally, the TME induces several immunosuppressive soluble factors such as TGF β , prostaglandin E2 (PGE2), adenine, indoleamine 2,3-dioxygenase (IDO) and a range of ligands that inhibit their function, including KIRs, CD94/NKG2A, PD1, CTLA4, TIM3, TIGIT, CD96, KLRG-1, LAG3, and, recently discovered, IL-1R8 [106,107]. Another aspect contributing to the impaired NK cells function in the TME is the poor availability of nutrients, such as glucose and glutamine. Research showed that CD56^{bright} NK cells require glycolysis to produce IFN- γ and promote their survival, while the lung TME favors more gluconeogenesis due to up-regulation of the fructose diphosphates enzyme[108]. This leads to inhibition of glycolysis and eventually leading to impaired NK cell viability.

Taken together, several studies have shown that heterogeneity is the function of intrinsic as well as extrinsic factors eventually shaping different stages within the development, thereby generating wide variations within cell types, and resulting in the diverse NK cell populations (Figure 4).

3. Plasmacytoid dendritic cells (pDCs):

Plasmacytoid dendritic cells (pDCs) were first described by the Liu and Colonna groups as the major IFN producing cells of the immune system[109,110]. They are generated continuously in the bone marrow from hematopoietic stem cells via both myeloid and lymphoid precursors. The development of pDCs highly depends on the ligation of CD135 cytokine receptors by Flt3L that even in absence of other proliferative signals is enough to induce their development in vivo[111]. Plasmacytoid DCs also require the high-level expression of IRF-8, TCF-4 (also known as E2-2), and BCL-11A for their development, functional specification, and maintenance[112–114]. Plasmacytoid DCs are characterized as BDCA-2⁺BDCA-4⁺CD4⁺CD45RA⁺IL-3R α ⁺ILT3⁺ILT1⁻CD11c⁻ lineage⁻ cells[115]. After the development, proteins such as CXCR4 (context-dependently) mediate pDC trafficking to peripheral blood and lymphoid organs where they remain non-proliferative and show a short life span of a few days[116]. Furthermore, pDCs express TLR-7 and TLR-9 in their endosomal compartments which upon ligand ligation led to the immense production of type I interferons (IFN-I). Lastly, upon activation they become larger and more branched like other DCs.

3.1 Diversity within the pDCs compartment:

Plasmacytoid DCs are known as natural IFN secreting cells because of their immense capacity to secrete IFN-I against infections. These cells are exclusively known for their ability to mount antiviral immune response along with a response towards a bacterial, fungal, and parasitic infection. Although pDCs constitute less than 1% of the total PBMCs population in peripheral blood, they still produce over 80% of total IFN-I secreted upon infection[109,117]. They also have other functions, including adaptive, regulatory, and tolerogenic roles, however, it is not yet clear how they show these ranges of functions[118]. There are two different theories regarding the origin of diversity within pDCs population: Development of distinct functional subsets during the maturation or acquired plasticity upon stimulation[119]. Data generated from single-cell transcriptomic analysis support acquired plasticity over-development subsets theory by showing a homogenous pDCs population in homeostatic conditions[120]. It was also observed that pDCs could convert into conventional (cDC)-like cells upon stimulation with IL-3 or CpG-B[121,122]. A slight difference in the signal integration at single-cell level is already enough to drive such functional plasticity[119,123]. However, in the absence of enough information regarding the development and maturation scheme of pDCs and identification of several phenotypes within the DC population, it is still hard to gather consensus regarding the origin of pDC heterogeneity[119]. In the following section, the phenotypical and functional diversity within the pDC population is discussed.

4.1.1 Phenotypical heterogeneity within pDC

pDCs with different phenotypical characteristics have been identified, mostly differing in the degree of their differentiation and capacity for secreting IFN-I. In mice, different markers such as CCR9, SCA-1, CD9, and Ly-49Q are expressed by peripheral pDCs and can distinguish between different phenotypes[124–126]. Human pDCs were characterized into two subsets based on the expression of CD2 surface molecules where CD2^{high} pDCs showed the higher capacity to promote T cell stimulation when activated while CD2 sparse populations secreted IFN-I upon activation[127]. Similarly, Siglec-1 was also used to distinguish between IFN-I secreting and non-secreting cells. However, this marker also described the IFN-I non-secreting cells as immature phenotypes of pDCs[128]. Positive expression of CD5 and CD81 was later described together with CD2 to describe the IFN-1 secreting potential of pDCs and linked this expression to tyrosine kinase receptor AXL[119,129]. It has also been found that pDCs upon

activation with the tick-borne encephalitis vaccine (FSME) upregulate CD56 in their cell surface that enables them to induce cytotoxic effector function against MHC-I negative tumor cells along with priming antigen specific T cells[130,131].

Transcriptional profiling of individual pDCs revealed an unprecedented phenotypic heterogeneity within a cellular compartment that could be directed towards the early lineage priming of the progenitor cells. A DC population was identified that displayed similar features between pDCs and cDCs, eg: the surface phenotypes and functionality of cDCs while the transcriptional profile of pDCs. A more recent study highlighted the phenotypical diversity within pDCS compartment where the cells upon activation showed three specific subpopulations with the differential functional ability for IFN-I secretion and T cell priming[123].

4.1.2 Functionally diverse pDCs

4.1.2.1 Innate and adaptive role of pDCs

Plasmacytoid DCs sense pathogen associated molecular patterns via specific endosomal toll-like receptors: TLR-9 (unmethylated CpG motif-containing DNA), TLR-7 (viral single-stranded RNA) ultimately leading to its activation[132–134]. This activation starts the downstream IFN signaling pathways via myeloid differentiation primary response protein 88. Additionally, pDCs can also produce IFN-I through cyclic GMP-AMP synthase and stimulator of IFN genes and retinoic acid-inducible gene 1 like receptor cytoplasmic pathways[135,136]. Thus, secreted IFNs play an important role in restricting viral entry and replication. This overall process of pDCs activation by directly sensing the pathogens has been described as cell-intrinsic activation. Although it is a well-known phenomenon in pDCs study, it has also been shown that some pDC subpopulation requires additional IFN-I boost for activation rather than direct pathogen sensing[137]. Some pDCs can self-regulate and activate other pDCs via autocrine and paracrine signaling of IFN-I signaling[138,139]. There is also the indication that a direct cellular interaction also enables the activation and IFN-I secretion machinery within these cell types[140,141]. Hence, the overall process of pDCs activation and IFN-I secretion is modulated via integrating multiple pathways and cellular processes that remain to be fully explained.

Besides their innate protective function, pDCs also play a key role in shaping the adaptive responses to viruses. Upon activation, these cells undergo morphological changes and increase upregulation of MHC molecules and co-stimulatory molecules, along with secreting

different proinflammatory cytokines[142]. These changes further adapt pDCs for their role as antigen-presenting cells. Several studies have highlighted the fact that pDCs can more efficiently take up and present endogenous antigens compared to exogenous antigens, thus showing an enhanced MHC-I and MHC-II presentation[143]. Apart from IFN-I, pDCs also produce pro-inflammatory cytokines such as IL-6, and tumor necrosis factor in response to TLR activation, thus activating the adaptive immune response[137]. Besides, pDCs have also been shown to induce activation of NK cells in a juxtacrine or paracrine manner, leading to the augmented lytic function of NK cells and secretion of IFN- γ [33]. IFN- γ enhances the function of T cells and B cells. This crosstalk between two cells is important for proper recruitment of either cell towards the site of infection and induces the suited immune response. In this way, pDCs either directly or indirectly facilitate the smooth functioning of the adaptive immune responses.

4.1.2.2 Immunosuppressive and Cytotoxic effector pDCs

Plasmacytoid DCs along with different co-stimulatory molecules also upregulate program death ligands, which are well-known checkpoint inhibitors for T cells. Additionally, pDCs also promote the induction of Foxp3⁺ regulatory T cells. Besides peripheral tolerance, pDCs are reported to transport antigen to the thymus to promote central tolerance through clonal deletion[144] pDCs exert immunosuppressive effects via mechanisms that involve T cell anergy and deletion[145,146]. This demonstrates that pDCs have multiple mechanisms devoted to immune tolerance, and these may be engaged in a context-dependent manner. However, identification of regulatory pDCs in the tumor microenvironment could also be detrimental. Plasmacytoid DCs have been reported to infiltrate in head and neck cancer, lung cancer, breast cancer, ovarian cancer, and skin cancer thereby contributing to the suppressive tumor microenvironment via generation of regulatory T cells and correlated to their poor prognosis[147–149].

Plasmacytoid DCs have also been associated with the unique cytotoxic properties that are endowed upon TLR-7 mediated activation[131]. Viruses such as influenza virus and synthetic components such as imiquimod are the ligand for TLR-7 that could induce functionally active TRAIL⁺ pDCs that can lyse appropriate tumor targets[150–154]. HIV-infected pDCs also upregulate TRAIL that has been shown to kill CD4⁺ T cells and thus might be involved in the depletion of T cells in HIV patients.

4. Next generation immuno-technologies: Microfluidics for Single-Cell Analysis

Although ample evidence obtained in bulk-based studies suggest the presence of phenotypical and functional heterogeneity, in-depth understanding remains quite limited. Amongst immunologists, flow and mass cytometry are among well-established, high-throughput, and high-content single-cell analysis tools[155–157]. Flow cytometers measure fluorescently labelled cells and mass cytometers use transition element isotopes for mapping the functional heterogeneity and phenotypes of different immune cells by quantification of multiple cytokines, chemokines, and surface protein markers of individual cells[158,159]. Although cytometers are a powerful tool for single-cell analysis, they are still predominantly an end-point measurement tool that can only provide a snapshot in time and quantify static markers on cells to provide information on immune cell heterogeneity.

Over the last decade, microfluidics made significant contributions to the field of single-cell research. This method allows cells to be monitored dynamically with high degree of control over the cellular microenvironment[160,161]. These approaches have offered new information by creating innovative conditions that are limited in conventional bulk methods. Microfluidic systems were also developed for applications in several areas such as protein purification and PCR on a drastically decreased scale[162,163]. Microfluidic chips are capable of accurately replicating *in vivo* biological environments to allow high-throughput analysis of cells[164]. It also allows precise automation and control of analytical functions as well as manipulation of cells and their microenvironments with high resolution in both space and time[165,166]. With microfluidics, scientists can implement techniques and protocols for single-cell analysis through DNA sequencing, RNA expression, and protein quantification to understand the mechanism of cell activation, proliferation, protein expression, motility and morphology, secretion, and cellular communication[167–170].

The ability to rapidly fabricate microfluidic devices in PDMS by soft lithography greatly stimulated the development of microfluidic designs[171]. Besides being inexpensive, PDMS is biocompatible and permeable to gases, two properties that are a necessary for replication of artificial cellular microenvironments, *in vitro*[172,173]. The flexibility of PDMS allows easy integration of membrane valves and pumps on more complex microfluidic designs to create an intricate network of microchannels wherein protocols can be realized in full automation with programming software[174]. Microfluidic chip designs can be broadly classified in three

categories: microfluidics with passive traps, valve-based microfluidics, and droplet microfluidics. The trap based and well based microfluidic platforms are often limited by limited by their ability to replicate the dynamically variable immune cell microenvironment in which immune cells work. Also, for more efficient single-cell level analysis of immune cells it is essential that cells are isolated, stimulated and analyzed in a noise-free environment to negate the effects of paracrine communication from neighboring cells which are not easily obtained in these platforms. Valve-based platforms provides an optimal platform for cell isolation yet, it is severely limited in terms of throughput. All the above-mentioned limitation are catered to by droplet-based microfluidics, thus making it a robust tool for studying single cell. This thesis focuses on droplet based microfluidic system to further study the interaction within immune cells.

5.1 Droplet-Based Microfluidics

The idea to perform biological analysis in water-in-oil droplets was first published in the 1950s by Nossal and Lederberg[175]. Since then droplet microfluidics has continued fueled growing body of research leading to multiple applications in fields of biology and chemistry[176–178]. Droplet microfluidics has been widely implemented for high-throughput screening of biological and chemical reactions, single-cell analysis, genomics, and transcriptomics[179–183]. It also finds applications in molecular detection, imaging, drug delivery, antibody screening, toxicity screening, and diagnostics[184–190]. On a microfluidic chip, using two immiscible liquids, droplets, in one liquid phase, are generated in another liquid phase by breaking off either at a T-junction or flow-focusing junction[191,192]. In such a setup, passive generation of droplets relies on drag forces and viscous dissipation[193]. Variations in channel geometries help to pair, trap, merge, mix, release, and split droplets[194]. Pneumatic membrane valves, electrical forces, optical manipulations, and acoustic waves are other alternatives for active production of droplets on microfluidic chips[195–198].

Droplet-based microfluidic platforms provide scientists with the ability to investigate immune cell behavior in complete isolation by creating a noise-free and controlled cellular microenvironment[199]. Specifically, it allows to map immune cell subsets, quantify secretion of signaling molecules from single cells, and investigate cellular communication. In 2015, Sarkar et al. demonstrated an array-based droplet device that allowed monitoring of nanoliter-sized droplets for T-cell activation longitudinally right from the onset of

activation[200]. Their results suggested that the activation of single T-cells is faster when cells encounter dendritic cells in comparison to other activation methods. Furthermore, they developed a method to probe into the potentially heterogeneous cytolytic behavior of human NK cells[201]. They demonstrated a hundred percent killing efficiency of NK cells, which is in contrast to earlier findings by various groups who performed such studies, either, in bulk or at single cell resolution[202,203].

In order to quantify secreted molecules in droplets, cells are often paired with functionalized beads or other sensing molecules to capture target analytes during incubation, prior to analysis[204]. The droplet interface ensures that encapsulated cells are shielded from external factors that might influence their secretory behavior. Concurrently, this interface in combination with the small droplet volume, confines secreted molecules within the droplet resulting in increased sensitivity. Qiu et al. employed aptamer-based DNA sensors to quantify IFN γ secretion by encapsulating single T-cells in droplets followed by flow-cytometric and microscopic analysis (Figure 5A)[205]. This study demonstrated the versatility of droplet microfluidics to be integrated with multiple detection methodologies. In another recent study, Eyer et al. used Drop-Map technology for phenotyping IgG secreting plasma cells at single-cell level (Figure 5B)[206]. In this study, they paired antibody secreting cells with multiple paramagnetic functionalized nanoparticles that captures target antibodies in picolitre sized droplets. For the purpose of analysis, the generated droplets were immobilized in a glass observation chamber to measure fluorescence intensity of each droplet and quantify secreted antibodies for mapping different plasma cell phenotypes. With this technology it was possible to monitor and quantify antibody secretion by encapsulated cells in droplets, real-time.

Besides aqueous based droplets, hydrogels like agarose can also be used to create droplets in oil phase, which allows washing steps and permits staining with antibodies in droplets by slow diffusion. This conceptual advantage of using hydrogel based droplets was exploited in the Huck laboratory, where agarose droplets were used for encapsulation of Jurkat T-cells to capture multiple cytokines on functionalized beads to demonstrate cellular heterogeneity and map cellular subsets (Figure 6)[207]. Generally, for cytometry, droplets need to be broken to retrieve cells and beads. On the contrary, cells and beads encapsulated in hydrogels can be analyzed directly with flow cytometry, preventing the loss of cells, and saving significant amount of time.

Recently, researchers have also implemented protocols for single-cell sequencing in droplet microfluidics[208]. In 2015, Macosko et al. developed Drop-seq technology where the transcriptomics of thousands of retinal cells were analyzed in droplets using barcoded microparticles[209]. Later, the Abate lab also demonstrated the genomic sequencing of more than fifty thousand single cells in agarose microgels[210]. Single-cell sequencing allows researchers to identify differences in cellular behavior and understand the functionalities of individual cells that assists in decoding immune cell heterogeneity[211]. Genomic amplification for sequencing can be performed in droplet microfluidics with high accuracy and specificity in a massively parallel fashion[208]. The work of Shahi et al., demonstrated the efficiency of droplet microfluidics to profile protein secretion by single immune cells using a high-throughput droplet-microfluidic barcoding technique, Abseq[212]. This microfluidic device was integrated with functions to amplify DNA in nanoliter sized droplets to allow for more than tens of thousands of cells to be analyzed in parallel.

Together, all these studies highlighted the role of droplet microfluidics in single-cell analysis of immune cells. Droplet-based microfluidics is a highly versatile and flexible technology and is widely applicable in multiple realms of immunology. The ability to carry out high-throughput analysis of hundreds to thousands of individual immune cells and paired immune cells in parallel makes droplet microfluidics a highly reliable and popular single-cell analysis tool.

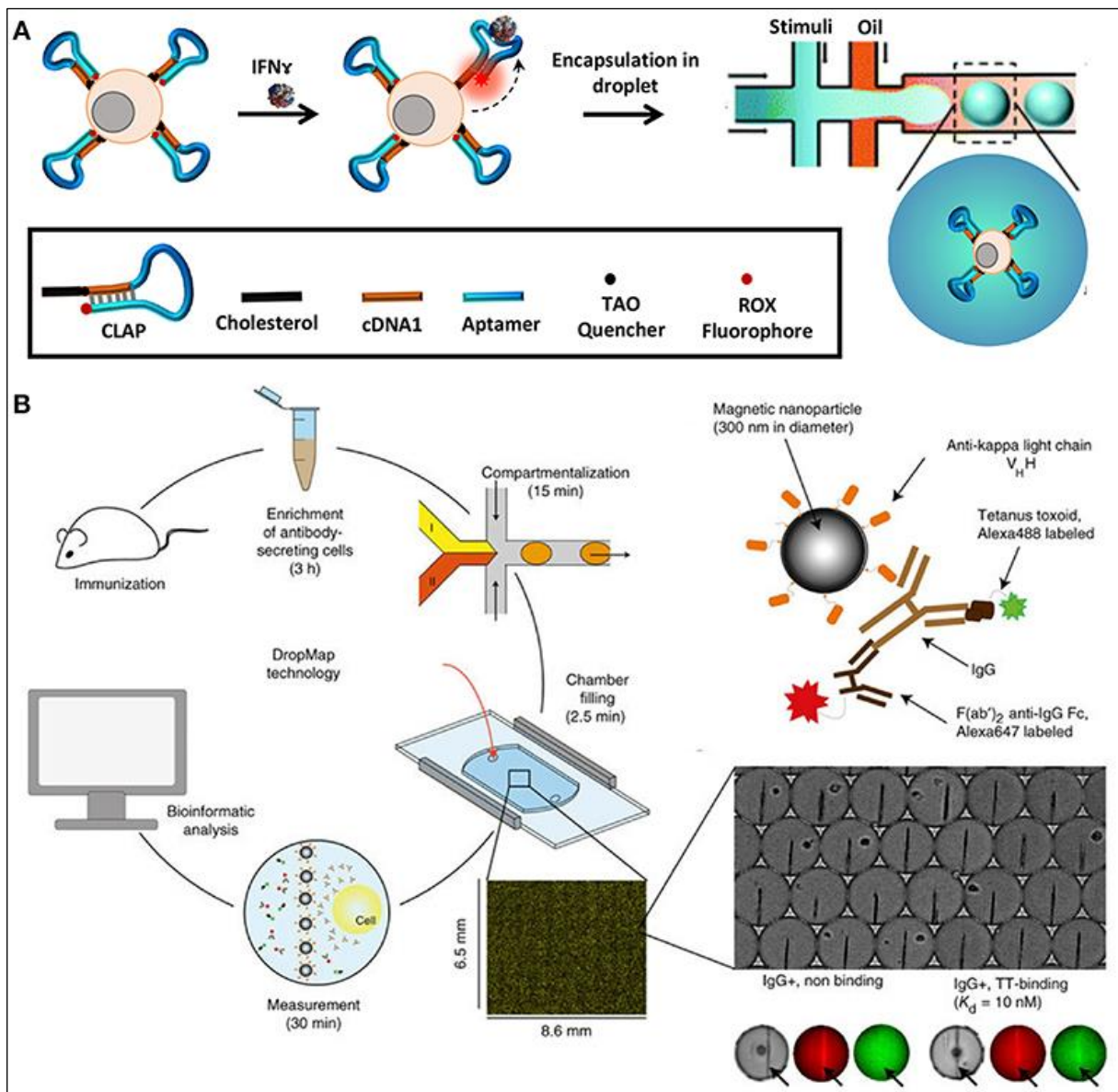


Figure 5. Droplet microfluidics is a very versatile tool that allows single-cell analysis of immune cells in a noise-free environment. The cells are often paired with functionalized beads or sensors such as aptamer sensors for quantification of secreted molecules and proteins. Droplet microfluidics is combined with flow cytometry, mass cytometry, and automated microscopy for downstream analysis. **A.** Adapted from Qiu et al.[205]. **B.** Adapted from Eyer et al.[206]. Reproduced with permission from Springer Nature.

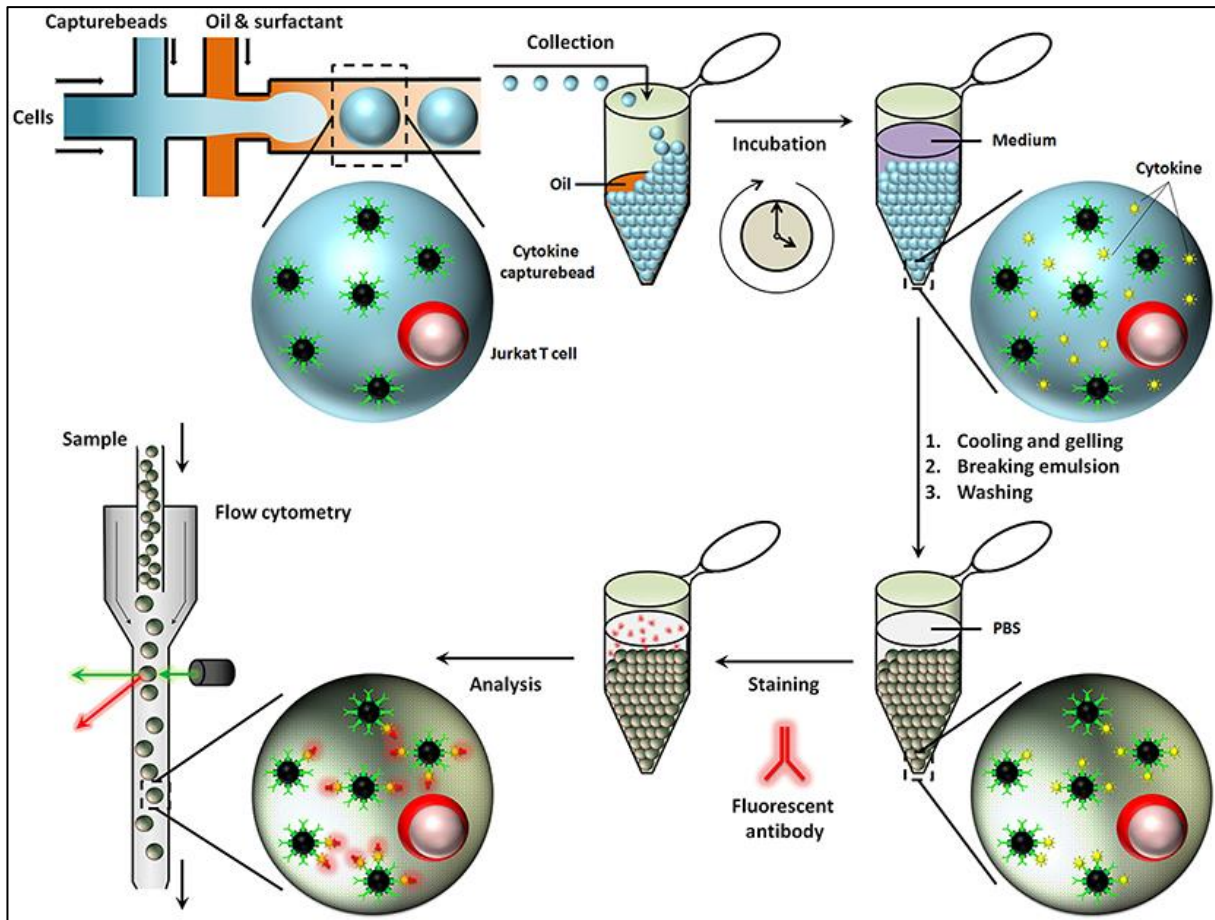


Figure 6. Hydrogel agarose gel droplets used in the Huck laboratory for measurement of cytokine secretion. The advantage of hydrogel droplets is that it allows washing steps for immunoassays. Also, cells encapsulated in hydrogel droplets can directly be analyzed by cytometry. Figure adapted from Chokkalingam et al.[207].

5. Scope of the Thesis

A well-coordinated interaction between immune components is crucial for successful immunotherapy, however, the underlying cellular heterogeneity within both the immune cells and tumorous cells adds complexity to this interplay. Although cellular heterogeneity in the immune system is widely appreciated, many aspects of it remain understudied. Use of conventional population-based technologies, cannot dissect this complex variation since it can only estimate the average distribution of responses. For long, flow cytometry and microscopy-based techniques have been the gold standard for the analysis of cellular behavior. These tools can measure with single cell resolution, however, lack single cell manipulation and often involve activation of cells in bulk-assays, which ultimately leads to paracrine and juxtacrine signaling among cells. Recent breakthroughs in single-technologies such as mass cytometry, single-cell RNA sequencing (scRNA-seq), and a combination of different microfluidics and micro systems-based studies, integrated with flow cytometry and microscopy, have allowed new ventures to study, identify, and correlate the phenotypical characteristic with functional diversity. In this thesis I aim to achieve a balanced integration of single cell technology to investigate functional heterogeneity and cellular interactions in immune system to channel new avenues for immunotherapy.

Part 1

The aim of this part is to develop single cell-based platforms that facilitates monitoring of cellular interaction and functional outputs. Droplet based microfluidics provides a robust tool for isolating and analyzing cells at the single-cell level by eliminating or controlling the influence of external factors on the cellular microenvironment. In the following chapters, I addressed the two major challenges namely: efficient cellular encapsulation, and high-throughput real time monitoring of the cells in droplets, thus enhancing the performance of in-droplet immunoassays.

In **Chapter 2**, I utilized a simple yet innovative “Tip-loading” technique to overcome the loss of scarce immune cells during encapsulation. The higher encapsulation efficiency is ensured by circumventing the chances of cell sedimentation in the tube or cell clumping due to longer tube length.

In **Chapter 3**, I integrated our droplet-based platform with real time microscopy and automated analysis scripts to monitor the dynamics of immune cell mediated cytotoxicity in droplets. This adaptation facilitates efficient cell pairing and high throughput monitoring of droplets in real time.

Part 2

In Part 2, I dove into the application of the previously developed platform to study intriguing biological processes. In the following sections, I studied functional heterogeneity in immune cells (NK cells and pDCs) and the consequences of their interaction at single cell level using the platform.

In **Chapter 4**, I investigated the functional heterogeneity in NK cell population by monitoring the dynamics of their interaction with different target cells. I also studied the cytotoxic and secretory functions of individual NK cells separately and together with cancer cells to understand how different functions are performed by a single NK cell. By identifying rare serial killers and assessing stem cell differentiated NK cells (for adoptive NK cell therapy), I demonstrated how studying these interactions at single cell level provide novel and relevant insights.

In **Chapter 5**, I probed the heterogeneity within the pDCs population and understand how the IFN-I secretion mechanism is regulated by its microenvironment.

In **Chapter 6**, I studied how bidirectional talk in between immune cells regulate each other's function. I facilitated interaction between single pDCs and single NK cells in droplets and monitor their functional output in terms of cytotoxicity and secretion of interferons using microscopy or FACS.

In **Chapter 7**, I summarized the findings of this thesis and provide an outlook for the future research. I also provided the information on how the insights from single cell studies in immune system be used to create avenues for immunotherapy.

6. References

- [1] R. Satija, A.K. Shalek, Heterogeneity in immune responses: From populations to single cells, *Trends Immunol.* 35 (2014) 219–229. <https://doi.org/10.1016/j.it.2014.03.004>.
- [2] S.M. Kaech, E.J. Wherry, Heterogeneity and Cell-Fate Decisions in Effector and Memory CD8+ T Cell Differentiation during Viral Infection, *Immunity.* 27 (2007) 393–405. <https://doi.org/10.1016/j.immuni.2007.08.007>.
- [3] A. O’Garra, Cytokines induce the development of functionally heterogeneous T helper cell subsets, *Immunity.* (1998). [https://doi.org/10.1016/S1074-7613\(00\)80533-6](https://doi.org/10.1016/S1074-7613(00)80533-6).
- [4] N.M. Toriello, E.S. Douglas, N. Thaitrong, S.C. Hsiao, M.B. Francis, C.R. Bertozzi, R.A. Mathies, Integrated microfluidic bioprocessor for single-cell gene expression analysis., *Proc. Natl. Acad. Sci. U. S. A.* 105 (2008) 20173–8. <https://doi.org/10.1073/pnas.0806355106>.
- [5] D. Wang, S. Bodovitz, Single cell analysis: the new frontier in “omics”., *Trends Biotechnol.* 28 (2010) 281–90. <https://doi.org/10.1016/j.tibtech.2010.03.002>.
- [6] E.W. Newell, N. Sigal, N. Nair, B.A. Kidd, H.B. Greenberg, M.M. Davis, Combinatorial tetramer staining and mass cytometry analysis facilitate T-cell epitope mapping and characterization, *Nat. Biotechnol.* 31 (2013) 623–629. <https://doi.org/10.1038/nbt.2593>.
- [7] H.G. Polikowsky, C.E. Wogoland, K.E. Diggins, K. Huse, J.M. Irish, Cutting Edge: Redox Signaling Hypersensitivity Distinguishes Human Germinal Center B Cells, *J. Immunol.* 195 (2015) 1364–1367. <https://doi.org/10.4049/jimmunol.1500904>.
- [8] T. Liu, Y. Yamaguchi, Y. Shirasaki, K. Shikada, M. Yamagishi, K. Hoshino, T. Kaisho, K. Takemoto, T. Suzuki, E. Kuranaga, O. Ohara, M. Miura, Single-cell imaging of caspase-1 dynamics reveals an all-or-none inflammasome signaling response, *Cell Rep.* 8 (2014) 974–982. <https://doi.org/10.1016/j.celrep.2014.07.012>.
- [9] A.K. Shalek, R. Satija, J. Shuga, J.J. Trombetta, D. Gennert, D. Lu, P. Chen, R.S. Gertner, J.T. Gaubblomme, N. Yosef, S. Schwartz, B. Fowler, S. Weaver, J. Wang, X. Wang, R. Ding, R. Raychowdhury, N. Friedman, N. Hacohen, H. Park, A.P. May, A. Regev, Single-cell RNA-seq reveals dynamic paracrine control of cellular variation, *Nature.* 510 (2014) 363–369. <https://doi.org/10.1038/nature13437>.
- [10] M. Junkin, S. Tay, Microfluidic single-cell analysis for systems immunology, *Lab Chip.* 14 (2014) 1246–60. <https://doi.org/10.1039/c3lc51182k>.
- [11] I. Zaretsky, M. Polonsky, E. Shifrut, S. Reich-Zeliger, Y. Antebi, G. Aidelberg, N. Waysbort, N. Friedman, Monitoring the dynamics of primary T cell activation and differentiation using long term live cell imaging in microwell arrays, *Lab Chip.* 12 (2012) 5007–5015. <https://doi.org/10.1039/c2lc40808b>.
- [12] J. Wang, D. Tham, W. Wei, Y.S. Shin, C. Ma, H. Ahmad, Q. Shi, J. Yu, R.D. Levine, J.R. Heath, Quantitating cell-cell interaction functions with applications to glioblastoma multiforme cancer cells, *Nano Lett.* 12 (2012) 6101–6106. <https://doi.org/10.1021/nl302748q>.
- [13] S.C. De Rosa, L.A. Herzenberg, L.A. Herzenberg, M. Roederer, 11-color, 13-parameter flow cytometry: Identification of human naive T cells by phenotype, function, and T-cell receptor diversity, *Nat. Med.* 7 (2001) 245–248. <https://doi.org/10.1038/84701>.
- [14] G. Roncador, P.J. Brown, L. Maestre, S. Hue, J.L. Martínez-Torrecuadrada, K.-L. Ling, S. Pratap, C. Toms, B.C. Fox, V. Cerundolo, F. Powrie, A.H. Banham, Analysis of FOXP3 protein expression in human CD4+CD25+ regulatory T cells at the single-cell level, *Eur. J. Immunol.* 35 (2005) 1681–1691. <https://doi.org/10.1002/eji.200526189>.
- [15] S.Z. Josefowicz, A. Rudensky, Control of Regulatory T Cell Lineage Commitment and Maintenance, *Immunity.* 30 (2009) 616–625. <https://doi.org/10.1016/j.immuni.2009.04.009>.
- [16] E. Schmitt, M. Klein, T. Bopp, Th9 cells, new players in adaptive immunity, *Trends Immunol.* 35 (2014) 61–68. <https://doi.org/10.1016/j.it.2013.10.004>.
- [17] S. Eyerich, K. Eyerich, D. Pennino, T. Carbone, F. Nasorri, S. Pallotta, F. Cianfarani, T. Odorasio, C. Traidl-Hoffmann, H. Behrendt, S.R. Durham, C.B. Schmidt-Weber, A. Cavani, Th22 cells represent a distinct human T cell subset involved in epidermal immunity and remodeling, *J. Clin. Invest.* 119 (2009) 3573–3585. <https://doi.org/10.1172/JCI40202>.
- [18] J.T. Gaubblomme, N. Yosef, Y. Lee, R.S. Gertner, L. V. Yang, C. Wu, P.P. Pandolfi, T. Mak, R. Satija, A.K. Shalek, V.K. Kuchroo, H. Park, A. Regev, Single-Cell Genomics Unveils Critical Regulators of Th17 Cell Pathogenicity, *Cell.* 163 (2015) 1400–1412.

- <https://doi.org/10.1016/j.cell.2015.11.009>.
- [19] A. Yağın, Y.J. Yamanaka, J.C. Love, Analytical technologies for integrated single-cell analysis of human immune responses., *Methods Mol. Biol.* 853 (2012) 211–35. https://doi.org/10.1007/978-1-61779-567-1_16.
- [20] M.M. Davis, C.M. Tato, D. Furman, Systems immunology: Just getting started, *Nat. Immunol.* 18 (2017) 725–732. <https://doi.org/10.1038/ni.3768>.
- [21] R.J. Kimmerling, G. Lee Szeto, J.W. Li, A.S. Genshaft, S.W. Kazer, K.R. Payer, J. De Riba Borrajo, P.C. Blainey, D.J. Irvine, A.K. Shalek, S.R. Manalis, A microfluidic platform enabling single-cell RNA-seq of multigenerational lineages, *Nat. Commun.* 7 (2016). <https://doi.org/10.1038/ncomms10220>.
- [22] E. Papalexi, R. Satija, Single-cell RNA sequencing to explore immune cell heterogeneity, *Nat. Rev. Immunol.* 18 (2018) 35–45. <https://doi.org/10.1038/nri.2017.76>.
- [23] D.A. Jaitin, E. Kenigsberg, H. Keren-Shaul, N. Elefant, F. Paul, I. Zaretsky, A. Mildner, N. Cohen, S. Jung, A. Tanay, I. Amit, Massively parallel single-cell RNA-seq for marker-free decomposition of tissues into cell types, *Science* (80-.). 343 (2014) 776–779. <https://doi.org/10.1126/science.1247651>.
- [24] W.K. Decker, A. Safdar, Bioimmunoadjuvants for the treatment of neoplastic and infectious disease: Coley’s legacy revisited, *Cytokine Growth Factor Rev.* (2009). <https://doi.org/10.1016/j.cytogfr.2009.07.004>.
- [25] W.K. Decker, R.F. da Silva, M.H. Sanabria, L.S. Angelo, F. Guimarães, B.M. Burt, F. Kheradmand, S. Paust, Cancer immunotherapy: Historical perspective of a clinical revolution and emerging preclinical animal models, *Front. Immunol.* (2017). <https://doi.org/10.3389/fimmu.2017.00829>.
- [26] L.L. Liu, V. Béziat, V.Y.S. Oei, A. Pfefferle, M. Schaffer, S. Lehmann, E. Hellström-Lindberg, S. Söderhäll, M. Heyman, D. Grandér, K.J. Malmberg, Ex vivo expanded adaptive NK cells effectively kill primary acute lymphoblastic leukemia cells, *Cancer Immunol. Res.* (2017). <https://doi.org/10.1158/2326-6066.CIR-16-0296>.
- [27] S.K. Grossenbacher, R.J. Canter, W.J. Murphy, Natural killer cell immunotherapy to target stem-like tumor cells, *J. Immunother. Cancer.* (2016). <https://doi.org/10.1186/s40425-016-0124-2>.
- [28] S. Oh, J.H. Lee, K. Kwack, S.W. Choi, Natural killer cell therapy: A new treatment paradigm for solid tumors, *Cancers (Basel)*. (2019). <https://doi.org/10.3390/cancers11101534>.
- [29] J. Spanholtz, M. Tordoir, D. Eissens, F. Preijers, A. Van Meer Der, I. Joosten, N. Schaap, T.M. De Witte, H. Dolstra, High log-scale expansion of functional human natural killer cells from umbilical cord blood CD34-positive cells for adoptive cancer immunotherapy, *PLoS One.* (2010). <https://doi.org/10.1371/journal.pone.0009221>.
- [30] A. Malhotra, A. Shanker, NK cells: Immune cross-talk and therapeutic implications, *Immunotherapy.* (2011). <https://doi.org/10.2217/imt.11.102>.
- [31] C.A. Biron, K.B. Nguyen, G.C. Pien, L.P. Cousens, T.P. Salazar-Mather, Natural killer cells in antiviral defense: Function and regulation by innate cytokines, *Annu. Rev. Immunol.* (1999). <https://doi.org/10.1146/annurev.immunol.17.1.189>.
- [32] J. Tel, H.J.G.A. Erik, T. Baba, G. Schreibelt, B.M. Schulte, D. Benitez-Ribas, O.C. Boerman, S. Croockewit, J.G.O. Wim, M. Van Rossum, G. Winkels, P.G. Coulie, J.A.P. Cornelis, C.G. Figdor, I.J.M. De Vries, Natural human plasmacytoid dendritic cells induce antigen-specific T-cell responses in melanoma patients, *Cancer Res.* (2013). <https://doi.org/10.1158/0008-5472.CAN-12-2583>.
- [33] K.N. Reitano, S. Kottitil, C.M. Gille, X. Zhang, M. Yan, M.A. O’Shea, G. Roby, C.W. Hallahan, J. Yang, R.A. Lempicki, J. Arthos, A.S. Fauci, Defective plasmacytoid dendritic cell-NK cell cross-talk in HIV infection, *AIDS Res. Hum. Retroviruses.* (2009). <https://doi.org/10.1089/aid.2008.0311>.
- [34] R. Thomas, X. Yang, NK-DC Crosstalk in Immunity to Microbial Infection, *J. Immunol. Res.* (2016). <https://doi.org/10.1155/2016/6374379>.
- [35] R. Kiessling, E. Klein, H. Wigzell, „Natural” killer cells in the mouse. I. Cytotoxic cells with specificity for mouse Moloney leukemia cells. Specificity and distribution according to genotype, *Eur. J. Immunol.* (1975). <https://doi.org/10.1002/eji.1830050208>.
- [36] A. Moretta, C. Bottino, M.C. Mingari, R. Biassoni, L. Moretta, What is a natural killer cell?, *Nat. Immunol.* (2002). <https://doi.org/10.1038/ni0102-6>.
- [37] E. Vivier, E. Tomasello, M. Baratin, T. Walzer, S. Ugolini, Functions of natural killer cells, *Nat. Immunol.* 9 (2008) 503–510. <https://doi.org/10.1038/ni1582>.
- [38] M.A. Caligiuri, Human natural killer cells, *Blood.* (2008). <https://doi.org/10.1182/blood-2007-09-077438>.
- [39] F. Cichocki, B. Grzywacz, J.S. Miller, Human NK cell development: One road or many?, *Front. Immunol.* (2019).

- <https://doi.org/10.3389/fimmu.2019.02078>.
- [40] B. Grzywacz, J.S. Miller, M.R. Verneris, Developmental stages and pathways of NK cell maturation, in: *Nat. Kill. Cells*, 2010. <https://doi.org/10.1016/B978-0-12-370454-2.00001-6>.
- [41] Q. Chen, W. Ye, W. Jian Tan, K.S. Mei Yong, M. Liu, S. Qi Tan, E. Loh, K. Te Chang, T. Chye Tan, P.R. Preiser, J. Chen, Delineation of Natural Killer Cell Differentiation from Myeloid Progenitors in Human, *Sci. Rep.* (2015). <https://doi.org/10.1038/srep15118>.
- [42] C. Wu, B. Li, R. Lu, S.J. Koelle, Y. Yang, A. Jares, A.E. Krouse, M. Metzger, F. Liang, K. Loré, C.O. Wu, R.E. Donahue, I.S.Y. Chen, I. Weissman, C.E. Dunbar, Clonal tracking of rhesus macaque hematopoiesis highlights a distinct lineage origin for natural killer cells, *Cell Stem Cell.* (2014). <https://doi.org/10.1016/j.stem.2014.01.020>.
- [43] P. Dogra, C. Rancan, W. Ma, M. Toth, T. Senda, D.J. Carpenter, M. Kubota, R. Matsumoto, P. Thapa, P.A. Szabo, M.M. Li Poon, J. Li, J. Arakawa-Hoyt, Y. Shen, L. Fong, L.L. Lanier, D.L. Farber, Tissue Determinants of Human NK Cell Development, Function, and Residence, *Cell.* (2020). <https://doi.org/10.1016/j.cell.2020.01.022>.
- [44] L. Moretta, A. Moretta, Unravelling natural killer cell function: Triggering and inhibitory human NK receptors, *EMBO J.* (2004). <https://doi.org/10.1038/sj.emboj.7600019>.
- [45] E. Vivier, J.A. Nunès, F. Vély, Natural killer cell signaling pathways, *Science* (80-.). (2004). <https://doi.org/10.1126/science.1103478>.
- [46] M.T. Orr, L.L. Lanier, Natural Killer Cell Education and Tolerance, *Cell.* (2010). <https://doi.org/10.1016/j.cell.2010.08.031>.
- [47] W.M. Yokoyama, B.F.M. Plougastel, Immune functions encoded by the natural killer gene complex, *Nat. Rev. Immunol.* (2003). <https://doi.org/10.1038/nri1055>.
- [48] P. Parham, MHC class I molecules and KIRS in human history, health and survival, *Nat. Rev. Immunol.* (2005). <https://doi.org/10.1038/nri1570>.
- [49] D.H. Raulet, N. Guerra, Oncogenic stress sensed by the immune system: Role of natural killer cell receptors, *Nat. Rev. Immunol.* (2009). <https://doi.org/10.1038/nri2604>.
- [50] L. L, Up on the tightrope: natural killer cell activation and inhibition, *Nat. Immunol.* (2009).
- [51] Y.T. Bryceson, M.E. March, H.G. Ljunggren, E.O. Long, Synergy among receptors on resting NK cells for the activation of natural cytotoxicity and cytokine secretion, *Blood.* (2006). <https://doi.org/10.1182/blood-2005-04-1351>.
- [52] J.C. Sun, L.L. Lanier, NK cell development, homeostasis and function: Parallels with CD8 + T cells, *Nat. Rev. Immunol.* (2011). <https://doi.org/10.1038/nri3044>.
- [53] E. Vivier, D.H. Raulet, A. Moretta, M.A. Caligiuri, L. Zitvogel, L.L. Lanier, W.M. Yokoyama, S. Ugolini, Innate or adaptive immunity? The example of natural killer cells, *Science* (80-.). (2011). <https://doi.org/10.1126/science.1198687>.
- [54] J.C. Sun, J.N. Beilke, L.L. Lanier, Adaptive immune features of natural killer cells, *Nature.* (2009). <https://doi.org/10.1038/nature07665>.
- [55] S. Paust, C.A. Blish, R.K. Reeves, Redefining Memory: Building the Case for Adaptive NK Cells, *J. Virol.* (2017). <https://doi.org/10.1128/jvi.00169-17>.
- [56] P. Carrega, G. Ferlazzo, Natural killer cell distribution and trafficking in human tissues, *Front. Immunol.* (2012). <https://doi.org/10.3389/fimmu.2012.00347>.
- [57] J.S. Schleypen, N. Baur, R. Kammerer, P.J. Nelson, K. Rohrmann, E.F. Gröne, M. Hohenfellner, A. Haferkamp, H. Pohla, D.J. Schendel, C.S. Falk, E. Noessner, Cytotoxic markers and frequency predict functional capacity of natural killer cells infiltrating renal cell carcinoma, *Clin. Cancer Res.* (2006). <https://doi.org/10.1158/1078-0432.CCR-05-0857>.
- [58] N. Dalbeth, R. Gundle, R.J.O. Davies, Y.C.G. Lee, A.J. McMichael, M.F.C. Callan, CD56 bright NK Cells Are Enriched at Inflammatory Sites and Can Engage with Monocytes in a Reciprocal Program of Activation , *J. Immunol.* (2004). <https://doi.org/10.4049/jimmunol.173.10.6418>.
- [59] J. Faget, C. Biota, T. Bachelot, M. Gobert, C. Dezutter-Dambuyant, I. Treilleux, S. Goddard-Leon, J.Y. Blay, C. Caux, C. Menetrier-Caux, Abstract 1341: Early detection of tumor cells by innate immune cells leads to Treg recruitment through CCL22 production by tumor cells, in: 2010. <https://doi.org/10.1158/1538-7445.am10-1341>.
- [60] A.G. Freud, B.L. Mundy-Bosse, J. Yu, M.A. Caligiuri, The Broad Spectrum of Human Natural Killer Cell Diversity, *Immunity.* (2017). <https://doi.org/10.1016/j.immuni.2017.10.008>.
- [61] D.K. Sojka, B. Plougastel-Douglas, L. Yang, M.A. Pak-Wittel, M.N. Artyomov, Y. Ivanova, C. Zhong, J.M. Chase, P.B. Rothman, J. Yu, J.K. Riley, J. Zhu, Z. Tian, W.M. Yokoyama, Tissue-resident natural killer (NK) cells are cell lineages distinct from thymic and

- conventional splenic NK cells, *Elife*. (2014). <https://doi.org/10.7554/eLife.01659>.
- [62] A. Crinier, P. Milpied, B. Escalière, C. Piperoglou, J. Galluso, A. Balsamo, L. Spinelli, I. Cervera-Marzal, M. Ebbo, M. Girard-Madoux, S. Jaeger, E. Bollon, S. Hamed, J. Hardwigsen, S. Ugolini, F. Vély, E. Narni-Mancinelli, E. Vivier, High-Dimensional Single-Cell Analysis Identifies Organ-Specific Signatures and Conserved NK Cell Subsets in Humans and Mice, *Immunity*. (2018). <https://doi.org/10.1016/j.immuni.2018.09.009>.
- [63] A. Crinier, P.Y. Dumas, B. Escalière, C. Piperoglou, L. Gil, A. Villacreces, F. Vély, Z. Ivanovic, P. Milpied, É. Narni-Mancinelli, É. Vivier, Single-cell profiling reveals the trajectories of natural killer cell differentiation in bone marrow and a stress signature induced by acute myeloid leukemia, *Cell. Mol. Immunol.* (2021). <https://doi.org/10.1038/s41423-020-00574-8>.
- [64] A.K. Björklund, M. Forkel, S. Picelli, V. Konya, J. Theorell, D. Friberg, R. Sandberg, J. Mjösberg, The heterogeneity of human CD127+ innate lymphoid cells revealed by single-cell RNA sequencing, *Nat. Immunol.* (2016). <https://doi.org/10.1038/ni.3368>.
- [65] M.L. Robinette, A. Fuchs, V.S. Cortez, J.S. Lee, Y. Wang, S.K. Durum, S. Gilfillan, M. Colonna, Transcriptional programs define molecular characteristics of innate lymphoid cell classes and subsets, *Nat. Immunol.* (2015). <https://doi.org/10.1038/ni.3094>.
- [66] M.G. Constantinides, B.D. McDonald, P.A. Verhoef, A. Bendelac, A committed precursor to innate lymphoid cells, *Nature*. (2014). <https://doi.org/10.1038/nature13047>.
- [67] O. El Weizman, N.M. Adams, I.S. Schuster, C. Krishna, Y. Pritykin, C. Lau, M.A. Degli-Esposti, C.S. Leslie, J.C. Sun, T.E. O'Sullivan, ILC1 Confer Early Host Protection at Initial Sites of Viral Infection, *Cell*. (2017). <https://doi.org/10.1016/j.cell.2017.09.052>.
- [68] A.P. McFarland, A. Yalin, S.Y. Wang, V.S. Cortez, T. Landsberger, R. Sudan, V. Peng, H.L. Miller, B. Ricci, E. David, R. Faccio, I. Amit, M. Colonna, Multi-tissue single-cell analysis deconstructs the complex programs of mouse natural killer and type 1 innate lymphoid cells in tissues and circulation, *Immunity*. (2021). <https://doi.org/10.1016/j.immuni.2021.03.024>.
- [69] L. Moretta, Dissecting CD56dim human NK cells, *Blood*. (2010). <https://doi.org/10.1182/blood-2010-09-303057>.
- [70] B. Fu, Z. Tian, H. Wei, Subsets of human natural killer cells and their regulatory effects, *Immunology*. (2014). <https://doi.org/10.1111/imm.12224>.
- [71] V. Stary, G. Stary, NK Cell-Mediated Recall Responses: Memory-Like, Adaptive, or Antigen-Specific?, *Front. Cell. Infect. Microbiol.* (2020). <https://doi.org/10.3389/fcimb.2020.00208>.
- [72] L.L. Liu, A. Pfefferle, V.O. Yi Sheng, A.T. Björklund, V. Béziat, J.P. Goodridge, K.J. Malmberg, Harnessing adaptive natural killer cells in cancer immunotherapy, *Mol. Oncol.* (2015). <https://doi.org/10.1016/j.molonc.2015.10.001>.
- [73] J.G. O'Leary, M. Goodarzi, D.L. Drayton, U.H. von Andrian, T cell- and B cell-independent adaptive immunity mediated by natural killer cells, *Nat. Immunol.* (2006). <https://doi.org/10.1038/ni1332>.
- [74] R. Romee, S.E. Schneider, J.W. Leong, J.M. Chase, C.R. Keppel, R.P. Sullivan, M.A. Cooper, T.A. Fehniger, Cytokine activation induces human memory-like NK cells, *Blood*. (2012). <https://doi.org/10.1182/blood-2012-04-419283>.
- [75] H. Schlums, F. Cichocki, B. Tesi, J. Theorell, V. Beziat, T.D. Holmes, H. Han, S.C.C. Chiang, B. Foley, K. Mattsson, S. Larsson, M. Schaffer, K.J. Malmberg, H.G. Ljunggren, J.S. Miller, Y.T. Bryceson, Cytomegalovirus infection drives adaptive epigenetic diversification of NK cells with altered signaling and effector function, *Immunity*. (2015). <https://doi.org/10.1016/j.immuni.2015.02.008>.
- [76] M. Gumá, A. Angulo, C. Vilches, N. Gómez-Lozano, N. Malats, M. López-Botet, Imprint of human cytomegalovirus infection on the NK cell receptor repertoire, *Blood*. (2004). <https://doi.org/10.1182/blood-2004-05-2058>.
- [77] J. Lee, T. Zhang, I. Hwang, A. Kim, L. Nitschke, M.J. Kim, J.M. Scott, Y. Kamimura, L.L. Lanier, S. Kim, Epigenetic Modification and Antibody-Dependent Expansion of Memory-like NK Cells in Human Cytomegalovirus-Infected Individuals, *Immunity*. 42 (2015) 431–442. <https://doi.org/10.1016/J.IMMUNI.2015.02.013>.
- [78] L. Quatrini, M. Della Chiesa, S. Sivori, M.C. Mingari, D. Pende, L. Moretta, Human NK cells, their receptors and function, *Eur. J. Immunol.* (2021). <https://doi.org/10.1002/eji.202049028>.
- [79] M. Luetke-Eversloh, Q. Hammer, P. Durek, K. Nordström, G. Gasparoni, M. Pink, A. Hamann, J. Walter, H.D. Chang, J. Dong, C. Romagnani, Human Cytomegalovirus Drives Epigenetic Imprinting of the IFNG Locus in NKG2Chi Natural Killer Cells, *PLoS Pathog.* (2014). <https://doi.org/10.1371/journal.ppat.1004441>.
- [80] A. Merino, B. Zhang, P. Dougherty, X. Luo, J. Wang, B.R. Blazar, J.S. Miller, F. Cichocki, Chronic stimulation drives human NK cell dysfunction and epigenetic reprogramming, *J. Clin. Invest.* (2019). <https://doi.org/10.1172/JCI125916>.
- [81] Valiante NM, Uhrberg M, Shilling HG, Lienert-Weidenbach K, Arnett KL, D'Andrea A, Phillips JH, Lanier LL, Parham P, N.M. Valiante, M. Uhrberg, H.G. Shilling, K. Lienert-Weidenbach, K.L. Arnett, A. D'Andrea, J.H. Phillips, L.L. Lanier, P. Parham,

- Functionally and structurally distinct NK cell receptor repertoires in the peripheral blood of two human donors, *Immunity*. (1997).
- [82] A. Horowitz, D.M. Strauss-Albee, M. Leipold, J. Kubo, N. Nemat-Gorgani, O.C. Dogan, C.L. Dekker, S. Mackey, H. Maecker, G.E. Swan, M.M. Davis, P.J. Norman, L.A. Guethlein, M. Desai, P. Parham, C.A. Blish, Genetic and environmental determinants of human NK cell diversity revealed by mass cytometry, *Sci. Transl. Med.* (2013). <https://doi.org/10.1126/scitranslmed.3006702>.
- [83] J.K. Wiencke, R. Butler, G. Hsuang, M. Eliot, S. Kim, M.A. Sepulveda, D. Siegel, E.A. Houseman, K.T. Kelsey, The DNA methylation profile of activated human natural killer cells, *Epigenetics*. (2016). <https://doi.org/10.1080/15592294.2016.1163454>.
- [84] T.D. Holmes, R.V. Pandey, E.Y. Helm, H. Schlums, H. Han, T.M. Campbell, T.T. Drashansky, S. Chiang, C.Y. Wu, C. Tao, M. Shoukier, E. Tolosa, S. Von Hardenberg, M. Sun, C. Klemann, R.A. Marsh, C.M. Lau, Y. Lin, J.C. Sun, R. Månsson, F. Cichocki, D. Avram, Y.T. Bryceson, The transcription factor Bcl11b promotes both canonical and adaptive NK cell differentiation, *Sci. Immunol.* (2021). <https://doi.org/10.1126/SCIIMMUNOL.ABC9801>.
- [85] D. Wang, S. Malarkannan, Transcriptional regulation of natural killer cell development and functions, *Cancers (Basel)*. (2020). <https://doi.org/10.3390/cancers12061591>.
- [86] J. Bi, X. Wang, Molecular Regulation of NK Cell Maturation, *Front. Immunol.* (2020). <https://doi.org/10.3389/fimmu.2020.01945>.
- [87] C. Yang, J.R. Siebert, R. Burns, Z.J. Gerbec, B. Bonacci, A. Rymaszewski, M. Rau, M.J. Riese, S. Rao, K.S. Carlson, J.M. Routes, J.W. Verbsky, M.S. Thakar, S. Malarkannan, Heterogeneity of human bone marrow and blood natural killer cells defined by single-cell transcriptome, *Nat. Commun.* (2019). <https://doi.org/10.1038/s41467-019-11947-7>.
- [88] J. Zhao, S. Zhang, Y. Liu, X. He, M. Qu, G. Xu, H. Wang, M. Huang, J. Pan, Z. Liu, Z. Li, L. Liu, Z. Zhang, Single-cell RNA sequencing reveals the heterogeneity of liver-resident immune cells in human, *Cell Discov.* (2020). <https://doi.org/10.1038/s41421-020-0157-z>.
- [89] C. Yang, J.R. Siebert, R. Burns, Y. Zheng, A. Mei, B. Bonacci, D. Wang, R.A. Urrutia, M.J. Riese, S. Rao, K.S. Carlson, M.S. Thakar, S. Malarkannan, Single-cell transcriptome reveals the novel role of t-bet in suppressing the immature NK gene signature, *Elife*. (2020). <https://doi.org/10.7554/eLife.51339>.
- [90] S.M. Gordon, J. Chaix, L.J. Rupp, J. Wu, S. Madera, J.C. Sun, T. Lindsten, S.L. Reiner, The Transcription Factors T-bet and Eomes Control Key Checkpoints of Natural Killer Cell Maturation, *Immunity*. (2012). <https://doi.org/10.1016/j.immuni.2011.11.016>.
- [91] S. Lunemann, G. Martrus, H. Goebels, T. Kautz, A. Langeneckert, W. Salzberger, M. Koch, M.J. Bunders, B. Nashan, K.P.J.M. Van Gisbergen, M. Altfeld, Hobit expression by a subset of human liver-resident CD56bright Natural Killer, *Sci. Rep.* (2017). <https://doi.org/10.1038/s41598-017-06011-7>.
- [92] S. Kim, J. Poursine-Laurent, S.M. Truscott, L. Lybarger, Y.J. Song, L. Yang, A.R. French, J.B. Sunwoo, S. Lemieux, T.H. Hansen, W.M. Yokoyama, Licensing of natural killer cells by host major histocompatibility complex class I molecules, *Nature*. (2005). <https://doi.org/10.1038/nature03847>.
- [93] K.M. Lee, M.E. McNerney, S.E. Stepp, P.A. Mathew, J.D. Schatzle, M. Bennett, V. Kumar, 2B4 Acts As a Non-Major Histocompatibility Complex Binding Inhibitory Receptor on Mouse Natural Killer Cells, *J. Exp. Med.* (2004). <https://doi.org/10.1084/jem.20031989>.
- [94] Y. He, Z. Tian, NK cell education via nonclassical MHC and non-MHC ligands, *Cell. Mol. Immunol.* (2017). <https://doi.org/10.1038/cmi.2016.26>.
- [95] S. Cooley, F. Xiao, M. Pitt, M. Gleason, V. McCullar, T.L. Bergemann, K.L. McQueen, L.A. Guethlein, P. Parham, J.S. Miller, A subpopulation of human peripheral blood NK cells that lacks inhibitory receptors for self-MHC is developmentally immature, *Blood*. (2007). <https://doi.org/10.1182/blood-2006-07-036228>.
- [96] C. Pfeifer, A.J. Highton, S. Peine, J. Sauter, A.H. Schmidt, M.J. Bunders, M. Altfeld, C. Körner, Natural Killer Cell Education Is Associated With a Distinct Glycolytic Profile, *Front. Immunol.* (2018). <https://doi.org/10.3389/fimmu.2018.03020>.
- [97] N.C. Fernandez, E. Treiner, R.E. Vance, A.M. Jamieson, S. Lemieux, D.H. Raulet, A subset of natural killer cells achieves self-tolerance without expressing inhibitory receptors specific for self-MHC molecules, *Blood*. (2005). <https://doi.org/10.1182/blood-2004-08-3156>.
- [98] H. Wei, F. Li, H. Wei, Y. Gao, L. Xu, W. Yin, R. Sun, Z. Tian, Blocking the natural killer cell inhibitory receptor NKG2A increases activity of human natural killer cells and clears hepatitis B virus infection in mice, *Gastroenterology*. (2013). <https://doi.org/10.1053/j.gastro.2012.10.039>.
- [99] N. Tarek, J.B. Le Luque, M.M. Gallagher, J. Zheng, J.M. Venstrom, E. Chamberlain, S. Modak, G. Heller, B. Dupont, N.K. V. Cheung, K.C. Hsu, Unlicensed NK cells target neuroblastoma following anti-GD2 antibody treatment, *J. Clin. Invest.* (2012).

- <https://doi.org/10.1172/JCI62749>.
- [100] K. Juelke, M. Killig, A. Thiel, J. Dong, C. Romagnani, Education of hyporesponsive NK cells by cytokines, *Eur. J. Immunol.* (2009). <https://doi.org/10.1002/eji.200939307>.
- [101] A. Pfefferle, B. Jacobs, H. Netskar, E.H. Ask, S. Lorenz, T. Clancy, J.P. Goodridge, E. Sohlberg, K.J. Malmberg, Intra-lineage Plasticity and Functional Reprogramming Maintain Natural Killer Cell Repertoire Diversity, *Cell Rep.* (2019). <https://doi.org/10.1016/j.celrep.2019.10.058>.
- [102] A. Marçais, J. Cherfils-Vicini, C. Viant, S. Degouve, S. Viel, A. Fenis, J. Rabilloud, K. Mayol, A. Tavares, J. Bienvenu, Y.G. Gangloff, E. Gilson, E. Vivier, T. Walzer, The metabolic checkpoint kinase mTOR is essential for IL-15 signaling during the development and activation of NK cells, *Nat. Immunol.* (2014). <https://doi.org/10.1038/ni.2936>.
- [103] L.M. Gaynor, F. Colucci, Uterine natural killer cells: Functional distinctions and influence on pregnancy in humans and mice, *Front. Immunol.* (2017). <https://doi.org/10.3389/fimmu.2017.00467>.
- [104] J. Hanna, D. Goldman-Wohl, Y. Hamani, I. Avraham, C. Greenfield, S. Natanson-Yaron, D. Prus, L. Cohen-Daniel, T.I. Arnon, I. Manaster, R. Gazit, V. Yutkin, D. Benharroch, A. Porgador, E. Keshet, S. Yagel, O. Mandelboim, Decidual NK cells regulate key developmental processes at the human fetal-maternal interface, *Nat. Med.* (2006). <https://doi.org/10.1038/nm1452>.
- [105] D.M. Strauss-Albee, J. Fukuyama, E.C. Liang, Y. Yao, J.A. Jarrell, A.L. Drake, J. Kinuthia, R.R. Montgomery, G. John-Stewart, S. Holmes, C.A. Blish, Human NK cell repertoire diversity reflects immune experience and correlates with viral susceptibility, *Sci. Transl. Med.* (2015). <https://doi.org/10.1126/scitranslmed.aac5722>.
- [106] S. Platonova, J. Cherfils-Vicini, D. Damotte, L. Crozet, V. Vieillard, P. Validire, P. André, M.C. Dieu-Nosjean, M. Alifano, J.F. Régnerard, W.H. Fridman, C. Sautès-Fridman, I. Cremer, Profound coordinated alterations of intratumoral NK cell phenotype and function in lung carcinoma, *Cancer Res.* (2011). <https://doi.org/10.1158/0008-5472.CAN-10-4179>.
- [107] N.C. Horton, S.O. Mathew, P.A. Mathew, Novel Interaction between Proliferating Cell Nuclear Antigen and HLA I on the Surface of Tumor Cells Inhibits NK Cell Function through Nkp44, *PLoS One.* (2013). <https://doi.org/10.1371/journal.pone.0059552>.
- [108] J. Cong, X. Wang, X. Zheng, D. Wang, B. Fu, R. Sun, Z. Tian, H. Wei, Dysfunction of Natural Killer Cells by FBP1-Induced Inhibition of Glycolysis during Lung Cancer Progression, *Cell Metab.* (2018). <https://doi.org/10.1016/j.cmet.2018.06.021>.
- [109] F.P. Siegal, N. Kadowaki, M. Shodell, P.A. Fitzgerald-Bocarsly, K. Shah, S. Ho, S. Antonenko, Y.J. Liu, The nature of the principal Type 1 interferon-producing cells in human blood, *Science* (80-.). (1999). <https://doi.org/10.1126/science.284.5421.1835>.
- [110] M. Cella, F. Facchetti, A. Lanzavecchia, M. Colonna, Plasmacytoid dendritic cells activated by influenza virus and CD40L drive a potent TH1 polarization, *Nat. Immunol.* (2000). <https://doi.org/10.1038/79747>.
- [111] P. Sathe, D. Vremec, L. Wu, L. Corcoran, K. Shortman, Convergent differentiation: Myeloid and lymphoid pathways to murine plasmacytoid dendritic cells, in: *Blood*, 2013. <https://doi.org/10.1182/blood-2012-02-413336>.
- [112] B. Cisse, M.L. Caton, M. Lehner, T. Maeda, S. Scheu, R. Locksley, D. Holmberg, C. Zweier, N.S. den Hollander, S.G. Kant, W. Holter, A. Rauch, Y. Zhuang, B. Reizis, Transcription Factor E2-2 Is an Essential and Specific Regulator of Plasmacytoid Dendritic Cell Development, *Cell.* (2008). <https://doi.org/10.1016/j.cell.2008.09.016>.
- [113] S. Upadhaya, C.M. Sawai, E. Papalex, A. Rashidfarrokhi, G. Jang, P. Chattopadhyay, R. Satija, B. Reizis, Kinetics of adult hematopoietic stem cell differentiation in vivo, *J. Exp. Med.* (2018). <https://doi.org/10.1084/jem.20180136>.
- [114] G.C. Ippolito, J.D. Dekker, Y.H. Wang, B.K. Lee, A.L. Shaffer, J. Lin, J.K. Wall, B.S. Lee, L.M. Staudt, Y.J. Liu, V.R. Iyer, H.O. Tucker, Dendritic cell fate is determined by BCL11A, *Proc. Natl. Acad. Sci. U. S. A.* (2014). <https://doi.org/10.1073/pnas.1319228111>.
- [115] A. Dzionek, Y. Inagaki, K. Okawa, J. Nagafune, J. Röck, Y. Sohma, G. Winkels, M. Zysk, Y. Yamaguchi, J. Schmitz, Plasmacytoid dendritic cells: From specific surface markers to specific cellular functions, *Hum. Immunol.* (2002). [https://doi.org/10.1016/S0198-8859\(02\)00752-8](https://doi.org/10.1016/S0198-8859(02)00752-8).
- [116] Y. Zhan, K. V. Chow, P. Soo, Z. Xu, J.L. Brady, K.E. Lawlor, S.L. Masters, M. O'Keeffe, K. Shortman, J.G. Zhang, A.M. Lew, Plasmacytoid dendritic cells are short-lived: Reappraising the influence of migration, genetic factors and activation on estimation of lifespan, *Sci. Rep.* (2016). <https://doi.org/10.1038/srep25060>.
- [117] M. Cella, D. Jarrossay, F. Facchetti, O. Alebardi, H. Nakajima, A. Lanzavecchia, M. Colonna, Plasmacytoid monocytes migrate to inflamed lymph nodes and produce large amounts of type I interferon, *Nat. Med.* (1999). <https://doi.org/10.1038/11360>.
- [118] L. Guéry, S. Hugues, Tolerogenic and activatory plasmacytoid dendritic cells in autoimmunity, *Front. Immunol.* (2013). <https://doi.org/10.3389/fimmu.2013.00059>.
- [119] R. Leylek, J. Idoyaga, The versatile plasmacytoid dendritic cell: Function, heterogeneity, and plasticity, in: *Int. Rev. Cell Mol. Biol.*,

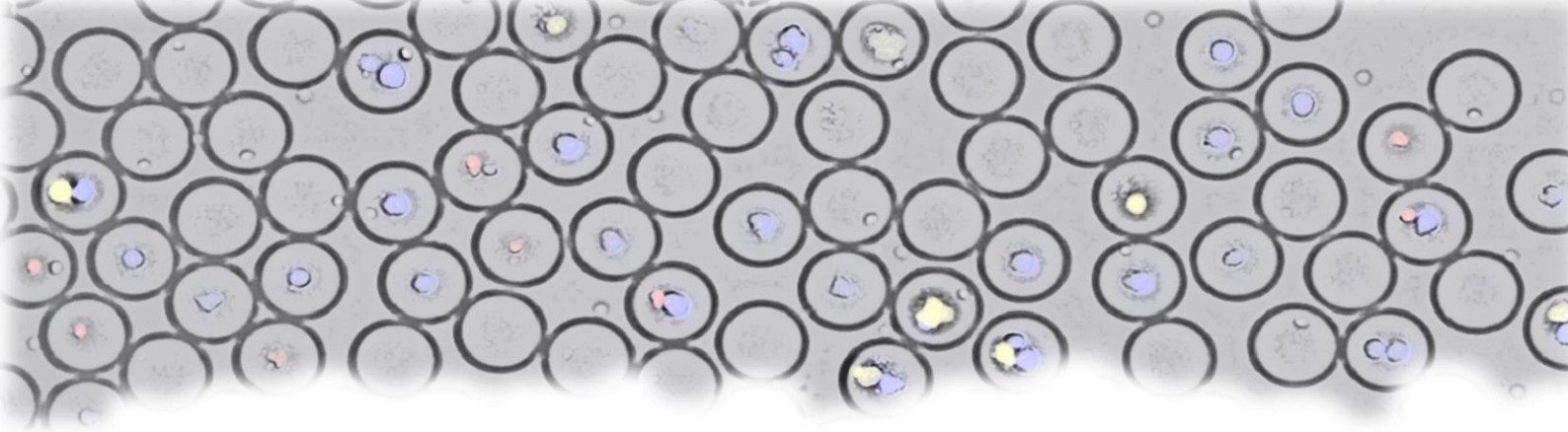
2019. <https://doi.org/10.1016/bs.ircmb.2019.10.002>.
- [120] A.C. Villani, R. Satija, G. Reynolds, S. Sarkizova, K. Shekhar, J. Fletcher, M. Griesbeck, A. Butler, S. Zheng, S. Lazo, L. Jardine, D. Dixon, E. Stephenson, E. Nilsson, I. Grundberg, D. McDonald, A. Filby, W. Li, P.L. De Jager, O. Rozenblatt-Rosen, A.A. Lane, M. Haniffa, A. Regev, N. Hacohen, Single-cell RNA-seq reveals new types of human blood dendritic cells, monocytes, and progenitors, *Science* (80-.). (2017). <https://doi.org/10.1126/science.aah4573>.
- [121] C. Guiducci, G. Ott, J.H. Chan, E. Damon, C. Calacsan, T. Matray, K.D. Lee, R.L. Coffman, F.J. Barrat, Properties regulating the nature of the plasmacytoid dendritic cell response to Toll-like receptor 9 activation, *J. Exp. Med.* (2006). <https://doi.org/10.1084/jem.20060401>.
- [122] N. Kadowaki, S. Antonenko, J.Y.N. Lau, Y.J. Liu, Natural interferon α/β -producing cells link innate and adaptive immunity, *J. Exp. Med.* (2000). <https://doi.org/10.1084/jem.192.2.219>.
- [123] S.G. Alculumbre, V. Saint-André, J. Di Domizio, P. Vargas, P. Sirven, P. Bost, M. Maurin, P. Maiuri, M. Wery, M.S. Roman, L. Savey, M. Touzot, B. Terrier, D. Saadoun, C. Conrad, M. Gilliet, A. Morillon, V. Soumelis, Diversification of human plasmacytoid predendritic cells in response to a single stimulus article, *Nat. Immunol.* (2018). <https://doi.org/10.1038/s41590-017-0012-z>.
- [124] A. Schlitzer, J. Loschko, K. Mair, R. Vogemann, L. Henkel, H. Einwächter, M. Schiemann, J.H. Niess, W. Reindl, A. Krug, Identification of CCR9- murine plasmacytoid DC precursors with plasticity to differentiate into conventional DCs, *Blood.* (2011). <https://doi.org/10.1182/blood-2010-12-326678>.
- [125] M. Niederquell, S. Kurig, J.A.A. Fischer, S. Tomiuk, M. Swiecki, M. Colonna, I.C.D. Johnston, A. Dzionek, Sca-1 expression defines developmental stages of mouse pDCs that show functional heterogeneity in the endosomal but not lysosomal TLR9 response, *Eur. J. Immunol.* (2013). <https://doi.org/10.1002/eji.201343498>.
- [126] Y. Kamogawa-Schifter, J. Ohkawa, S. Namiki, N. Arai, K.I. Arai, Y.J. Liu, Ly49Q defines 2 pDC subsets in mice, *Blood.* (2005). <https://doi.org/10.1182/blood-2004-09-3388>.
- [127] T. Matsui, J.E. Connolly, M. Michnevitz, D. Chaussabel, C.-I. Yu, C. Glaser, S. Tindle, M. Pypaert, H. Freitas, B. Piqueras, J. Banchereau, A.K. Palucka, CD2 Distinguishes Two Subsets of Human Plasmacytoid Dendritic Cells with Distinct Phenotype and Functions, *J. Immunol.* (2009). <https://doi.org/10.4049/jimmunol.0802008>.
- [128] T.R. Wilhelm, A. Taddeo, O. Winter, A.R. Schulz, J.N. Mälzer, C. Domingo, R. Biesen, T. Alexander, A. Thiel, A. Radbruch, F. Hiepe, V. Gerl, Siglec-1-positive plasmacytoid dendritic cells (pDCs) in human peripheral blood: A semi-mature and myeloid-like subset imbalanced during protective and autoimmune responses, *Clin. Immunol.* (2016). <https://doi.org/10.1016/j.clim.2015.12.001>.
- [129] H. Zhang, J.D. Gregorio, T. Iwahori, X. Zhang, O. Choi, L.L. Tolentino, T. Prestwood, Y. Carmi, E.G. Engleman, A distinct subset of plasmacytoid dendritic cells induces activation and differentiation of B and T lymphocytes, *Proc. Natl. Acad. Sci. U. S. A.* (2017). <https://doi.org/10.1073/pnas.1610630114>.
- [130] D. Roothans, E. Smits, E. Lion, J. Tel, S. Anguille, CD56 marks human dendritic cell subsets with cytotoxic potential, *Oncoimmunology.* (2013). <https://doi.org/10.4161/onci.23037>.
- [131] J. Tel, E.L. Smits, S. Anguille, R.N. Joshi, C.G. Figdor, I.J.M. De Vries, Human plasmacytoid dendritic cells are equipped with antigen-presenting and tumoricidal capacities, *Blood.* (2012). <https://doi.org/10.1182/blood-2012-06-435941>.
- [132] A.D. Edwards, S.S. Diebold, E.M.C. Slack, H. Tomizawa, H. Hemmi, T. Kaisho, S. Akira, C. Reis e Sousa, Toll-like receptor expression in murine DC subsets: Lack of TLR7 expression of CD8 α + DC correlates with unresponsiveness to imidazoquinolines, *Eur. J. Immunol.* (2003). <https://doi.org/10.1002/eji.200323797>.
- [133] M. Gilliet, W. Cao, Y.J. Liu, Plasmacytoid dendritic cells: Sensing nucleic acids in viral infection and autoimmune diseases, *Nat. Rev. Immunol.* (2008). <https://doi.org/10.1038/nri2358>.
- [134] D. Jarrossay, G. Napolitani, M. Colonna, F. Sallusto, A. Lanzavecchia, Specialization and complementarity in microbial molecule recognition by human myeloid and plasmacytoid dendritic cells, *Eur. J. Immunol.* (2001). [https://doi.org/10.1002/1521-4141\(200111\)31:11<3388::AID-IMMU3388>3.0.CO;2-Q](https://doi.org/10.1002/1521-4141(200111)31:11<3388::AID-IMMU3388>3.0.CO;2-Q).
- [135] C. Bode, M. Fox, P. Tewary, A. Steinhagen, R.K. Ellerkmann, D. Klinman, G. Baumgarten, V. Hornung, F. Steinhagen, Human plasmacytoid dendritic cells elicit a Type I Interferon response by sensing DNA via the cGAS-STING signaling pathway, *Eur. J. Immunol.* (2016). <https://doi.org/10.1002/eji.201546113>.
- [136] D. Bruni, M. Chazal, L. Sinigaglia, L. Chauveau, O. Schwartz, P. Desprès, N. Jouvenet, Viral entry route determines how human plasmacytoid dendritic cells produce type I interferons, *Sci. Signal.* (2015). <https://doi.org/10.1126/scisignal.aaa1552>.
- [137] B. Reizis, Plasmacytoid Dendritic Cells: Development, Regulation, and Function, *Immunity.* (2019).

- <https://doi.org/10.1016/j.immuni.2018.12.027>.
- [138] F. Wimmers, N. Subedi, N. van Buuringen, D. Heister, J. Vivié, I. Beeren-Reinieren, R. Woestenenk, H. Dolstra, A. Piruska, J.F.M. Jacobs, A. van Oudenaarden, C.G. Figdor, W.T.S. Huck, I.J.M. de Vries, J. Tel, Single-cell analysis reveals that stochasticity and paracrine signaling control interferon-alpha production by plasmacytoid dendritic cells, *Nat. Commun.* 9 (2018) 3317. <https://doi.org/10.1038/s41467-018-05784-3>.
- [139] L.C. Van Eyndhoven, E. Chouri, N. Subedi, J. Tel, Phenotypical Diversification of Early IFN α -Producing Human Plasmacytoid Dendritic Cells Using Droplet-Based Microfluidics, *Front. Immunol.* (2021). <https://doi.org/10.3389/fimmu.2021.672729>.
- [140] S.I. Saitoh, F. Abe, A. Kanno, N. Tanimura, Y. Mori Saitoh, R. Fukui, T. Shibata, K. Sato, T. Ichinohe, M. Hayashi, K. Kubota, H. Kozuka-Hata, M. Oyama, Y. Kikko, T. Katada, K. Kontani, K. Miyake, TLR7 mediated viral recognition results in focal type I interferon secretion by dendritic cells, *Nat. Commun.* (2017). <https://doi.org/10.1038/s41467-017-01687-x>.
- [141] E. Tomasello, K. Naciri, R. Chelbi, G. Bessou, A. Fries, E. Gressier, A. Abbas, E. Pollet, P. Pierre, T. Lawrence, T. Vu Manh, M. Dalod, Molecular dissection of plasmacytoid dendritic cell activation in vivo during a viral infection, *EMBO J.* (2018). <https://doi.org/10.15252/embj.201798836>.
- [142] J.A. Villadangos, L. Young, Antigen-Presentation Properties of Plasmacytoid Dendritic Cells, *Immunity.* (2008). <https://doi.org/10.1016/j.immuni.2008.09.002>.
- [143] A. Krug, R. Veeraswamy, A. Pekosz, O. Kanagawa, E.R. Unanue, M. Colonna, M. Cella, Interferon-producing cells fail to induce proliferation of naive T cells but can promote expansion and T helper 1 differentiation of antigen-experienced unpolarized T cells, *J. Exp. Med.* (2003). <https://doi.org/10.1084/jem.20021091>.
- [144] H. Hadeiba, K. Lahl, A. Edalati, C. Oderup, A. Habtezion, R. Pachynski, L. Nguyen, A. Ghodsi, S. Adler, E.C. Butcher, Plasmacytoid Dendritic Cells Transport Peripheral Antigens to the Thymus to Promote Central Tolerance, *Immunity.* (2012). <https://doi.org/10.1016/j.immuni.2012.01.017>.
- [145] A. Goubier, B. Dubois, H. Gheit, G. Joubert, F. Villard-Truc, C. Asselin-Paturel, G. Trinchieri, D. Kaiserlian, Plasmacytoid Dendritic Cells Mediate Oral Tolerance, *Immunity.* (2008). <https://doi.org/10.1016/j.immuni.2008.06.017>.
- [146] M. Kool, M. van Nimwegen, M.A.M. Willart, F. Muskens, L. Boon, J.J. Smit, A. Coyle, B.E. Clausen, H.C. Hoogsteden, B.N. Lambrecht, H. Hammad, An Anti-Inflammatory Role for Plasmacytoid Dendritic Cells in Allergic Airway Inflammation, *J. Immunol.* (2009). <https://doi.org/10.4049/jimmunol.0900471>.
- [147] I. Treilleux, J.Y. Blay, N. Bendriss-Vermare, I. Ray-Coquard, T. Bachelot, J.P. Guastolla, A. Bremond, S. Goddard, J.J. Pin, C. Barfaelemy-Dubois, S. Lebecque, Dendritic cell infiltration and prognosis of early stage breast cancer, *Clin. Cancer Res.* (2004). <https://doi.org/10.1158/1078-0432.CCR-04-0684>.
- [148] E. Hartmann, B. Wollenberg, S. Rothenfusser, M. Wagner, D. Wellisch, B. Mack, T. Giese, O. Gires, S. Endres, G. Hartmann, Identification and functional analysis of tumor-infiltrating plasmacytoid dendritic cells in head and neck cancer, *Cancer Res.* (2003).
- [149] S. Wei, I. Kryczek, L. Zou, B. Daniel, P. Cheng, P. Mottram, T. Curiel, A. Lange, W. Zou, Plasmacytoid dendritic cells induce CD8⁺ regulatory T cells in human ovarian carcinoma, *Cancer Res.* (2005). <https://doi.org/10.1158/0008-5472.CAN-04-4043>.
- [150] J. Tel, S. Anguille, C.E.J. Waterborg, E.L. Smits, C.G. Figdor, I.J.M. de Vries, Tumoricidal activity of human dendritic cells, *Trends Immunol.* (2014). <https://doi.org/10.1016/j.it.2013.10.007>.
- [151] M.L. Kalb, A. Glaser, G. Stary, F. Koszik, G. Stingl, TRAIL + Human Plasmacytoid Dendritic Cells Kill Tumor Cells In Vitro: Mechanisms of Imiquimod- and IFN- α -Mediated Antitumor Reactivity, *J. Immunol.* (2012). <https://doi.org/10.4049/jimmunol.1102437>.
- [152] A.W. Hardy, D.R. Graham, G.M. Shearer, J.P. Herbeval, HIV turns plasmacytoid dendritic cells (pDC) into TRAIL-expressing killer pDC and down-regulates HIV coreceptors by Toll-like receptor 7-induced IFN- α , *Proc. Natl. Acad. Sci. U. S. A.* (2007). <https://doi.org/10.1073/pnas.0707244104>.
- [153] G. Stary, C. Bangert, M. Tauber, R. Strohal, T. Kopp, G. Stingl, Tumoricidal activity of TLR7/8-activated inflammatory dendritic cells, *J. Exp. Med.* (2007). <https://doi.org/10.1084/jem.20070021>.
- [154] L. Chaperot, A. Blum, O. Manches, G. Lui, J. Angel, J.-P. Molens, J. Plumas, Virus or TLR Agonists Induce TRAIL-Mediated Cytotoxic Activity of Plasmacytoid Dendritic Cells, *J. Immunol.* (2006). <https://doi.org/10.4049/jimmunol.176.1.248>.
- [155] R.S. Ahn, K. Taravati, K. Lai, K.M. Lee, J. Nititham, R. Gupta, D.S. Chang, S.T. Arron, M. Rosenblum, W. Liao, Transcriptional landscape of epithelial and immune cell populations revealed through FACS-seq of healthy human skin, *Sci. Rep.* 7 (2017).

- <https://doi.org/10.1038/s41598-017-01468-y>.
- [156] X. Yan, C. Wu, T. Chen, M.M. Santos, C.L. Liu, C. Yang, L. Zhang, J. Ren, S. Liao, H. Guo, G.K. Sukhova, G.P. Shi, Cathepsin S inhibition changes regulatory T-cell activity in regulating bladder cancer and immune cell proliferation and apoptosis, *Mol. Immunol.* 82 (2017) 66–74. <https://doi.org/10.1016/j.molimm.2016.12.018>.
- [157] B. Korin, T. Dubovik, A. Rolls, Mass cytometry analysis of immune cells in the brain, *Nat. Protoc.* 13 (2018) 377–391. <https://doi.org/10.1038/nprot.2017.155>.
- [158] C. Goetz, L.J. Peng, B. Aggeler, J. Bonnevier, Phenotyping CD4+ hTh2 cells by flow cytometry: Simultaneous detection of transcription factors, secreted cytokines, and surface markers, in: *Methods Mol. Biol.*, 2017: pp. 175–184. https://doi.org/10.1007/978-1-4939-6759-9_10.
- [159] D. Lin, H.T. Maecker, Mass Cytometry Assays for Antigen-Specific T Cells Using CyTOF., *Methods Mol. Biol.* 1678 (2018) 37–47. https://doi.org/10.1007/978-1-4939-7346-0_3.
- [160] E.K. Sackmann, A.L. Fulton, D.J. Beebe, The present and future role of microfluidics in biomedical research, *Nature.* 507 (2014) 181–189. <https://doi.org/10.1038/nature13118>.
- [161] E.W.K. Young, D.J. Beebe, Fundamentals of microfluidic cell culture in controlled microenvironments, *J. Chem. Soc.* (2010) 1036–1048. <https://doi.org/10.1039/B813328J/Analyst>.
- [162] Q. Zhu, L. Qiu, Y. Xu, G. Li, Y. Mu, Single cell digital polymerase chain reaction on self-priming compartmentalization chip, *Biomicrofluidics.* 11 (2017). <https://doi.org/10.1063/1.4975192>.
- [163] I. Rodríguez-Ruiz, V. Babenko, S. Martínez-Rodríguez, J.A. Gavira, Protein separation under a microfluidic regime, *Analyst.* 143 (2018) 606–619. <https://doi.org/10.1039/c7an01568b>.
- [164] D. Kim, X. Wu, A.T. Young, C.L. Haynes, Microfluidics-based in vivo mimetic systems for the study of cellular biology, *Acc. Chem. Res.* (2014). <https://doi.org/10.1021/ar4002608>.
- [165] C. Yi, C.W. Li, S. Ji, M. Yang, Microfluidics technology for manipulation and analysis of biological cells, *Anal. Chim. Acta.* 560 (2006) 1–23. <https://doi.org/10.1016/j.aca.2005.12.037>.
- [166] I. Meyvantsson, D.J. Beebe, Cell Culture Models in Microfluidic Systems, *Annu. Rev. Anal. Chem.* 1 (2008) 423–429. <https://doi.org/10.1007/s13398-014-0173-7.2>.
- [167] Y. Deng, Y. Zhang, S. Sun, Z. Wang, M. Wang, B. Yu, D.M. Czajkowsky, B. Liu, Y. Li, W. Wei, Q. Shi, An integrated microfluidic chip system for single-cell secretion profiling of rare circulating tumor cells, *Sci. Rep.* 4 (2014). <https://doi.org/10.1038/srep07499>.
- [168] J. Hultström, O. Manneberg, K. Dopf, H.M. Hertz, H. Brismar, M. Wiklund, Proliferation and viability of adherent cells manipulated by standing-wave ultrasound in a microfluidic chip, *Ultrasound Med. Biol.* 33 (2007) 145–151. <https://doi.org/10.1016/j.ultrasmedbio.2006.07.024>.
- [169] A.H. Diercks, A. Ozinsky, C.L. Hansen, J.M. Spotts, D.J. Rodriguez, A. Aderem, A microfluidic device for multiplexed protein detection in nano-liter volumes, *Anal. Biochem.* 386 (2009) 30–35. <https://doi.org/10.1016/j.ab.2008.12.012>.
- [170] V. Lecault, A.K. White, A. Singhal, C.L. Hansen, Microfluidic single cell analysis: From promise to practice, *Curr. Opin. Chem. Biol.* 16 (2012) 381–390. <https://doi.org/10.1016/j.cbpa.2012.03.022>.
- [171] S.K. Sia, G.M. Whitesides, Microfluidic devices fabricated in poly(dimethylsiloxane) for biological studies, *Electrophoresis.* 24 (2003) 3563–3576.
- [172] R.S. Kane, S. Takayama, E. Ostuni, D.E. Ingber, G.M. Whitesides, Patterning proteins and cells using soft lithography., *Biomaterials.* 20 (1999) 2363–2376. [https://doi.org/10.1016/S0142-9612\(99\)00165-9](https://doi.org/10.1016/S0142-9612(99)00165-9).
- [173] A.A.S. Bhagat, P. Jothimuthu, I. Papautsky, Photodefinable polydimethylsiloxane (PDMS) for rapid lab-on-a-chip prototyping, *Lab Chip.* 7 (2007) 1192. <https://doi.org/10.1039/b704946c>.
- [174] T. Thorsen, S.J. Maerkl, S.R. Quake, A.G. Hadd, S.C. Jacobson, J.M. Ramsey, D.J. Harrison, P.C.H. Li, D.J. Harrison, A.G. Hadd, D.E. Raymond, J.W. Haliwell, S.C. Jacobson, S.C. Ramsey, E.T. Lagally, I. Medintz, R.A. Mathies, J. Khandurina, E. Eteshola, D. Leckband, J. Wang, A. Ibanez, M.P. Chatrathi, A. Escarpa, M.A. Unger, H.-P. Chou, T. Thorsen, A. Scherer, S.R. Quake, L. Buchillot, E. Farnault, M. Hoummady, H. Fujita, H.P. Chou, C.S. Spence, A. Scherer, S.R. Quake, V. Linder, E. Verpoorte, W. Thormann, N.F. de Rooij, H. Sigrist, T. Yang, S. Jung, H. Mao, P.S. Cremer, D.C. Duffy, J.C. MacDonald, O.J.A. Schueller, G.M. Whitesides, B.A. Grzybowski, R. Haag, N. Bowden, G.M. Whitesides, Microfluidic large-scale integration., *Science.* 298 (2002) 580–4. <https://doi.org/10.1126/science.1076996>.
- [175] G.V.J. Nossal, J. Lederberg, Antibody production by single cells, *Nature.* 181 (1958) 1419–1420.

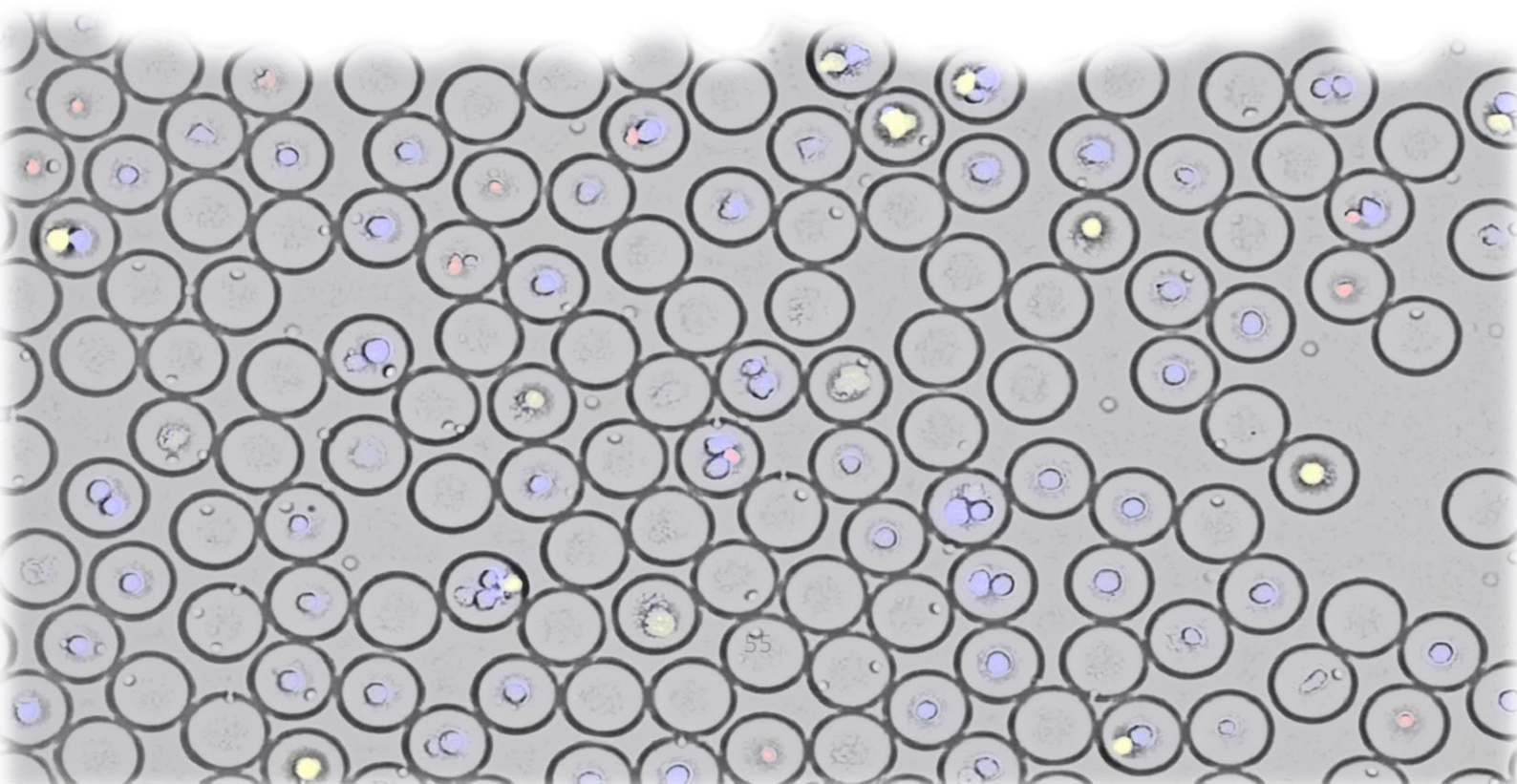
- [176] S. Jakiela, T.S. Kaminski, O. Cybulski, D.B. Weibel, P. Garstecki, Bacterial growth and adaptation in microdroplet chemostats, *Angew. Chemie - Int. Ed.* 52 (2013) 8908–8911. <https://doi.org/10.1002/anie.201301524>.
- [177] S. Abalde-Cela, P. Taladriz-Blanco, M.G. De Oliveira, C. Abell, Droplet microfluidics for the highly controlled synthesis of branched gold nanoparticles, *Sci. Rep.* 8 (2018). <https://doi.org/10.1038/s41598-018-20754-x>.
- [178] S.C. Kim, I.C. Clark, P. Shahi, A.R. Abate, Single-Cell RT-PCR in Microfluidic Droplets with Integrated Chemical Lysis, *Anal. Chem.* 90 (2018) 1273–1279. <https://doi.org/10.1021/acs.analchem.7b04050>.
- [179] Q. Chen, S. Utech, D. Chen, R. Prodanovic, J.-M. Lin, D.A. Weitz, Controlled assembly of heterotypic cells in a core–shell scaffold: organ in a droplet, *Lab Chip.* 16 (2016) 1346–1349. <https://doi.org/10.1039/C6LC00231E>.
- [180] N. Nuti, P.E. Verboket, P.S. Dittrich, Multivesicular droplets: A cell model system to study compartmentalised biochemical reactions, *Lab Chip.* 17 (2017). <https://doi.org/10.1039/C7LC00710H>.
- [181] S.K. Küster, M. Pabst, R. Zenobi, P.S. Dittrich, Screening for protein phosphorylation using nanoscale reactions on microdroplet arrays, *Angew. Chemie - Int. Ed.* 54 (2015) 1671–1675. <https://doi.org/10.1002/anie.201409440>.
- [182] A.M. Klein, L. Mazutis, I. Akartuna, N. Tallapragada, A. Veres, V. Li, L. Peshkin, D.A. Weitz, M.W. Kirschner, Droplet barcoding for single-cell transcriptomics applied to embryonic stem cells., *Cell.* (2015). <https://doi.org/10.1016/j.cell.2015.04.044>.
- [183] B.E. Debs, R. Utharala, I. V. Balyasnikova, A.D. Griffiths, C.A. Merten, Functional single-cell hybridoma screening using droplet-based microfluidics, *Proc. Natl. Acad. Sci.* 109 (2012) 11570–11575. <https://doi.org/10.1073/pnas.1204514109>.
- [184] Z. Guan, Y. Zou, M. Zhang, J. Lv, H. Shen, P. Yang, H. Zhang, Z. Zhu, C.J. Yang, A highly parallel microfluidic droplet method enabling single-molecule counting for digital enzyme detection, *Biomicrofluidics.* 8 (2014). <https://doi.org/10.1063/1.4866766>.
- [185] J.W. Park, S.C. Na, T.Q. Nguyen, S.M. Paik, M. Kang, D. Hong, I.S. Choi, J.H. Lee, N.L. Jeon, Live cell imaging compatible immobilization of *Chlamydomonas reinhardtii* in microfluidic platform for biodiesel research, *Biotechnol. Bioeng.* 112 (2015) 494–501. <https://doi.org/10.1002/bit.25453>.
- [186] J. Pessi, H.A. Santos, I. Miroshnyk, Joukoyliruusi, D.A. Weitz, S. Mirza, Microfluidics-assisted engineering of polymeric microcapsules with high encapsulation efficiency for protein drug delivery, *Int. J. Pharm.* 472 (2014) 82–87. <https://doi.org/10.1016/j.ijpharm.2014.06.012>.
- [187] J. Shuga, Y. Zeng, R. Novak, Q. Lan, X. Tang, N. Rothman, R. Vermeulen, L. Li, A. Hubbard, L. Zhang, R.A. Mathies, M.T. Smith, Single molecule quantitation and sequencing of rare translocations using microfluidic nested digital PCR, *Nucleic Acids Res.* 41 (2013). <https://doi.org/10.1093/nar/gkt613>.
- [188] N. Shembekar, H. Hu, D. Eustace, C.A. Merten, Single-Cell Droplet Microfluidic Screening for Antibodies Specifically Binding to Target Cells, *Cell Rep.* 22 (2018) 2094–2106. <https://doi.org/10.1016/j.celrep.2018.01.071>.
- [189] A. Rakszewska, J. Tel, V. Chokkalingam, W.T. Huck, One drop at a time: toward droplet microfluidics as a versatile tool for single-cell analysis, *NPG Asia Mater.* 6 (2014) e133. <https://doi.org/10.1038/am.2014.86>.
- [190] K. Churski, T.S. Kaminski, S. Jakiela, W. Kamysz, W. Baranska-Rybak, D.B. Weibel, P. Garstecki, Rapid screening of antibiotic toxicity in an automated microdroplet system, *Lab Chip.* 12 (2012) 1629. <https://doi.org/10.1039/c2lc21284f>.
- [191] P. Garstecki, M.J. Fuerstman, H.A. Stone, G.M. Whitesides, Formation of droplets and bubbles in a microfluidic T-junction—scaling and mechanism of break-up, *Lab Chip.* 6 (2006) 437. <https://doi.org/10.1039/b510841a>.
- [192] M. Seo, C. Paquet, Z. Nie, S. Xu, E. Kumacheva, Microfluidic consecutive flow-focusing droplet generators, *Soft Matter.* 3 (2007) 986. <https://doi.org/10.1039/b700687j>.
- [193] A.M. Pit, M.H.G. Duits, F. Mugele, Droplet manipulations in two phase flow microfluidics, *Micromachines.* 6 (2015) 1768–1793. <https://doi.org/10.3390/mi6111455>.
- [194] X. Chen, C.L. Ren, A microfluidic chip integrated with droplet generation, pairing, trapping, merging, mixing and releasing, *RSC Adv.* 7 (2017) 16738–16750. <https://doi.org/10.1039/C7RA02336G>.
- [195] S. Padmanabhan, T. Misteli, D.L. DeVoe, Controlled droplet discretization and manipulation using membrane displacement traps, *Lab Chip.* 17 (2017). <https://doi.org/10.1039/C7LC00910K>.
- [196] R.M. Lorenz, J.S. Edgar, G.D.M. Jeffries, D.T. Chiu, Microfluidic and optical systems for the on-demand generation and manipulation of single femtoliter-volume aqueous droplets, *Anal. Chem.* 78 (2006) 6433–6439. <https://doi.org/10.1021/ac060748l>.
- [197] T. Franke, A.R. Abate, D.A. Weitz, A. Wixforth, Surface acoustic wave (SAW) directed droplet flow in microfluidics for PDMS devices, *Lab Chip.* 9 (2009) 2625. <https://doi.org/10.1039/b906819h>.

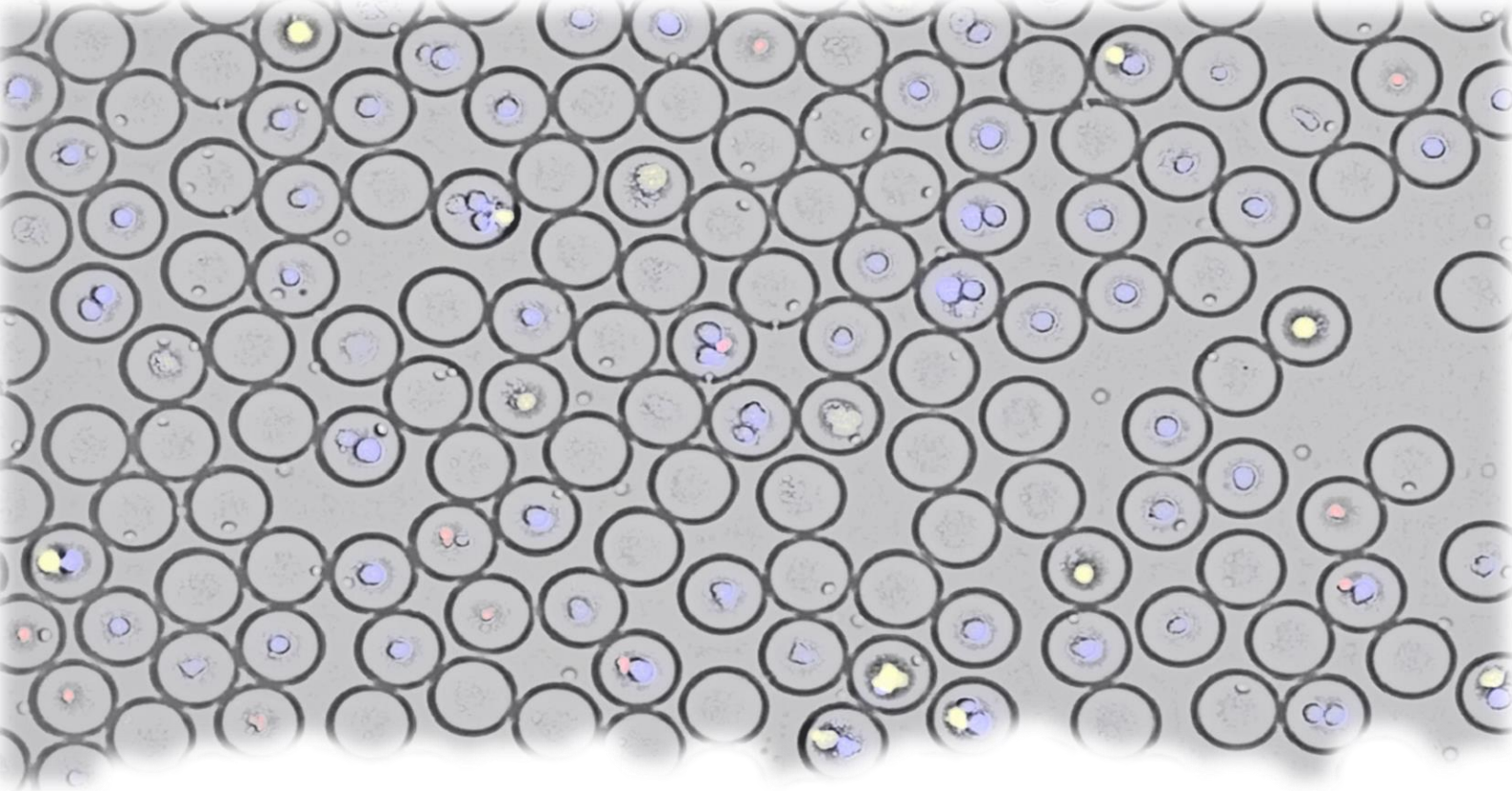
- [198] M.Y. Chiang, Y.W. Hsu, H.Y. Hsieh, S.Y. Chen, S.K. Fan, Constructing 3D heterogeneous hydrogels from electrically manipulated prepolymer droplets and crosslinked microgels, *Sci. Adv.* 2 (2016). <https://doi.org/10.1126/sciadv.1600964>.
- [199] D.J. Collins, A. Neild, A. deMello, A.Q. Liu, Y. Ai, The Poisson distribution and beyond: Methods for microfluidic droplet production and single cell encapsulation, *Lab Chip.* 15 (2015) 3439–3459. <https://doi.org/10.1039/c5lc00614g>.
- [200] S. Sarkar, B. Motwani, P. Sabhachandani, N. Cohen, T. Konry, T Cell Dynamic Activation and Functional Analysis in Nanoliter Droplet Microarray, *J. Clin. Cell. Immunol.* 06 (2015). <https://doi.org/10.4172/2155-9899.1000334>.
- [201] S. Sarkar, P. Sabhachandani, D. Ravi, S. Potdar, S. Purvey, A. Beheshti, A.M. Evens, T. Konry, Dynamic analysis of human natural killer cell response at single-cell resolution in B-Cell Non-Hodgkin Lymphoma, *Front. Immunol.* 8 (2017) 1–13. <https://doi.org/10.3389/fimmu.2017.01736>.
- [202] K. Guldevall, L. Brandt, E. Forslund, K. Olofsson, T.W. Frisk, P.E. Olofsson, K. Gustafsson, O. Manneberg, B. Vanherberghen, H. Brismar, K. Kärre, M. Uhlin, B. Önfelt, Microchip screening platform for single cell assessment of NK cell cytotoxicity, *Front. Immunol.* (2016). <https://doi.org/10.3389/fimmu.2016.00119>.
- [203] B. Dura, M.M. Servos, R.M. Barry, H.L. Ploegh, S.K. Dougan, J. Voldman, Longitudinal multiparameter assay of lymphocyte interactions from onset by microfluidic cell pairing and culture, *Proc. Natl. Acad. Sci.* 113 (2016) E3599–E3608. <https://doi.org/10.1073/pnas.1515364113>.
- [204] T. Konry, M. Dominguez-Villar, C. Baecher-Allan, D.A. Hafler, M.L. Yarmush, Droplet-based microfluidic platforms for single T cell secretion analysis of IL-10 cytokine, *Biosens. Bioelectron.* 26 (2011) 2707–2710. <https://doi.org/10.1016/j.bios.2010.09.006>.
- [205] L. Qiu, F. Wimmers, J. Weiden, H.A. Heus, J. Tel, C.G. Figdor, A membrane-anchored aptamer sensor for probing IFN γ secretion by single cells, *Chem. Commun.* (2017). <https://doi.org/10.1039/c7cc03576d>.
- [206] K. Eyer, R.C.L. Doineau, C.E. Castrillon, L. Briseño-Roa, V. Menrath, G. Mottet, P. England, A. Godina, E. Brient-Litzler, C. Nizak, A. Jensen, A.D. Griffiths, J. Bibette, P. Bruhns, J. Baudry, Single-cell deep phenotyping of IgG-secreting cells for high-resolution immune monitoring, *Nat. Biotechnol.* 35 (2017) 977–982. <https://doi.org/10.1038/nbt.3964>.
- [207] V. Chokkalingam, J. Tel, F. Wimmers, X. Liu, S. Semenov, J. Thiele, C.G. Figdor, W.T.S. Huck, Probing cellular heterogeneity in cytokine-secreting immune cells using droplet-based microfluidics, *Lab Chip.* 13 (2013) 4740. <https://doi.org/10.1039/c3lc50945a>.
- [208] M. Hosokawa, Y. Nishikawa, M. Kogawa, H. Takeyama, Massively parallel whole genome amplification for single-cell sequencing using droplet microfluidics, *Sci. Rep.* 7 (2017). <https://doi.org/10.1038/s41598-017-05436-4>.
- [209] E.Z. Macosko, A. Basu, R. Satija, J. Nemeshe, K. Shekhar, M. Goldman, I. Tirosh, A.R. Bialas, N. Kamitaki, E.M. Martersteck, J.J. Trombetta, D.A. Weitz, J.R. Sanes, A.K. Shalek, A. Regev, S.A. McCarroll, Highly parallel genome-wide expression profiling of individual cells using nanoliter droplets, *Cell.* 161 (2015) 1202–1214. <https://doi.org/10.1016/j.cell.2015.05.002>.
- [210] F. Lan, B. Demaree, N. Ahmed, A.R. Abate, Single-cell genome sequencing at ultra-high-throughput with microfluidic droplet barcoding, *Nat. Biotechnol.* 35 (2017) 640–646. <https://doi.org/10.1038/nbt.3880>.
- [211] J. Eberwine, J.Y. Sul, T. Bartfai, J. Kim, The promise of single-cell sequencing, *Nat. Methods.* 11 (2014) 25–27. <https://doi.org/10.1038/nmeth.2769>.
- [212] P. Shahi, S.C. Kim, J.R. Haliburton, Z.J. Gartner, A.R. Abate, Abseq: Ultrahigh-throughput single cell protein profiling with droplet microfluidic barcoding, *Sci. Rep.* 7 (2017). <https://doi.org/10.1038/srep44447>.



PART 1

DROPLET BASED MICROFLUIDICS





CHAPTER 2

A PIPETTE-TIP BASED METHOD FOR SEEDING CELLS TO DROPLET MICROFLUIDIC PLATFORMS

This chapter is published as:

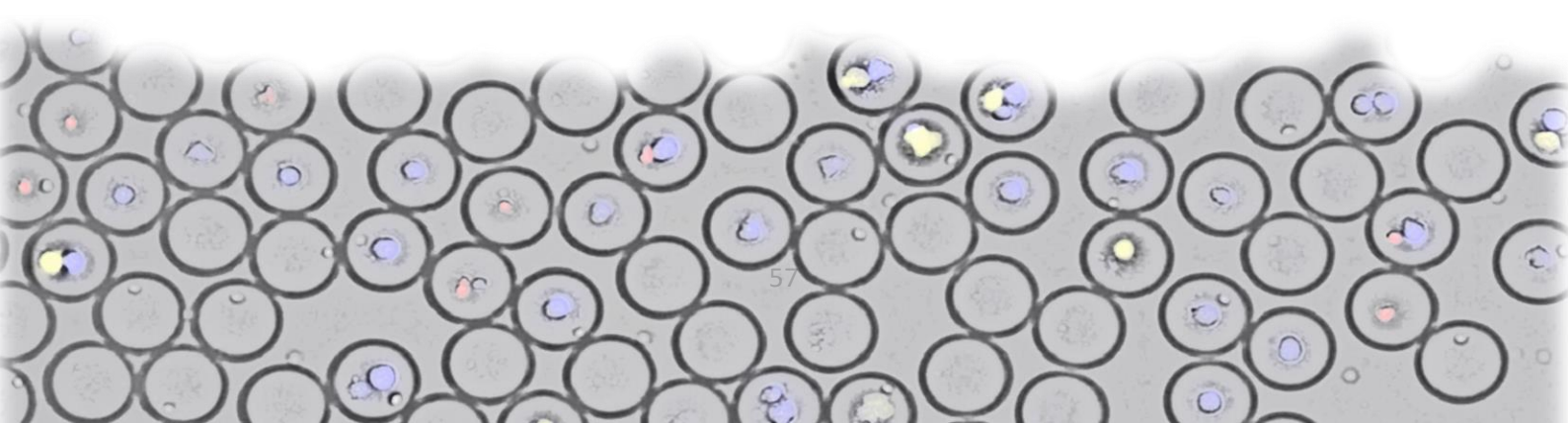
A pipette-tip based method for seeding cells to droplet microfluidic platforms

Nidhi Sinha*, Nikita Subedi*, Florian Wimmers*, Melf Soennichsen, Jurjen Tel

Journal of Visualized Experiments (JoVE), 144:e57848

Published: February 11, 2019

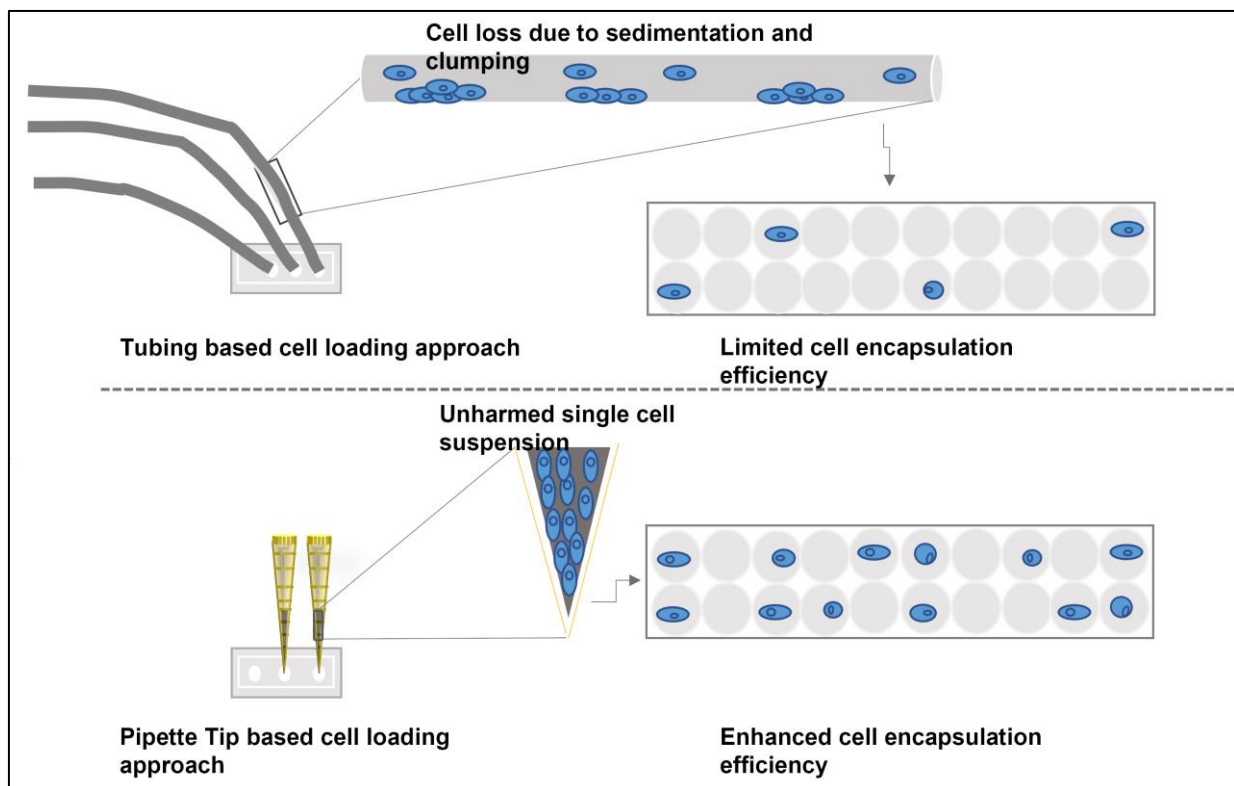
*Authors contributed equally



Abstract

Amongst various microfluidic platform designs frequently used for cellular analysis, droplet-microfluidics provides a robust tool for isolating and analyzing cells at the single-cell level by eliminating the influence of external factors on the cellular microenvironment. Encapsulation of cells in droplets is dictated by the Poisson distribution as a function of the number of cells present in each droplet and the average number of cells per volume of droplet. Primary cells, especially immune cells, or clinical specimens can be scarce and loss-less encapsulation of cells remains challenging. In this paper, we present a new methodology that uses pipette-tips to load cells to droplet-based microfluidic devices without the significant loss of cells. We demonstrate, with various cell types, efficient cell encapsulation in droplets that closely corresponds to the encapsulation efficiency predicted by the Poisson distribution. Our method ensures loss-less loading of cells to microfluidic platforms and can be easily adapted for downstream single cell analysis, e.g. to decode cellular interactions between different cell types.

Graphical Abstract



1. Introduction

In recent years, the use of microfluidics as a robust and versatile platform for cellular analysis at the single cell level has rapidly increased[1]. These platforms provide high-throughput screening of single cells and biological molecules with high precision and sensitivity using very small sample volume[2–4]. Among different types of microfluidic designs, droplet-based platforms enable high-throughput analysis of single cells by isolating them in an aqueous phase droplet surrounded by an immiscible phase that allows precise and accurate control over the cellular microenvironment[5,6]. Droplet-based microfluidics gives the flexibility to isolate single or multiple-cells in, both, aqueous and hydrogel droplets and is valuable in probing complex cellular behavior, such as protein secretion or cellular interactions[7–9]. Signaling and cross-talk amongst immune cells can be influenced by interactions with other cells in the microenvironment[10]. Isolation of single cells in droplets provides an effective noise-free analytical laboratory, free from the influence of external environmental factors for more efficient and accurate results[11,12]. Modifying the design of a droplet-microfluidic platform with multiple inlets allows the encapsulation of multiple cell types to study cellular interactions via cell-pairing[12,13].

The process of encapsulation of cells in droplets is random and the rate of encapsulation of cells can be statistically determined using the formula for the Poisson distribution[14,15]. This rate of encapsulation can be estimated by considering the average rate of the arrival of cells at the droplet junction and assuming that the arrival of each cell is independent from the arrival of other cells[16]. Even though independent cell arrival cannot be guaranteed, in cases of sparsely distributed cells, the assumption of independence can be considered and the probability of a droplet containing one or more cells can be predicted as a function of the number of cells present in each droplet and the average number of cells per droplet[16,17]. Since this estimation of cellular encapsulation in droplets is dependent on the number of cells present in each droplet, one can suggest that increasing the concentration of the cells at the inlet will increase the average number of cells present in each droplet[16]. Therefore, to ensure single cell encapsulation, the cell concentrations must be reduced but this often leads to a large number of empty droplets[18].

Loss of cells during loading by either attachment, sedimentation, and/or clumping in the syringe, tubing, or production device is a common drawback responsible for the deviation of actual encapsulation values from the predicted encapsulation values[19]. This problem gets further exaggerated when seeding rare immune cells or clinical specimens as they are already scarce in population and the encapsulation of only a few cells, much lower than expected, does not provide sufficient data for experimental analysis. Plasmacytoid dendritic cells (pDCs) are a rare subset of immune cells that only constitutes approximately 0.2 - 0.6 percent of the entire white blood cell population[20]. These cells secrete massive amounts of type I interferons upon activation and thereby play a critical role in immune responses[21]. When studying the cellular behavior of such rare cells in droplets, it is imperative to prevent cell loss during cell seeding and encapsulation[22]. There are several design related developments that have ensured the encapsulation of single cells in droplets using active encapsulation methods that utilize different physical forces such as acoustic or electrical forces for generation of droplets containing single-cells[23,24]. However, these methods have their own limitations in terms of droplet production[16].

In this study, we established a robust and straightforward method that circumvents the shortcomings of traditional methods for loading single or multiple cells to microfluidic devices. Our method, inspired by Rho et al., utilizes differently-sized pipette tips for seeding small volumes of rare immune cells to droplet microfluidic platforms without significant sample loss and yielded results that are coherent with theoretical predictions[25]. This methodology can be easily and successfully adapted for several applications involving droplet-based microfluidics and applied for a wide variety of cell types or even microparticles.

2. Protocol

2.1.-inlet Polydimethylsiloxane (PDMS) device fabrication

- 2.1.1 Measure 40 g PDMS base in a conditioning mixer cup and add 4 g PDMS curing agent to the base reagent in the cup, carefully, using a dropper.
- 2.1.2 2.1.2 Place the cup in the holder of the conditioning mixer and measure the total weight of the cup with the holder. Set the value of the centrifuge balance weight on the conditioning mixer accordingly.
- 2.1.3 2.1.3 Mix the base and curing agent in the conditioning mixer at 2000 rpm for 2 min followed by de-foaming at 2000 rpm for 2 min.
- 2.1.4 Prepare an aluminum boat, with a diameter approximately the same size as that of a 100 mm silicon wafer. Place the silicon wafer, fabricated for the replica molding process, in the aluminum boat and put this setup in a petri dish (diameter = 120 mm, height = 20 mm).

Note: The size of the petri dish depends on the size of the silicon wafer.

- 2.1.5 Remove the cup from the holder and the pour pre-cured PDMS mixture (contents of the cup), carefully, on the silicon wafer.
- 2.1.6 Place the petri dish, containing the silicon wafer with the pre-cured PDMS mixture, in a desiccator for about 20 min to remove all the air bubbles.
- 2.1.7 Remove the petri dish after 20 min and check for any remaining air bubbles that can be removed.
- 2.1.8 Place the petri dish in an oven, set at 65 °C, for at least 3 h.
- 2.1.9 Remove the petri dish from the oven after 3 h and carefully peel the cured PDMS from the silicon wafer.
- 2.1.10 Cut PDMS devices along the cut lines, using a knife or a scalpel. Punch holes at the inlets and outlet of each device using a 1.2 mm puncher. Clean each PDMS device with scotch tape to remove any dust or residual pieces of PDMS.

Optional: Blow with nitrogen to remove residual PDMS pieces.

- 2.1.11 Prepare glass slides by cleaning them with soap-water, followed by isopropanol and dry with nitrogen.

2.1.12 Bond a clean PDMS device with a clean glass slide in a plasma asher to close the flow lines. The settings used in this setup are as follows: Power: 50 W, Time: 45 s, Bleed delay time: 2 s, Process gas: Gas 1 (Air), Vent: Both valves, Restricted vent time: 60 s, Pump spin down time: 10 s, Vent hold time: 0 s, Gas shutoff time: 1 s, Turbo pumping enabled: 0. All the other gas lines are disconnected.

Note: The settings used for the plasma asher can vary according to the brand of the plasma asher used.

2.1.13 Prepare the silane solution by adding 50 μL silane (1H,1H,2H,2H-Perfluorooctyltriethoxysilane) to 950 μL fluorinated oil.

Note: Silane is toxic. Please operate under fume hood.

2.1.14 Draw the prepared silane solution in a syringe, which is connected to a teflon tubing.

2.1.15 Salinize the device by flushing the prepared silane solution through the outlet of the device.

2.1.16 Place the device in an oven, set at 65 $^{\circ}\text{C}$, for 30 min.

2.1.17 Remove the salinized device from the oven and flush excess silane out of the device with fluorinated oil.

2.1.18 Place the device back in an oven, set at 65 $^{\circ}\text{C}$, for at least 1 h to complete the bonding process.

Note: The Protocol can be paused here.

2.2 Loss-less cell encapsulation

2.2.1 Cell harvesting

Re-suspend Jurkat T cells in Roswell Park Memorial Institute (RPMI) medium at concentrations of 1.0E6 cells/mL, 2.0E6 cells/mL, 4.0E6 cells/mL, and 8.0E6 cells/mL; pDCs in X vivo 15 medium at concentrations of 1.3E6 cells/mL, 3.0E6 cells/mL, and 13.0E6 cells/mL; A549 cells in Dulbecco's Modified Eagle's Medium (DMEM) at a concentration of 1.0E6 cells/mL.

Note: The type of cells and concentration of cells can vary based on the experiment. Labelling of cells can also be done based on the experiment.

2.2.1 Tip-loading for aqueous droplet generation

2.2.1.1 Prepare fluorinated oil with 3% biocompatible surfactant mixture by adding 30 mL

surfactant to 20 mL fluorinated oil (oil phase).

Note: The concentration of the surfactant added to the fluorinated oil determines the stability of the emulsion for different incubation periods. The concentration of the surfactant varies depending on the media used for specific cell-types.

2.2.1.2 Draw the oil phase mixture in a syringe (1 mL). Remove air bubbles from the syringe and connect it to a teflon tubing of appropriate length.

2.2.1.3 Prepare a sample syringe by drawing biocompatible mineral oil in a syringe. Remove air bubbles and connect the syringe to a teflon tubing of appropriate length.

2.2.1.4 Punch a PDMS plug with a diameter of 5 mm from a cured PDMS slab.

Note: The cured PDMS slab can be prepared using steps 1.1 to 1.9. Use a plain silicon wafer instead of a fabricated silicon wafer.

2.2.1.5 Punch another hole in the center of the plug with a 1 mm puncher.

2.2.1.6 Insert the plug in a 200 μ L pipette tip, from the larger end, such that it fits tightly.

Note: Use a 1000 μ L pipette tip for larger sample volume and larger cells. For 1000 μ L pipette tip, plugs of diameter ranging between 5 mm and 7 mm can be used. With a plug of diameter 5 mm, a sample volume of around 400 μ L can be aspirated in the pipette tip. If a plug of larger diameter is used (7 mm), more sample volume can be aspirated (around 900 μ L).

2.2.1.7 Insert the tubing, which is connected to the syringe, in the PDMS plug, which has been inserted in the pipette tip. Push the syringe plunger slowly to fill the connected pipette tip with mineral oil. Push out all the residual air from the pipette tip.

2.2.1.8 Lower the pipette tip, connected to the syringe, in the sample solution and aspirate about 150 μ L of sample in the tip.

2.2.1.9 Repeat steps 2.2.4 to 2.2.8 to prepare a second sample syringe.

2.2.1.10 Carefully place all the three prepared syringes on the syringe pump.

2.2.1.11 Insert both the pipette tips, containing the sample, in the two inner inlets of the PDMS chip. Insert the tube containing the oil phase mixture in the outer inlet.

2.2.1.12 Set the value of the flow rates on the syringe pump as follows: continuous phase solution: 600 μ L/h, cell samples: 100 μ L/h, each. Enter and set the dimensions of the syringe.

Note: The diameter settings will vary based on the type of syringe.

- 2.2.1.13 Start the pump to flush sample solution through the inner channels of the device and oil phase through the outer channel of the device.
- 2.2.1.14 Plug in a tubing of appropriate length to the outlet to start collecting the droplets when the droplet formation is stable. The time of collection varies based on the experiment.
- 2.2.1.15 Collect droplets in a lock tube. Add 200 μ L RPMI medium (without serum) on top of the collected droplets and incubate the sample.

Note: Incubation time of the collected droplets varies based on the experiment.

Note: Droplets are collected in a lock tube when flow cytometry-based analysis or isolation is performed after retrieving the cells from droplets by breaking the emulsion. It is possible to collect the droplets in a glass chamber if the experiment requires in-droplet microscopic analysis.

2.3 Emulsion breaking and cell retrieval for flow cytometric analysis

- 2.3.1 Prepare 20% 1H,1H,2H,2H-Perfluoro-1-octanol (PFO) solution (v/v) in fluorinated oil by adding 2 mL PFO in 10 mL fluorinated oil.
- 2.3.2 Remove excess oil from the bottom of the collection tube, containing the droplets, using a syringe.
- 2.3.3 Add 100 μ L of 20% PFO solution to the emulsion to break the emulsion and release the encapsulated cells into the aqueous phase. Tap and mix briefly. Do not vortex at this point. Incubate for 1-2 min.

Note: The amount of PFO added depends on the quantity of droplets produced. Keep adding additional PFO until the oil layer is completely dissolved. Keep in mind that PFO is toxic for the cells and that too high PFO concentrations or too long incubation in PFO might lead to increased cell death.

- 2.3.4 Spin the solution shortly at the lowest possible rcf for 30 s.
- 2.3.5 Prepare 100 mL cold Phosphate-Buffered Saline (PBS) solution supplemented with 2% Fetal Calf Serum (FCS) (2 mL FCS in 98 mL PBS).
- 2.3.6 Pipette 550 μ L of aqueous fraction, immediately after centrifugation and transfer it to a new lock tube containing 500 μ L cold PBS solution supplemented with 2% FCS, as

prepared in step 2.3.5. Let any residual oil sink to the bottom of the new lock tube.

2.3.7 Aspirate 950 μL of the aqueous phase containing the cells from this lock tube, carefully, without aspirating any residual oil and transfer the solution to a new lock tube.

2.3.8 Spin down the cells in the new lock tube for 10 min.

2.3.9 Re-suspend the cells in 300 μL cold PBS solution supplemented with 2% FCS, as prepared in step 2.3.5.

Note: The cells can be also re-suspended in any other suitable solution such as media depending on the experiment.

Note: Stain the cells, based on the experiment, for analysis using flow cytometry.

2.4 Cell pairing

2.4.1 Cell harvesting and staining

2.4.1.1 Count Jurkat T cells, from culture flask, and spin down the cells at 1500 rpm for 5 min.

2.4.1.2 Remove the supernatant and re-suspend $1.0\text{E}6$ cells in 1 mL PBS to get a concentration of $1.0\text{E}6$ cells/mL. The amount of PBS added depends on the cell count.

2.4.1.3 Repeat steps 3.1.1 to 3.1.2 to prepare a second sample of Jurkat T-cells with the same cell concentration.

2.4.1.4 Wash both samples twice with 1 mL of PBS at 1500 rpm for 5 min.

2.4.1.5 Re-suspend one cell sample with $1.25 \mu\text{M}$ carboxyfluorescein succinimidyl ester (CFSE) dye and the other cell sample with $1.25 \mu\text{M}$ far red dye or $1.25 \mu\text{M}$ cell proliferation dye at a cell concentration of $1.0\text{E}6$ cells/mL. The total staining solution is 1 mL for $1.0\text{E}6$ cells.

Note: Cells can be labelled with different dyes depending on the filters available in the flow cytometer or in the fluorescence microscope.

2.4.1.6 Incubate the cell samples with dyes for 10 min at 37°C .

2.4.1.7 Stop the staining reaction by adding 1 mL ice cold FCS after 10 min.

2.4.1.8 Wash the cell samples twice with 1 mL PBS at 1500 rpm for 5 min.

2.4.1.9 Re-suspend the cell samples in RPMI media at a concentration of 10.0×10^6 cells/mL, for each color.

2.5 Tip-loading for production of agarose hydrogel droplets for cell pairing

Note: For cell pairing using agarose hydrogel droplets, maintain the temperature of the system between 27 °C and 37 °C throughout the droplet generation and collection process to prevent gelling of the hydrogels and to warrant cellular viability[9].

2.5.1 Dissolve ultra-low gelling temperature agarose by heating it upto 75 °C in PBS at a concentration of 4% (w/v) and stir the mixture for 20 min.

2.5.2 Mix the agarose solution with labelled Jurkat T cells to yield an agarose concentration of 2% (w/v). Repeat this for the other sample with differently labelled cells.

2.5.3 Prepare fluorinated oil with 2% surfactant mixture by adding 20 mL surfactant to 30 mL fluorinated oil (oil phase mixture).

2.5.4 Follow the steps 2.2.2 – 2.2.14.

Note: Because of the viscous nature of low melting agarose and to ensure stable droplet production, set the value of the flow rates on the syringe pumps as follows: oil phase mixture: 2000 μ L/h, cell samples: 200 μ L/h. Enter and set the dimensions of the syringe.

2.5.5 Collect the droplets in a lock tube and incubate the droplets at 4 °C for 60 min.

2.6 Emulsion breaking and agarose bead retrieval for FACS analysis

2.6.1 After incubation of droplets for 60 min, remove excess oil from the lock tube, containing the droplets, using a syringe.

2.6.2 Add 200 μ L PFO to remove the oil interphase from the droplets.

Note: The amount of PFO added to the tube depends on the quantity of droplets produced. Keep adding additional PFO until the oil layer is completely dissolved.

2.6.3 Wash the collected agarose beads twice with 1 mL of cold PBS to remove oil completely by centrifugation at 1500 rpm for 10 min.

2.6.4 Analyze collected agarose beads using flow cytometry.

Note: It is also possible to observe the beads under a fluorescence microscope.

3. Representative results

For our experiments, we used a 3-inlet PDMS based microfluidic device with the height of 25 microns (Figure 1). In this device setup, we used the outer inlet for flushing the oil with surfactant and the two inner inlets for flushing the aqueous phases with cell suspensions or media. After generation and collection, the droplets were incubated for a couple of hours off chip before downstream analysis using flow cytometry. During the incubation period, serum components present in the media can interact with the surfactant and cause droplets to become unstable and disintegrate. It is therefore important to add an optimized concentration of surfactant to the fluorinated oil. We tested the stability of the monodispersed droplets containing X vivo 15 medium supplemented with 2% human serum with different concentrations of surfactant in fluorinated oil. It can be inferred from Figure 2 that these monodispersed droplets are highly stable for up to 24 hours when at least 3% surfactant is added to the oil phase. Similar results were obtained with RPMI media with and without the addition of 10% FCS (data not shown). Therefore, droplet stability is highly dependent on optimal surfactant concentrations when working with different sources of culture media and serum components.

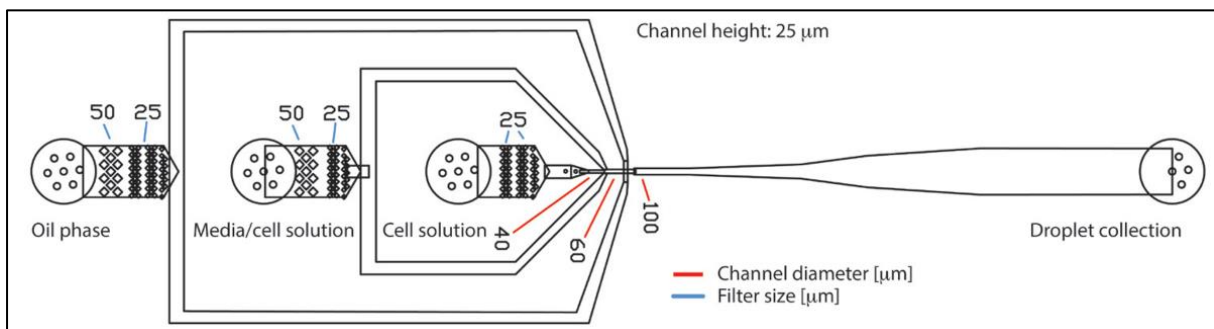


Figure 1. PDMS based droplet microfluidic device with three inlets and one outlet. The device consists of three inlets for continuous oil phase, cell culture media, and cell suspension, respectively. The generated droplets are collected at the outlet. The samples flow lamarily to the flow-focusing junction where they are encapsulated in droplets. At the inlets, filter structures hold large particles like protein or cell aggregates back. The diameter of the gaps in the filter structure are indicated by blue lines. The diameter of the channels at the production nozzle are indicated by red lines. The channel height on the entire chip was 25 μm .

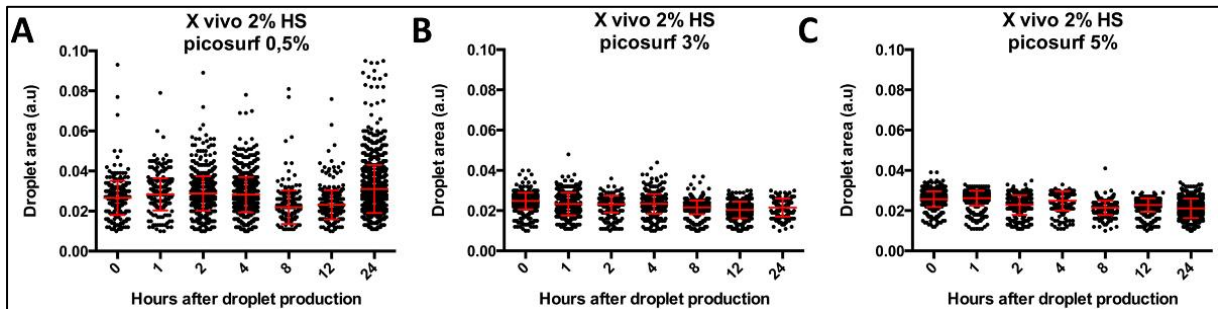


Figure 2. Droplet stability over 24 hours. The graphs show the area of droplets containing *X vivo* 15 + 2 % human serum, over time for three different concentrations of surfactant **A.** 0.5% **B.** 3% **C.** 5%.

To demonstrate the encapsulation efficiency of our approach we first seeded the cells using tubing connected to syringes, which is the most conventional approach for seeding cells (Figure 3A). We harvested Jurkat T cells at different concentrations of 1.0E6 cells/mL, 2.0E6 cells/mL, and 4.0E6 cells/mL and obtained an encapsulation efficiency that was lower than predicted values (Figure 3B). At 1.0E6 cells/mL, the fraction of droplets that contained a single cell was 2.5%, which did not increase even upon using higher cell concentrations.

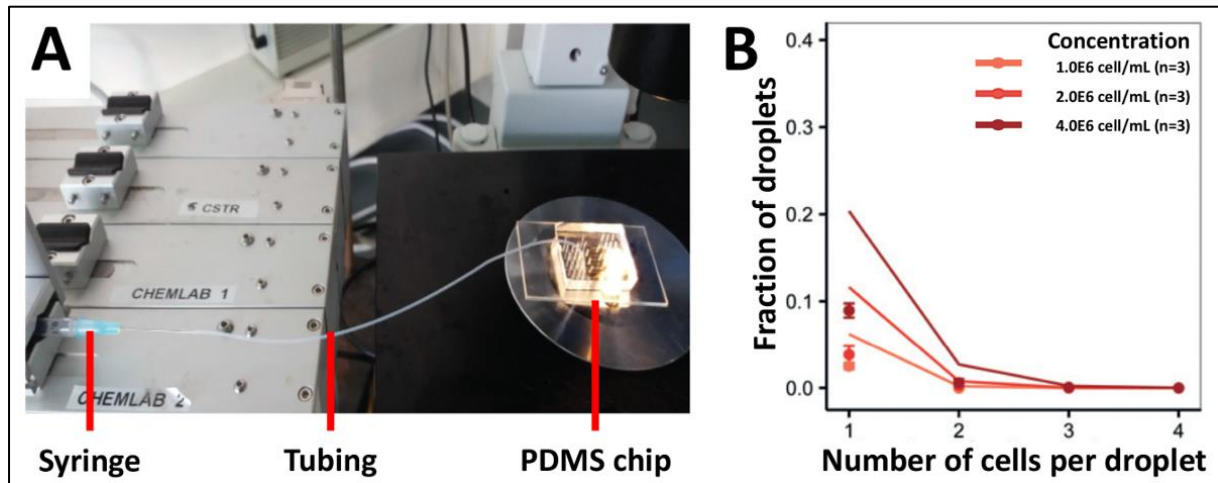


Figure 3. Tubing based cell loading approach. Jurkat-T cells are loaded at different concentrations to the device using a syringe connected to tubing. **A.** The illustration shows the experimental setup. **B.** The cell encapsulation rate as determined by light microscopy. Dots: experimentally determined values; Closed lines: Poisson distribution. Error bar represents standard error of mean.

To increase the cell-loading efficiency, we modified our previous approach and mounted the tubing at half the length to an elevated tripod and loaded the cell suspension in the half that was attached to the PDMS device (Figure 4A). Using this approach, we encapsulated Jurkat T cells at different concentrations of 1.0×10^6 cells/mL, 2.0×10^6 cells/mL, and 4.0×10^6 cells/mL, and also rare pDCs at different concentrations of 1.0×10^6 cells/mL, 2.0×10^6 cells/mL, and 12.0×10^6 cells/mL. We expected improved encapsulation rates by preventing cell sedimentation with this method. However, at all the concentrations tested, the experimental results were much lower than the predicted Poisson values (Figure 4B and Figure 4C).

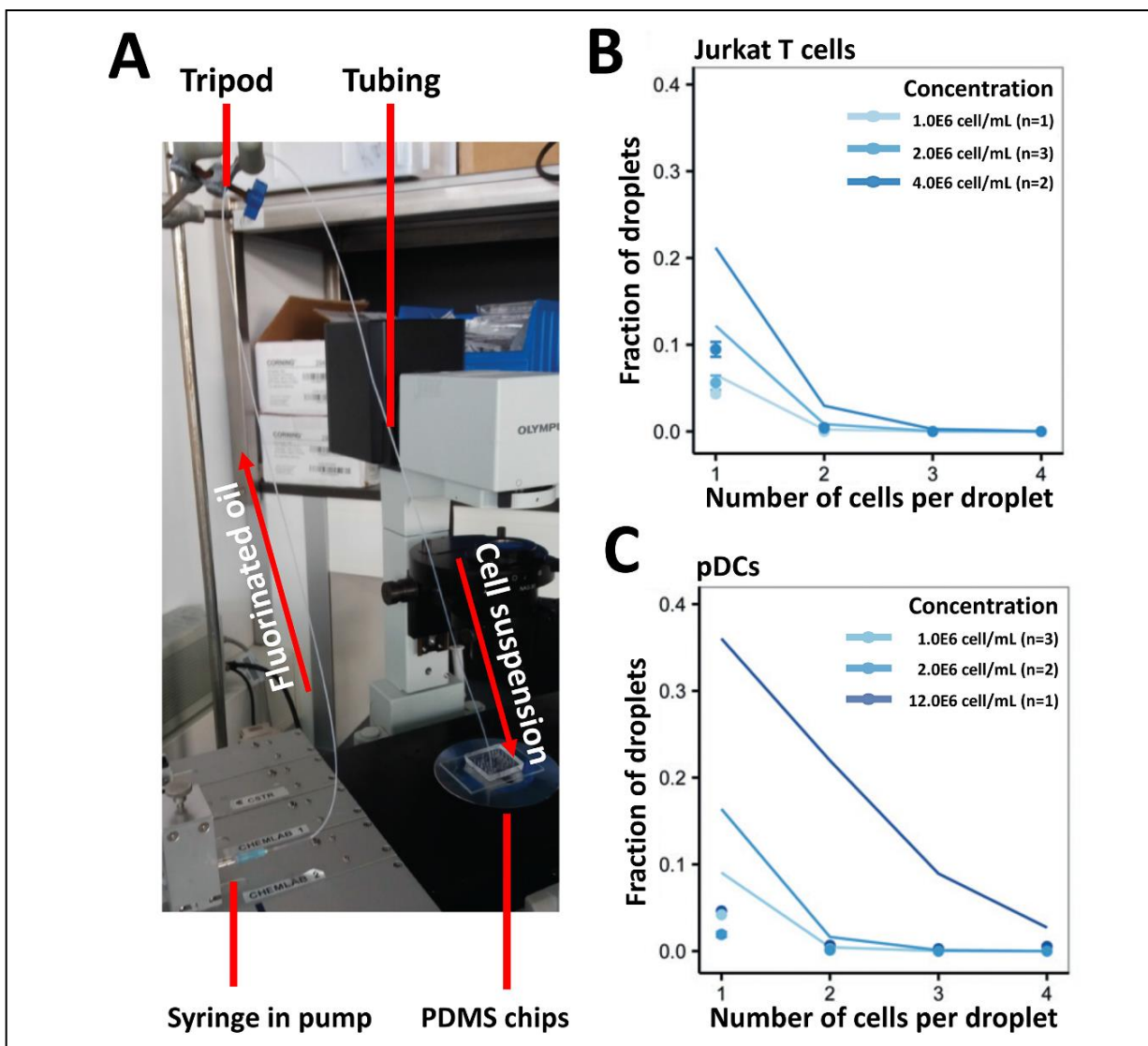


Figure 4. Encapsulation of various cell types at different concentrations using a vertical tube loading approach. Jurkat T cells and pDCs (of different concentrations) were encapsulated to determine the efficiency of cell encapsulation. **A.** The illustration shows the experimental setup for the vertical tube loading approach. **B.** The graph shows the encapsulation efficiency of Jurkat T cells. **C.** The graph shows

the encapsulation efficiency of pDCs. Dots: experimentally determined values; Closed lines: Poisson distribution. Error bar represents standard error of mean.

Using our tip-loading approach we optimized our cell encapsulation rates to obtain experimental results coherent with the statistically predicted values (Figure 5A). For different concentrations of Jurkat T cells, the obtained encapsulation efficiency matched our calculated values at all concentrations (Figure 5B). Remarkably, even with adherent cells like A549 tumor cells, which tend to clump, we observed a slightly improved encapsulation efficiency at a cellular concentration of 1.0×10^6 cells/mL (Figure 5C). We also assessed the efficacy of our system to encapsulate less available and scarce pDCs at different cell concentrations of 1.3×10^6 cells/mL, 3.0×10^6 cells/mL, and 13.0×10^6 cells/mL (Figure 5D). To facilitate the loading of possibly larger volumes exceeding 200 μ L, e.g when working with cell lines or more abundant primary immune cells, we also investigated the cell encapsulation efficiency by using 1000 μ L tips (blue). We demonstrated that these 1000 μ L tips gave a similar encapsulation efficiency in comparison to the 200 μ L tips (yellow) (Figure 5E).

Dependent on the chip design and research question at hand, our tip loading technique can be used to load cells through either one inlet, for probing into cellular heterogeneity, or multiple inlets in parallel, for decoding cellular interactions. We compared the loading of Jurkat T cells (at a final concentration of 10.0×10^6 cells/mL) from one inlet to two differently labeled populations of Jurkat T cells (at a final concentration of 10.0×10^6 cells/mL) from two inlets (Figure 6A and Figure 6B). During encapsulation, the droplets were generated using ultra-low gelling temperature agarose and gelled after production to form agarose hydrogel beads that allowed subsequent downstream analysis via microscopy and flow cytometry (Figure 6C and Figure 6D). Microscopic analysis revealed that cell pairing was achieved at different combinations indicating for high throughput cell pairing (Figure 6C). Furthermore, analysis of the same population of hydrogel beads by flow cytometry revealed that beads without cells could be separated from beads with cells based on the distinct forward (FSC, size) and sideward (SSC, granularity) scatter pattern (Figure 6D). Gating on the population of beads without cells confirmed a lack of cell encapsulation by the absence of fluorescent signals. Additionally, gating on the bead population with cells revealed the existence of multiple sub-populations indicative for the encapsulation of differently labeled Jurkat T cells. Our results demonstrate that efficient cell pairing can be achieved, based on both microscopic

and flow cytometric analysis, and showed a slightly increased encapsulation efficiency compared to the Poisson prediction (Figure 6E).

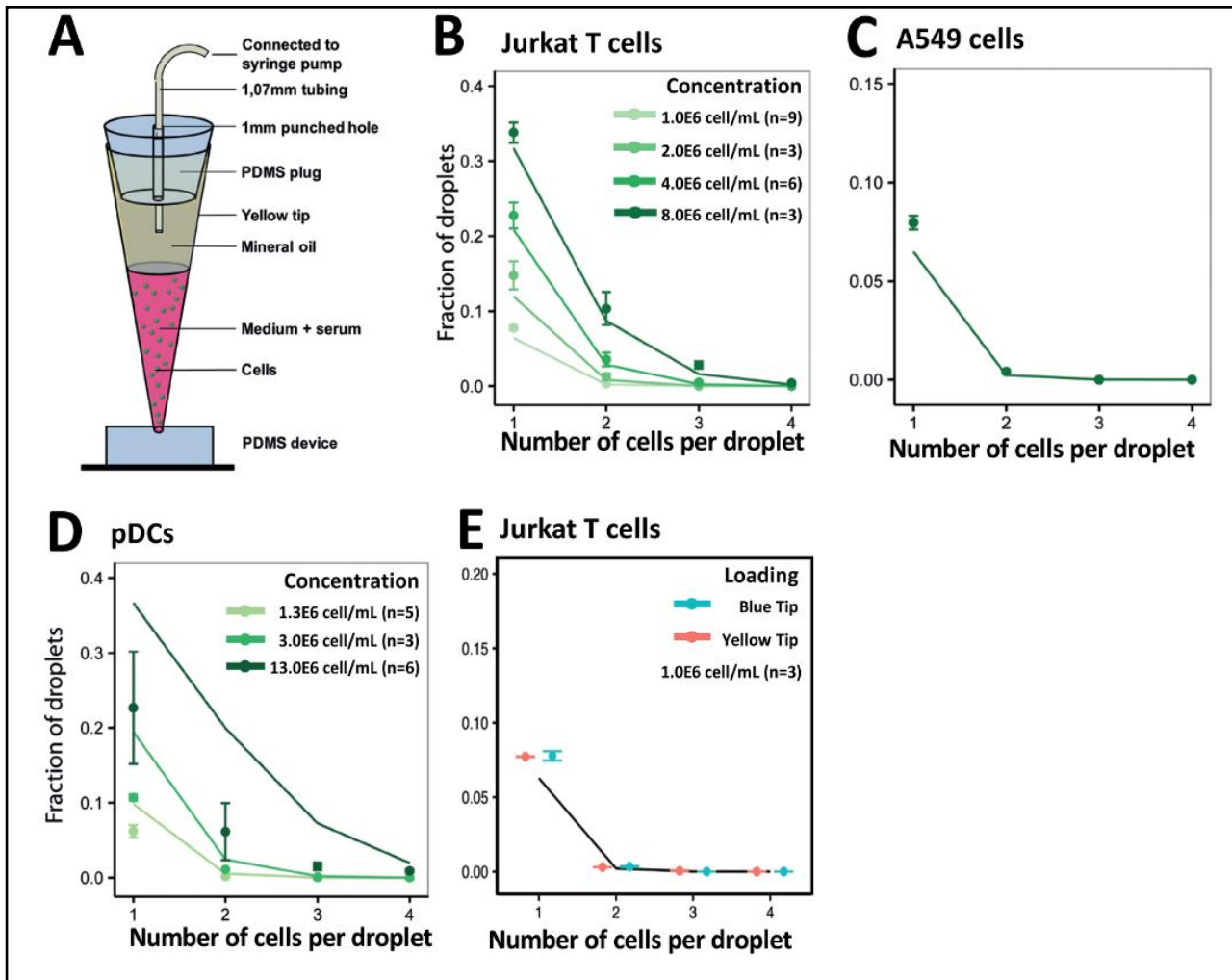


Figure 5. Tip loading approach to encapsulate different cells types. **A.** Schematic illustration of the tip loading technique. **B.** The graph shows the encapsulation efficiency of Jurkat cells. **C.** The graph shows the encapsulation efficiency of A549 cells. **D.** The graph shows the encapsulation efficiency of pDCs. **E.** The graph shows the encapsulation efficiency of Jurkat T cells using 200 μ L pipette tips (yellow) and 1,000 μ L pipette tips (blue). Dots: experimentally determined values; Closed lines: Poisson distribution. Error bar represents standard error of mean.

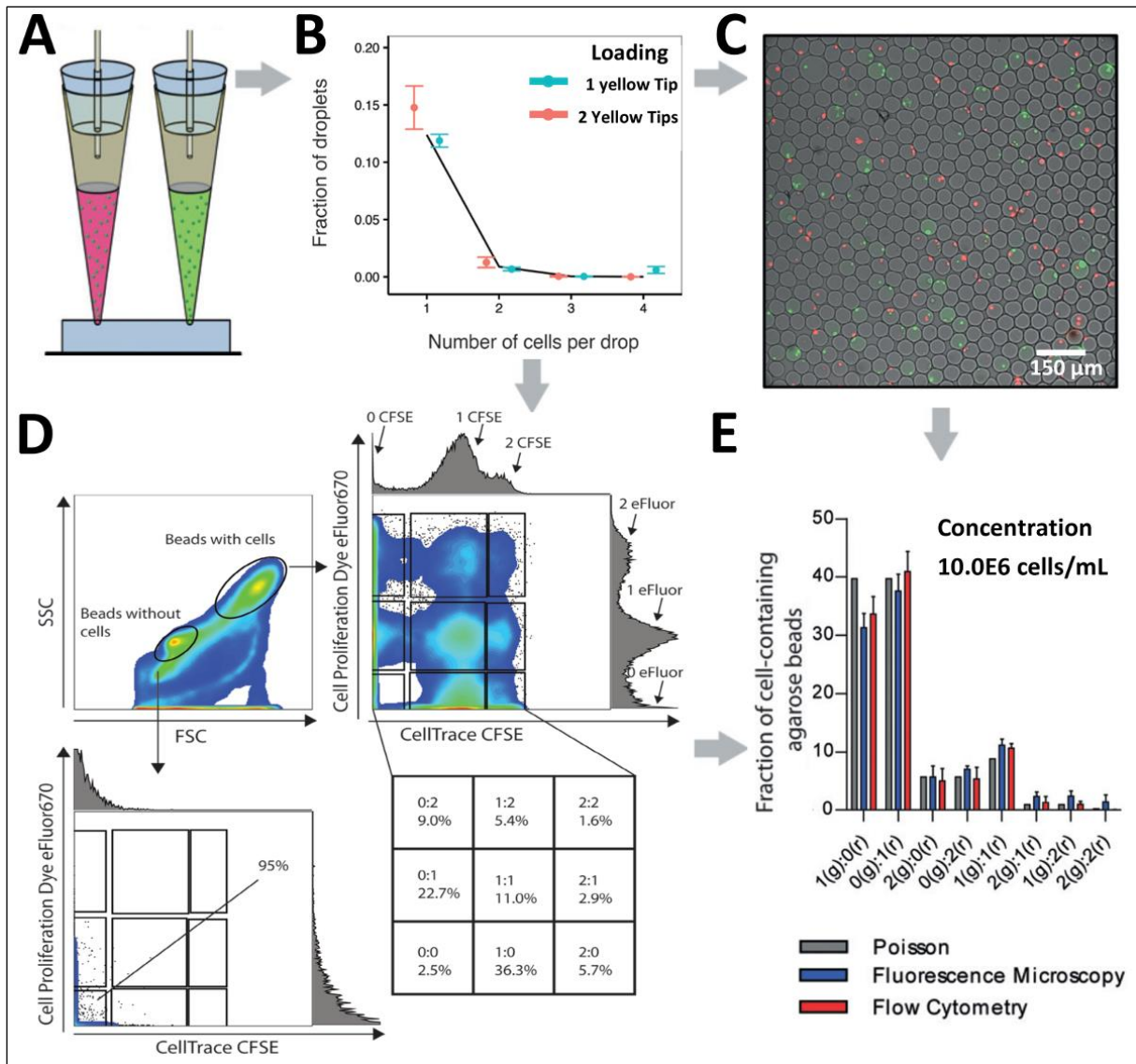


Figure 6. Cell pairing in droplets. **A.** Schematic illustration of the tip loading approach for pairing distinct cells from 2 inlets in droplets. **B.** The graph shows the encapsulation of Jurkat T cells using one inlet or two inlets in parallel. The cell concentration for one tip is 20×10^6 cells/mL and the cell concentration used for two tips both 10×10^6 cells/mL maintaining the final concentration of 10×10^6 cells/mL in both the setups. Dots: experimentally determined values; Closed lines: Poisson distribution. **C.** The Fluorescence microscopic overlays of hydrogel beads and labelled Jurkat T cells. **D.** The graph shows the flow cytometric analysis of paired cells in agarose hydrogel beads. The plot demonstrates both forward scatter and sideward scatter. **E.** Comparison of cell numbers in agarose hydrogel beads as detected by fluorescence microscopy and flow cytometry. Bars: mean value; Whiskers: standard error of mean, $n \geq 4$. Error bar represents standard error of mean.

4. Discussion

In this protocol, we have demonstrated an efficient and straightforward technique to load and encapsulate cells in droplets for high-throughput, single-cell analysis and to perform controlled cell pairing for cellular interaction studies. Furthermore, we have compared several conventional approaches to load cells to microfluidic devices and showed that our tip loading approach is a more efficient technique in comparison to other methods.

Studying clinical specimens or rare cell types scarce in number by droplet based microfluidics possess some inherent challenges. Like we have also demonstrated, cells tend to sediment in syringes and surface of the tubing, thereby, preventing cellular encapsulation to conform to the predicted values. To evade this problem, some groups use stirring bars in the syringes. However, when using rare and limited cell populations, the total cell volume is also limited, thereby, limiting the use of large syringes and stirring bars. Furthermore, we also replaced more commonly used tubing with Teflon coated tubing to prevent cell attachment but this method did not improve the results and if the tubing is too long, the problem of cell attachment aggravates (data not shown). Alternatively, we used a vertical tube loading approach where the cells were loaded in the tubing and not in the syringe to prevent the loss of cells in large syringe volumes. Using this technique, cells with small sample volume can be loaded, e.g. pDCs which are rare and limited. Also, the sample from the tubing is loaded to the device vertically to prevent cell sedimentation. The tubing used for cell seeding has small dimensions and can be compared to microchannels. The flow in the tubing is pressure driven and follows a parabolic velocity profile[26]. This implies that the maximum flow velocity is at the center of the tubing and minimum velocity is at the edges of the tubing [27]. When flushing a population of cells through the tubing, the velocity gradient causes the cells to be pushed towards the edges where they settle down because the velocity at the boundary is close to zero. The sedimentation or settlement of cells in the tubing, thereby, reduces the encapsulation efficiency as shown in the representative results where the experimental data did not match with the predicted model.

Another commonly adopted solution used by scientists, working with droplet microfluidics, is to increase the density of the cell culture media by addition of density matching reagents such as Iodinaxol to prevent cell sedimentation in syringes[19]. However, density matching

reagents can influence cellular behavior and adversely affect the cytokine secretion by cells (data not shown)[28].

Even though several small and big modifications in conventional cell loading techniques showed slight improvements in encapsulation efficiencies, the obtained experimental results still did not match the theoretical calculations. However, with the tip loading approach we could overcome the limitations of previous methods and encapsulation efficiency governed by Poisson statistics. This technique is not only advantageous for loading suspension cells but can also be applied for loading adherent cells, such as primary keratinocytes and A549 to microfluidic chips. When using abundant cell lines, for example A549, K562 etc., larger sample volume can be used.

Therefore, depending on the volume of the sample, different sized pipette-tips can also be used and this simple technique can be adapted for both single-cell encapsulation and multiple cell encapsulation.

While low cell concentration is required to ensure the encapsulation of single cells in droplets, higher cells concentrations are desired to increase the average number of cells encapsulated in each droplet for studies related to cell pairing. There are several single-cell methods that have been previously described to pair immune cells on microfluidic chips or microfabricated nanowells[29–31]. In droplet microfluidics, Poisson statistics dictates that 1:1 cell pairing for two different cell types can be achieved at optimal cell concentrations. Based on the Poisson prediction, there is also a probability that droplets might contain other combinations. While 1:1 cell pairing can be desirable to study cellular interactions at single cell level and results in increased cellular understanding, multiple cell pairing also has major advantages. It allows to comprehend the influence of multiple cells of one cell type on the other cell type. Cross talk between different immune cells help to generate an effective immune response against several infections and pathogens and also adds robustness to our immune system[32]. As such, cellular communication can be interrogated with high precision in distinct contexts, e.g. 1:1, 2:1, 1:2, 2:2, 3:1, etcetera yielding increased understanding on how single or pairs of cells control the induction of immune responses. This is particularly interesting to study for example the capacity of natural killer cells or cytotoxic T cells to serially kill their respective target cells.

As discussed, for multiple encapsulation of cells in droplets, higher cell concentrations are desired. However, when loading cells from one inlet for cell encapsulation, higher concentrations of cell sample can cause cells to aggregate at the inlet. This results in lower encapsulation rates and higher deviation from the theoretical values. To evade this problem, the cells can be loaded from two separate inlets as well. Theoretically, it would be possible to develop other microfluidic devices with multiple inlets to achieve even higher levels of cell encapsulation where an average on x number of cells is warranted. In this study we investigated the encapsulation efficiency of Jurkat T cells when loaded from both one inlet and two inlets using the same total concentration and obtained similar encapsulation efficiency. This modification allows researchers to pair different cell types on chip.

While this method aids in loading cells to microfluidic devices without significant loss of cells, there are certain precautions that need to be kept in mind. When filling the syringes with mineral oil and aspirating the cell sample in pipette tips, incorporation of air bubbles should be avoided and the entire system should be air-free. It is also important to keep in mind that the mineral oil should not mix with the sample. Pipette tips, containing samples, should be inserted firmly in the inlets of the microfluidic device, with utmost precaution, to prevent leakage and further incorporation of air bubbles. To summarize, tip-loading is a straightforward, yet, robust technique that allows for high-throughput analysis of cellular behavior through cell encapsulation without significant loss of cells in a cost-effective manner. When used with optimal sample concentrations at the inlet, this approach of loading cells with pipette-tips is very flexible and can be adapted for different cell types, especially for rare primary immune cells, to obtain higher encapsulation efficiency, close to predicted models.

5. Acknowledgments:

We thank the Eindhoven University of Technology for generous support.

6. References

- [1] H. Yin, D. Marshall, *Microfluidics for single cell analysis*, *Curr. Opin. Biotechnol.* 23 (2012) 110–119. <https://doi.org/10.1016/j.copbio.2011.11.002>.
- [2] I. Meyvantsson, D.J. Beebe, *Cell Culture Models in Microfluidic Systems*, *Annu. Rev. Anal. Chem.* 1 (2008) 423–429. <https://doi.org/10.1007/s13398-014-0173-7.2>.
- [3] C. Yi, C.W. Li, S. Ji, M. Yang, *Microfluidics technology for manipulation and analysis of biological cells*, *Anal. Chim. Acta.* 560 (2006) 1–23. <https://doi.org/10.1016/j.aca.2005.12.037>.
- [4] H.Y. Wang, N. Bao, C. Lu, *A microfluidic cell array with individually addressable culture chambers*, *Biosens. Bioelectron.* 24 (2008) 613–617. <https://doi.org/10.1016/j.bios.2008.06.005>.
- [5] Y. Zhang, Y.P. Ho, Y.L. Chiu, H.F. Chan, B. Chlebina, T. Schuhmann, L. You, K.W. Leong, *A programmable microenvironment for cellular studies via microfluidics-generated double emulsions*, *Biomaterials.* 34 (2013) 4564–4572. <https://doi.org/10.1016/j.biomaterials.2013.03.002>.
- [6] S.-Y. Teh, R. Lin, L.-H. Hung, A.P. Lee, *Droplet microfluidics*, *Lab Chip.* 8 (2008) 198–220. <https://doi.org/10.1039/b715524g>.
- [7] H. Hu, D. Eustace, C.A. Merten, H.N. Joensson, M.L. Samuels, E.R. Brouzes, M. Medkova, M. Uhlen, D.R. Link, H. Andersson-Svahn, E. Brouzes, M. Medkova, N. Savenelli, D. Marran, M. Twardowski, J.B. Hutchison, J.M. Rothberg, D.R. Link, N. Perrimon, M.L. Samuels, B. El Debs, R. Utharala, I. V. Balyasnikova, A.D. Griffiths, C.A. Merten, M. Najah, R. Calbrix, I.P. Mahendra-Wijaya, T. Beneyton, A.D. Griffiths, A. Drevelle, D.J. Eastburn, A. Sciambi, A.R. Abate, K. Leung, H. Zahn, T. Leaver, K.M. Konwar, N.W. Hanson, A.P. Page, C.C. Lo, P.S. Chain, S.J. Hallam, C.L. Hansen, A.M. Klein, L. Mazutis, I. Akartuna, N. Tallapragada, A. Veres, V. Li, L. Peshkin, D.A. Weitz, M.W. Kirschner, E. Traggiai, S. Becker, K. Subbarao, L. Kolesnikova, Y. Uematsu, M.R. Gismondo, B.R. Murphy, R. Rappuoli, A. Lanzavecchia, H. Hu, J. Voss, G. Zhang, P. Buchy, T. Zuo, L. Wang, F. Wang, F. Zhou, G. Wang, C. Tsai, L. Calder, S.J. Gambin, L. Zhang, V. Deubel, B. Zhou, J.J. Skehel, P. Zhou, S.N. Christo, K.R. Diener, R.E. Nordon, M.P. Brown, H.J. Griesser, K. Vasilev, F.C. Christo, J.D. Hayball, B. Dura, S.K. Dougan, M. Barisa, M.M. Hoehl, C.T. Lo, H.L. Ploegh, J. Voldman, J. Clausell-Tormos, D. Lieber, J.C. Baret, A. El-Harrak, O.J. Miller, L. Frenz, J. Blouwolf, K.J. Humphry, S. Koster, H. Duan, C. Holtze, D.A. Weitz, A.D. Griffiths, C.A. Merten, E.W.M. Kemna, R.M. Schoeman, F. Wolbers, I. Vermes, D.A. Weitz, A. van den Berg, A.R. Abate, C.H. Chen, J.J. Agresti, D.A. Weitz, T.P. Lagus, J.F. Edd, Z.N. Cao, F.Y. Chen, N. Bao, H.C. He, P.S. Xu, S. Jana, S.H. Jung, H.Z. Lian, C. Lu, C.M. Edwards, S. Heptinstall, K.C. Lowe, J.C. Baret, S.P. Andrews, G.A. Brown, J.A. Christopher, S.A. Voloshin, A.S. Kaprelyants, C. Ma, R. Fan, H. Ahmad, Q.H. Shi, B. Comin-Anduix, T. Chodon, R.C. Koya, C.C. Liu, G.A. Kwong, C.G. Radu, A. Ribas, J.R. Heath, M. Abonnenc, M. Borgatti, E. Fabbri, R. Gavioli, C. Fortini, F. Destro, L. Altomare, N. Manaresi, G. Medoro, A. Romani, M. Tartagni, E. Lo Monaco, P. Giacomini, R. Guerrieri, R. Gambari, A. Zeleznik, S. Andrejev, O. Ponomarova, D.R. Mende, P. Bork, K.R. Patil, *Efficient cell pairing in droplets using dual-color sorting*, *Lab Chip.* 15 (2015) 3989–3993. <https://doi.org/10.1039/C5LC00686D>.
- [8] E. Brouzes, M. Medkova, N. Savenelli, D. Marran, M. Twardowski, J.B. Hutchison, J.M. Rothberg, D.R. Link, N. Perrimon, M.L. Samuels, *Droplet microfluidic technology for single-cell high-throughput screening*, *Proc. Natl. Acad. Sci.* 106 (2009) 14195–14200. <https://doi.org/10.1073/pnas.0903542106>.
- [9] V. Chokkalingam, J. Tel, F. Wimmers, X. Liu, S. Semenov, J. Thiele, C.G. Figdor, W.T.S. Huck, *Probing cellular heterogeneity in cytokine-secreting immune cells using droplet-based microfluidics*, *Lab Chip.* 13 (2013) 4740. <https://doi.org/10.1039/c3lc50945a>.
- [10] J.M.M. den Haan, R. Arens, M.C. van Zelm, *The activation of the adaptive immune system: Cross-talk between antigen-presenting cells, T cells and B cells*, *Immunol. Lett.* 162 (2014) 103–112. <https://doi.org/10.1016/j.imlet.2014.10.011>.
- [11] G.J. Shah, A.T. Ohta, E.P.-Y. Chiou, M.C. Wu, C.-J. “CJ” Kim, *EWOD-driven droplet microfluidic device integrated with optoelectronic tweezers as an automated platform for cellular isolation and analysis*, *Lab Chip.* 9 (2009) 1732. <https://doi.org/10.1039/b821508a>.
- [12] A.D. Griffiths, D.S. Tawfik, *Miniaturising the laboratory in emulsion droplets*, *Trends Biotechnol.* 24 (2006) 395–402. <https://doi.org/10.1071/MF05190>.
- [13] T.P. Lagus, J.F. Edd, *High-throughput co-encapsulation of self-ordered cell trains: cell pair interactions in microdroplets*, *RSC Adv.* 3 (2013) 20512. <https://doi.org/10.1039/c3ra43624a>.

Chapter 2- A pipette tip-based method for cell loading on chip

- [14] S.J. Moon, E. Ceyhan, U.A. Gurkan, U. Demirci, Statistical modeling of single target cell encapsulation, *PLoS One*. 6 (2011). <https://doi.org/10.1371/journal.pone.0021580>.
- [15] A.R. Abate, C.H. Chen, J.J. Agresti, D.A. Weitz, Beating Poisson encapsulation statistics using close-packed ordering, *Lab Chip*. (2009). <https://doi.org/10.1039/b909386a>.
- [16] D.J. Collins, A. Neild, A. deMello, A.-Q. Liu, Y. Ai, The Poisson distribution and beyond: methods for microfluidic droplet production and single cell encapsulation, *Lab Chip*. 15 (2015) 3439–3459. <https://doi.org/10.1039/C5LC00614G>.
- [17] E.W.M. Kemna, R.M. Schoeman, F. Wolbers, I. Vermes, D.A. Weitz, A. Van Den Berg, High-yield cell ordering and deterministic cell-in-droplet encapsulation using Dean flow in a curved microchannel, *Lab Chip*. (2012). <https://doi.org/10.1039/c2lc00013j>.
- [18] S. Köster, F.E. Angilè, H. Duan, J.J. Agresti, A. Wintner, C. Schmitz, A.C. Rowat, C.A. Merten, D. Pisignano, A.D. Griffiths, D.A. Weitz, Drop-based microfluidic devices for encapsulation of single cells, *Lab Chip*. 8 (2008) 1110. <https://doi.org/10.1039/b802941e>.
- [19] L. Mazutis, J. Gilbert, W.L. Ung, D.A. Weitz, A.D. Griffiths, J.A. Heyman, Single-cell analysis and sorting using droplet-based microfluidics, *Nat. Protoc.* (2013). <https://doi.org/10.1038/nprot.2013.046>.
- [20] P. Sun, S. Fernandez, M.A. Marovich, D.R. Palmer, C.M. Celluzzi, K. Boonnak, Z. Liang, H. Subramanian, K.R. Porter, W. Sun, T.H. Burgess, Functional characterization of ex vivo blood myeloid and plasmacytoid dendritic cells after infection with dengue virus, *Virology*. 383 (2009) 207–215. <https://doi.org/10.1016/j.virol.2008.10.022>.
- [21] J. Tel, S. V. Hato, R. Torensma, S.I. Buschow, C.G. Figdor, W.J. Lesterhuis, I.J.M. De Vries, The chemotherapeutic drug oxaliplatin differentially affects blood DC function dependent on environmental cues, *Cancer Immunol. Immunother.* 61 (2012) 1101–1111. <https://doi.org/10.1007/s00262-011-1189-x>.
- [22] F. Wimmers, N. Subedi, N. van Buuringen, D. Heister, J. VIVIÉ, I. Beeren-Reinieren, R. Woestenenk, H. Dolstra, A. Piruska, J.F.M. Jacobs, A. van Oudenaarden, C.G. Figdor, W.T.S. Huck, I.J.M. de Vries, J. Tel, Single-cell analysis reveals that stochasticity and paracrine signaling control interferon-alpha production by plasmacytoid dendritic cells, *Nat. Commun.* (2018). <https://doi.org/10.1038/s41467-018-05784-3>.
- [23] J. Gong, C.-J. “CJ” Kim, All-electronic droplet generation on-chip with real-time feedback control for EWOD digital microfluidics, *Lab Chip*. 8 (2008) 898. <https://doi.org/10.1039/b717417a>.
- [24] U. Demirci, G. Montesano, Single cell epitaxy by acoustic picolitre droplets, *Lab Chip*. (2007). <https://doi.org/10.1039/b704965j>.
- [25] H.S. Rho, Y. Yang, H.-Willem Veltkamp, H. Gardeniers, Direct Delivery of Reagents from a Pipette Tip to a PDMS Microfluidic Device, *Chips Tips*. (2015).
- [26] P.H. Paul, M.G. Garguilo, D.J. Rakestraw, Imaging of Pressure- And Electrokinetically Driven Flows through Open Capillaries, *Anal. Chem.* 70 (1998) 2459–2467. <https://doi.org/10.1021/ac9709662>.
- [27] G.M. Whitesides, A.D. Stroock, Flexible methods for microfluidics, *Phys. Today*. 54 (2001) 42. <https://doi.org/10.1063/1.1387591>.
- [28] A. Mita, C. Ricordi, S. Messinger, A. Miki, R. Misawa, S. Barker, R.D. Molani, R. Haertter, A. Khan, S. Miyagawa, A. Pileggi, L. Inverardi, R. Alejandro, B.J. Hering, H. Ichii, Anti-proinflammatory Effects of Iodixanol (OptiPrep)-Based Density Gradient Purification on Human Islet Preparations, *Cell Transpl.* 19 (2013) 1537–1546. <https://doi.org/10.3727/096368910X516600.Anti-proinflammatory>.
- [29] B. Dura, S.K. Dougan, M. Barisa, M.M. Hoehl, C.T. Lo, H.L. Ploegh, J. Voldman, Profiling lymphocyte interactions at the single-cell level by microfluidic cell pairing, *Nat. Commun.* (2015). <https://doi.org/10.1038/ncomms6940>.
- [30] B. Dura, M.M. Servos, R.M. Barry, H.L. Ploegh, S.K. Dougan, J. Voldman, Longitudinal multiparameter assay of lymphocyte interactions from onset by microfluidic cell pairing and culture, *Proc. Natl. Acad. Sci.* 113 (2016) E3599–E3608. <https://doi.org/10.1073/pnas.1515364113>.
- [31] Y.J. Yamanaka, C.T. Berger, M. Sips, P.C. Cheney, G. Alter, J.C. Love, Single-cell analysis of the dynamics and functional outcomes of interactions between human natural killer cells and target cells, *Integr. Biol. (United Kingdom)*. (2012). <https://doi.org/10.1039/c2ib20167d>.
- [32] R. Satija, A.K. Shalek, Heterogeneity in immune responses: From populations to single cells, *Trends Immunol.* 35 (2014) 219–229. <https://doi.org/10.1016/j.it.2014.03.004>.

The background of the page is a grayscale microfluidic chip with a grid of circular wells. Each well contains a cell, which is stained with various colors: blue for the nucleus, yellow for the cytoplasm, and red for specific organelles or markers. The cells are arranged in a regular pattern across the chip.

CHAPTER 3

AN AUTOMATED REAL-TIME MICROFLUIDIC PLATFORM TO PROBE SINGLE NK CELL HETEROGENEITY AND CYTOTOXICITY ON-CHIP

This chapter is published as:

An automated real-time microfluidic platform to probe single NK cell heterogeneity and cytotoxicity on-chip

Nikita Subedi, Laura C. Van Eyndhoven, Ayla M. Hokke, Lars Houben , Mark C. Van Turnhout, Carlijn V.C. Bouten, Klaus Eyer, Jurjen Tel

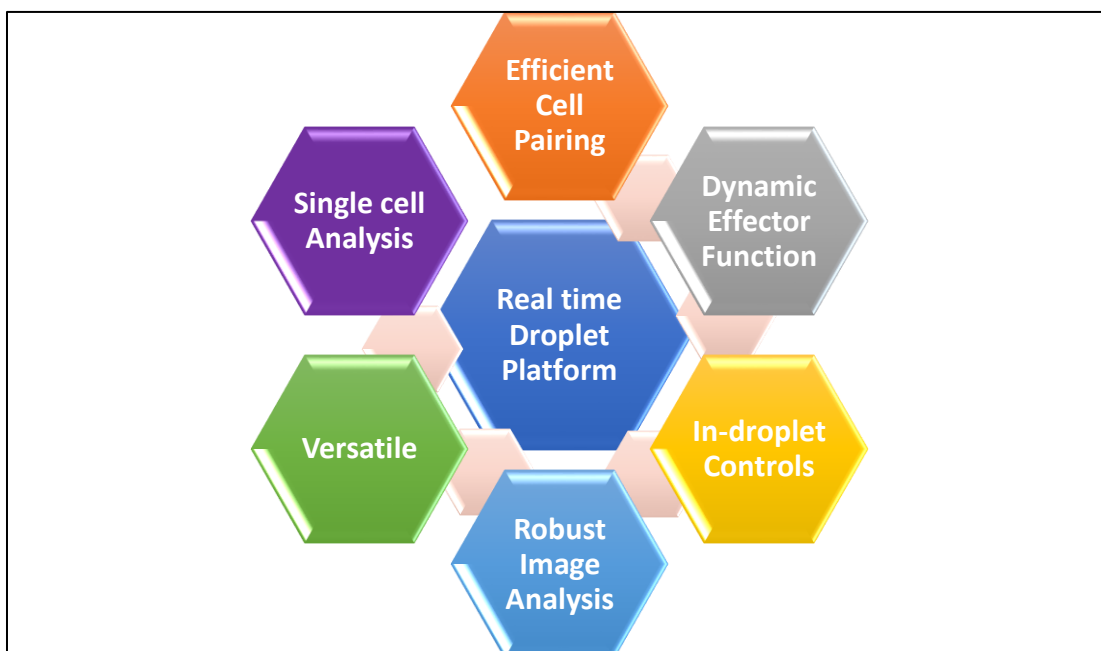
Scientific Reports; 17084

Published: August 24, 2021

Abstract

Cytotoxicity is a vital effector mechanism used by immune cells to combat pathogens and cancer cells. While conventional cytotoxicity assays rely on averaged end-point measures, crucial insights on the dynamics and heterogeneity of effector and target cell interactions cannot be extracted, emphasizing the need for dynamic single-cell analysis. Here, we present a fully automated droplet-based microfluidic platform that allowed the real-time monitoring of effector-target cell interactions and killing, allowing the screening of over 60,000 droplets identifying 2000 individual cellular interactions monitored over 10 hours. During incubation, we observed that the dynamics of cytotoxicity within the Natural Killer (NK) cell population varies significantly over the time. Around 20% of the total NK cells in droplets showed positive cytotoxicity against paired K562 cells, most of which was exhibited within first four hours of cellular interaction. Using our single cell analysis platform, we demonstrated that the population of NK cells is composed of individual cells with different strength in their effector functions, a behavior masked in conventional studies. Moreover, the versatility of our platform will allow the dynamic and resolved study of interactions between immune cell types and the finding and characterization of functional sub-populations, opening novel ways towards both fundamental and translational research.

Graphical Abstract



1. Introduction

The human immune system operates in an intricate environment that involves a complex and coordinated system to identify and eliminate threats. Since both pathogens and tumour cells can be highly variable, the immune system evolved into a highly heterogeneous, but tightly regulated system[1]. Traditionally, the diversity in immune cell populations is characterised predominantly by differences in morphology and expression of static markers. However, cellular effector functions, such as migration of immune cells to the site of infection, release of cytokines, or cytolytic activity, also exhibit enormous variation between and among well-defined cellular subsets, such as the cytolytic heterogeneity observed in NK cells[2,3]. Although several studies have highlighted how heterogeneity is a hallmark of immune system and plays an important role in shaping the overall immune response, the functional aspects of cellular heterogeneity remain largely unexplored[4]. So far, the majority of both *in vivo* animal models and *in vitro* experiments mainly only yielded an averaged outcome as a consequence of the interactions between multiple cells, rather than providing functional readouts of single-activated cells. Additionally, the current systems that can provide functional readout of individual cells either lack throughput or fail to isolate individual cell pairs to exclude possible effects of paracrine signalling. Since a well-functioning immune response is the result of combined efforts of multiple, and diverse individual cells, understanding heterogeneity within immune cell populations is crucial for a better understanding of the overall immune response and the effector functions in a cell population. Cytotoxicity is an important effector mechanism used by Cytotoxic T cells (CTLs) and Natural Killer (NK) cells to combat both pathogens and tumour cells. Cytotoxicity assays are essential to understand the functional activation and cytolytic impact of individual effector cells towards various target cells, including heterogeneous tumours. For decades, the gold standard to assess immune cell-mediated cytotoxicity used to be the chromium release assay, where the release of radioactive ^{51}Cr by dying target cells is indicative for specific lysis[5]. While quantitative and precise, this method requires the handling and disposal of radioactive compounds. Recently, several other alternative approaches have been developed, e.g. fluorescent probes to detect cell viability[6], metabolic MTT assay[7], enzyme-based LDH assays[8], and luciferase transduced cell-based bioluminescence assays[9]. Even though these assays have provided insight into fundamental cellular behaviour, these studies are performed

in bulk and generate averaged responses[10]. Bulk-based studies fail to address the functional heterogeneity underlying a given cell population by masking the phenotype, gene expression, and the mechanism of cellular communication in between individual immune cells[11,12]. To overcome the limitations of bulk methodologies, the study of cytotoxicity at a single-cell level can be performed using flow cytometry-based assays and single cell microscopy assays[13,14]. However, flow cytometric assays are snapshot-based and therefore not suited to monitor temporal dynamics of cellular interactions leading to cytotoxicity[10]. Besides, single cell microscopy systems average out the overall population dynamics by allowing paracrine signalling to steer individual cell behaviours[1].

Advances in technology and miniaturization yielded microsystem-based technologies that aim to overcome the limitations of conventional and flow cytometry-based assays[15,16]. These technologies enhanced the sensitivity of measurements, allowing the investigation of lower cell numbers using reduced reagent volumes. However, a major challenge of adopting microsystem technologies for interaction-based assays is the efficient pairing of effector and target cells[17]. Despite the numerous attempts to overcome this challenge, a novel approach that meets the requirements is a necessity.

Here we present a droplet-based microfluidic platform that, in conjunction with real-time fluorescence microscopy and an automated image analysis script, enables high-throughput monitoring of over 60,000 droplets therefore allowing to analyse around 20,000 droplets with cells. Droplet-based microfluidics is highly tuneable and provides the opportunity to pair cells in a compartmentalized and noise-free microenvironment[18–21]. The cellular encapsulation and pairing can be precisely controlled to achieve different effector:target ratios[22]. By studying the interaction between NK cells and different target tumour cells we present the possibility to study the underlying dynamics of cytotoxicity. Our data reveals heterogenous NK cell behaviour with a consistent percentage of the population displaying cytolytic abilities.

2. Materials and methods

2.1 Cell isolation and culture

K562 cells were cultured in 1:1 (v/v) mixture of RPMI 1640 (Gibco, Catalog no. 22400089) and IMDM (Gibco, Catalog no.12440053) supplemented with 10% fetal bovine serum (FBS; Gibco) and 1% penicillin/streptomycin (PS; Gibco). Jurkat T cells were cultured in RPMI, supplemented with 10% FBS and 1% PS. Both cell lines were regularly tested for mycoplasma contamination. Primary NK cells were obtained from buffy coats of healthy donors (Sanquin) after written informed consent according to the Declaration of Helsinki and all experimental protocols concur to institutional guidelines. In short, peripheral blood mononuclear cells (PBMCs) were isolated from donor blood via density gradient centrifugation using Lymphoprep Density Gradient Medium (Stem cell). The NK cells were subsequently isolated using magnet-activated cell sorting (MACS) by negative selection using the NK cell isolation kit (Miltenyi Biotech, Catalog no. 130-092-657) following the manufacturer's instructions. Cells were counted and purity was routinely assessed using flow cytometry by cell surface marker staining for 10 minutes at 4°C, using PE-CY7-labeled anti-CD56 (Biolegend, Catalog no. 362509), PE-labeled anti-CD16 (Biolegend, Catalog no. 302007), and PerCP-labeled anti CD3 (Biolegend, Catalog no. 300328) antibodies in 50 µL FACS buffer (2% FBS in PBS). The NK cells were identified as CD16⁺CD56⁺CD3⁻, and purity was on average 91%. Subsequently, isolated NK cells were encapsulated into droplets with K562 pair in presence of 1400 ng/mL IL2, as stimulant (Peprotech, Catalog no. 200-02) to monitor the cytotoxicity function of NK cells.

2.2 Microfluidic chip for droplet production

The microfluidic device was molded using an SU-8 photo resist structure on a silicon wafer and a commercially available polydimethylsiloxane silicone elastomer (Sylgard 184, Dow Corning), mixed with curing agent at the ratio 10:1 (w/w) and allowed to cure for 3 hours at 60°C. The surface of the Sylgard 184 was activated by exposure to plasma and sealed with a plasma-treated glass cover slide to yield closed micro channels. Channels were subsequently treated with a 5% (v/v) silane (1H,1H,2H,2H-Perfluorooctyltriethoxysilane; Fluorochem, Catalog no. S13150) solution in fluorinated oil (Novec HFE7500, 3M, Catalog no. 51243) and thermally bonded for 12 hours at 60°C. The dimensions of the microfluidic

Chapter 3- An automated real-time microfluidic platform to probe cytotoxicity on chip channels are $40\ \mu\text{m} \times 30\ \mu\text{m}$ at the first inlet, $60\ \mu\text{m} \times 30\ \mu\text{m}$ at the second inlet and the production nozzle, and $100\ \mu\text{m} \times 30\ \mu\text{m}$ at the collection channel (Figure 1B).

2.3 Assembly of Droplet observation chamber

Glass microscopy slides ($76 \times 26 \times 1\ \text{mm}$; Corning) were used as top and bottom covers ($76 \times 26 \times 1\ \text{mm}$). Two access holes of 1.5 mm diameter were drilled in the top glass. Both slides were thoroughly cleaned using soap, water, and ethanol, and were exposed to air plasma (60 W) for 5 minutes. A cutout sheet of $60\ \mu\text{m}$ thick double-sided tape (ORAFOL) was carefully placed above the bottom glass slide. Afterwards, the glass slides were stacked on top of each other, and the assembly was pressed using Atlas Manual 15T Hydraulic Press (Specac) for 5 minutes at 155°C at $400\ \text{kg per m}^2$ pressure load (Supplementary Figure 1). Next, two nano ports (Idex) were attached to the holes using UV curable glue (Loctite 3221 Henkel) which was cured under UV light for 5 min. Subsequently, the surface of the 2D chamber was treated with 5% (v/v) silane solution. Lastly, the chamber was dried, filled with fluorinated oil, and sealed until used. The chamber was reused multiple times and cleaned after each experiment by flushing fluorinated oil to remove droplets and stored filled until the next use.

2.4 Cell Staining

$5\ \mu\text{M}$ Calcein Red AM (AAT Bioquest, Catalog no. 21900) and $10\ \mu\text{M}$ Cell Tracker Blue dyes (Invitrogen, C2110) were used to stain primary NK cells and target cells (K562 or Jurkat), respectively. For staining, around 2 million cells were washed with RPMI free of supplements and Phenol red (Gibco, Catalog no. 11835030), resuspended in the freshly prepared dye solution in-RPMI (1 mL) and incubated at 37°C for 30 min. Thereafter, cells were subsequently washed twice and resuspended in RPMI medium supplemented with 25 mM HEPES (Gibco, Catalog no. 15630056), 2% human serum (Sanquin), without Phenol red containing $2.5\ \mu\text{M}$ Sytox green (Invitrogen, Catalog no. S7020) and $7\ \mu\text{M}$ CellEvent Caspase-3/7 Green Detection Reagent (Invitrogen, Catalog no. C10423), respectively. The stained cells were then proceeded for cell encapsulation.

2.5 Cell loading in microfluidic chip

2.5 mL glass syringe and tubing polytetrafluoroethylene tubing were filled with biocompatible mineral oil (Sigma Aldrich, Catalog no. M8410-1L). The end of the tubing was attached to a PDMS plug of 5 μm diameter, which was then squeezed tightly into the large end of a pipette tip (200 μL). Subsequently, the pipette tip was filled with mineral oil from the syringe. To load cell suspension, the pipette tip was lowered into a cell solution and the syringe pump was used to aspirate the solution into the tip. Finally, the pipette tip was connected tightly to the inlet of a microfluidic chip and droplet production was started. The syringes were driven by computer-controlled syringe pumps (Nemesys, Cetoni GmbH). The droplets of ~ 50 μm diameter were generated using flow speed of 30 $\mu\text{L}/\text{min}$ for oil and 5 $\mu\text{L}/\text{min}$ for each sample inlet. The droplets were produced for around 5 minutes, thus generating 700,000 droplets in total. For the stability of droplets, 2.5% (v/v) Pico-Surf surfactant (Sphere Fluidics, Catalog no. C024) was used in fluorinated oil.

2.6 Single NK cell cytotoxicity assay

Primary NK cells and target cells were loaded into different inlets at the concentration of 7 million cells/mL and 10 million cells/mL, respectively. The viability dyes Sytox Green and Cell Event Caspase-3/7 Green were loaded along with the cells, and droplets were collected in the observation chamber. Droplets were generated at room temperature while collected into the observation chamber over a warm water bath at 37 $^{\circ}\text{C}$. After collection, the droplets were incubated in a stage top incubator (Okolab) set at 5% CO_2 and 37 $^{\circ}\text{C}$ temperature and observed using Nikon Ti2 microscope for 10 hours. The 0h were considered everything after ± 10 mins.

2.7 Image acquisition and analysis

Fluorescence imaging was performed using a Nikon Eclipse Ti2 microscope, using a 10X objective and mCherry, DAPI, and FITC/YFP filters every hour. 15×15 tiles with resolution of 20477×20477 were framed per experiment. The images were viewed using NIS Element and Image J. Automated Image analysis was performed using custom-made in-built MATLAB script (Mathworks), DMALAB (available on request). The script generated droplet mask that was overlaid onto the fluorescence images, and each droplet was analyzed separately. Over 60,000 droplets per experiment were analyzed using this script. The cell

division of the target or effector cell was not considered during the analysis. The output received are in terms of droplet index, cell count, fluorescence intensity and dead cell count. Detailed description of image analysis script is provided in Result and Discussion section.

2.8 Statistics and software

The Graphs were generated using GraphPad Prism 9.0.0. The results are expressed as mean \pm SEM. Significant differences between two groups were analyzed by two-tailed unpaired Student's t-test. P values < 0.05 were considered statistically significant.

3. Results and Discussion

3.1. Droplet-based microfluidic platform to detect immune cell cytotoxicity

Cell-mediated cytotoxicity is a very dynamic and heterogeneous process since not all effector-target-cell interactions lead to targeted cell death[20]. Although molecular mechanisms mediating cytotoxicity have been extensively studied, the understanding of the determinants that govern the differential killing of specific target cells is yet elusive and often based on averaged and end-point readouts. Therefore, we developed a high-throughput cytotoxicity platform that combines (i) droplet generation and cell pairing using microfluidics, (ii) droplet immobilization for real-time microscopy, and (iii) automated image analysis to allow unbiased and high-throughput detection of cytotoxic events (Figure 1A).

To automate cell tracking and the image analysis process, we labelled immune cells and target cells with different membrane permeable dyes. Next, we co-encapsulated them in water-in-oil droplets (~ 70 pL) using a 3-inlet microfluidic chip of $30 \mu\text{m}$ height, along with the viability dye and cell stimulus in the medium (Figure 1B). An important aspect of our platform is the ability to track large numbers of droplets over time. For this purpose, we adapted a droplet immobilization chamber from Bounab *et al.* made by stacking two glass slides on top of each other that are glued together with thermo-responsive double-sided tape[23,24]. To ensure the sealing quality of the chamber, they were tested visually for deformation of the tape in the chamber and experimentally by testing the mobility of the droplets that were collected and were monitored over 10 hours. We observed that the droplets barely moved over time and the chamber did not contain any air bubbles (Figure 1C), indicative for an efficiently

Chapter 3- An automated real-time microfluidic platform to probe cytotoxicity on chip pressed and sealed chamber. The versatility of our approach lies in the flexibility of controlling the height of the chamber to allow immobilization of differently sized droplets.

In summary, our single-cell cytotoxicity platform allows for the imaging of over 50,000 droplets, thus allowing high-throughput monitoring of cellular interactions in a noise-free and controllable microenvironment in real-time.

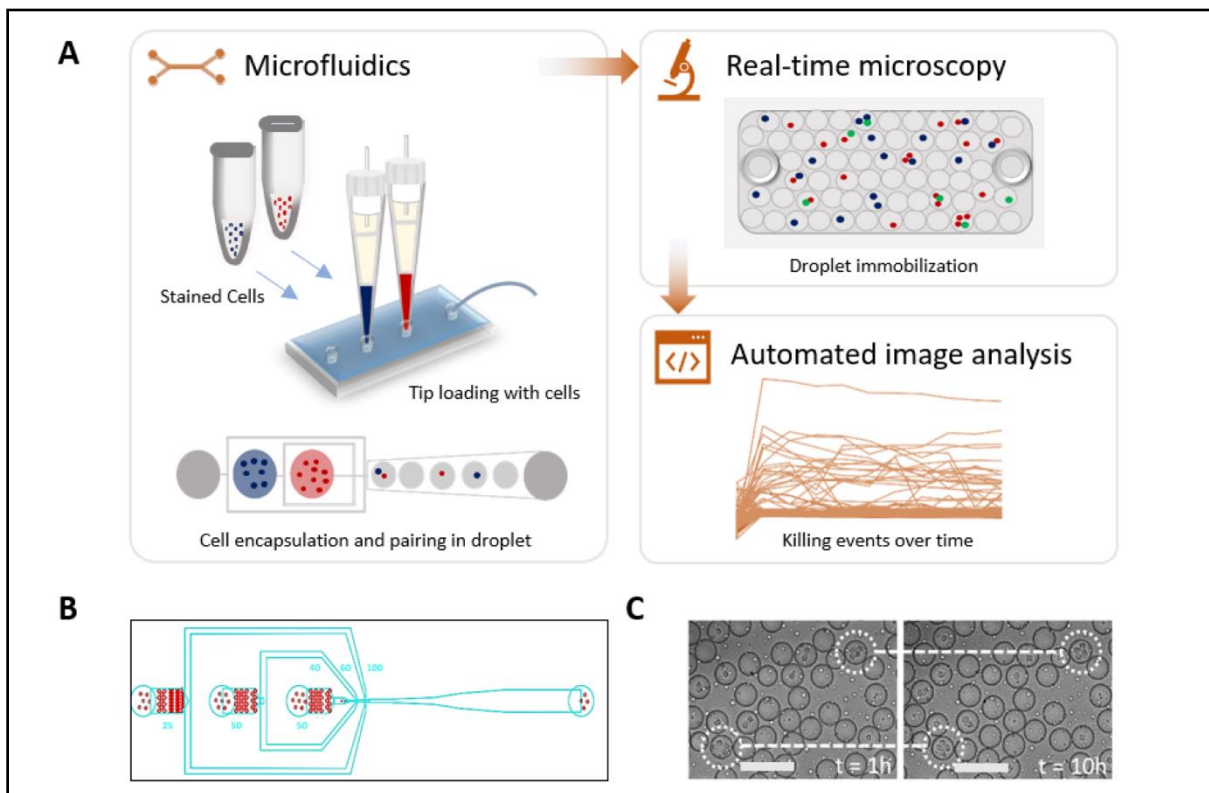


Figure 1. Experimental setup of high-throughput droplet-based cytotoxicity platform. A. Experimental schematics showing cytotoxicity platform that combines (i) droplet generation and cell pairing using microfluidics, (ii) droplet immobilization for real-time microscopy, (iii) automated image analysis using custom-made MATLAB script to allow unbiased and high throughput detection of cytotoxic events. Stained NK cells and K562 cells were loaded into the chip using 200 μ L pipette tips and encapsulated into droplets using a 3-inlet microfluidic chip. The viability dyes were included within the cell medium. The immobilized droplets were incubated in a stage top incubator set at 5% CO_2 and 37°C. Image acquisition was performed at every hour interval for 10 hours. **B.** The three-inlet microfluidic device with flow-focusing junction to generate droplets. **C.** A qualitative test of the observation chamber was performed by monitoring droplets movement in the chamber under the microscope for 10 hours.

3.2. Highly tunable and controllable co-encapsulation of cells in droplets

Single cell cytotoxicity assays with primary cells, containing rare cell populations, emphasize the necessity to ensure efficient and controllable encapsulation. In practice, cell encapsulation does not always match the predicted values due to technical variables such as cellular sedimentation, and attachment or clumping of cells in the tubes. Over the years, there have been several design-related developments that have improved the encapsulation of single cells in droplets. Examples of such developments include the use of active encapsulation methods that utilize either acoustic or electrical forces for the generation of droplets containing single cells[25,26]. However, these methods have their own limitations in terms of bio-incompatibility and total expense compared to passive droplet generation techniques[27]. To combat those limitations, we utilized the tip-loading method that we had optimized before, ensuring efficient cellular encapsulation that closely matched the Poisson distribution[22] (Figure 2A & Supplementary Figure 2A, B, C, D). The rate of cell arrival at the junction is a function of cell seeding density. Therefore, by varying the concentrations of cells, we can maximize cell pairing. By using different cell concentrations for effector and target cells, different Effector:Target (E:T) ratios in droplets were obtained. We aimed for the highest 1:1 (E:T) encapsulation ratios while avoiding excessive cell clumping, which we achieved using concentrations of 7 and 10 million cells/mL for effector and target cells, respectively. At this concentration, we showed that around 3% (~2000 droplets) of the total fraction of droplets had 1:1 cell pairing (Figure 2A). At concentrations above 10 million/mL, the encapsulation became unstable because of the large number of cells clustering at the inlet and resulting in channel blockage, (Supplementary Figure 3 A, B).

Until now, cell pairing efficiency in droplets at high throughput had been the limiting factor in developing a platform that combines real-time microscopy with cellular interactions-based assays. Several groups have developed a variety of approaches such as hydrodynamic trap-based or microwell/nanowell-based platforms to tackle this problem[3,28,29]. Even though these platforms achieved high pairing efficiencies and dynamic monitoring, they failed to exclude paracrine signalling between neighbouring cells and lack high throughput, important factors that need to be considered when studying and understanding functional heterogeneity in immune cells[30]. Furthermore, the droplet-based cytotoxicity platform developed by Sarkar et al. utilized a docking array-based system, allowing the visualization of around 4000

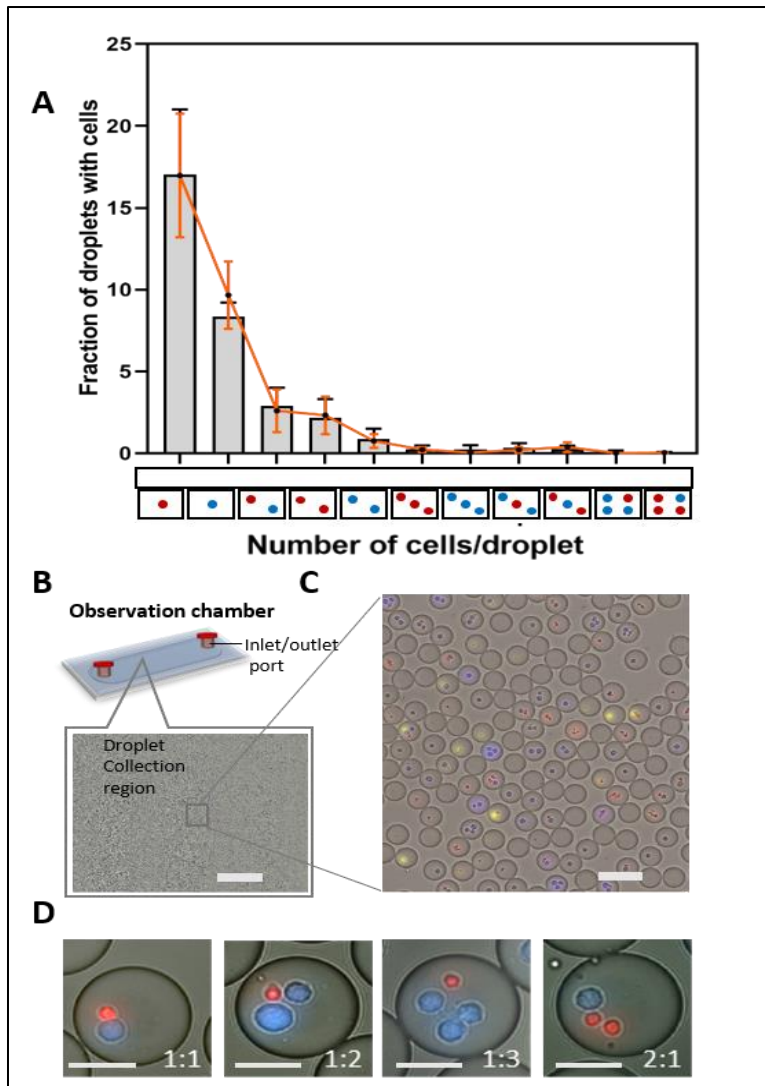


Figure 2: Cell encapsulation and pairing in droplets. **A.** Graph showing the predicted fraction of droplets containing a different combination of cells illustrated on the x-axis according to Poisson distribution (red solid line) and the observed fraction of droplets containing given combinations of cells (bar diagram) at 7 million/mL NK cells (red) and 10 million/mL K562 cells (blue); $n=3$ independent experiments; red and black dots represent mean value for given combination for Poisson distribution and observed distribution respectively. Error bars represents standard error of mean. **B.** Schematic and Macroscopic view of the observation chamber. The image represents around 229 mm²

viewing area of the chamber, allowing to image ~100,000 droplets of 70 μ L volume; scale bar =1 mm. Droplets without cells (representing approximately 66.66 percentage of total droplets fraction) are not shown in the figure. **C.** Magnified segment in the observation chamber showing distribution of different cells in droplets; scale bar = 100 μ m. **D.** Visualization of different E:T ratios in droplets at the cell seeding concentration of 7 million/mL and 10 million/mL for effector and target cells, respectively; scale bar = 25 μ m.

droplets and the platform developed by Antona et al. utilized spherical traps, allowing the visualization of around 6500 droplets per experiment[20,21]. These studies analyzed approximately 100 droplets to study the cellular interaction in between NK cells and target wells. Since immune cells can be highly heterogeneous in their effector functions, throughput is vital to discover small and distinct subsets. So far, to the best of our knowledge, no other droplet-based cytotoxicity platform has been able to meet that requirement in such a way as

our platform, allowing the visualization of around 60,000 droplets per experiment (Figure 2B, C). Among those droplets, this platform allows to analyse 20,000 droplets with cells including cell pairs at different E:T ratio thereby allowing to do proper statistical analysis and even identification of rare cells (Figure 2D). Droplets with only either effector or target cells serve as an internal negative control for viability (Supplementary Figure 4A, B). Droplets with multiple effector cells encapsulated with one or more target cells are used to examine the effect of intercellular interactions and paracrine stimulation. Finally, the droplets with only one effector cell and multiple target cells are monitored to examine the so-called serial killing effect of effector cells. Concluding, our droplet-based microfluidic platform allows for easy, highly controllable effector-target co-encapsulation efficiencies, including proper biological controls and the possibilities to examine the effects of paracrine signaling and serial killing in parallel.

3.3. Live fluorescent cell labelling allows for cell tracking and identification of cytotoxic events

A crucial aspect of the droplet-based cytotoxicity platform is the accurate monitoring of cell viability in droplets. Additionally, it is also important to trace if either an effector cell or a target cell died once a cytotoxic event is measured (Figure 3A). To trace cells over time, they were labelled with the commonly used live cell imaging dyes, Cell Tracker Blue, and Calcein Red AM. The latter is also used as a viability marker in some cytotoxicity-based studies, however, the possibility of signal loss caused by membrane pumps can make it difficult to use this dye for real-time assays with longer incubation times[31,32]. The stability and toxicity of the dyes were tested using our custom-made DMLAB script over time. We observed that the signal from Cell Tracker Blue labelled cells remained stable, whereas the signal from Calcein Red AM reduced gradually over time without inducing toxic effects (Supplementary Figure 5A, B, C, D).

To achieve an accurate and dynamic readout of the viability of cells in droplets, two viability markers were tested: Sytox Green, for necrotic and late apoptotic events, and Cell Event Caspase, to detect early apoptotic event. In droplets, we observed, for both candidate dyes, that they can dynamically stain apoptotic cells, while remaining stable over time, therefore being the perfect candidate to also detect early and late apoptotic events (Figure 3B, C & Supplementary Figure 6A, B).

These results show that different dyes can be used together with our script to trace and identify cytotoxic events in real time.

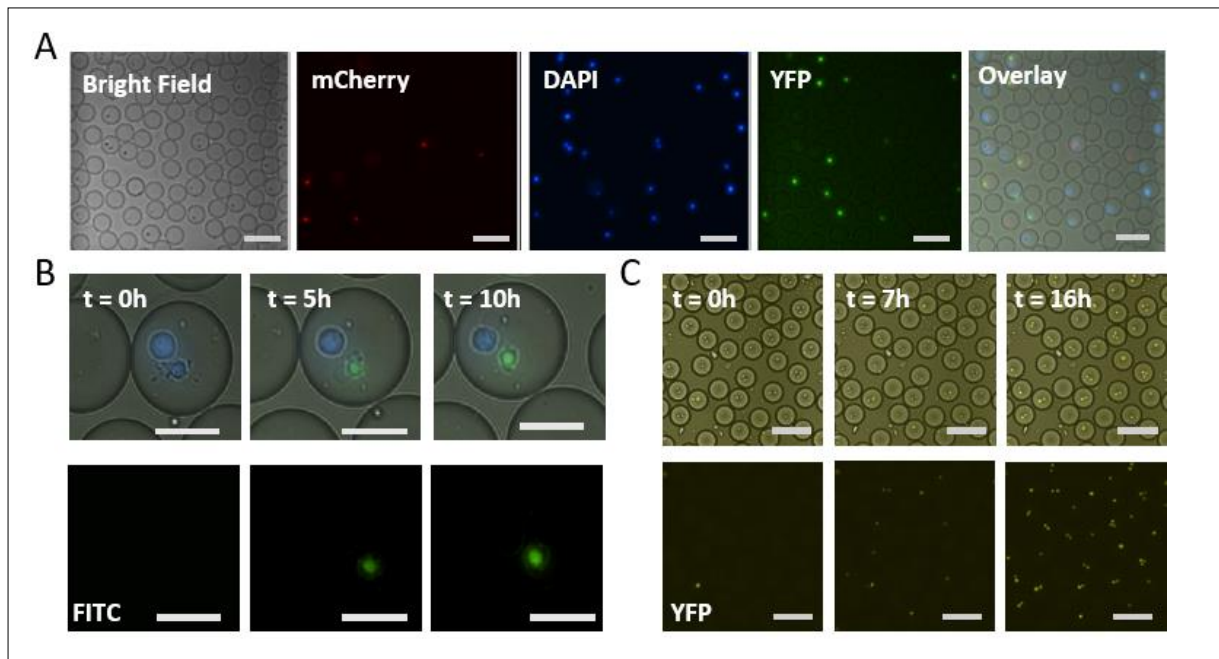


Figure 3: Real-time viability tracking. NK cells and target cells (here K562 cells and Jurkat T cells) were labelled with Calcein Red AM (5 μ M) and Cell Tracker Blue (10 μ M), respectively. The viability dyes Sytox Green (2.5 μ M) and Cell Event Caspase 3/7 (7 μ M) were encapsulated in droplets with cells and culture medium. **A.** Image showing different cells in droplets that are monitored using mCherry for NK cells, DAPI for K562 cells, and YFP/FITC for dead cells; scale bar = 100 μ m. **B.** K562 cells were labelled with Cell Tracker Blue (25 μ M) and co-encapsulated with Sytox Green as viability marker. The signal remains stable over 10 hours; scale bars = 25 μ m. **C.** Jurkat T cells were encapsulated in droplets along with (Cell Event Caspase3/7 (7 μ M) and 5% DMSO to induce apoptosis. In presence of DMSO, the cell undergoes apoptosis after 6 hours, and the staining remains stable over 10 hours; scale bars = 100 μ m.

3.4. Script for robust, automated, high throughput image analysis of cytotoxic events

The droplet-based cytotoxicity assay yields fluorescence images with thousands of droplets at multiple time points. To maintain the high-throughput character of the assay, and to gain accurate results, an automated readout of these images is pivotal. For a complete automation of the image analysis, certain requirements were fulfilled. First, the script should be able to track the droplets over several hours. Second, the script should be able to distinguish the different cell types and corresponding numbers of cells in each of the tracked droplets. Third,

it should be able to accurately track the change in viability signal for each cell type to connect the viability signal to the corresponding cell, which could either be the effector or target cell. To this end we developed a custom-made In-Droplet Viability Analysis script, or DMALAB script, to allow for automated detection of thousands of cells, corresponding cytotoxic events, and full control over the image processing procedure.

In short, the image analysis script consists of three steps: (i) droplet tracing (BF), (ii) fluorescence image pre-processing (fluo), (iii) and cell counting (ncel; Figure 4A). The process starts with detecting individual droplets in the bright field channel using the commercially available “imfindcircle” function. The script allows to optimize the settings for the droplet identification, which are based on the shape, size, and immobilization of the droplets. Using contrast stretching, the edges of the individual droplets get identified, allowing the accurate monitoring of moving droplets over time. Next, each droplet will be given an index number, while the coordinates determine the droplet position. The script allows for the control over contrast stretching parameters and tracks and removes the moving droplets, thus ensuring the accuracy of droplets detection over different time frames (Figure 4B). After the script has traced the individual droplets, the next step is to detect the individual cells per droplet. To facilitate the cell detection in the droplets, we pre-labeled the cells with fluorescent dyes. With the objective of obtaining a binary image that represents the object (here cells), the fluorescent images are preprocessed by cropping, applying a top hat filter, setting the intensity of non-droplet pixel to zero and applying the threshold to get the binary image (Figure 4C). The final part of the analysis consists of cell counting within droplets and the detection of changes in fluorescence. Finally, all objects can be counted, and the change in fluorescence can be detected at sequential time points.

To validate the performance of the script, overnight activated NK cells in presence of 50ng/ml IL2 were encapsulated with K562 cells in the droplets and the results from manual and automated analysis in terms of droplets count, cell distribution, cell pairing, and viability of cells at random time frames were compared. Upon comparing, we obtained coherent results between the two methods with a maximum deviation of only 2% (Figure 4D & Supplementary Figure 7A, B). In case of doubts, there is also an inbuilt droplet trace function that allows for the visualization of the individual droplets, for all fluorescent channels, and the possibility to exclude droplets from downstream analysis if needed. Altogether, our script enables high-throughput analysis of images with large amounts of data by automatically detecting cells and

their viability in droplets. It gives a high level of control over the analysis parameters, making it easily applicable in various kinds of functional droplet-based assays.

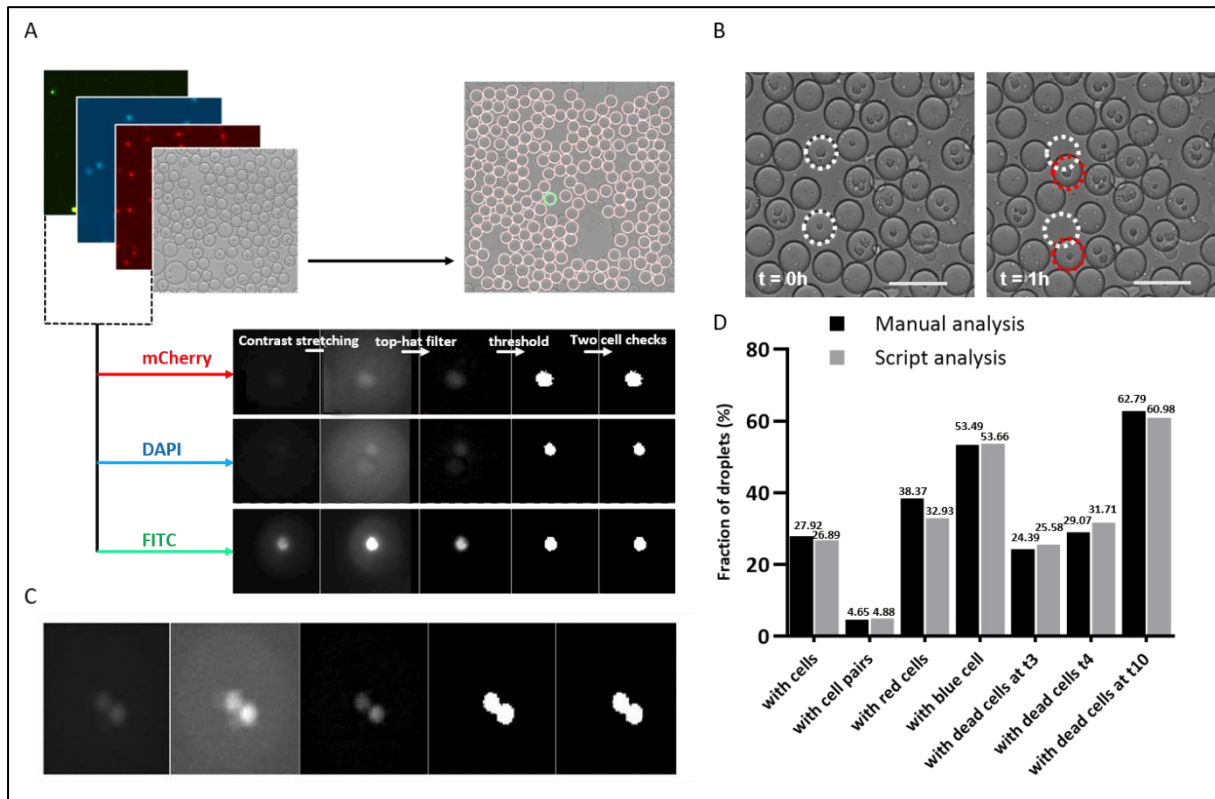


Figure 4: Image processing and analyzing steps in MATLAB script. **A.** Image processing by stacking different channels, droplet tracing, and detection of cells over each channel. **B.** Droplet movement over one hour. An adjustable amount of movement is allowed by the script, but if this allowed movement is more than the droplet radius, the risk exists of detecting a different droplet at the next time point. Droplet detection over time is done by comparing the coordinates of the center of the droplet between two consecutive time points and selecting the closest center within the allowed movement range. **C.** Evaluation of the script for cells recognition over different channels, here two cells labelled with cell tracker blue are identified in DAPI channel). **D.** Validation of the script by comparing differences in cell distribution, cell pairing, and dead cell identification at 3 different time points ($t=3$ hrs., $t=4$ hrs., and $t=10$ hrs.) in-between script generated data with manually counted data.

3.5. Dynamic nature of NK cell-mediated killing of tumor cells

NK cells are well known for the efficient identification of their targets to induce killing without prior antigen sensitization, making them an ideal target for anti-cancer immunotherapies[33].

They identify target cells that lack or have reduced expression of MHC-1 molecules and subsequently kill upon balanced signaling between activation and inhibitory receptors[34]. The use of several receptor interactions and signaling pathways makes NK cells a very complex and heterogeneous cell type[35]. The cytotoxic interactions are both effector-cell as well as target-cell dependent, which further enhances the variation in responses mediated by both types. Therefore, to address functional heterogeneity in the NK cell compartment, we co-cultured them with K562 as target cells. K562 is a myelogenous leukemia cell line that lacks MHC-1 expression and therefore is an attractive target to further characterize NK cell-mediated cytotoxicity. The effector (NK cells) and the target (K562) cells were paired together in 70 pL droplets, allowing them to interact. The study by Antona et al. showed that cells in a confined environment, such as droplets, increase the chances of cellular interaction[21]. However, we observed that only around 20% of NK cells were potent killers, while the large majority were not able to induce killing at all during the 10 hours of incubation, which is in agreement with the micro-well based study by Gudeval et al[3]., and earlier chromium release-based study by Vanherberghen et al.[3] (Figure 5A, B). In contrast to the work described by Sarkar et.al., we did not observe 100% NK cell-mediated killing in droplets, which we believe is explained by the characteristics of the utilized dye, which includes the sensitivity of being actively pumped out by the target cell[20]. Interestingly, our results reveal heterogeneity within the NK cell compartment with only part of the population displaying cytotoxic behavior. This indicates that only a small percentage of NK cells kill, whilst the majority are either inactive, very late killers (beyond our time frame of 10 hrs) or require passive support from paracrine signaling from the other cells to be able to induce cytotoxic ability.

Additionally, the dynamics of NK cell mediated cytotoxicity of K562 cells was monitored using our platform. During the incubation, we observed that different NK cells demonstrate different potential to kill. In a representative experiment, we analyzed 66,600 droplets in total (18,320 droplets with cells), of which 2052 droplets contained the desired cell pairing (Figure 5C, D). By plotting the intensity of viability dye over incubation time, we showed the dynamics of cellular interaction between NK cells and K562 cells. Our findings from this experiment revealed that 17.25% K562 cells were dead whereas 82.5% K562 cells were alive despite being incubated together with NK cells. We also observed that a large fraction of cytotoxic NK cells (77%) induces cytotoxicity within the first four hours of interaction. 40% of the NK

cells provided lytic hits within first hour of interaction while the incident of cell death decreased over time and was minimal after 10 hours (0.88%). These findings were consistent with other donors as well. Of all the NK cells that have the potential to kill K562 cells, approximately 86% delivered a lytic hit within four hours of incubation, and we refer to them as fast killers. Among these fast killer cells, 52% of cells initiated killing within 1 hour of incubation (Figure 5E). 25% of NK cells were able to mount the cytotoxic ability in the second hour of incubation and the number went down subsequently over time. In contrast, K562 in absence of NK cells had higher viability (around 95%) over 10 hours and most of the target cell death occurred only at the later phase of the incubation (Supplementary Figure 4B). These results suggested that a majority of NK cell population showed spontaneity on killing their target cells upon recognition. A fraction of NK cell population was not able to kill as quickly, however, for these late killing events, the possibility of natural cell death could be equally likely.

The data presented here supports the classification of NK cells based on their cytotoxic ability and the dynamics at which they kill their target cells[2]. Even though the time of target cell lysis varied considerably over different time point during the course of incubation, our result supports the notion of the existence of a NK cell subpopulation that induces killing as early as 30 minutes after interaction with a target cell[2,36,37]. The fast and slow killing ability of NK cells could be coupled to the granzyme dependent and independent mechanisms by which NK cells induces cell death. Furthermore, The size and content of the lytic granules along with the secretion and quantity of degranulation events can also be associated with the kinetics of target cell killing by NK cells[38]. We can associate these variations in killing capacities of NK cells to functional heterogeneity within NK cell population. However, the potential cause underlying these variations was not explored in this research and requires further investigation.

These distinctive properties within NK cell population can determine the capacity of NK cells mediating cytotoxicity indicating towards the heterogeneity within NK cell populations. However, the specific causes of such variation in the killing potentials are still not clear and requires further study.

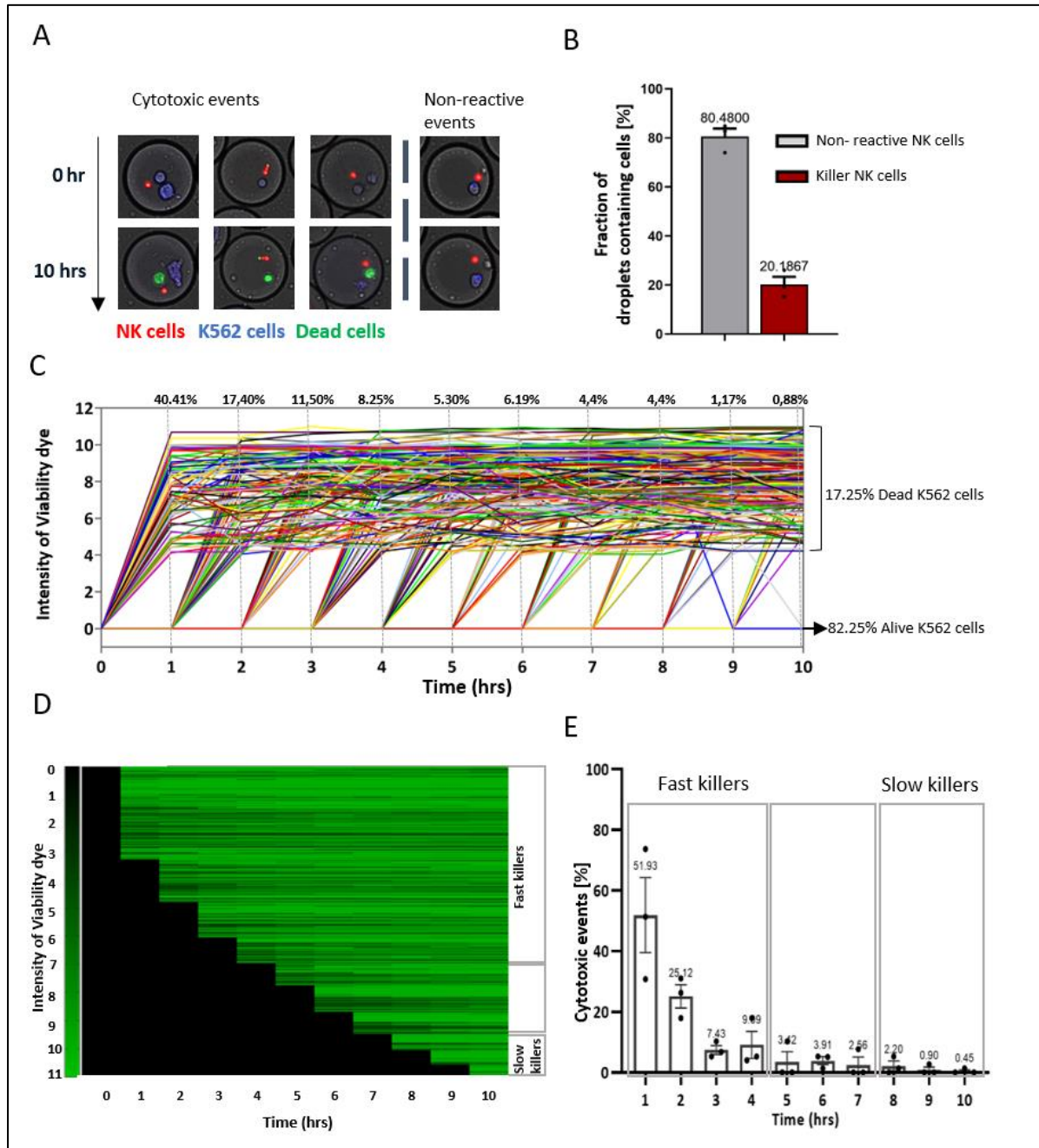


Figure 5: NK cytotoxicity in real-time. A. Microscopic overview of NK cell-mediated cytotoxicity in droplets. NK cells were labelled with Calcein Red AM dye (red cells) and K562 cells with Cell Tracker Blue (blue cells) and paired together in 70 pL droplets in presence of viability dye (Sytox green and Cell event Caspase 3/7). They were then incubated at 37°C and 5% CO₂ for 10 hrs. Image acquisition was done at an hour interval. Over the interval of 10 hours, NK cells are interacting with target cells, either, with (left) or without inducing cytotoxicity (right). The cells that die are stained with the viability dye and thus turn green. The live cell retains the original color. **B.** Bar diagram representing killer fraction of NK cells in droplets; data analysis performed on E:T 1:1; n=3 independent experiments; error bar represents

standard error of mean. **C.** A representative experiment showing intensity of the viability for K526 cells upon interaction with NK cells plotted over time. Each line represents individual cells; $n=66,600$ total droplets with 20,860 droplets containing cells. The graph does not include the droplets with 0, or 1 cell and droplets with dead cells at $t=0$ hr. An alive cell gives the intensity of viability dye as "0", cells with values above zero are considered as dead. **D.** Heat Map showing the dynamics of cytotoxicity within an experiment. Each line represents individual cells. The viability was assessed over the period of 10 hours. **E.** Graph representing the dynamics of cytotoxic events in droplets for different donors. The dynamics were determined for the killer fraction of NK cells, thus showing the percentage of the fast and slow killer population in NK cells; data analysis performed on E:T 1:1; $n=3$ independent experiments; error bar represents standard error of mean.

Some NK cells have the capacity to kill multiple target cells, referred to as serial killers[2,39]. For years, translational researchers that aim to use NK cells for immunotherapy have aimed to harness this extremely relevant and promising feature[2,40]. Although this search goes beyond the scope of this study, we investigated the pairing distribution and the cytotoxicity induced by different E:T ratios (Supplementary Figure 8A) to characterize serial killing ability of NK cells. Even with a limited sample size, we could identify several instances (around 2.5% of droplets with the combination of multiple K562 and a single NK cells; data not shown) where a single NK cell could kill two target cells, supporting the previously observed serial killing ability of NK cells[40]. Future studies will be needed to assess the serial killing potential of NK cells, which can be achieved by minimal adaptations to our experimental workflow.

Concluding, our droplet-based microfluidic platform allows for easy, highly controllable effector-target co-encapsulation efficiencies, including proper biological controls and the possibilities to examine the effects of paracrine signaling and serial killing in parallel.

4. Conclusion and outlook

In this paper, we have presented an integrated platform that allows for monitoring and decoding cellular interactions between immune and tumor cells in high throughput. This methodology was built on the already available and broadly utilized principles of cytotoxicity assessment and live-cell imaging. Here we combined (i) the assessment of different E:T ratios, (ii) a dynamic readout, and (iii) an automated image analysis script that allows an unbiased and high-throughput detection of cytotoxic events. Besides, this cytotoxicity platform is

designed to be easily adjusted according to different experimental needs, allowing the assessment of cytotoxicity in a wide variety of both immune cells and target cells.

We show that NK cell cytotoxic effector functions are highly dynamic and heterogeneous, which could otherwise not have been possibly studied with conventional assays. The value of this microfluidic setup is its simplicity, both in fabrication and experimental workflow. Future minor modifications to adapt this platform for droplet sorting and barcoding will also allow the use of this setup for omics-based studies, thereby opening new avenues of research in cellular and functional diversity. Apart from NK cells, there are several cell types including CTLs, macrophages, and killer dendritic cells that can exhibit cytotoxic abilities, and have been widely explored for immunotherapeutic purposes. *In vitro* cytotoxicity assays have been an important assessment tool for measuring the maturation and functional activities of these immune cells. Therefore, a comprehensive evaluation of cell-mediated cytotoxicity can become an important parameter to correlate the treatment with the clinical outcome. Since we deliberately designed our platform to allow flexibility, other cell types can easily be studied without the need for modifications. Therefore, this platform can be easily adapted to the abovementioned cell types and their killing dynamics can be assessed for clinical as well as for research purposes.

5. Acknowledgments

The authors want to thank Nidhi Sinha for all the enthusiastic discussions and proofreading of the manuscript. We also want to thank Bart Tiemeijer and Liesbeth Varion-Verhagen for providing PBMCs. This work is supported by an ERC Starting Grant ImmunoCode (802791), and furthermore, we acknowledge generous support by the Eindhoven University of Technology.

6. References

- [1] R. Satija, A.K. Shalek, Heterogeneity in immune responses: from populations to single cells, *Trends Immunol.* 35 (2014) 219–229. <https://doi.org/10.1016/j.it.2014.03.004>.
- [2] B. Vanherberghen, P.E. Olofsson, E. Forslund, M. Sternberg-Simon, M.A. Khorshidi, S. Pacouret, K. Guldevall, M. Enqvist, K.J. Malmberg, R. Mehr, B. Önfelt, Classification of human natural killer cells based on migration behavior and cytotoxic response, *Blood.* 121 (2013) 1326–1334. <https://doi.org/10.1182/blood-2012-06-439851>.
- [3] K. Guldevall, L. Brandt, E. Forslund, K. Olofsson, T.W. Frisk, P.E. Olofsson, K. Gustafsson, O. Manneberg, B. Vanherberghen, H.

Chapter 3- An automated real-time microfluidic platform to probe cytotoxicity on chip

- Brismar, K. Kärre, M. Uhlin, B. Önfelt, Microchip screening platform for single cell assessment of NK cell cytotoxicity, *Front. Immunol.* 7 (2016) 1–7. <https://doi.org/10.3389/fimmu.2016.00119>.
- [4] S.M. Kaech, E.J. Wherry, Heterogeneity and Cell-Fate Decisions in Effector and Memory CD8+ T Cell Differentiation during Viral Infection, *Immunity.* 27 (2007) 393–405. <https://doi.org/10.1016/j.immuni.2007.08.007>.
- [5] K.T. Brunner, J. Mael, J.C. Cerottini, B. Chapuis, Quantitative assay of the lytic action of immune lymphoid cells on 51-Cr-labelled allogeneic target cells in vitro; inhibition by isoantibody and by drugs., *Immunology.* 14 (1968) 181–96. <http://www.ncbi.nlm.nih.gov/pubmed/4966657><http://www.pubmedcentral.nih.gov/articlerender.fcgi?artid=PMC1409286>.
- [6] M.T. Scimone, H.C. Cramer, P. Hopkins, J.B. Estrada, C. Franck, Application of mild hypothermia successfully mitigates neural injury in a 3D in-vitro model of traumatic brain injury, *PLoS One.* 15 (2020) 1–15. <https://doi.org/10.1371/journal.pone.0229520>.
- [7] Y. Rai, R. Pathak, N. Kumari, D.K. Sah, S. Pandey, N. Kalra, R. Soni, B.S. Dwarakanath, A.N. Bhatt, Mitochondrial biogenesis and metabolic hyperactivation limits the application of MTT assay in the estimation of radiation induced growth inhibition, *Sci. Rep.* (2018). <https://doi.org/10.1038/s41598-018-19930-w>.
- [8] C. Korzeniewski, D.M. Callewaert, An enzyme-release assay for natural cytotoxicity, *J. Immunol. Methods.* 64 (1983) 313–320. [https://doi.org/10.1016/0022-1759\(83\)90438-6](https://doi.org/10.1016/0022-1759(83)90438-6).
- [9] M.A. Karimi, E. Lee, M.H. Bachmann, A.M. Salicioni, E.M. Behrens, T. Kambayashi, C.L. Baldwin, Measuring Cytotoxicity by Bioluminescence Imaging Outperforms the Standard Chromium-51 Release Assay, *PLoS One.* 9 (2014) e89357. <https://doi.org/10.1371/journal.pone.0089357>.
- [10] P.K. Chattopadhyay, T.M. Gierahn, M. Roederer, J.C. Love, Single-cell technologies for monitoring immune systems, *Nat. Immunol.* 15 (2014) 128–135. <https://doi.org/10.1038/ni.2796>.
- [11] N.M. Toriello, E.S. Douglas, N. Thaitrong, S.C. Hsiao, M.B. Francis, C.R. Bertozzi, R.A. Mathies, Integrated microfluidic bioprocessor for single-cell gene expression analysis., *Proc. Natl. Acad. Sci. U. S. A.* 105 (2008) 20173–8. <https://doi.org/10.1073/pnas.0806355106>.
- [12] D. Wang, S. Bodovitz, Single cell analysis: the new frontier in “omics”., *Trends Biotechnol.* 28 (2010) 281–90. <https://doi.org/10.1016/j.tibtech.2010.03.002>.
- [13] J. Kim, M.-T.T. Phan, S. Kweon, H. Yu, J. Park, K.-H. Kim, I. Hwang, S. Han, M.-J. Kwon, D. Cho, A Flow Cytometry-Based Whole Blood Natural Killer Cell Cytotoxicity Assay Using Overnight Cytokine Activation., *Front. Immunol.* 11 (2020) 1851. <https://doi.org/10.3389/fimmu.2020.01851>.
- [14] A. Murschhauser, P.J.F. Röttgermann, D. Woschée, M.F. Ober, Y. Yan, K.A. Dawson, J.O. Rädler, A high-throughput microscopy method for single-cell analysis of event-time correlations in nanoparticle-induced cell death, *Commun. Biol.* (2019). <https://doi.org/10.1038/s42003-019-0282-0>.
- [15] J.C. Love, J.L. Ronan, G.M. Grotenbreg, A.G. van der Veen, H.L. Ploegh, A microengraving method for rapid selection of single cells producing antigen-specific antibodies, *Nat. Biotechnol.* 24 (2006) 703–707. <https://doi.org/10.1038/nbt1210>.
- [16] J. Clausell-Tormos, D. Lieber, J.-C. Baret, A. El-Harrak, O.J. Miller, L. Frenz, J. Blouwolff, K.J. Humphry, S. Köster, H. Duan, C. Holtze, D.A. Weitz, A.D. Griffiths, C.A. Merten, Droplet-Based Microfluidic Platforms for the Encapsulation and Screening of Mammalian Cells and Multicellular Organisms, *Chem. Biol.* 15 (2008) 427–437. <https://doi.org/10.1016/j.chembiol.2008.04.004>.
- [17] Y. Zhou, N. Shao, R. Bessa de Castro, P. Zhang, Y. Ma, X. Liu, F. Huang, R.F. Wang, L. Qin, Evaluation of Single-Cell Cytokine Secretion and Cell-Cell Interactions with a Hierarchical Loading Microwell Chip, *Cell Rep.* 31 (2020) 107574. <https://doi.org/10.1016/j.celrep.2020.107574>.
- [18] F. Wimmers, N. Subedi, N. van Buuringen, D. Heister, J. Vivié, I. Beeren-Reinieren, R. Woestenenk, H. Dolstra, A. Piruska, J.F.M.

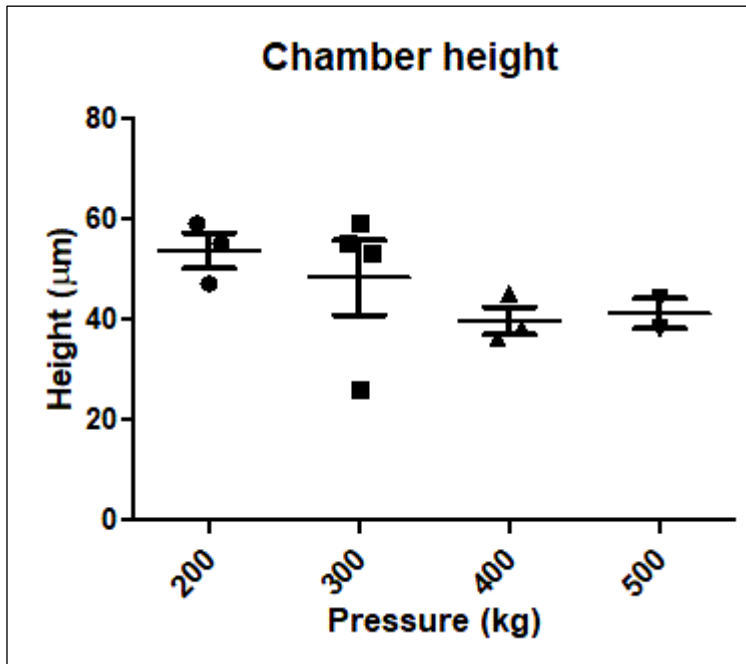
Chapter 3- An automated real-time microfluidic platform to probe cytotoxicity on chip

- Jacobs, A. van Oudenaarden, C.G. Figdor, W.T.S. Huck, I.J.M. de Vries, J. Tel, Single-cell analysis reveals that stochasticity and paracrine signaling control interferon-alpha production by plasmacytoid dendritic cells, *Nat. Commun.* 9 (2018) 3317. <https://doi.org/10.1038/s41467-018-05784-3>.
- [19] V. Chokkalingam, J. Tel, F. Wimmers, X. Liu, S. Semenov, J. Thiele, C.G. Figdor, W.T.S. Huck, Probing cellular heterogeneity in cytokine-secreting immune cells using droplet-based microfluidics, *Lab Chip.* 13 (2013) 4740. <https://doi.org/10.1039/c3lc50945a>.
- [20] S. Sarkar, P. Sabhachandani, D. Ravi, S. Potdar, S. Purvey, A. Beheshti, A.M. Evens, T. Konry, Dynamic analysis of human natural killer cell response at single-cell resolution in B-Cell Non-Hodgkin Lymphoma, *Front. Immunol.* 8 (2017) 1–13. <https://doi.org/10.3389/fimmu.2017.01736>.
- [21] S. Antona, I. Platzman, J.P. Spatz, Droplet-Based Cytotoxicity Assay: Implementation of Time-Efficient Screening of Antitumor Activity of Natural Killer Cells, *ACS Omega.* 5 (2020) 24674–24683. <https://doi.org/10.1021/acsomega.0c03264>.
- [22] N. Sinha, N. Subedi, F. Wimmers, M. Soennichsen, J. Tel, A Pipette-Tip Based Method for Seeding Cells to Droplet Microfluidic Platforms., *J. Vis. Exp.* (2019) 1–10. <https://doi.org/10.3791/57848>.
- [23] Y. Bounab, K. Eyer, S. Dixneuf, M. Rybczynska, C. Chauvel, M. Mistretta, T. Tran, N. Aymerich, G. Chenon, J.F. Llitjos, F. Venet, G. Monneret, I.A. Gillespie, P. Cortez, V. Moucadel, A. Pachot, A. Troesch, P. Leissner, J. Textoris, J. Bibette, C. Guyard, J. Baudry, A.D. Griffiths, C. Védrine, Dynamic single-cell phenotyping of immune cells using the microfluidic platform DropMap, *Nat. Protoc.* 15 (2020) 2920–2955. <https://doi.org/10.1038/s41596-020-0354-0>.
- [24] K. Eyer, R.C.L. Doineau, C.E. Castrillon, L. Briseño-Roa, V. Menrath, G. Mottet, P. England, A. Godina, E. Brient-Litzler, C. Nizak, A. Jensen, A.D. Griffiths, J. Bibette, P. Bruhns, J. Baudry, Single-cell deep phenotyping of IgG-secreting cells for high-resolution immune monitoring, *Nat. Biotechnol.* 35 (2017) 977–982. <https://doi.org/10.1038/nbt.3964>.
- [25] J. Gong, C.J. Kim, All-electronic droplet generation on-chip with real-time feedback control for EWOD digital microfluidics, *Lab Chip.* 8 (2008) 898–906. <https://doi.org/10.1039/b717417a>.
- [26] U. Demirci, G. Montesano, Single cell epitaxy by acoustic picolitre droplets, *Lab Chip.* 7 (2007) 1139–1145. <https://doi.org/10.1039/b704965j>.
- [27] D.J. Collins, A. Neild, A. deMello, A.Q. Liu, Y. Ai, The Poisson distribution and beyond: Methods for microfluidic droplet production and single cell encapsulation, *Lab Chip.* 15 (2015) 3439–3459. <https://doi.org/10.1039/c5lc00614g>.
- [28] B. Dura, M.M. Servos, R.M. Barry, H.L. Ploegh, S.K. Dougan, J. Voldman, Longitudinal multiparameter assay of lymphocyte interactions from onset by microfluidic cell pairing and culture, *Proc. Natl. Acad. Sci.* 113 (2016) E3599–E3608. <https://doi.org/10.1073/pnas.1515364113>.
- [29] Y.J. Yamanaka, C.T. Berger, M. Sips, P.C. Cheney, G. Alter, J.C. Love, Single-cell analysis of the dynamics and functional outcomes of interactions between human natural killer cells and target cells, *Integr. Biol. (United Kingdom).* 4 (2012) 1175–1184. <https://doi.org/10.1039/c2ib20167d>.
- [30] N. Sinha, N. Subedi, J. Tel, Integrating Immunology and Microfluidics for Single Immune Cell Analysis., *Front. Immunol.* 9 (2018) 2373. <https://doi.org/10.3389/fimmu.2018.02373>.
- [31] S. Neri, E. Mariani, A. Meneghetti, L. Cattini, A. Facchini, Calcein-acetyoxymethyl cytotoxicity assay: Standardization of a method allowing additional analyses on recovered effector cells and supernatants, *Clin. Diagn. Lab. Immunol.* 8 (2001) 1131–1135. <https://doi.org/10.1128/CDLI.8.6.1131-1135.2001>.
- [32] R. Lichtenfels, W.E. Biddison, H. Schulz, A.B. Vogt, R. Martin, CARE-LASS (calcein-release-assay), an improved fluorescence-based test system to measure cytotoxic T lymphocyte activity, *J. Immunol. Methods.* 172 (1994) 227–239. [https://doi.org/10.1016/0022-1759\(94\)90110-4](https://doi.org/10.1016/0022-1759(94)90110-4).

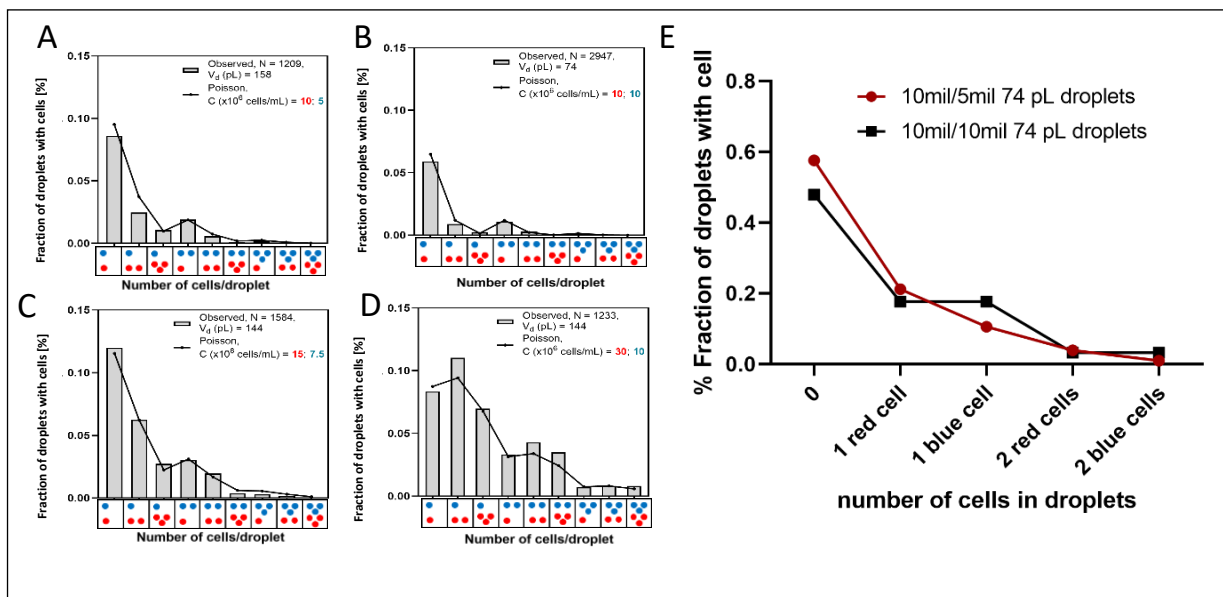
Chapter 3- An automated real-time microfluidic platform to probe cytotoxicity on chip

- [33] M.A. Caligiuri, Human natural killer cells, *Blood*. (2008). <https://doi.org/10.1182/blood-2007-09-077438>.
- [34] E. Vivier, E. Tomasello, M. Baratin, T. Walzer, S. Ugolini, Functions of natural killer cells, *Nat. Immunol.* 9 (2008) 503–510. <https://doi.org/10.1038/ni1582>.
- [35] E. Forslund, K. Guldevall, P.E. Olofsson, T. Frisk, A.E. Christakou, M. Wiklund, B. Önfelt, Novel microchip-based tools facilitating live cell imaging and assessment of functional heterogeneity within NK cell populations, *Front. Immunol.* 3 (2012) 1–7. <https://doi.org/10.3389/fimmu.2012.00300>.
- [36] P.E. Olofsson, L. Brandt, K.E.G. Magnusson, T. Frisk, J. Jaldén, B. Önfelt, A collagen-based microwell migration assay to study NK-target cell interactions, *Sci. Rep.* 9 (2019) 1–10. <https://doi.org/10.1038/s41598-019-46958-3>.
- [37] P.J. Choi, T.J. Mitchison, Quantitative analysis of resistance to natural killer attacks reveals stepwise killing kinetics, *Integr. Biol.* 6 (2014) 1153–1161. <https://doi.org/10.1039/C4IB00096J>.
- [38] L.A. Gwalani, J.S. Orange, Single Degranulations in NK Cells Can Mediate Target Cell Killing, *J. Immunol.* 200 (2018) 3231–3243. <https://doi.org/10.4049/jimmunol.1701500>.
- [39] P.J. Choi, T.J. Mitchison, Imaging burst kinetics and spatial coordination during serial killing by single natural killer cells, *Proc. Natl. Acad. Sci. U. S. A.* 110 (2013) 6488–6493. <https://doi.org/10.1073/pnas.1221312110>.
- [40] R. Bhat, C. Watzl, Serial Killing of Tumor Cells by Human Natural Killer Cells – Enhancement by Therapeutic Antibodies, *PLoS One.* 2 (2007) e326. <https://doi.org/10.1371/journal.pone.0000326>.

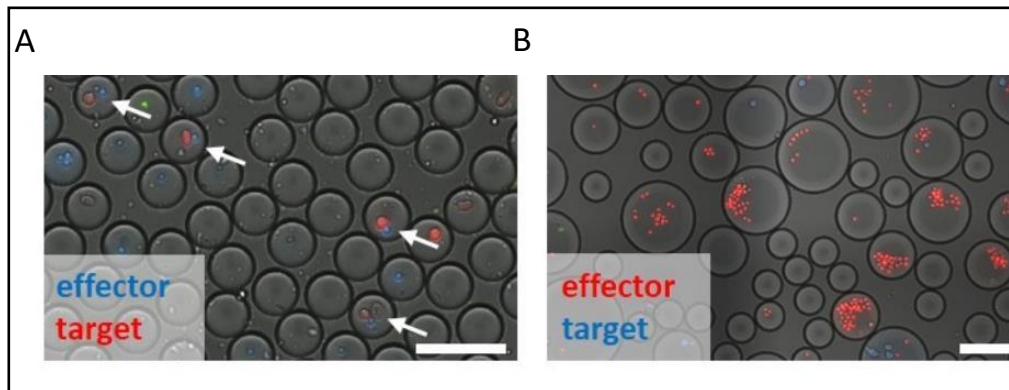
7. Supplementary Information



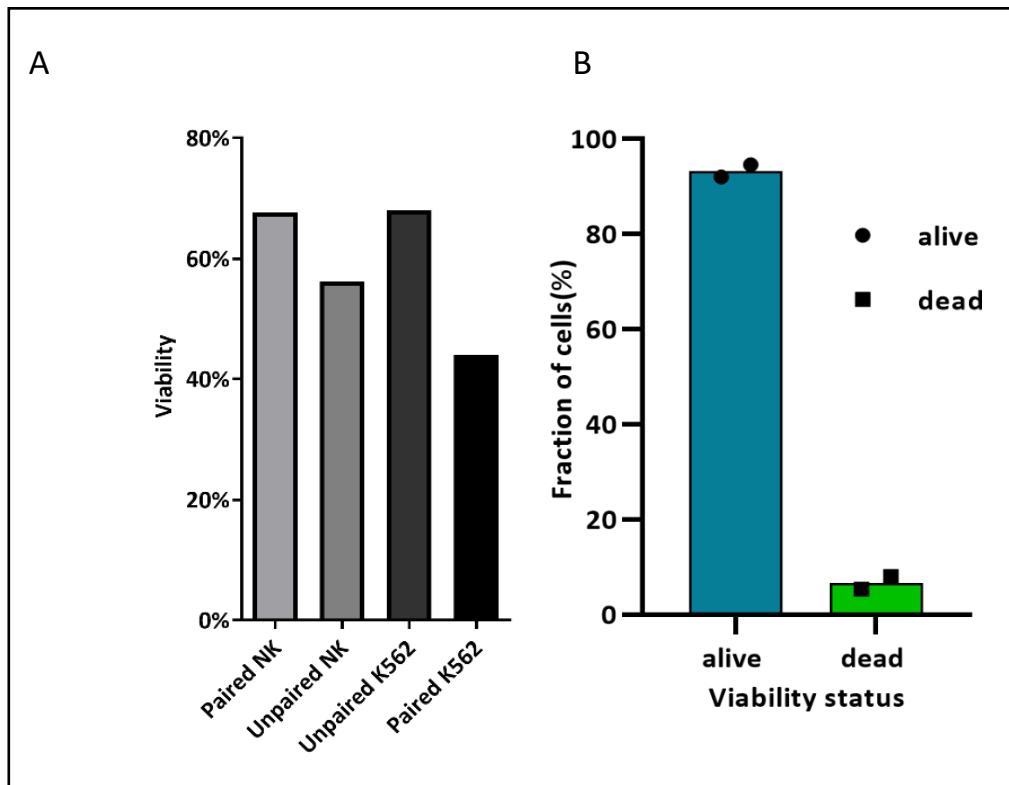
Supplementary Figure 1. Graph showing effect of different pressure loads (200 kgs, 300 kgs, 400 kgs, and 500 kgs) on the height of the collection chamber; Error bar represents standard error of mean.



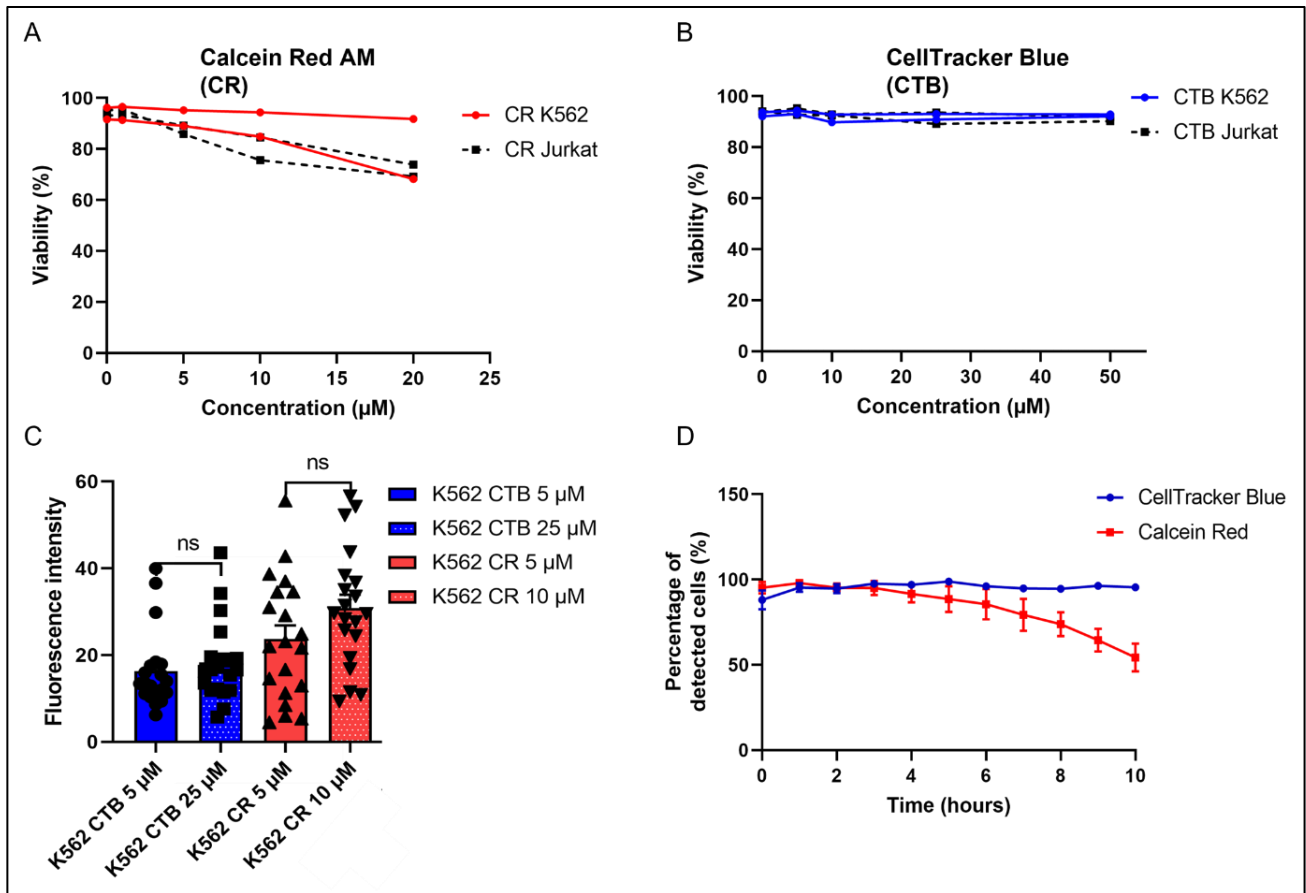
Supplementary Figure 2. Co-encapsulation efficiency of effector cells and target cells at various seeding densities. Graphs showing the predicted fraction of droplets containing the combination of cells illustrated on the x-axis according to Poisson distribution (lines) and the observed fraction of droplets containing those combinations of cells (bars) at various seeding densities. The seeding densities were: **A.** 10×10^6 red cells/mL and 5×10^6 blue cells/mL, **B.** 10×10^6 cells/mL for both cell types, **C.** 15×10^6 red cells/mL and 7.5×10^6 blue cells/mL, **D.** 30×10^6 red cells/mL and 10×10^6 blue cells/mL. **E.** line graph representing the fraction of droplets with and without cells (irrespective of cell pairing) at different concentration.



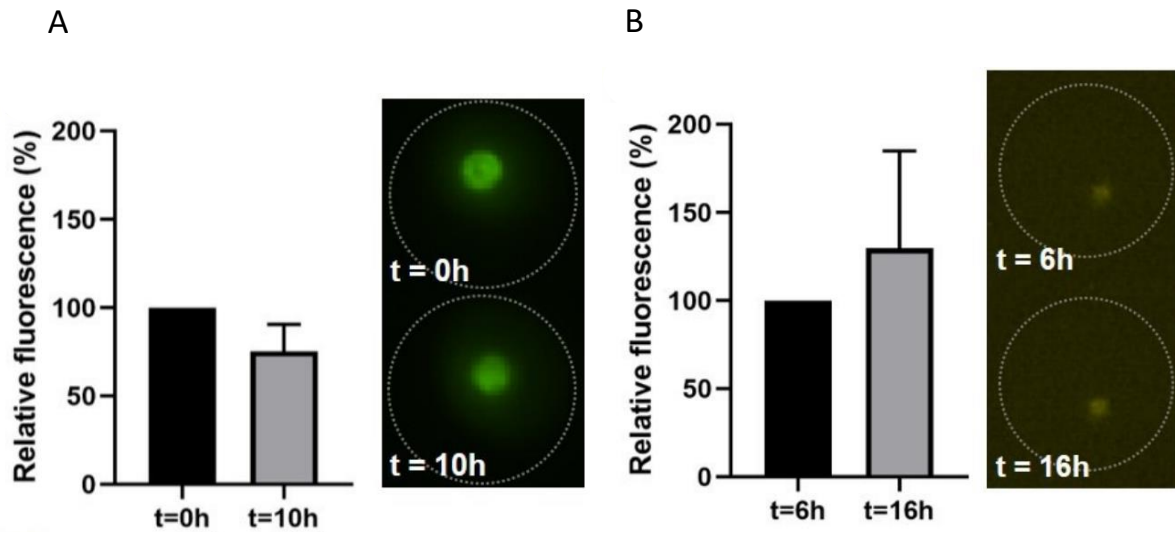
Supplementary Figure 3. Overview of droplets containing different numbers of cells. The seeding densities in this experiment were $10 \cdot 10^6$ cells/mL for both cell types. **(A)** Droplet with cell pairing is indicated with arrows. **(B)** Cell clumps in polydisperse droplets. Here, the seeding density of the effector cells was $15 \cdot 10^6$ cells/mL, and the seeding density of the target cells was $7,5 \cdot 10^6$ cells/mL. Scale bars are 100 μ m.



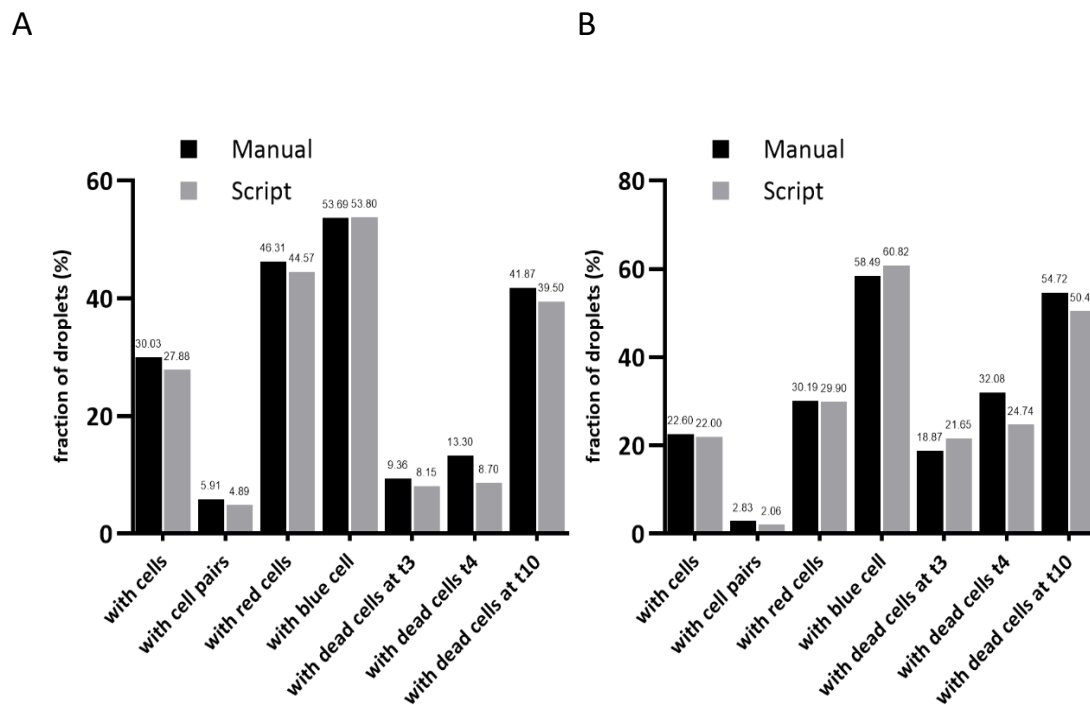
Supplementary Figure 4. Distribution of viabilities within droplets. **A.** The total counted viabilities of NK cells and target cells ($n=1000$ droplets). The graph depicts the experiment with NK cells paired together with K562 were all E:T ratios were taken together to show the difference between unpaired and paired cells. **B.** the viability of K562 cells in droplets; The graph depicts the experiment with only K562 in the droplets. Error bar represents Standard error of mean; $n=2$; $t=10h$.



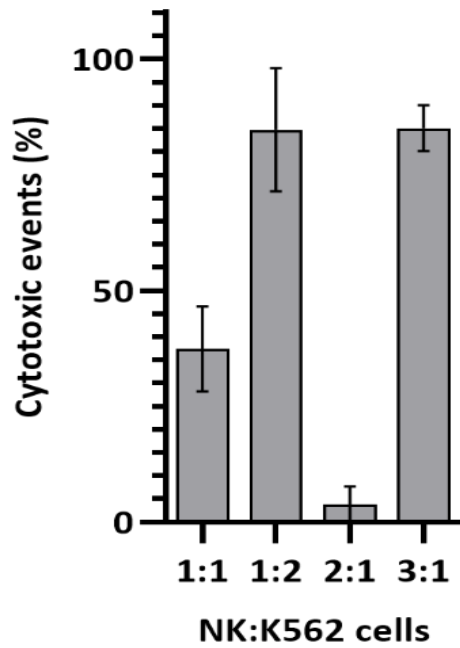
Supplementary Figure 5. Characterization of the use of Calcein Red AM (CR) and CellTracker Blue (CTB). **A-B.** K562 cells and Jurkat cells were labelled with different concentrations of CellTracker Blue and Calcein Red AM, washed, and cultured overnight. Necrosis and apoptosis were assessed using flow cytometry. $n=2$ for both graphs. **C.** K562 cells were labelled with different concentrations of CellTracker Blue (both cell types) and Calcein Red AM (K562 cells), washed, and encapsulated in droplets. Fluorescent signal of 20 randomly sampled cells was then measured using ImageJ and corrected for background. Significance was tested with unpaired Student's *t*-test, two-tailed. **D.** Jurkat cells were labelled with Calcein Red at 5 µM and CellTracker Blue at 5 µM and were encapsulated in droplets. The DMLAB script was then used to detect cells. The percentage of cells that was detected over time over the maximum number of cells that was detected is depicted in the graph. $n=3$ for both cell dyes; Error bar represents SEM.



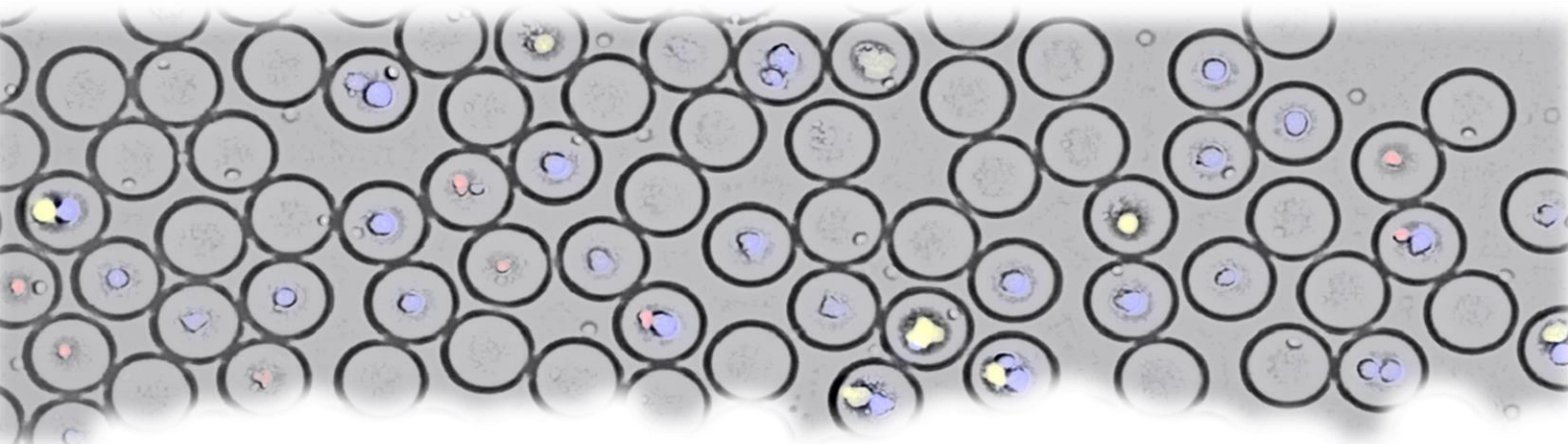
Supplementary Figure 6. Stability of viability dye over time **A.** Sytoxgreen (Nucleic acid binding) dye stability was measured on K562 cells that were labelled with CR at a concentration of 10 μ M; n=20; Error bar represents SD. **B.** Caspase detection reagent signal intensity was measured on Jurkat cells (not labelled with CR); n=20; Error bar represent SD.



Supplementary Figure 7. Distribution of viabilities within droplets. **A-B.** Validation of the script by comparing differences in cell distribution, cell pairing, and dead cell identification at 3 different time points (t=3, t=4, and t=10) in-between script generated data with manually counted data.

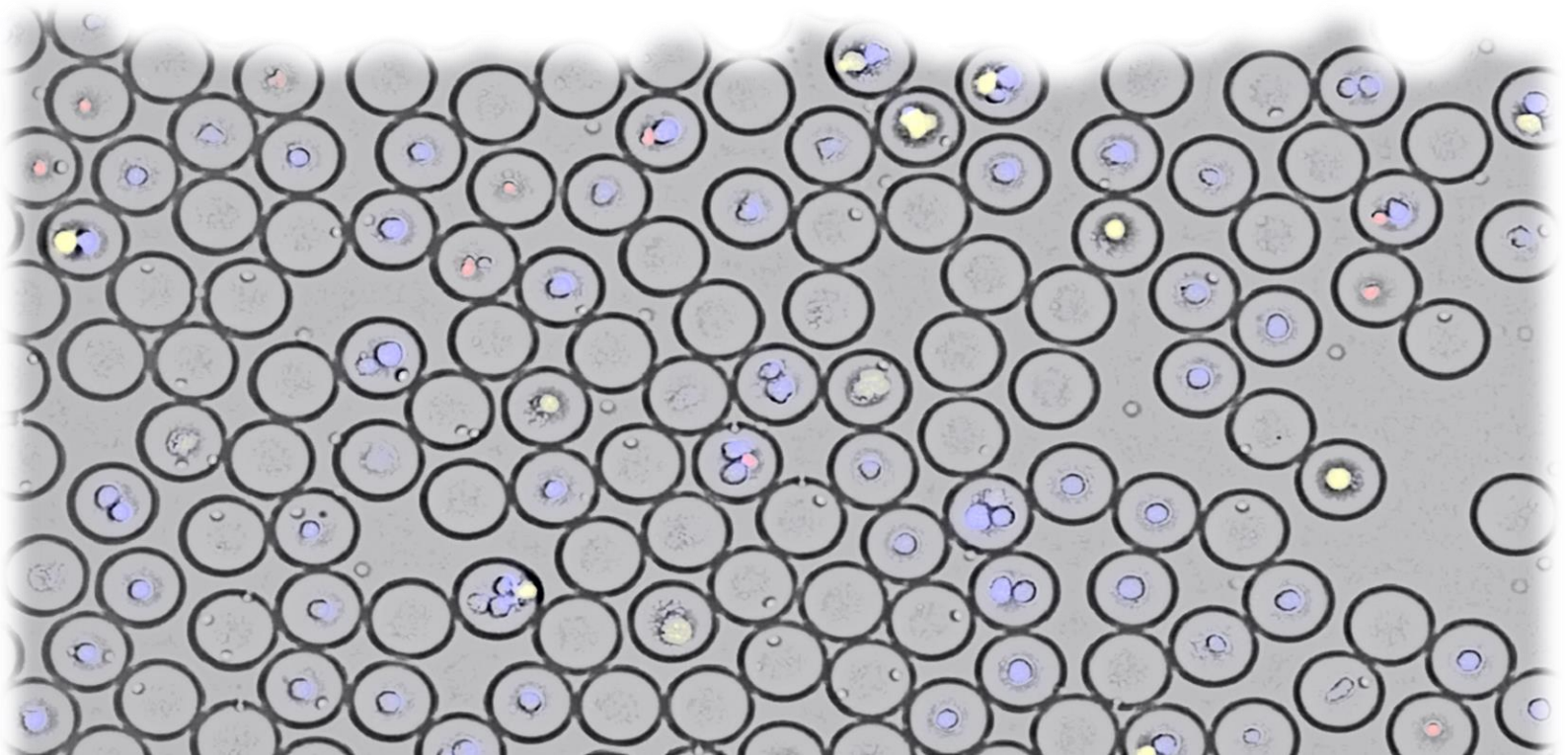
A

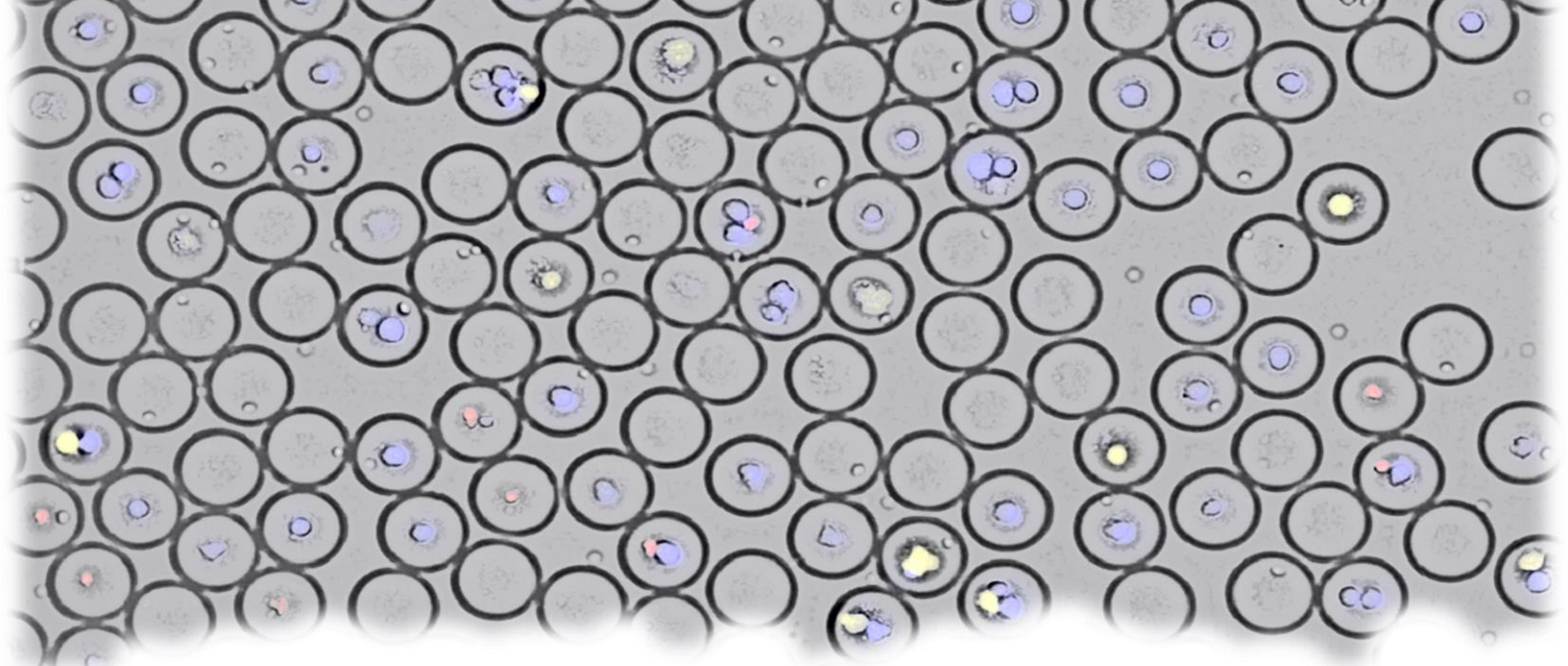
Supplementary Figure 8. Distribution of different E:T ratio in droplets: Difference in cytotoxicity at different cellular distributions (E:T 1:1,1:2,2:1,3:1); $n=3$ (for representative $n=1$ total droplets pair analyzed 1143; for 1:1 1066 droplets; 1:2 13 droplets; 2:1 49 droplets; 3:1 15;); error bar represents SEM.



PART 2

DECODING FUNCTIONAL HETEROGENEITY IN IMMUNE CELLS





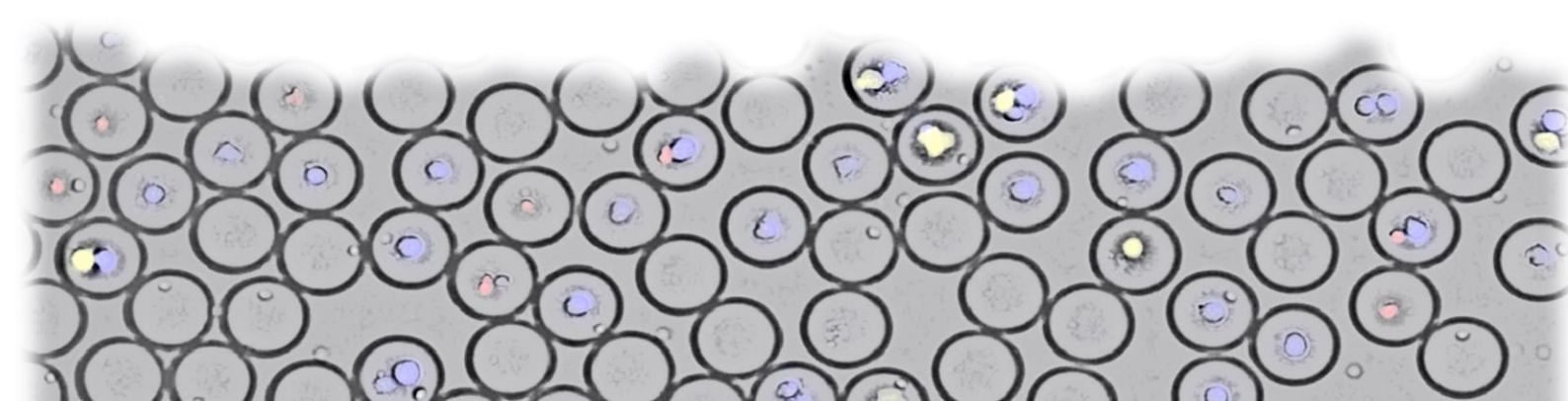
CHAPTER 4

SINGLE CELL PROFILING REVEALS FUNCTIONAL HETEROGENEITY AND SERIAL KILLING IN HUMAN PERIPHERAL AND EX VIVO-GENERATED CD34⁺ PROGENITOR DERIVED NATURAL KILLER CELLS

This chapter is submitted for publication as:

Single cell profiling reveals functional heterogeneity and serial killing in human peripheral and ex vivo-generated CD34⁺ progenitor derived natural killer cells

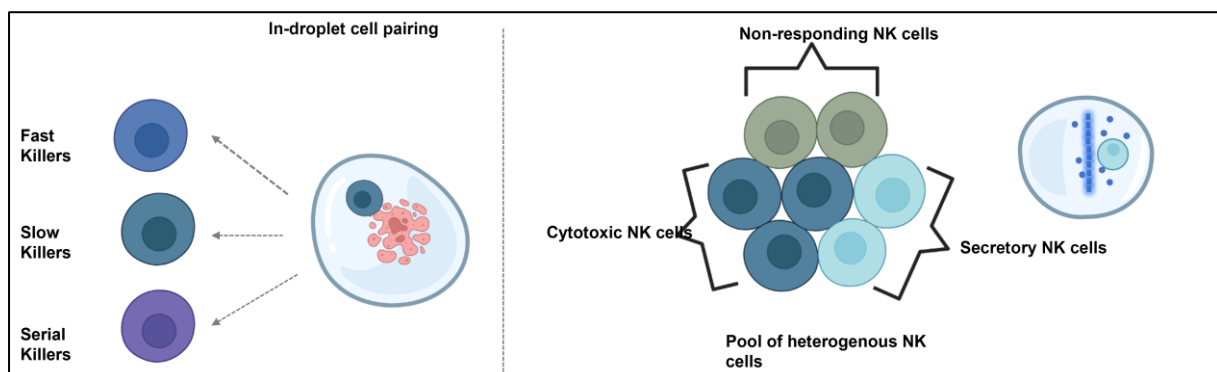
Nikita Subedi, Liesbeth Petronella Verhagen, Paul de Jonge, Laura Van Eyndhoven, Mark C. van Turnhout, Vera Koomen, Jean Baudry, Klaus Eyer, Harry Dolstra, Jurjen Tel



Abstract

Increasing evidence suggest that Natural killer (NK) cells are composed of distinct functional subsets. This multi-functional role displayed by NK cells have made them an attractive choice for anti-cancer immunotherapy. A functional NK cell repertoire is generated through cellular education, resulting in heterogeneous NK cell population with distinct capabilities to respond to different stimuli. The application of a high-throughput droplet-based microfluidic platform allows monitoring of NK cell-target cell interactions at single-cell level and in real-time. Through fluorescence-based screening of around 80,000 droplets, with different Effector:Target ratios, a fully automated image analysis allows for the assessment of individual killing events in each droplet over time. We observed a variable response of single NK cells towards different target cells and identified a distinct population of NK cells capable of inducing multiple target lysis, coined as serial killers. To meet the increasing clinical demand for NK cells several sources, such as umbilical cord blood (UCB), have successfully been explored. By assessing the cytotoxic dynamics, we showed that single UCB-derived CD34⁺ hematopoietic progenitor (HPC)-NK cells display superior anti-tumor cytotoxicity. Additionally, with an integrated analysis of cytotoxicity and cytokine secretion we showed that target cell interactions augmented cytotoxic as well as secretory behavior of NK cells. By providing an in-depth assessment over NK cell functions, this study provides crucial information on diversity and functional characteristics of peripheral blood NK cells and *ex vivo*-generated HPC-NK cells to develop and improve of NK cell-based cancer immunotherapy.

Graphical Abstract



1. Introduction

Natural killer (NK) cells are a subgroup of type 1 innate lymphoid cells capable of inducing cytolytic activity against virus-infected or cancer cells. Unlike other lymphocytes, these cells do not need prior antigen sensitization and induce rapid lysis of target cells upon identification without harming healthy tissue[1]. Apart from cytotoxicity, NK cells also secrete immune-stimulating molecules that modulate the functions of other immune cells[2]. This functional versatility has enhanced the popularity to exploit NK cells in anti-cancer immunotherapy. More importantly, clinical effects have been demonstrated upon infusion in cancer-bearing patients[3,4]. Recent developments in NK cell-based immunotherapy consist of different strategies, including the use of different cytokines to enhance autologous NK cells or to use allogeneic NK cells (both in their endogenous or genetically engineered form) as the mode of adoptive therapy. Even in allogeneic conditions, NK cell infusion is safe they match the criteria for the off-the-shelf immunotherapy[5]. A major hurdle is that only a small fraction of peripheral blood mononuclear cells comprises of NK cells, and thus generating them in sufficient numbers to meet clinical requirements is challenging[5]. Recently, other sources for NK cells, such as umbilical cord blood (UCB) and G-SCF mobilized blood, have therefore been successfully explored[6–8]. As a major advantage, UCB-derived CD34⁺ hematopoietic progenitor cells (HPCs) are more easily available and have several NK cell progenitors with fewer requirements for HLA matching compared to T cells.[9]. This makes UCB-derived HPCs a flexible and attractive source for NK cells[7]. Upon expansion, these cells display significantly more cytotoxicity in bulk experiments compared to their blood-derived counterparts[10].

In addition to their clinical relevance, it is also important to understand the functional potency of individual NK cells to optimize immunotherapeutic efficacy. Namely, NK cells exhibit a high degree of heterogeneity, both phenotypically and functionally[11–13]. Mass cytometry-based data demonstrated how diverse the NK cell population can be by revealing over 100,000 different phenotypes within a healthy individual[14]. Therefore, the overall function of NK cells results from combined efforts of multiple diverse individual cells. Although these cells lack genetic rearrangement and recombination, like T and B lymphocytes, this high variation shapes them into becoming a versatile cell type[15]. Recent studies utilized single-cell RNA sequencing to profile NK cells transcriptomic and identified specific markers that could be clustered into different functional subpopulation[11,13,16,17]. Furthermore, using a

microwell-based single-cell platform Vanherberghen and coworkers identified rare serial killer NK cells with superior cytotoxic behavior which accounted for more than 50% of total lysis[1]. Hence, single-cell-based tools lay the basis for a new era in dissecting heterogeneity within the NK cell compartment to address the functional ability of individual cells[18].

Previously, we developed a high throughput droplet-based microfluidic platform to monitor the cytotoxic effector function of immune cells at single-cell level[19]. In this current study, we monitored around 80,000 droplets over 10 hours in real time to probe the phenotypical and functional heterogeneity of single human PB-NK cells and *ex vivo*-generated HPC-NK cells. Furthermore, we identified a cell population within these NK cell sources with superior serial killing ability. By pairing NK cells with distinct target cells, we demonstrate that NK cell-mediated cytotoxicity and cytokine secretion is a dynamic process restricted to a percentage of single NK cells equipped with this ability. By providing an in-depth assessment of NK cell functions, this research provides crucial information on the diversity and functional characteristics of PB-NK cells and HPC-NK cells to channel new avenues in NK cell-based cancer immunotherapy.

2. Materials and Methods

2.1 Cell isolation and culture

K562 cells were cultured in 1:1 (v/v) mixture of RPMI 1640 (Gibco, Catalog no. 22400089) and IMDM (Gibco, Catalog no.12440053) supplemented with 10% fetal bovine serum (FBS; Gibco) and 1% penicillin/streptomycin (PS; Gibco). THP-1 and Daudi cells were cultured in RPMI, supplemented with 10% FBS and 1% PS. All the cell lines were regularly tested for mycoplasma contamination. PB-NK cells were obtained from buffy coats of healthy donors (Sanquin) after written informed consent according to the Declaration of Helsinki and all experimental protocols concur to institutional guidelines. In short, peripheral blood mononuclear cells (PBMCs) were isolated from donor blood via density gradient centrifugation using Lymphoprep Density Gradient Medium (Stem cell). The NK cells were subsequently isolated using magnet-activated cell sorting (MACS) by negative selection using an NK cell isolation kit (Miltenyi Biotech, Catalog no. 130-092-657) following the manufacturer's instructions. Cells were counted and purity was routinely assessed using flow cytometry by cell surface marker staining for 10 minutes at 4°C, using PE-CY7-labeled anti-CD56 (Biolegend, Catalog no. 362509), PE-labeled anti-CD16 (Biolegend, Catalog no. 302007), and PerCP-labeled anti CD3 (Biolegend, Catalog no. 300328) antibodies in 50 µL FACS buffer (2% FBS in PBS). The NK cells were identified as CD16⁺CD56⁺CD3⁻, and purity was on average 91%. Subsequently, isolated NK cells were encapsulated into droplets with K562 in presence of 1400 ng/mL IL2, as stimulant (Peprotech, Catalog no. 200-02).

2.2 HPC-NK cell culture and expansion

Cryopreserved UCB CD34⁺ progenitor-derived HPC- NK cells from different donors were kindly provided by Dr. Harry Dolstra (Radboudumc, Nijmegen)[10]. The cells were thawed in medium with 71% Human Serum (HS; Sanquin), 0.03% DNase and 0.1%MgCL₂ and were washed (at 300 g for 15 minutes) after 10 minutes resting. The cells were then resuspended in NK MACS medium (Miltenyi, Catalog no. 130-107-209) supplemented with 10% HS and 1% NK MACS supplement (Miltenyi) at the concentration of 3 million cells/mL. 1.5 mL of the cell suspension was loaded into the 6 well plate and were supplemented by 50 ng/mL IL-15 (Immunotools, Catalog no. 352310) and 0.2 ng/mL IL-12 (Miltenyi, Catalog no. 130-096-704). On every second day, 1 mL NK MACS medium (with 10%HS, 1% NK MACS

Supplement, 50 ng IL-15 and 0.2 ng/mL IL-12) was added to the cells, thus allowing them to expand for 7 days. All the assays were performed after the 6th day of expansion. The culture was kept for 2 weeks after thawing.

2.3 Microfluidic chip for droplet production

The three-inlet microfluidic device was developed following the protocols as described in Sinha et. al[20]. The microfluidic device was molded using an SU-8 photo resist structure on a silicon wafer and a commercially available polydimethylsiloxane silicone elastomer (Sylgard 184, Dow Corning), mixed with curing agent at the ratio 10:1 (w/w) and allowed to cure for 3 hours at 60°C. The surface of the Sylgard 184 was activated by exposure to plasma and sealed with a plasma-treated glass cover slide to yield closed micro channels. Channels were subsequently treated with a 5% (v/v) silane (1H,1H,2H,2H-Perfluorooctyltriethoxysilane; Fluorochem, Catalog no. S13150) solution in fluorinated oil (Novec HFE7500, 3M, Catalog no. 51243) and thermally bonded for 12 hours at 60°C. The dimensions of the microfluidic channels are 40 μm \times 30 μm at the first inlet, 60 μm \times 30 μm at the second inlet and the production nozzle, and 100 μm \times 30 μm at the collection channel.

2.4 Assembly of Droplet observation chamber

Glass microscopy slides (76 \times 26 \times 1 mm; Corning) were used as top and bottom covers (76 \times 26 \times 1 mm). Two access holes of 1.5 mm diameter were drilled in the top glass. Both slides were thoroughly cleaned using soap, water, and ethanol, and were exposed to air plasma (60 W) for 5 minutes. A cutout sheet of 60 μm thick double-sided tape (ORAFOL) was carefully placed above the bottom glass slide. Afterwards, the glass slides were stacked on top of each other, and the assembly was pressed using Atlas Manual 15T Hydraulic Press (Specac) for 5 minutes at 155°C at 400 kg per m² pressure load. Next, two nano ports (Idex) were attached to the holes using UV curable glue (Loctite 3221 Henkel) which was cured under UV light for 5 min. Subsequently, the surface of the 2D chamber was treated with 5% (v/v) silane solution. Lastly, the chamber was dried, filled with fluorinated oil, and sealed until use. The chamber was reused multiple times and cleaned after each experiment by flushing fluorinated oil to remove droplets and was stored filled until the next use.

2.5 Cell loading in microfluidic chip

Droplets were produced with a three-inlet microfluidic device. The protocol for loading cells in the microfluidic chips is described in Subedi et al[19]. The droplets of ~50 μm diameter were generated using flow speeds of 30 $\mu\text{L}/\text{min}$ for oil and 5 $\mu\text{L}/\text{min}$ for each sample inlet. For serial killer experiments, droplets of ~130 μm diameter were produced using flow speeds of 20 $\mu\text{L}/\text{min}$ for oil and 5 $\mu\text{L}/\text{min}$ for each sample inlet. The droplets were produced for around 5-10 minutes, thus generating 700,000 droplets in total. For the stability of droplets, 2.5% (v/v) Pico-Surf[®] surfactant (Sphere Fluidics, Catalog no. C024) was used in fluorinated oil.

2.5 Bulk Activation Assay

NK cells were incubated at 1 million cells per 100 μL in PBA containing IFN γ Catch Reagent (Miltenyi, Catalog no. 130-090-443) and TNF α Catch Reagent (Miltenyi, Catalog no. 130-091-268) at 4°C for 20 minutes. Next, cells were washed and resuspended in RPMI cell culture medium supplemented with 2% HS, 1% PS, at 25,000 cells per 100 μL in U-bottom microwell plates together with stimulants (K562 cells at E:T 1:1 or IL2 50 ng/ml or K562+IL-2 at above mentioned concentrations). The cells were incubated at 5% CO₂ and 37 °C temperature for 4 hours.

2.7 Single NK cell Activation Assay

NK cells were incubated at 1 million cells per 100 μL in PBA containing IFN γ Cytokine Catch Reagent and TNF α Cytokine Catch Reagent at 4°C for 20 minutes. Cells were then washed and resuspended in RPMI culture medium supplemented with 2% HS and 1%PS, at 2 million cells/mL for single-cell encapsulation. Next, the NK cells were encapsulated in 70 pL (~50 μm) droplets together with stimulus (final concentration of K562 cells, 15 million cells/mL or IL-2, 700 ng/ml or K562+IL-2, earlier mentioned concentrations) loaded from another inlet. The concentrations of stimulus have been adjusted such that each single-cell received same absolute number of molecules as in bulk-based experiments. Droplet production and encapsulation rates were carefully monitored using a microscope (Nikon) at 10x magnification and a high-speed camera. The droplet emulsion was collected and covered with culture medium to protect droplets from evaporation. The encapsulated cells were incubated in Eppendorf tubes with a few punched holes to allow gas exchange, at 5% CO₂ and 37 °C temperature. After 4 hours of incubation, the droplets were de-emulsified by

adding 100 μ L 20 v/v% 1H,1H,2H,2H-Perfluoro-1-octanol (PFO; Sigma Aldrich, 370533) in HFE-7500 and stained for FACS analysis.

2.8 FACS-Antibody Staining

Cells were washed once with PBS and dead cells were stained with Zombie Green fixable viability dye (Biolegend, 423111), 1:10.000 in PBS, 50 μ L) at 4°C for 20 minutes. Subsequently, cells were washed once with PBS and incubated with anti-human antibodies against CD3 (PerCP-Cy5.5, Biolegend), CD56 (BV510, Biolegend), CD16 (BV605, Biolegend), CD11b (PE-Cy5, Biolegend) CD27 (AF700, Biolegend) NKp46 (PE, Biolegend), NKg2A (PE-Dazzle 594, Biolegend), IFN γ (FITC, Miltenyi) and TNF α (APC, Miltenyi) at 4°C for 30 minutes. Next, the cells were washed twice with PBS buffer with 0.5% BSA and analyzed via BD FACS Arial.

2.9 Single NK cell cytotoxicity assay

NK cells and target cells were labelled with Calcein red (5 μ M) (ATT Bioquest) and Cell tracker blue, CMAC (10 μ M) (Invitrogen) respectively. The labelled NK cells and target cells were then loaded into droplet chip via different inlets at the concentration of 7 million cells/mL and 10 million cells/mL, respectively. The viability dyes Sytox Green (Invitrogen) and Cell Event Caspase-3/7 Green (Invitrogen) were loaded at the final concentration of 5 μ M and 7 μ M respectively along with the cells, and droplets were collected in the observation chamber. Droplets were generated at room temperature while collected into the observation chamber over a warm water bath. The immobilized droplets were incubated in a stage top incubator set at 5% CO₂ and 37 °C. Image acquisition was performed at every hour interval for 10 h.

2.10 Nanoparticle functionalization

50 μ g of Paramagnetic nanoparticles (Bio-Adembeads Streptavidin Plus 300nm, Ademtech) were washed with 50 μ g PBS(Gibco) using a magnet. The supernatant was removed, and the nanoparticles were resuspended in 990 μ L PBS with biotinylated anti-IFN- γ (Biolegend) antibodies and incubated for 30 min at room temperature while mixing. 10 μ L Biotin was added with a final concentration of 1 mM in the solution and incubated for 10 min at room temperature. The beads were washed again with PBS using magnets and resuspended in 5% Pluronic F-68 (Gibco) PBS solution and incubated for 30 min at room temperature. The beads were washed and resuspended in assay buffer containing RPMI 1640 (Gibco, life

technologies), 5% Human Serum (HS) (Sanquin), and 25 mM HEPES (Gibco) and incubated for 10 min at room temperature. The nanoparticles were washed again and finally resuspended in the 100 μ L of assay buffer containing fluorescently labeled AlexaFlora568-detection antibody for IFN- γ (Biolegend).

When performing time-lapse experiments with cells, the final nanoparticle suspension contained 700 ng/ml IL-2 stimuli (Peprotech) and 10 μ M Sytox Green (Invitrogen) as final concentration in droplets. For experiments concerning the calibration curve and optimization steps, IFN- γ (Peprotech) cytokine samples ranging from 0.001 - 100 nM were prepared in assay buffer. All calculations were made considering the final concentration inside the droplets.

2.11 Image acquisition and analysis

Fluorescence imaging was performed using a Nikon Eclipse Ti2 microscope, using a 10X objective and mCherry, DAPI, and FITC/YFP filters every hour. The images were viewed using NIS Element and Image J. Automated Image analysis was performed using custom-made in-build MATLAB script (Mathworks), DMALAB (available with submission). The script generated a droplet mask that was overlaid onto the fluorescence images, and each droplet was analyzed separately. Over 80,000 droplets were analyzed using this script. The output received are in terms of droplet index, cell count, fluorescence intensity and dead cell count. Detailed description of image analysis script is provided in Subedi et al[19]. For the experiments with serial killers, microscopy images were analyzed manually.

2.12 Statistics and software

The graphs were generated using GraphPad Prism 9.0.0. The results are expressed as mean \pm SEM. Significant differences between two groups were analyzed by two-tailed unpaired Student's t-test (Mann-Whitney test). P values < 0.05 were considered statistically significant. Flow cytometry data were analyzed using FlowJo X (Tree Star). FMO staining served as controls for gating strategy. For the gating strategy, the readers are referred to Supplementary Figure 1A.

3. Results

3.1 Single-NK cell activation in droplets using K562 and IL2

To study the diversity within the NK cell compartment, we utilized droplets-based microfluidics to activate single NK cells with K562 cells and cytokines in an isolated environment with reduced paracrine interaction within cells. Similar to our previous work, NK cells were labelled with cytokine catch reagents for IFN- γ and TNF- α to allow for capturing and monitoring cytokine secretion by single-cells[21,22]. After 4 hours of activation cells were retrieved from the droplets by breaking the emulsion with PFO and prepared the cells for downstream Flowcytometric analysis (Figure 1A).

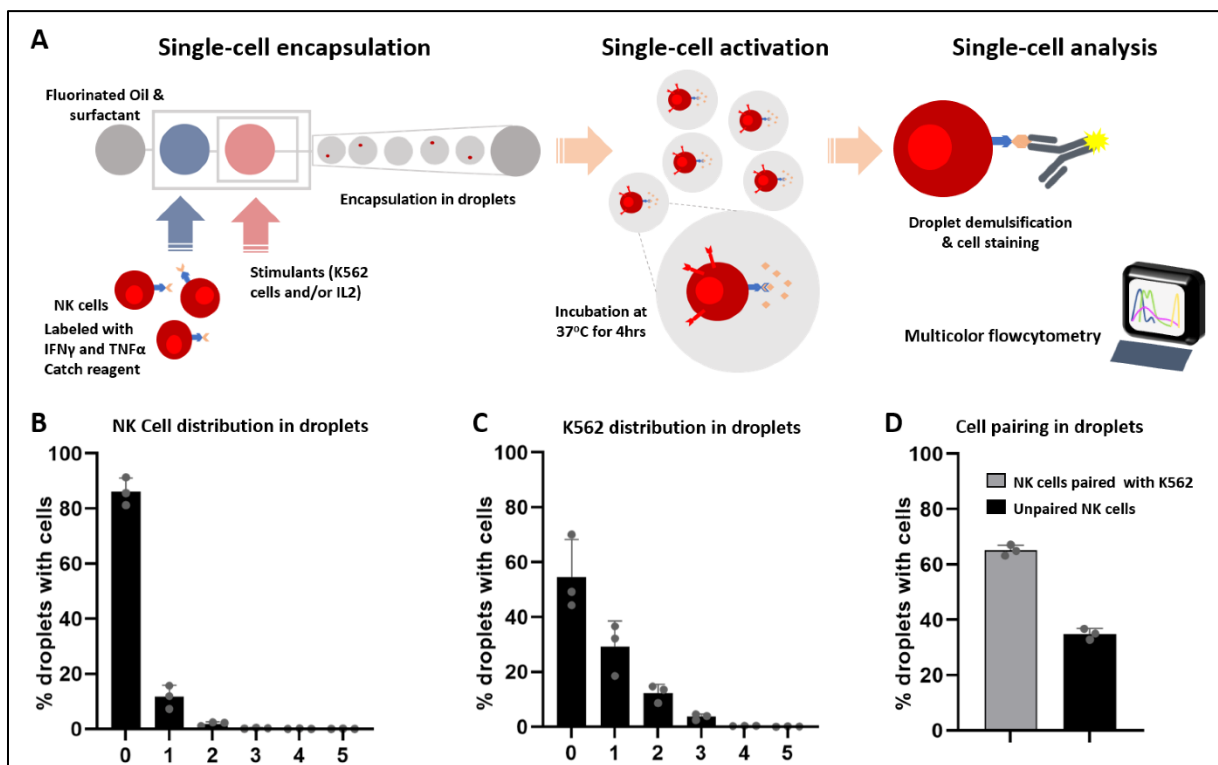


Figure 1. Experimental Schematics showing NK cell activation and cytokine secretion assay in droplet:

A. Freshly isolated human peripheral blood NK cells were labelled with IFN- γ and TNF- α catch reagent and encapsulated together with stimulants (K562/IL-2) into oil/water droplets using a 3-inlet flow-focusing droplet chip with 25 μ m height. After 4 hours, the droplets were dissolved using PFO solution to retrieve the cells, which were thereafter labelled for FACS analysis. The distribution of cellular encapsulation of NK cells **B.** or K562 cells **C.** in the droplets. **D.** Cell pairing distribution in droplets. Results are shown as the mean \pm SEM of 3 independent experiments with different donors.

Similar to our previous studies with other cell types, the viability of NK cells after culturing in droplets was preserved (Supplementary figure 1B). We used pipette tips for loading cells in microfluidic chips to increase the probability of cellular encapsulation, and to achieve optimal cell pairing at a ratio of 1:1 in the oil-water droplets (~70 pL)[20]. The cell loading concentrations were adjusted such that NK cells were optimally paired with K562 cells, and the percentage of activated cells reflected the cellular interaction. With optimal loading conditions we generated droplets containing 65% single NK cells co-encapsulated together with K562 cells (Figure 1B-D). In summary, our platform allowed us to probe NK cell activation at single-cell level and interaction with target cells.

3.2 Functional heterogeneity within peripheral blood NK cells - phenotypical correlation at different maturation stages

Studies associated stages of NK cell maturation with functional variations[23,24]. Here, we combined CD56 and CD16 with CD11b and CD27 to define different functional subsets within PB-NK cells. Even though CD11b and CD27 are generally not considered conventional markers for maturation in humans, their functional role has recently been documented[25,26]. Additionally, recent studies showed a correlation between murine maturation phenotypes and human phenotypes[27]. This prompted us to investigate these specific markers in association with human maturation stages. With our platform, we assessed the phases of maturation and characterized them into three distinct phenotypical subsets: 1. Tolerant NK cells (CD56⁺CD16⁻CD27⁻CD11b⁻), 2. Regulatory NK cells (CD56⁺CD16⁻CD27⁺CD11b⁺), and 3. Cytotoxic NK cells (CD56⁺CD16⁺CD27⁻CD11b⁻) (Figure 2A). We also identified an intermediate stage that showed dim expression of both CD56 and CD16 (CD56⁺CD16^{+/}-CD27⁻CD11b⁺), here described as pre-cytotoxic NK cells. The distribution of the different NK cell subsets was investigated in freshly isolated cells and analyzed after bulk and single-cell culture without addition of external stimuli. The composition within the population was dominated by mature NK cells, ~80% CD56⁺ cytotoxic phenotypes (Figure 2B,C). Activating NK cell with IL2 induced a 2-fold increment in tolerant phenotypes (Figure 2D,F, Supplementary Figure 2) whereas interaction with K562 led to an increase in the cytotoxic subsets (Figure 2E,F, Supplementary Figure 2). For both single and bulk stimulated cells, we hardly observed the regulatory NK cell phenotype (Figure 2).

Taken together, the overall composition of the PB-NK cell population with distinct subsets was not altered by external factors such as cytokines and cellular interactions. Even at single-cell level, the observed NK cell diversity was similar as was defined in earlier studies, thus confirming that droplets-based platforms are suited for studying NK cell heterogeneity.

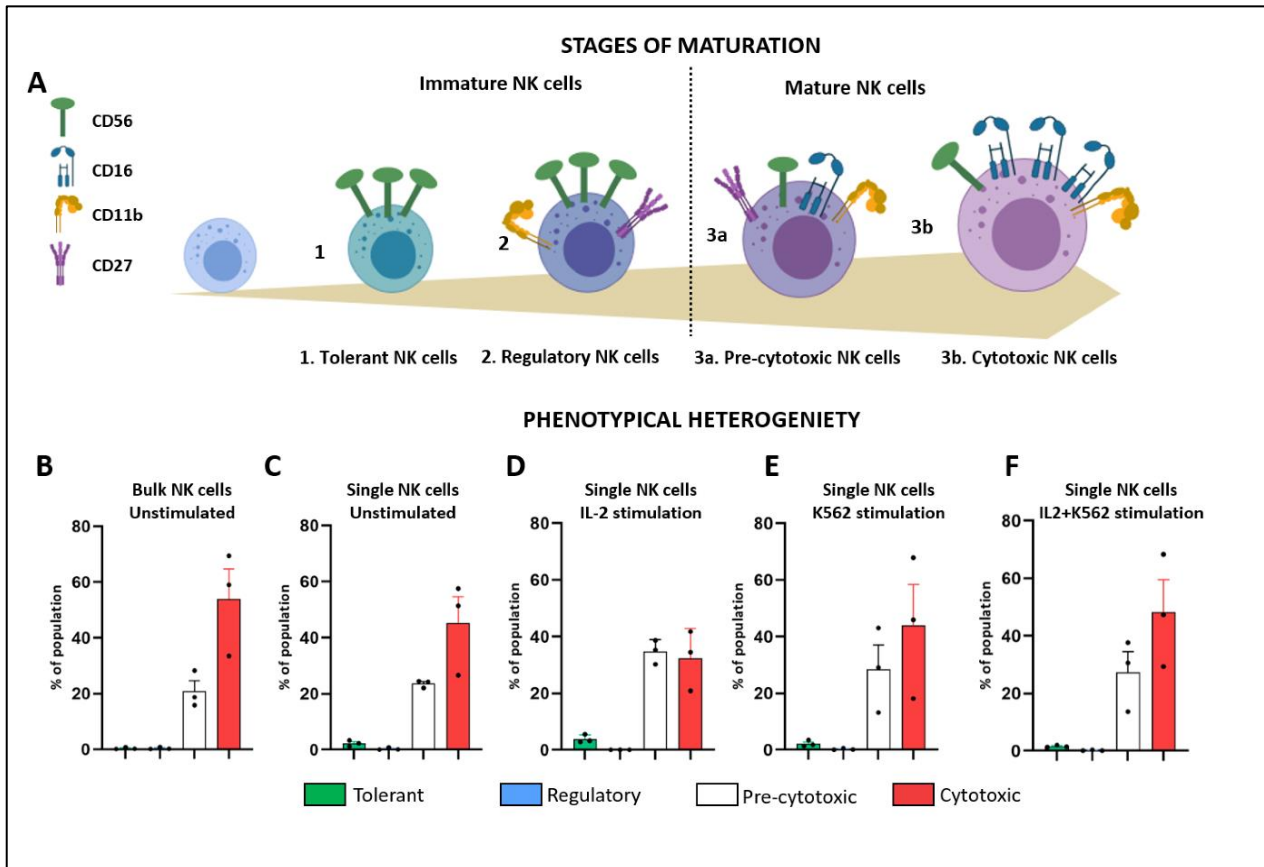


Figure 2. Phenotypical heterogeneity within peripheral blood NK cells and correlation at different maturation stages: **A.** Schematics of NK cell maturation versus different functional subgroups within the NK cell population. **B-F,** Graphs showing distribution of different NK cell population for different conditions upon incubation for 4 hours. **B.** Unstimulated NK cells in a traditional bulk-based assay. **C.** Unstimulated NK cells in droplets, **D.** Activation of single NK cells with IL-2 in droplets. **E.** Activation of single NK cells with K562 in droplets. **F.** Activation of single NK cells with K562 and IL-2. Green, blue, white, and red bars represent tolerant, regulatory, pre-cytotoxic and cytotoxic phenotypes respectively. Results are shown as the mean \pm SEM of 3 independent experiments with different donors.

3.3 Functional diversity of PB-NK cells at single-cell level

Next, we studied different functions of PB-NK cells at single-cell level to associate them with the respective phenotypes. IFN- γ and TNF- α secretion were included as functional markers for immune regulation, CD107a (degranulation marker) as measure for cytotoxicity and NKG2A

and NKp46 as maturation markers[28–30]. The combined stimulation with IL-2 and K562 induced the most secretion of IFN γ by all four defined subsets (Figure 3A). Regulatory and tolerant phenotypes (CD56⁺⁺⁺) showed the highest percentage (approximately 10%) of cytokine secreting cells, however, the total number of events observed for these subtypes was very low (at most 2%). Therefore, compared to the absolute number of events, both of the cytotoxic phenotypes showed the largest number of positive cells upon combined stimulation.

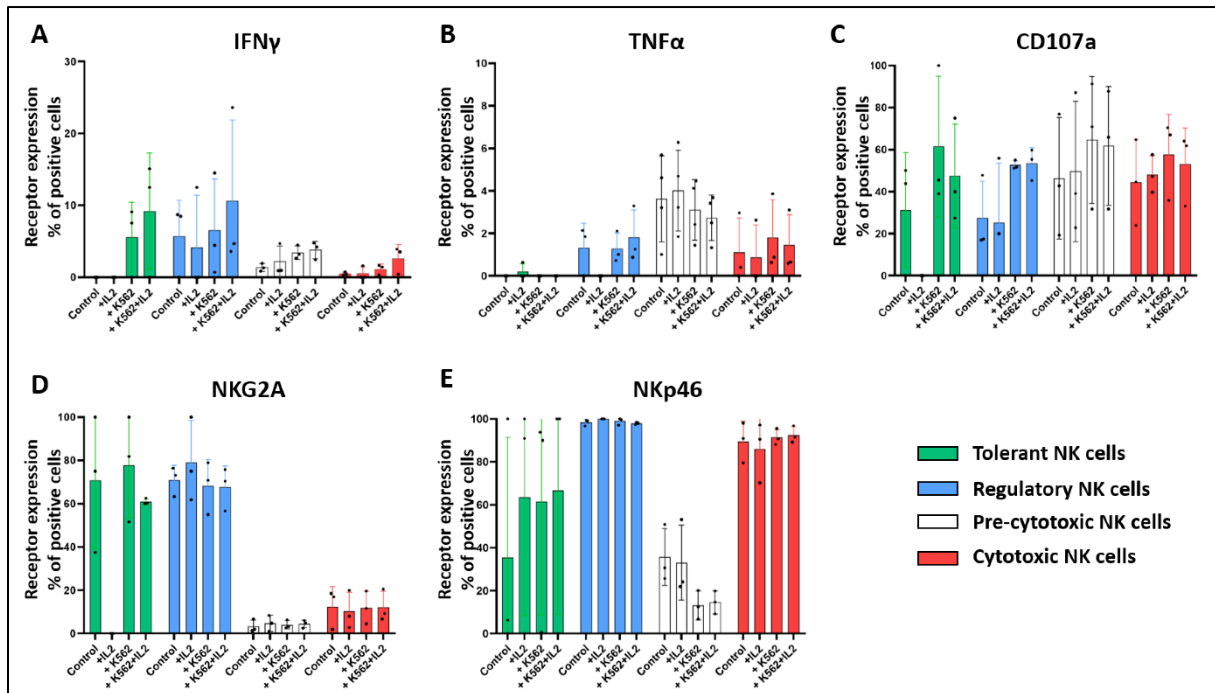


Figure 3. Functional diversity of NK cells at single-cell level: A-E, Graphs showing the percentage of NK cells population positive for **A.** IFN- γ , **B.** TNF- α , **C.** CD107a, **D.** NKG2A, **E.** NKp46 when stimulated in droplets with IL-2, K562 or IL-2 and K562 combination. Green, blue, white, and red bars represent tolerant, regulatory, pre-cytotoxic and cytotoxic phenotypes respectively. Results are shown as the mean \pm SEM of 3 independent experiments with different donors.

Both the regulatory and the cytotoxic phenotypes showed high TNF α secretion upon stimulation (Figure 3B). Notably, no difference in CD107a expression upon stimulation was observed with the cytotoxic phenotypes while the pre-cytotoxic phenotype dominated the CD107a expression thus showing an enhanced cytotoxic behavior (Figure 3C). Furthermore, pre-cytotoxic phenotype also formed a major component of the PB-NK cell compartment and expressed intermediate levels of NKp46 (Figure 3E). These findings strengthen the notion that this subset could be the immediate precursor of the cytotoxic population. As expected, the tolerant and regulatory phenotypes showed higher expression of NKG2A, while NKp46 was

highly upregulated by more mature regulatory and cytotoxic phenotype (Figure 3D,E). Collectively, we showed functional variation among different PB-NK cell phenotypes upon stimulation at single-cell level indicative for heterogeneity within the NK cell compartment.

3.4 NK cell mediated cytotoxicity is a dynamic process and highly dependent upon target cell interaction

The interaction dynamics of single NK cells with different target cell types were closely monitored to improve the understanding of cytolytic function. Previously, we developed a droplet-based single-cell platform for high throughput and real time analysis of cellular cytotoxicity[19]. We used this platform to monitor over 80,000 droplets per experiment which approximately contained 3,500 droplets with a 1:1 NK cell: target cell ratio (Figure 4A). Individual droplets were monitored for 10 hours and subsequently analyzed with an automated script to identify possible cytotoxic events (Figure 4B). During the course of incubation, we observed around 3% target cell division (data not shown) however, all the E:T ratio were defined based on observation at t=0.

PB-NK cells showed a significant variation in the cytolytic function upon interaction with different target cells (Figure 4C). Where single PB-NK cells lysed around 25% (± 2.25 ; n=3) K562 cells, only 10% (± 4.318 ; n=3) of THP-1 and 8% (± 0.271 ; n=3) of Daudi cells were killed by single PB-NK cells. We observed similar variation using a bulk-based cytotoxicity assay, thereby benchmarking our single-cell findings. For K562 and Daudi cells, most of the cytotoxic events were observed within the first four hours of cellular interaction, while lysis of THP-1 cells occurred at later time points (Figure 4D). This variation in lytic abilities of PB-NK cells could be linked with the differential expression of the MHC-I molecules expressed by different target cells (Supplementary figure 3).

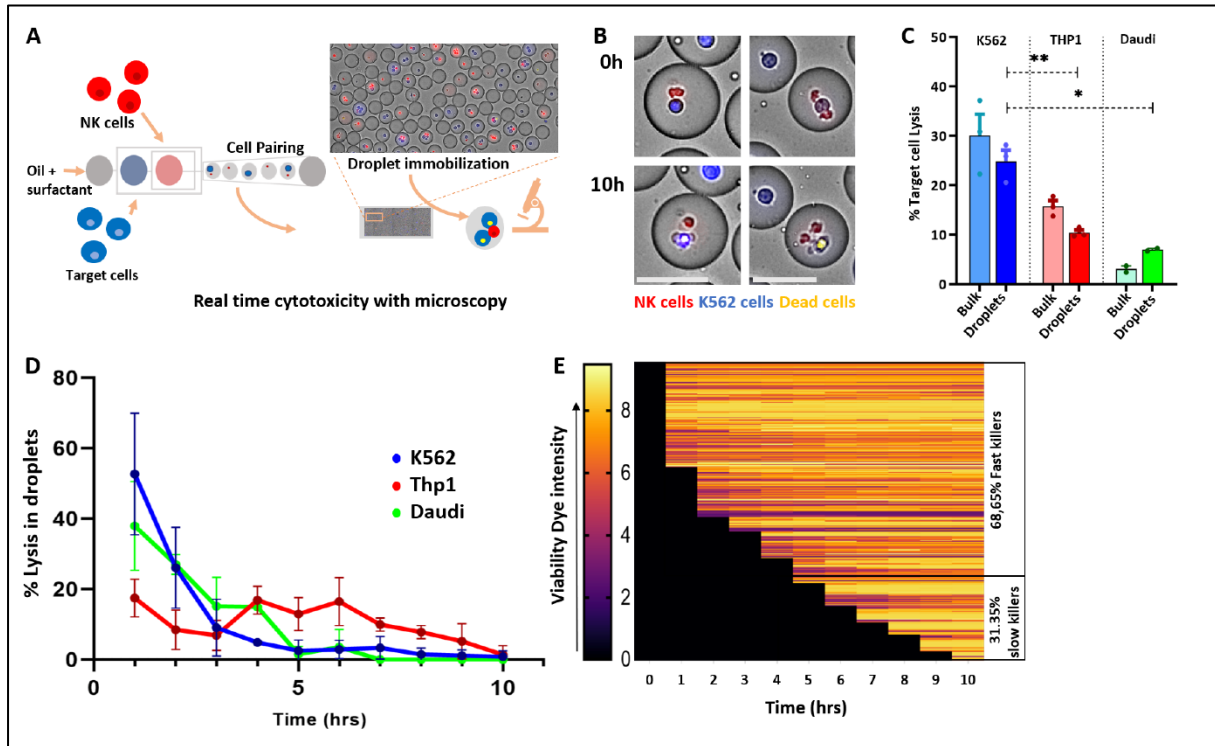


Figure 4. NK cell mediated cytotoxicity at single-cell level: **A.** Schematic representation of single-cell cytotoxicity. NK cells were labelled with Calcein Red AM dye (red cells) and K562 cells with Cell Tracker Blue (blue cells) and paired together in 70 μ L droplets in the presence of viability dye (Sytox green and Cell event Caspase 3/7; yellow cells). Cells were incubated at 37 $^{\circ}$ C and 5% CO_2 for 10 h. **B.** Microscopic overview of NK cell-mediated cytotoxicity in droplets. Over the interval of 10 h, NK cells interacted with target cells inducing cytotoxicity. The dead cells were stained with the viability dye turning yellow. Scale bar = 50 μ m. **C.** Bulk versus droplets cytotoxicity assay with K562 (Blue), Thp1 (Red) and Daudi cells (green). Light and dark colors represent bulk and droplets experiments respectively. **D.** Graph representing the dynamics of cytotoxic events in droplets for different donors. The dynamics were determined for the killer fraction of NK cells, thus showing the percentage of the fast and slow killer population in NK cells. Blue, green, and red lines represent K562, THP1 and Daudi cells respectively; data analysis performed on E:T 1:1. **E.** Heat Map showing the dynamics of cytotoxicity within an experiment. Each line represents individual cells. The graph does not include the droplets with 0, or 1 cell and droplets with dead cells at $t = 0$ h. Results are shown as the mean \pm SEM of 3 independent experiments with different donors.

Zooming in on the killing events revealed that 42% of NK cells (fast killers) induced killing as early as 1 hour. In total 69% NK cells were able to kill K562 cells during 4 hours of interaction (Figure 4E). The remaining 31% of cells (slow killers) only induced cytotoxicity at later time

intervals. The observation of these early and late lytic events implies differential regulation in target cell recognition and the involvement of different cytotoxic mechanisms shown by different NK cells with regards to different target cells. Two distinct cytotoxic mechanisms were shown to act on different time scales, with rapid granule-mediated cell death and slower CD95-induced or TRAIL induced apoptosis[31]. These striking differences in lytic ability observed between individual NK cells, together with their variation in killing behavior towards different target cells further strengthens the existence of heterogeneity within the PB-NK cell population.

3.5 Identification of rare serial killing events executed by NK cells using droplet-based single-cell platform

There exists a small fraction of NK cells endowed with an immense capacity to kill and handle most of the target cell lysis[1,31]. These cells, also known as serial killers, can kill over 3 target cells consecutively and are a pursued phenotype for application in cancer immunotherapy. The fraction of serial killer NK cells is however relatively low and other than their superior killing ability, not much is known yet about them.

We therefore adapted the microfluidic platform by tuning the droplet size and cell loading concentrations and utilized the strength of our approach to study these potent serial killers in high throughput. With larger droplets (1.2 nL volume) we increased the fraction of droplets containing multiple target cells (≥ 3) with single NK cells to around 3% (242 droplets) (Figure 5A,B). Exploring different E:T ratios i.e., 1:1, 1:2, 2:1 and 3:1, variations in lysis of target cells was distinctly observed (Figure 5C). At 1:1 ratio, lower fraction of death in K562 cells was seen in bulk than compared to droplets at a 1:1 ratio. In contrast, at 1:2 ratio around 50% (± 4.7 ; $n=4$) of paired K562 cells were killed by single encapsulated NK cells in the droplet and this was higher than observed in bulk-based measurements. When single K562 cells were paired with either 2 or 3 NK cells in droplets, the percentage of cell death increased and was somewhat higher than the corresponding bulk-based assay. By comparing with the significantly low killing events with unpaired K562 (in-droplet controls), we ruled out the possibility of spontaneous cell death in the droplets (Figure 5C).

We defined serial killing activity if a single NK cell could consecutively lyse ≥ 3 target cells over the period of 10 hours. Zooming in on droplets with 1 NK cell and 3 or more target cells, we observed 12% (± 0.736 , $n=3$) serial killing events by PB-NK cells (Figure 5D,E, Supplementary

figure 4). Additionally, we observed in 49% (± 8.06 , $n=3$) of droplets with less than 3 K562 cells target cell lysis and 37% (± 9.68 , $n=3$) droplets showed no target cell lysis. To ensure multiple cell encapsulation, we enhanced the droplet size which however resulted in later cellular interactions between NK and target cell, thus decreasing the percentage of positive cytotoxic events early upon incubation [32].

Interestingly, using our droplet-based assay we segregated and created multiple conditions with high-throughput resolution to scrutinize the killing properties of NK cells. This enabled us to identify a rare serial killer subset in the PB-NK cell population where single NK cells are capable of lysing over three K562 cells. This is a first and important step to open the possibility of studying these highly searched for cell types.

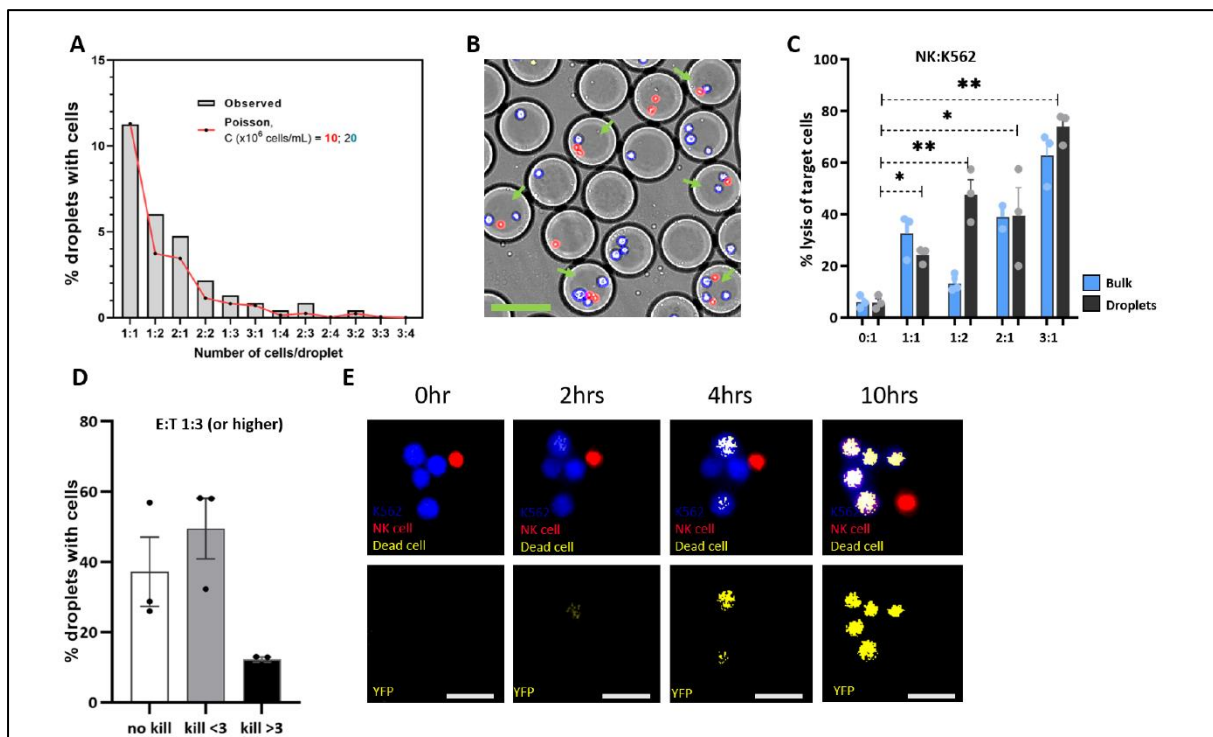


Figure 5. Adaptation of cytotoxicity platform to identify serial killer NK cells: **A.** Graph showing the experimental (grey bars) and predicted (red line) probability for different cell pairing ratios inside the 1.2 nL droplet. **B.** Microscopic overview of different E:T ratio for NK cells (red) and K562 (blue) observed inside the droplet. Scale bar=50 μ m. **C.** Bulk (blue) versus droplets (black) cytotoxicity assay with K562 (at 0:1; 1:1; 1:2, 2:1, 3:1 E:T ratio, respectively). **D.** Graph depicting percentage of alive K562, <3 dead K562 and ≥ 3 dead K562 within the droplets containing more ≥ 3 or more K562 cells. **E.** Microscopic overview of a serial killing event in droplets over the period of 10 hours. red = NK cells; Blue= K562 cells; yellow= dead cells; scale bar= 50 μ m.

3.6 Single *ex vivo*-generated HPC-NK cells display superior anti-tumor cytotoxicity

Given the potency and high translational efficacy of HPC-NK cells, we next sought to determine their tumoricidal activity. We observed an enhanced IFN γ and TNF α secretion by HPC-NK cells in droplets when paired together with target cells thus ensuring their activation in droplets (Figure 6 A). In total 53% (± 7.75 ; $n=4$) total lytic events was observed for these NK cells with an increasing trend of lytic events over the period of 10 hours (Figure 6B). HPC-NK cells were able to induce significantly higher lytic ability in comparison to PB-BK cells (Figure 6C). At different E:T ratios, both in bulk and at single-cell level, there was a significant increase in the percentage of cytotoxic events compared to unpaired target cells (Figure 6D). At 1:1, the cytotoxic event in both bulk (51%; ± 7.4 ; $n=4$) and at single-cell level (54%; ± 2.4 ; $n=4$) were similar, but with other E:T ratios the number of cytotoxic events increased in droplets despite the number of effector or target cells inside.

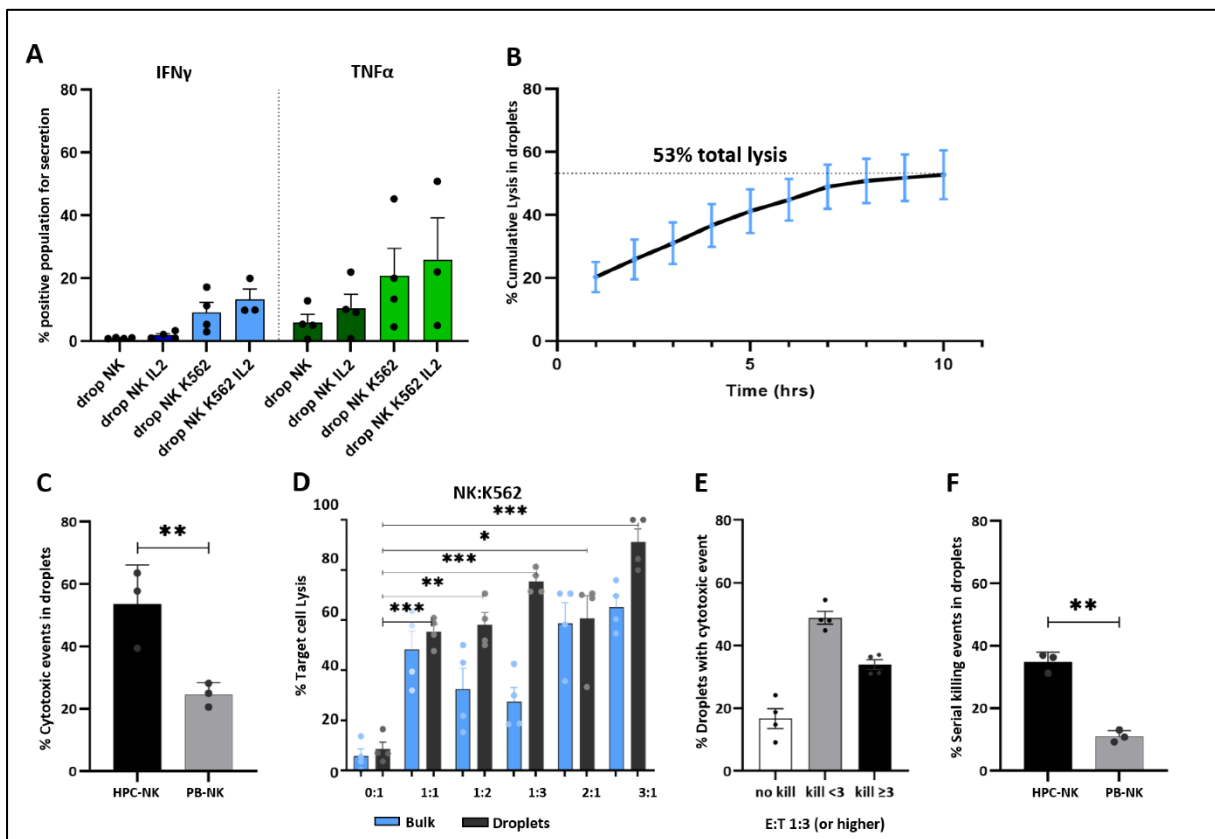


Figure 6. Functional assessment of HPC-NK cells in single-cell level: A. Activation of HPC-NK cells at single-cell level with different stimulants (IL2, K562 or IL2+K562) to measure the secretion of IFN γ (Blue bars) and TNF α (Green Bars). $n=4$ activation with IL2 and K562; $n=3$ activation with IL2 and K562. **B.** Graph representing the dynamics of cumulative cytotoxic events in droplets for different donor-derived HPC-NK cells. The dynamics were determined for the killer fraction of HPC-NK cells; data analysis

performed all possible E:T. **C.** Comparison between cytotoxic events between UCB-derived (HPC) NK cells (Black bars) and PB-NK cells (grey bars); n=3. **D.** Bulk (blue) versus droplets (black) cytotoxicity assay with K562 (at 0:1; 1:1; 1:2, 1:3; 2:1, 3:1 E:T ratio, respectively. **E.** Graph depicting percentage of no dead K562, <3 dead K562 and ≥ 3 dead K562 within the droplets containing ≥ 3 K562 cells. **F.** Comparison between percentage of serial killers NK cells in HPC-NK cells (UCB-derived; black bars) and PB-NK cells (Grey bars); n=3. Results are shown as the mean \pm SEM of 4 independent experiments with different donors (other than denoted differently).

A large fraction of NK cells with serial killing ability was identified in HPC-NK cells compared to PB-NK cells (Figure 6E and F). Of the total droplets with over 3 target cells, we observed around 34% (± 3.2 ; n=4) HPC-NK cells had lysed over 3 target cells successively. We also observed a higher percentage of droplets with positive cytotoxic events (48%; ± 4.0 ; n=4), while the droplets with no cytotoxic events remained at a minimum. In conclusion, we showed that *ex vivo*-generated HPC-NK cells are equipped with superior cytotoxic potential in comparison to PB-NK cells both at population as well as at single-cell level.

3.7 NK and target cell co-encapsulation augments IFN- γ secretion

To obtain insight in the distinct functional abilities of NK cells, we designed an in-droplet immunoassay to correlate two important functions: cytotoxicity and IFN- γ secretion. To the best of our knowledge, we report for the first time on a droplet-based platform that allows monitoring both functions in single primary NK cells simultaneously in real time. A similar platform was developed by Antona et al. that also studied these functions in droplets, however their platform was designed for end-point based analysis and thus cannot address the temporal dynamics of cellular interactions[33]. We adapted the “In-drop sandwich immunoassay”, as described by Eyer et al.[34,35] to allow the combinatorial investigation of IFN- γ release and NK cell cytotoxicity in a time dependent manner. In essence, each droplet functions as a bio-nanoreactor containing NK cells co-encapsulated together with target cells, soluble viability dyes, functionalized magnetic nanoparticles, and detection antibodies in solution. Within a magnetic field, the nanoparticles form a uniform bead line. Thus, making each individual droplet a screening chamber in which cytotoxicity and secretion can be investigated together (Figure 7A,B). To validate our approach, we first generated two batches

of droplets that both contained the magnetic capture beads and fluorescently labeled IFN- γ detection antibodies and co-encapsulated either 0 nM IFN- γ or 50 nM soluble IFN- γ . During microscopy we clearly observed a strong positive signal for the droplet batch with soluble IFN- γ (Figure 7C). Next, we integrated this technical advancement in our NK cell killing platform which yielded droplets with 7 different possible combinations (Figure 7D, Supplementary figure 5).

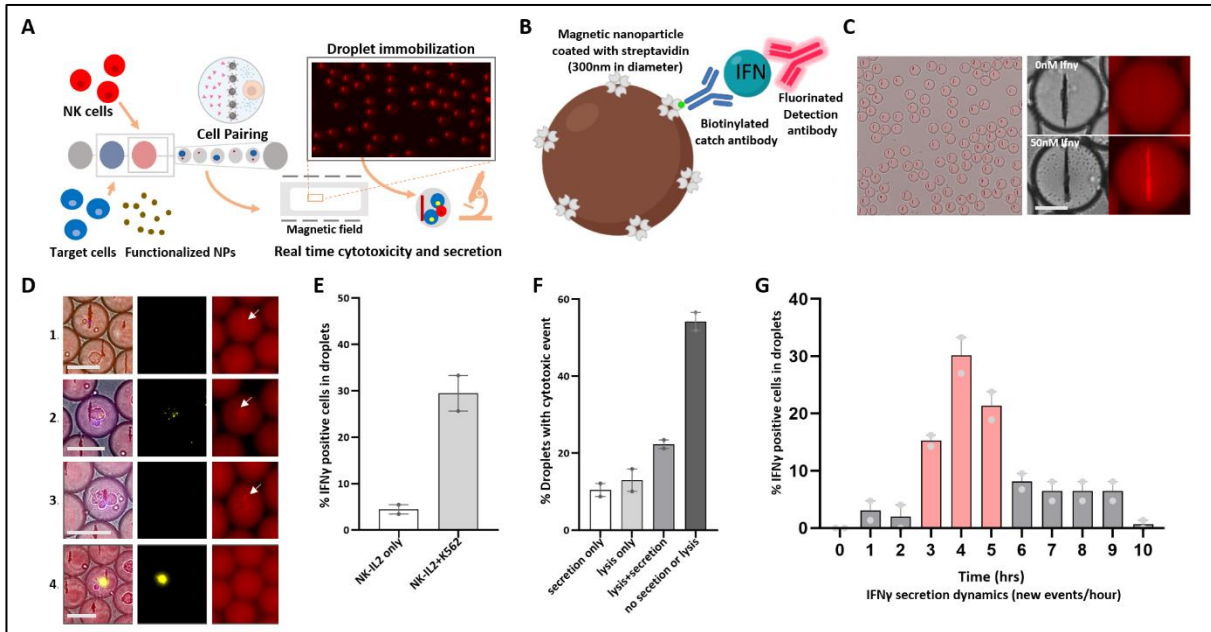


Figure 7. Combinatorial assessment of cytotoxic and secretory function of PB NK cells upon target cell interaction: **A.** Schematics of in-droplet combinatorial assay. NK cells were labelled with Cell tracker Blue (10 μ M) and encapsulated together with target cells and nanoparticles mix at the concentration of 10 million cells/mL. Mixture of viability dyes (Sytox green and Cell event caspase3/7 green) was added together with the cells. Oil/water droplets were immobilized in an observation chamber in presence of magnetic field and monitored for 10 hours at 37°C. Each image was captured at an hour interval. **B.** The magnetic nanoparticle coated with streptavidin allowed binding of biotinylated catch antibody. When secreted IFN γ binds to the catch antibody, the freely floating detection antibody is relocated into the beads thus forming a fluorescent bead line. **C.** Microscopic overview of droplet with fluorescent beadline (left) and zoomed in view of a droplet with 0 nM IFN- γ (upper right) or with 50 nM IFN- γ (lower right). Scale bar 50 μ m. **D.** Microscopic overview of several conditions analyzed inside droplets; (1) Droplets with only NK cells that secreted IFN- γ , (2) droplets with NK cells and K562 cells positive for both cytotoxicity and IFN- γ secretion, (3) droplets with NK cells and K562 and positive only for IFN- γ secretion, (4) droplets with K562 and NK cells positive only for cytotoxicity. Scale bar = 50 μ m. **E.** Graph representing percentage of NK cells secreting IFN- γ in droplets when incubated only with IL-2 (white bars) or with IL-2 and K562 (grey bars). **F.** Graph

representing percentage of droplets with cell pair showing secretion only (white), lysis only (light grey); lysis and secretion (dark grey) and no secretion or lysis (black). **G.** *Dynamics of IFN- γ secretion by NK cells measured over the period of 10 hours. Each vertical bar represents independent events per hour. Results are shown as the mean \pm SEM of 2 independent experiments with different donors.*

To examine whether target cell-induced secretory and cytolytic function were associated with individual NK cells, we monitored the secretion dynamics of an NK cell upon pairing with target cells in real time. Approximately, 33% droplets were positive when paired with K562 while only 5% droplets without target cells showed positive IFN- γ secretion (Figure 7E). Among the total number of droplets with E:T pairing, only 22% (± 1.12 ; n=2) showed both cytotoxicity and secretion, 13% (± 2.9 ; n=2) were positive only for cytolysis, and 10% (± 1.6 ; n=2) for secretion only. To investigate how the dynamics of contact with target cells could regulate cytolysis and secretion in single NK cells, the droplets with positive events for both cytolysis and secretion were monitored closely. On average, an NK cell would already induce a lytic event within the first three hours of interaction (data not shown) while the secretion followed around 4.7 hours. The highest fraction of IFN- γ producing cells ($\sim 67\%$) were observed positive within 3 to 6 hours (Figure 7G). Hence these results suggest that secretion follows the lytic event upon interaction with target cells, however the underlying mechanistic mode of action needs to be further explored.

4. Discussion

Cellular heterogeneity within the NK cell compartment is well appreciated, however, how functional cellular properties are tied to this phenotypical diversity remains largely understudied. It is important to study at a single-cell level in a noise-free environment to exclude juxtacrine or paracrine interactions to fully comprehend NK cell diversification and their ability to induce different effector functions. Therefore, an optimal experimental approach requires both stimulation and analysis with single-cell resolution. By activating NK cells in picolitre size droplets, we ensured that external noise is reduced, and that observed cellular responses reflect intrinsic behavior.

Using our microfluidic platform, we present the functional assessment of *ex vivo*-generated HPC-NK cells and compared them with peripheral blood NK cells at single-cell level. We successfully demonstrated that HPC-NK cells, upon expansion with cytokines, are significantly more cytotoxic than primary NK cells isolated from peripheral blood. Furthermore, we showed

that HPC-NK cells harbor a larger pool of serial killers which is consistent with the percentage of serial killers in HPC-NK cells identified in a recent study using a microwell-based platform[10]. Interestingly, for all E:T ratios tested (except for 1:1), we observed a higher percentage of cytotoxicity similar or higher than bulk-based analysis. These results suggest that the confinement within droplets enhances the probability for NK cells to interact with a target cell compared to a crowded microwell-based setup[32]. Similar cytotoxic events at different E:T ratio, for example similar percentage of lysis with 2:1 and 1:2 (or 3:1 or 1:3) was observed. This suggests that NK cells within a small group (as inside the droplets), operate independently to mediate the lysis of a single target cell and do not show cumulative cytolytic effect by cooperating with neighboring NK cell as in bulk based co-culture[36].

Serial killers have been studied previously for population-based IL-2-activated human PB-NK cells[1,37,38]. However, it is still not studied how NK cell activation at a single-cell level affects the phenomenon. We identified 12% serial killing events where a single NK cell (upon single-cell activation) could lyse ≥ 3 target cells consecutively. The percentage of serial killers identified in our study is higher than what had been observed in resting NK cells, as shown by Guldevall et.al., suggesting that IL-2 can enhance the serial killer behavior in NK cells[38,39]. In line with earlier studies, around 25% of NK cells showed positive cytotoxic events while remaining other NK cells did not induce target cell lysis[1,19,39]. In contrast to the work described by Sarkar et.al., we did not observe 100% NK cell-mediated killing in droplets. We believe 100% killing in earlier study could be due to the characteristics of the utilized dye being actively pumped out by the target cell[40].

The FACS based data from single-cell activation showed an augmented secretory activity of CD56⁺ phenotypes (both cytotoxic and pre-cytotoxic) upon interaction with their target cells[41]. We further investigated the correlation between target interaction induced cytotoxic event and secretory behavior of individual NK cells by incorporating an innovative in-droplet sandwich immunoassay together with our in-droplet cytotoxicity assay. This combinatorial platform provides a unique ability for high throughput monitoring of cytokine secretion in real time together with cytotoxicity at single-cell level. To this end we identified 74% of total lytic events in droplets that showed positive secretory function as well. In this way we demonstrated a correlation between cytotoxic and secretory function of NK cells, which others were not able to find[33,42]. We believe that this discrepancy is explained by a

short experimental protocol of 4 hours leading to a missed cytolytic fraction that also test positive for IFN- γ .

The dynamics of NK cell-mediated cytotoxicity are dependent on several factors such as the maturation state of NK cells, phenotypical variation based on the expression of several surface molecules, and lytic content of NK cells[40]. Besides these NK cell-specific factors, the expression of NK-responsive factors in target cells also determines the nature and speed of cell death. In our study, we presented the comparison of NK cell-mediated cytotoxicity with two leukemia (K562 and THP-1) and one lymphoma (Daudi) cell line, known to show different sensitivity towards NK cells[43,44]. Along with the number of cytotoxic events, the differences were also observed in the timeline of the cytotoxicity. This variation could be linked to the surface arrangements of these cells (expression patterns of different activating and inhibitory molecules) which eventually leads to activation of different killing mechanisms. In agreement with the literature, we observed upregulated expression of HLA molecules by all cell types[45–47]. NK cells lyse K562 target cells primarily by delivering perforin/granzyme-loaded cytolytic granules into the lytic synapse. However, the lysis of THP-1 cells had been found to be more dependent on cytokines, such as IFN γ that could lead to increase in ICAM-1 molecule upon exposure[48,49]. NK cells also kill THP-1 cells by forming nanotubes that generally occurs after certain hours of interaction[49,50]. Involvement of all these different pathways lead to later killing of THP-1 cells compared to K562.

Our research puts emphasis on unraveling the complex functional and phenotypical heterogeneity within the NK cell population. This research provided an integrated analysis of NK-target cell interactions and its implications on the cytolytic and secretory behavior of single NK cells. By adapting the droplet-based cytotoxicity platform, we identified rare serial killers, thus channeling exciting ways for easy identification and study of these rare cell types in future. Furthermore, with functional assessment of *ex vivo*-generated HPCNK cells, one of the important sources of adaptive NK cell therapy, we probed heterogeneity in these cell types. We believe that our data on functional heterogeneity underlying NK cell population, both peripheral NK cells as well as CD34+ HPC-derived NK cells, provides valuable contributions towards developing and elevating efficacy of NK cell-based cancer immunotherapy.

5. Acknowledgments

These results are part of the project that has received funding from the European Research Council (ERC) under the European Union's Horizon 2020 research and innovation programme (Grant agreement No.802791). Furthermore, we acknowledge generous support by the Eindhoven University of Technology.

6. References

- [1] B. Vanherberghen, P.E. Olofsson, E. Forslund, M. Sternberg-Simon, M.A. Khorshidi, S. Pacouret, K. Guldevall, M. Enqvist, K.J. Malmberg, R. Mehr, B. Önfelt, Classification of human natural killer cells based on migration behavior and cytotoxic response, *Blood*. 121 (2013) 1326–1334. <https://doi.org/10.1182/blood-2012-06-439851>.
- [2] E. Vivier, E. Tomasello, M. Baratin, T. Walzer, S. Ugolini, Functions of natural killer cells, *Nat. Immunol.* (2008). <https://doi.org/10.1038/ni1582>.
- [3] S. Liu, V. Galat, Y. Galat4, Y.K.A. Lee, D. Wainwright, J. Wu, NK cell-based cancer immunotherapy: from basic biology to clinical development, *J. Hematol. Oncol.* (2021). <https://doi.org/10.1186/s13045-020-01014-w>.
- [4] W. Hu, G. Wang, D. Huang, M. Sui, Y. Xu, Cancer immunotherapy based on natural killer cells: Current progress and new opportunities, *Front. Immunol.* (2019). <https://doi.org/10.3389/fimmu.2019.01205>.
- [5] H. Fujisaki, H. Kakuda, N. Shimasaki, C. Imai, J. Ma, T. Lockey, P. Eldridge, W.H. Leung, D. Campana, Expansion of highly cytotoxic human natural killer cells for cancer cell therapy, *Cancer Res.* (2009). <https://doi.org/10.1158/0008-5472.CAN-08-3712>.
- [6] M.W.H. Roeven, S. Thordardottir, A. Kohela, F. Maas, F. Preijers, J.H. Jansen, N.M. Blijlevens, J. Cany, N. Schaap, H. Dolstra, The Aryl Hydrocarbon Receptor Antagonist StemRegenin1 Improves in Vitro Generation of Highly Functional Natural Killer Cells from CD34+ Hematopoietic Stem and Progenitor Cells, *Stem Cells Dev.* (2015). <https://doi.org/10.1089/scd.2014.0597>.
- [7] J.S. Hoogstad-van Evert, J. Cany, D. van den Brand, M. Oudenampsen, R. Brock, R. Torensma, R.L. Bekkers, J.H. Jansen, L.F. Massuger, H. Dolstra, Umbilical cord blood CD34+ progenitor-derived NK cells efficiently kill ovarian cancer spheroids and intraperitoneal tumors in NOD/SCID/IL2Rgnull mice, *Oncoimmunology.* (2017). <https://doi.org/10.1080/2162402X.2017.1320630>.
- [8] E. Liu, D. Marin, P. Banerjee, H.A. Macapinlac, P. Thompson, R. Basar, L. Nassif Kerbauy, B. Overman, P. Thall, M. Kaplan, V. Nandivada, I. Kaur, A. Nunez Cortes, K. Cao, M. Daher, C. Hosing, E.N. Cohen, P. Kebriaei, R. Mehta, S. Neelapu, Y. Nieto, M. Wang, W. Wierda, M. Keating, R. Champlin, E.J. Shpall, K. Rezvani, Use of CAR-Transduced Natural Killer Cells in CD19-Positive Lymphoid Tumors, *N. Engl. J. Med.* (2020). <https://doi.org/10.1056/nejmoa1910607>.
- [9] M. Luevano, A. Madrigal, A. Saudemont, Generation of natural killer cells from hematopoietic stem cells in vitro for immunotherapy, *Cell. Mol. Immunol.* (2012). <https://doi.org/10.1038/cmi.2012.17>.
- [10] J.M.R. Van der Meer, R.J.A. Maas, K. Guldevall, K. Klarenaar, P.K.J.D. de Jonge, J.S.H. van Evert, A.B. van der Waart, J. Cany, J.T. Safrit, J.H. Lee, E. Wagena, P. Friedl, B. Önfelt, L.F. Massuger, N.P.M. Schaap, J.H. Jansen, W. Hobo, H. Dolstra, IL-15 superagonist N-803 improves IFN γ production and killing of leukemia and ovarian cancer cells by CD34+ progenitor-derived NK cells, *Cancer Immunol. Immunother.* (2021). <https://doi.org/10.1007/s00262-020-02749-8>.
- [11] C. Yang, J.R. Siebert, R. Burns, Z.J. Gerbec, B. Bonacci, A. Rymaszewski, M. Rau, M.J. Riese, S. Rao, K.S. Carlson, J.M. Routes, J.W. Verbsky, M.S. Thakar, S. Malarkannan, Heterogeneity of human bone marrow and blood natural killer cells defined by single-cell

Chapter 4 - Single cell profiling reveal functional heterogeneity in NK cells

- transcriptome, *Nat. Commun.* (2019). <https://doi.org/10.1038/s41467-019-11947-7>.
- [12] J.R. Ortaldo, R.B. Herberman, Heterogeneity of natural killer cells., *Annu. Rev. Immunol.* (1984). <https://doi.org/10.1146/annurev.iy.02.040184.002043>.
- [13] S.L. Smith, P.R. Kennedy, K.B. Stacey, J.D. Worboys, A. Yarwood, S. Seo, E.H. Solloa, B. Mistretta, S.S. Chatterjee, P. Gunaratne, K. Allette, Y.C. Wang, M.L. Smith, R. Sebra, E.M. Mace, A. Horowitz, W. Thomson, P. Martin, S. Eyre, D.M. Davis, Diversity of peripheral blood human NK cells identified by single-cell RNA sequencing, *Blood Adv.* (2020). <https://doi.org/10.1182/bloodadvances.2019000699>.
- [14] A. Horowitz, D.M. Strauss-Albee, M. Leipold, J. Kubo, N. Nemat-Gorgani, O.C. Dogan, C.L. Dekker, S. Mackey, H. Maecker, G.E. Swan, M.M. Davis, P.J. Norman, L.A. Guethlein, M. Desai, P. Parham, C.A. Blish, Genetic and environmental determinants of human NK cell diversity revealed by mass cytometry, *Sci. Transl. Med.* (2013). <https://doi.org/10.1126/scitranslmed.3006702>.
- [15] J.M. Karo, J.C. Sun, Novel molecular mechanism for generating NK-cell fitness and memory, *Eur. J. Immunol.* (2015). <https://doi.org/10.1002/eji.201445339>.
- [16] J. Zhao, S. Zhang, Y. Liu, X. He, M. Qu, G. Xu, H. Wang, M. Huang, J. Pan, Z. Liu, Z. Li, L. Liu, Z. Zhang, Single-cell RNA sequencing reveals the heterogeneity of liver-resident immune cells in human, *Cell Discov.* (2020). <https://doi.org/10.1038/s41421-020-0157-z>.
- [17] A. Crinier, P.Y. Dumas, B. Escalière, C. Piperoglou, L. Gil, A. Villacreces, F. Vély, Z. Ivanovic, P. Milpied, É. Narni-Mancinelli, É. Vivier, Single-cell profiling reveals the trajectories of natural killer cell differentiation in bone marrow and a stress signature induced by acute myeloid leukemia, *Cell. Mol. Immunol.* (2021). <https://doi.org/10.1038/s41423-020-00574-8>.
- [18] N. Sinha, N. Subedi, J. Tel, Integrating Immunology and Microfluidics for Single Immune Cell Analysis., *Front. Immunol.* 9 (2018) 2373. <https://doi.org/10.3389/fimmu.2018.02373>.
- [19] N. Subedi, L.C. Van Eindhoven, A.M. Hokke, L. Houben, M.C. Van Turnhout, C.V.C. Bouten, K. Eyer, J. Tel, An automated real-time microfluidic platform to probe single NK cell heterogeneity and cytotoxicity on-chip, *Sci. Rep.* 11 (2021) 17084. <https://doi.org/10.1038/s41598-021-96609-9>.
- [20] N. Sinha, N. Subedi, F. Wimmers, M. Soennichsen, J. Tel, A Pipette-Tip Based Method for Seeding Cells to Droplet Microfluidic Platforms., *J. Vis. Exp.* (2019) 1–10. <https://doi.org/10.3791/57848>.
- [21] L.C. Van Eindhoven, E. Chouri, N. Subedi, J. Tel, Phenotypical Diversification of Early IFN α -Producing Human Plasmacytoid Dendritic Cells Using Droplet-Based Microfluidics, *Front. Immunol.* (2021). <https://doi.org/10.3389/fimmu.2021.672729>.
- [22] F. Wimmers, N. Subedi, N. van Buuringen, D. Heister, J. Vivié, I. Beeren-Reinieren, R. Woestenenk, H. Dolstra, A. Piruska, J.F.M. Jacobs, A. van Oudenaarden, C.G. Figdor, W.T.S. Huck, I.J.M. de Vries, J. Tel, Single-cell analysis reveals that stochasticity and paracrine signaling control interferon-alpha production by plasmacytoid dendritic cells, *Nat. Commun.* 9 (2018) 3317. <https://doi.org/10.1038/s41467-018-05784-3>.
- [23] N.D. Huntington, C.A.J. Voshenrich, J.P. Di Santo, Developmental pathways that generate natural-killer-cell diversity in mice and humans, *Nat. Rev. Immunol.* (2007). <https://doi.org/10.1038/nri2154>.
- [24] A.G. Freud, B.L. Mundy-Bosse, J. Yu, M.A. Caligiuri, The Broad Spectrum of Human Natural Killer Cell Diversity, *Immunity.* (2017). <https://doi.org/10.1016/j.immuni.2017.10.008>.
- [25] B. Fu, F. Wang, R. Sun, B. Ling, Z. Tian, H. Wei, CD11b and CD27 reflect distinct population and functional specialization in human natural killer cells, *Immunology.* (2011). <https://doi.org/10.1111/j.1365-2567.2011.03446.x>.
- [26] M.T.M. Vossen, M. Matmati, K.M.L. Hertoghs, P.A. Baars, M.-R. Gent, G. Leclercq, J. Hamann, T.W. Kuijpers, R.A.W. van Lier, CD27 Defines Phenotypically and Functionally Different Human NK Cell Subsets, *J. Immunol.* (2008).

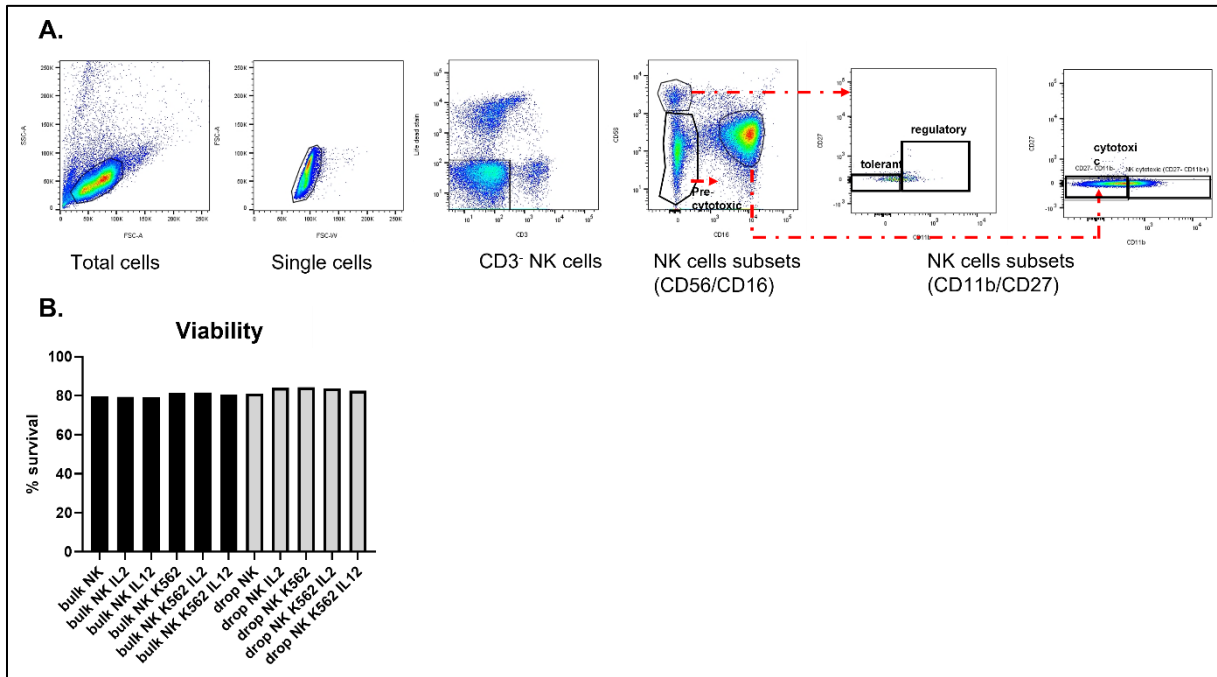
Chapter 4 - Single cell profiling reveal functional heterogeneity in NK cells

- <https://doi.org/10.4049/jimmunol.180.6.3739>.
- [27] A. Crinier, P. Milpied, B. Escalière, C. Piperoglou, J. Galluso, A. Balsamo, L. Spinelli, I. Cervera-Marzal, M. Ebbo, M. Girard-Madoux, S. Jaeger, E. Bollon, S. Hamed, J. Hardwigsen, S. Ugolini, F. Vély, E. Narni-Mancinelli, E. Vivier, High-Dimensional Single-Cell Analysis Identifies Organ-Specific Signatures and Conserved NK Cell Subsets in Humans and Mice, *Immunity*. (2018). <https://doi.org/10.1016/j.immuni.2018.09.009>.
- [28] I.S. Schuster, J.D. Coudert, C.E. Andoniou, M.A. Degli-Esposti, “Natural Regulators”: NK cells as modulators of T cell immunity, *Front. Immunol.* (2016). <https://doi.org/10.3389/fimmu.2016.00235>.
- [29] S. Shigeru, N. Akitoshi, M.H. Subaru, A. Shiozaki, The balance between cytotoxic NK cells and regulatory NK cells in human pregnancy, *J. Reprod. Immunol.* (2008). <https://doi.org/10.1016/j.jri.2007.04.007>.
- [30] A.M. Abel, C. Yang, M.S. Thakar, S. Malarkannan, Natural killer cells: Development, maturation, and clinical utilization, *Front. Immunol.* (2018). <https://doi.org/10.3389/fimmu.2018.01869>.
- [31] I. Prager, C. Liesche, H. Van Ooijen, D. Urlaub, Q. Verron, N. Sandström, F. Fasbender, M. Claus, R. Eils, J. Beaudouin, B. Önfelt, C. Watzl, NK cells switch from granzyme B to death receptor-mediated cytotoxicity during serial killing, *J. Exp. Med.* (2019). <https://doi.org/10.1084/jem.20181454>.
- [32] S. Antona, I. Platzman, J.P. Spatz, Droplet-Based Cytotoxicity Assay: Implementation of Time-Efficient Screening of Antitumor Activity of Natural Killer Cells, *ACS Omega*. 5 (2020) 24674–24683. <https://doi.org/10.1021/acsomega.0c03264>.
- [33] S. Antona, T. Abele, K. Jahnke, Y. Dreher, K. Göpfrich, I. Platzman, J.P. Spatz, Droplet-Based Combinatorial Assay for Cell Cytotoxicity and Cytokine Release Evaluation, *Adv. Funct. Mater.* (2020). <https://doi.org/10.1002/adfm.202003479>.
- [34] K. Eyer, R.C.L. Doineau, C.E. Castrillon, L. Briseño-Roa, V. Menrath, G. Mottet, P. England, A. Godina, E. Brient-Litzler, C. Nizak, A. Jensen, A.D. Griffiths, J. Bibette, P. Bruhns, J. Baudry, Single-cell deep phenotyping of IgG-secreting cells for high-resolution immune monitoring, *Nat. Biotechnol.* 35 (2017) 977–982. <https://doi.org/10.1038/nbt.3964>.
- [35] Y. Bounab, K. Eyer, S. Dixneuf, M. Rybczynska, C. Chauvel, M. Mistretta, T. Tran, N. Aymerich, G. Chenon, J.F. Llitjos, F. Venet, G. Monneret, I.A. Gillespie, P. Cortez, V. Moucadel, A. Pachot, A. Troesch, P. Leissner, J. Textoris, J. Bibette, C. Guyard, J. Baudry, A.D. Griffiths, C. Védrine, Dynamic single-cell phenotyping of immune cells using the microfluidic platform DropMap, *Nat. Protoc.* 15 (2020) 2920–2955. <https://doi.org/10.1038/s41596-020-0354-0>.
- [36] Y.J. Yamanaka, C.T. Berger, M. Sips, P.C. Cheney, G. Alter, J.C. Love, Single-cell analysis of the dynamics and functional outcomes of interactions between human natural killer cells and target cells, *Integr. Biol. (United Kingdom)*. 4 (2012) 1175–1184. <https://doi.org/10.1039/c2ib20167d>.
- [37] A.E. Christakou, M. Ohlin, B. Vanherberghen, M.A. Khorshidi, N. Kadri, T. Frisk, M. Wiklund, B. Önfelt, Live cell imaging in a microarray of acoustic traps facilitates quantification of natural killer cell heterogeneity, *Integr. Biol. (United Kingdom)*. 5 (2013) 712–719. <https://doi.org/10.1039/c3ib20253d>.
- [38] R. Bhat, C. Watzl, Serial Killing of Tumor Cells by Human Natural Killer Cells – Enhancement by Therapeutic Antibodies, *PLoS One*. 2 (2007) e326. <https://doi.org/10.1371/journal.pone.0000326>.
- [39] K. Guldevall, L. Brandt, E. Forslund, K. Olofsson, T.W. Frisk, P.E. Olofsson, K. Gustafsson, O. Manneberg, B. Vanherberghen, H. Brismar, K. Kärre, M. Uhlin, B. Önfelt, Microchip screening platform for single cell assessment of NK cell cytotoxicity, *Front. Immunol.* 7 (2016) 1–7. <https://doi.org/10.3389/fimmu.2016.00119>.
- [40] S. Sarkar, P. Sabhachandani, D. Ravi, S. Potdar, S. Purvey, A. Beheshti, A.M. Evens, T. Konry, Dynamic analysis of human natural killer cell response at single-cell resolution in B-Cell Non-Hodgkin Lymphoma, *Front. Immunol.* 8 (2017) 1–13. <https://doi.org/10.3389/fimmu.2017.01736>.

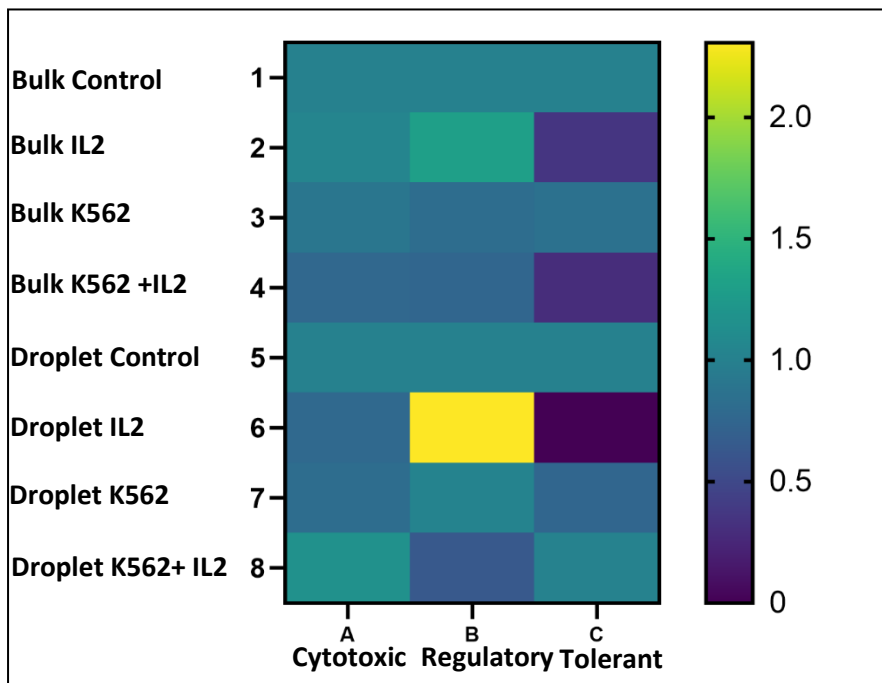
Chapter 4 - Single cell profiling reveal functional heterogeneity in NK cells

- [41] X. An, V.G. Sendra, I. Liadi, B. Ramesh, G. Romain, C. Haymaker, M. Martinez-Paniagua, Y. Lu, L.G. Radvanyi, B. Roysam, N. Varadarajan, Single-cell profiling of dynamic cytokine secretion and the phenotype of immune cells, *PLoS One*. (2017). <https://doi.org/10.1371/journal.pone.0181904>.
- [42] Y.J. Yamanaka, C.T. Berger, M. Sips, P.C. Cheney, G. Alter, J.C. Love, Single-cell analysis of the dynamics and functional outcomes of interactions between human natural killer cells and target cells, *Integr. Biol. (United Kingdom)*. (2012). <https://doi.org/10.1039/c2ib20167d>.
- [43] D. Zarcone, A.B. Tilden, H.M. Friedman, C.E. Grossi, Human Leukemia-derived Cell Lines and Clones as Models for Mechanistic Analysis of Natural Killer Cell-mediated Cytotoxicity, *Cancer Res.* (1987).
- [44] A. Müllbacher, K. NJ, Target cell lysis by natural killer cells is influenced by beta 2-microglobulin expression. *PG - 21-9*, (n.d.). <https://onlinelibrary.wiley.com/doi/abs/10.1111/j.1365-3083.1989.tb01184.x?sid=nlm%3Apubmed>.
- [45] R. Ramirez, R. Solana, J. Carracedo, M.C. Alonso, J. Peña, Mechanisms involved in NK resistance induced by interferon- γ , *Cell. Immunol.* (1992). [https://doi.org/10.1016/0008-8749\(92\)90191-Q](https://doi.org/10.1016/0008-8749(92)90191-Q).
- [46] S. Tsuchiya, M. Yamabe, Y. Yamaguchi, Y. Kobayashi, T. Konno, K. Tada, Establishment and characterization of a human acute monocytic leukemia cell line (THP-1), *Int. J. Cancer.* (1980). <https://doi.org/10.1002/ijc.2910260208>.
- [47] J.D. Fayen, M.L. Tykocinski, The expansion of human $\gamma\delta$ T cells in response to Daudi cells requires the participation of CD4+ T cells, *Immunology.* (1999). <https://doi.org/10.1046/j.1365-2567.1999.00761.x>.
- [48] C. Lehmann, M. Zeis, L. Uharek, Activation of natural killer cells with interleukin 2 (IL-2) and IL-12 increases perforin binding and subsequent lysis of tumour cells, *Br. J. Haematol.* (2001). <https://doi.org/10.1046/j.1365-2141.2001.02995.x>.
- [49] R. Wang, J.J. Jaw, N.C. Stutzman, Z. Zou, P.D. Sun, Natural killer cell-produced IFN- γ and TNF- α induce target cell cytolysis through up-regulation of ICAM-1, *J. Leukoc. Biol.* (2012). <https://doi.org/10.1189/jlb.0611308>.
- [50] A. Chauveau, A. Aucher, P. Eissmann, E. Vivier, D.M. Davis, Membrane nanotubes facilitate long-distance interactions between natural killer cells and target cells, *Proc. Natl. Acad. Sci. U. S. A.* (2010). <https://doi.org/10.1073/pnas.0910074107>.

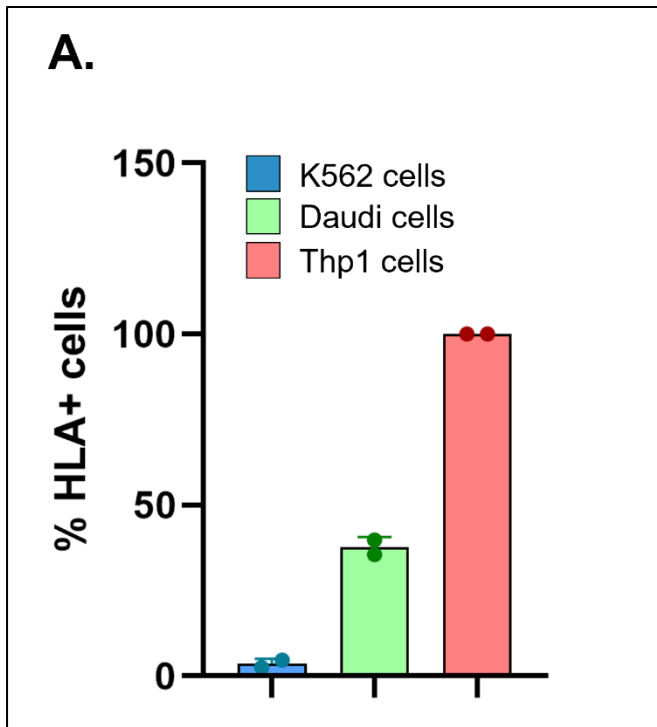
7. Supplementary Figures



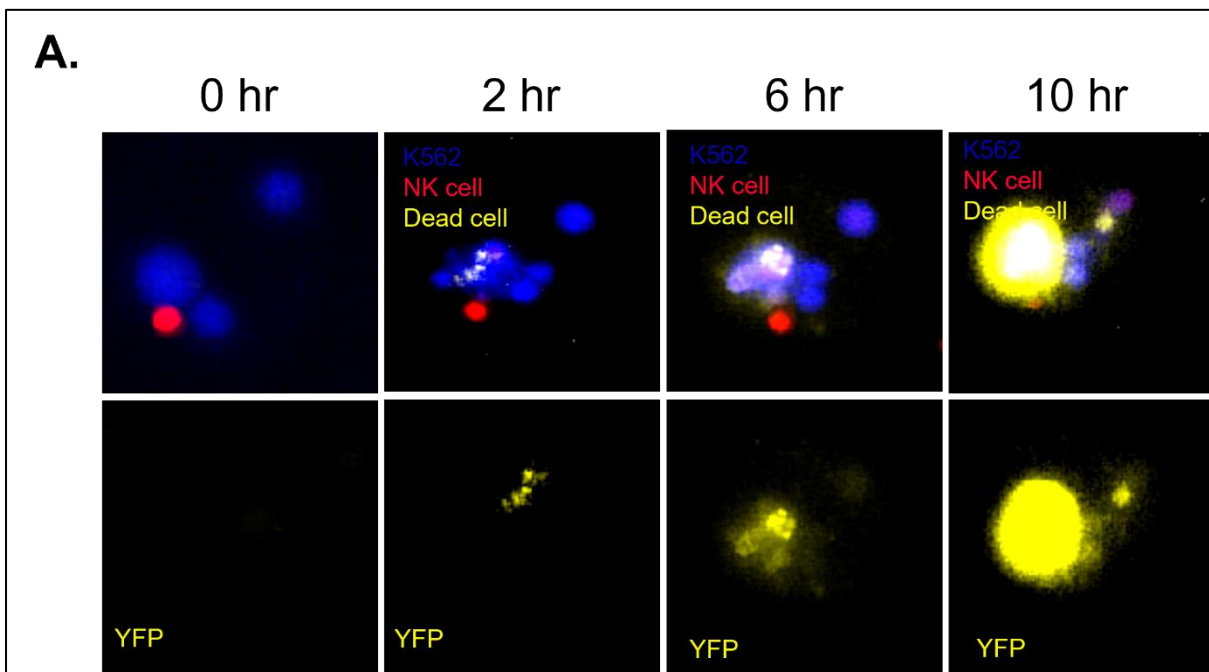
Supplementary Figure 1: A. Gating strategy for NK cells to identify different subpopulation based on CD56/CD16 and CD11b/CD27. **B.** Graph showing the viability of NK cells in bulk and droplets after activation.



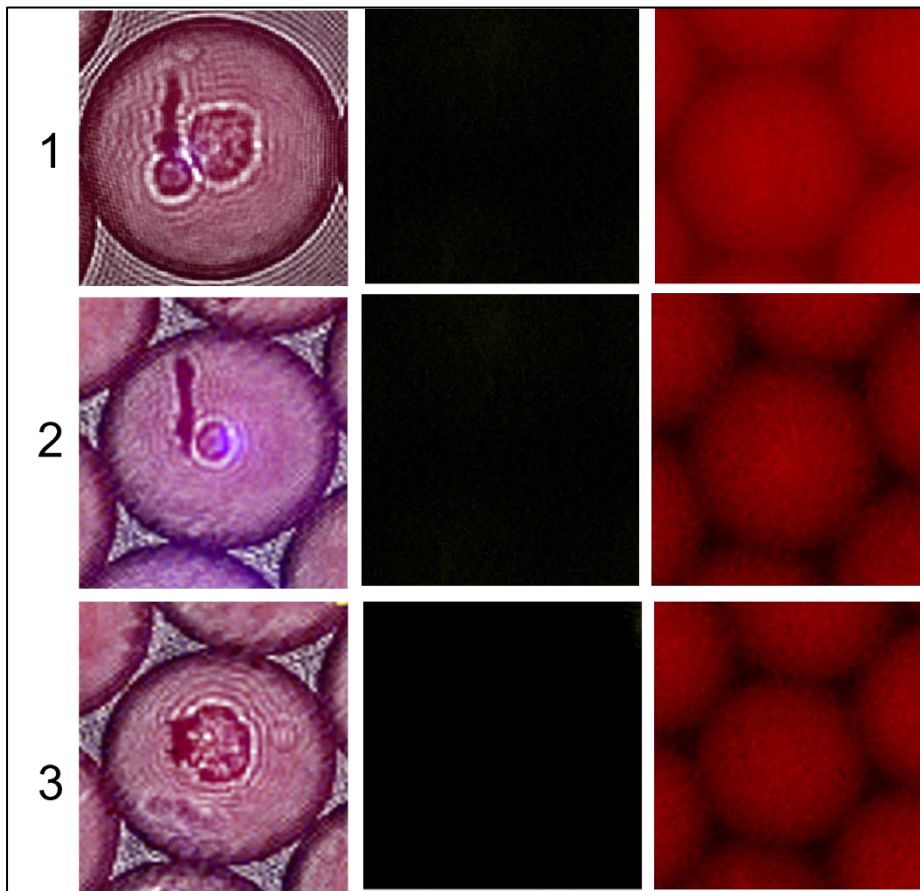
Supplementary Figure 2: A. Heat map demonstrating the fold increment of different markers in NK cell with and without stimulation in bulk and droplets.



Supplementary Figure 3: A. Expression of MHC-1 molecule by K562 (red), Daudi (green) and Thp1 cells (red); n=2 error bar represents standard error of mean.



Supplementary Figure 4: A. microscopic view of a single NK cell lysing 3 different K562 cells over 10 hours' time period. Blue: K562 cell, Red: NK cell, Yellow: Dead cell



Supplementary Figure 5: A. *microscopic view showing different conditions in combinatorial assay for cytotoxicity and IFN γ secretion. 1. NK-K562 with no positive signal for both lysis and secretion. 2. only NK with no positive signal for secretion. 3. only K562 cells with no positive signal for cytotoxicity and secretion*



CHAPTER 5

SINGLE-CELL ANALYSIS REVEALS THAT STOCHASTICITY AND PARACRINE SIGNALING CONTROL INTERFERON-ALPHA PRODUCTION BY PLASMACYTOID DENDRITIC CELLS

This chapter is published as:

Single-cell analysis reveals that stochasticity and paracrine signalling control interferon-alpha production by plasmacytoid dendritic cells

Florian Wimmers, [Nikita Subedi](#), Nicole van Buuringen, Daan Heister, Judith Vivié, Inge Beeren-Reinieren, Rob Woestenenk, Harry Dolstra, Aigars Piruska, Joannes F. M. Jacobs, Alexander van Oudenaarden, Carl G. Figdor, Wilhelm T. S. Huck, I. Jolanda M. de Vries , Jurjen Tel

Nature Communications; 3317

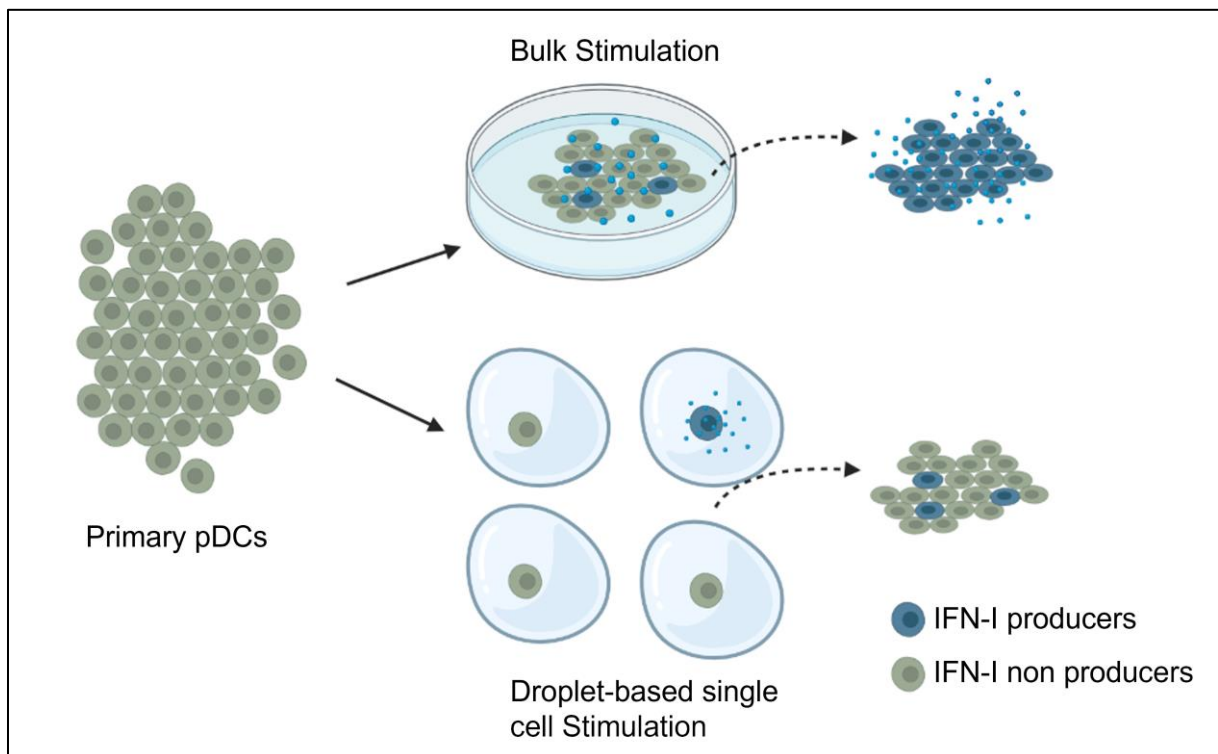
Published: Aug 18, 2018



Abstract

Type I interferon (IFN) is a key driver of immunity to infections and cancer. Plasmacytoid dendritic cells (pDCs) are uniquely equipped to produce large quantities of type I IFN but the mechanisms that control this process are poorly understood. Here we report on a droplet-based microfluidic platform to investigate type I IFN production in human pDCs at the single-cell level. We show that type I IFN but not TNF α production is limited to a small subpopulation of individually stimulated pDCs and controlled by stochastic gene regulation. Combining single-cell cytokine analysis with single-cell RNA-seq profiling reveals no evidence for a pre-existing subset of type I IFN-producing pDCs. By modulating the droplet microenvironment, we demonstrate that vigorous pDC population responses are driven by a type I IFN amplification loop. Our study highlights the significance of stochastic gene regulation and suggests strategies to dissect the characteristics of immune responses at the single-cell level.

Graphical Abstract



1. Introduction

Plasmacytoid dendritic cells (pDCs) are blood circulating innate immune cells with the unique ability to rapidly release large quantities of type I interferon (IFN) for anti-viral immunity[1–3]. pDC-produced type I IFN is associated with effective anti-cancer immunity but is also a driver of autoimmune diseases[4–8]. Type I IFN production by pDCs is initiated when nucleic acids trigger the endosomal Toll-like receptors (TLRs) 7 or 9 leading to the activation of transcription factor interferon regulatory factor-7 (IRF7), which only pDCs express constitutively and at high levels[9–11]. Several pDC subclasses were proposed and single-cell genomic profiling revealed ample variation in the molecular outfit of individual DCs[12–16]. These individual differences may have an impact on the ability of each pDC to produce type I IFN, and in non-pDC model systems random differences between virus-infected cell populations, attributed to stochastic gene regulation, caused significant variation in the production of type I IFN[17–21]. Additionally, type I IFN production by pDCs can be modulated by the microenvironment via soluble factors or cell surface receptors[22–27]. It is currently not known how pDC populations combine the complex information from TLR signaling and microenvironmental factors with random variations in the molecular outfit of individual pDCs to generate robust type I IFN responses. The question remains whether pDCs display stochastic expression of type I IFN despite high IRF7 expression, and whether pDC populations exploit environmental cues to counterbalance potential heterogeneity arising from this phenomenon.

Here, we developed a droplet-based microfluidic platform to dissect the human pDC-driven type I IFN response at the single-cell level within a tunable microenvironment. Generating thousands of identical droplets at high throughput allows massively parallelized single-cell experiments within these bioreactors. Recent technological breakthroughs in the field of droplet-based microfluidics increased the throughput of single-cell DNA and RNA-sequencing experiments by orders of magnitude[28,29]. Previous attempts by our lab and others to leverage this power for the analysis of cytokine secretion were hampered in their translation into practice due to complex detection equipment or difficult handling conditions[30,31]. Here, we demonstrate the detection of cytokine secretion and activation marker expression by individually stimulated cells in droplets and reveal stochastic differences in pDC-driven type I IFN production. Single-cell RNA-sequencing (ScRNA-seq) of these cells allowed us to profile

the transcriptional changes in each cell upon perturbation with TLR ligands and links transcriptional variation to cytokine secretion at the protein level. Finally, by varying key droplet parameters, we find that single pDCs collaborate to amplify their activity and generate population-driven type I IFN responses.

2. Material and Methods

2.1 Antibodies and cell stimuli

For a full list of utilized antibodies and reagents, the readers are referred to the Supplementary Methods.

2.2 Cell isolation and culture

Jurkat T cells (ATCC, Clone E6-1 (ATCC[®] TIB-152[™])) were cultured in RPMI (Thermo Fischer Scientific) supplemented with 10% fetal calf serum (FCS; Greiner Bio-One) and 1% Antibiotic-Antimycotic (Life Technologies), and regularly tested for mycoplasma contamination. The pDCs were obtained from buffy coats of healthy donors (Sanquin) after written informed consent per the Declaration of Helsinki and according to institutional guidelines. In short, peripheral blood mononuclear cells (PBMCs) were isolated from donor blood via Ficoll density gradient centrifugation (Axis-Shield). The pDCs were subsequently isolated using magnet-activated cell sorting (MACS) or fluorescence-activated cell sorting (FACS).

For MACS isolation, PBMCs were resuspended in X-Vivo 15 cell culture media (Lonza) supplemented with 2% pooled human serum (HS; Sanquin) and incubated for 1 h at 37 °C in cell culture flasks T75 (Corning) to deplete monocytes. Cells were washed thrice with phosphate-buffered saline (PBS; Braun) while non-adherent cells were collected. The pDCs were isolated from this cell population by positive selection using the CD304 Microbeat Kit (Miltenyi Biotec) following the manufacturer's instructions. Cells were counted and purity was assessed using flow cytometry. For this purpose, cells were washed with PBS supplemented with 0.5% bovine serum albumin fraction V (BSA, Roche) and 0.01% NaN₃ (Merck; subsequently referred to as PBA) and stained for 10 min at 4 °C using APC-labelled anti-CD303 and fluorescein isothiocyanate (FITC)-labelled anti-Lineage Cocktail 1 (LIN1) antibodies in 30 µL PBA. The pDCs were identified as CD303⁺LIN⁻ and purity was on average 93% (Std.: 3.76%, *n* = 67).

For FACS isolation, PBMCs were washed and FITC-labelled anti-LIN1 antibodies were added to the pellet. Cells were incubated for 20 min at 4 °C. Subsequently, cells were washed with PBS supplemented with 4 mM ethylenediaminetetraacetic acid (EDTA; Sigma) and 0.1% BSA (subsequently referred to as wash buffer) and anti-FITC microbeads (Miltenyi Biotec) were added to the pellet. Cells were incubated for 30 min at 4 °C and subsequently washed with wash buffer. LIN1-positive cells were magnetically depleted using an LD column (Miltenyi Biotec) following the manufacturer's instructions. Cells were washed with wash buffer and VioBlue- or PE-Cy7-labeled anti-HLA-DR and BV510- or PE-labeled anti-CD304 antibodies were added to the pellet. Cells were incubated for 30 min at 4 °C and afterwards washed with wash buffer. The pDCs were sorted as LIN1⁻HLA-DR⁺CD304⁺ cells on a FACS Aria II SORP (BD). During stimulation, pDCs were cultured in X-Vivo 15 supplemented with 2% HS or RPMI supplemented with 10% FCS.

2.3 Soft lithographic procedure

The microfluidic device was molded against an SU-8 photo resist structure on a silicon wafer using a commercially available polydimethylsiloxane silicone elastomer (Sylgard 184, Dow Corning). The surface of the Sylgard 184 was OH-terminated by exposure to plasma (Diener Electronic GmbH) and was sealed with another plasma-treated glass cover slide to yield closed micro channels. Channels were treated with a 2% silane solution.

2.4 Microfluidic setup

Soft lithographic techniques were used to fabricate microfluidic channels (see above). Liquids were dispensed from plastic syringes (Becton Dickinson), which were connected to the microfluidic device by polytetrafluoroethylene tubing (Novodirect GmbH). The syringes were driven by computer-controlled syringe pumps (Nemesys, Cetoni GmbH). For the stability of droplets, 3 w/w% Pico-Surf surfactant (Sphere Fluidics) was used in fluorinated HFE-7500 oil (Novec 7500, 3M). Cells and stimuli were loaded separately on the microfluidic chip. The dimensions of the microfluidic channels are 40 µm × 25 µm at the first inlet, 60 µm × 25 µm at the second inlet and the production nozzle, and 100 µm × 25 µm at the collection channel.

2.5 Priming and blocking

To block type I IFN signaling, pDCs were incubated at 37 °C for 30 min with medium containing blocking antibody against IFNAR2 (PBL Assay Science, 10 µg/mL) and neutralizing sera against IFN-α and IFN-β (both from PBL Biomedical Laboratories, both 1000 NU/mL). To prime, pDCs were resuspended in medium containing cytokines or conditioned medium and incubated for 2 h, 37 °C. Subsequently, cells were washed thrice with wash buffer and prepared for downstream applications.

2.6 Single-cell activation assay

Cells were washed twice with wash buffer and incubated in 100 µL per 10⁶ cells wash buffer containing Cytokine Catch Reagent (Miltenyi Biotec) at 4 °C for at least 40 min. Control experiments excluded that the employed Cytokine Catch Reagents affect viability or cellular functions (Supplementary Fig. 15). Next, cells were washed with wash buffer and medium and resuspended in medium at 2.6·10⁶ cells/mL for single-cell encapsulation in 70–100 pL droplets. In case of experiments using different droplet sizes or multiple cells per drop, these concentrations were adjusted to yield the desired Poisson distribution. Stimulus was dissolved in medium at twice the desired concentration to account for on-Chip dilution. For 90 pL droplet production, flow rates were adjusted to 900 µL/h for the oil phase and 200 µL/h for the aqueous fractions (Supplementary Table 4 for overview of all employed flow rates). In all experiments, constant volumetric flow rates were used. To assess the encapsulation rate, videos of the droplet production and images of the produced emulsion were acquired using a CKX41 microscope (Olympus) at ×10 magnification. Encapsulation rate was manually assessed using Fiji[32,33]. The emulsion was collected and covered with medium to protect droplets from evaporation. Cells were incubated with open lid at 37 °C and 5% CO₂. Next, the emulsion was broken by adding 150 µL HFE-7500 containing 20% w/w 1H,1H,2H,2H-Perfluoro-1-octanol and centrifuging briefly at 60 relative centrifugal force (RCF). The cell-containing aqueous phase was transferred into a new tube containing 500 µL PBA and left for 2 min to allow residual oil to settle. Finally, the aqueous phase was transferred into a clean tube and cells were washed with PBS. Dead cells were identified by staining with Fixable Viability Dye eFluor780 (eBioscience, 1:2000 in PBS, 100 µL) for 30 min at 4 °C. Cells were washed once with PBS and blocked with PBA supplemented with 1% HS for 10 min at 4 °C. To stain for surface

proteins and captured cytokines, cells were incubated with antibodies in 70 μ L PBA supplemented with 1% HS for 10 min on ice. After incubation, cells were washed and resuspended in PBA and kept at 4 °C until acquisition on a FACS Verse flow cytometer (BD).

2.7 RNA isolation and quantitative PCR

RNA was isolated using Trizol (Life Technologies) following the manufacturer's protocol. RNA quantity was determined on NanoDrop 2000c (Thermo Scientific) and RNA quality was determined via agarose gel electrophoresis. Then, 2 μ g of RNA was DNase I-treated to remove residual genomic DNA and reverse transcribed into complementary DNA (cDNA) by M-MLV reverse transcriptase (Life Technologies) to obtain 25 μ L of cDNA. The cDNA was diluted 25 \times in nuclease free water. For each reaction, 4 μ L diluted cDNA, 300 nM primers, 10 μ L SYBR Green (Roche), and water were added to a final volume of 20 μ L. Each sample was amplified using a CFX96 sequence detection system (Bio-Rad). The following quantitative PCR (qPCR) cycling conditions were used: 50 °C/2 min, 95 °C/10 min, 40 cycles of 95 °C/15 s; 60 °C/1 min, melt analysis 60 °C–95 °C with increment 0.5 °C/5 s. The gene-specific oligonucleotide primers used to determine the expression of the genes of interest are listed in Supplementary Table 2. To increase the chance of consistency, qPCR primers were based on the MA probes with highest differential expression. PCR products were monitored by measuring the increase of fluorescence caused by binding of SYBR Green. Quantitative PCR data were analyzed using CFX96 manager and relative expression of the gene of interest was determined using the cycle threshold method with GAPDH as reference genes[34].

2.8 Perturbation profiling–scRNA-seq

Using FACS as described above, single cells were sorted in 384-well plates containing a 50 nL droplet with CELseq2-primers and covered by mineral oil. A Mosquito[®] HTS (TTP Labtech) was used to dispense the droplets. To remove red blood cells, PBMCs were resuspended in 8 mL of ice-cold ACK buffer and incubated for 5 min on ice prior antibody staining with FITC-labeled anti-LIN1. Subsequently, the cells were washed with X-Vivo 15 supplemented with 2% HS and the standard protocol was further followed.

After sorting, plates were immediately frozen at –80 °C until further processing. Several days later, plates were thawed and incubated at 65 °C for 5 min to lyse cells. Perturbation profiling

was conducted using the SORT-Seq protocol[35]. In short, spike-in RNA, reverse transcriptase and second-strand mixes were added to the wells using the Nanodrop II liquid handling platform (GC Biotech). Subsequently, the mRNA of each cell was reverse transcribed and converted to double-stranded cDNA. Libraries were then pooled, and in vitro transcribed for linear amplification, following the CEL-Seq 2 protocol[36]. Primers consisted of a 24 bp polyT stretch, a 6 bp random molecular barcode (unique molecular identifier (UMI)), a cell-specific 8 bp barcode, the 5' Illumina TruSeq small RNA kit adaptor, and a T7 promoter. Illumina sequencing libraries were then prepared with the TruSeq small RNA primers (Illumina) and sequenced paired end at 75 bp read length (high output) on the Illumina NextSeq.

2.9 Stimulation in microtiter plate

The pDCs were resuspended in 100 μ L medium containing the appropriate stimulus (see supplementary methods) and cultured in 96-well round bottom plates (Costar, polystyrene) at a density of 25,000 cells per well if not stated differently. Depending on the experimental setting, Brefeldin A (Sigma, 10 μ g/mL) was added 2 h before harvesting the cells.

2.10 Antibody staining

Cells were washed once with PBS and dead cells were identified by staining with Fixable Viability Dye eFluor[®] 780 (eBioscience, 1:2000 in PBS, 100 μ L) at 4 °C for 30 min. Subsequently, cells were washed once with PBS and blocked with PBA supplemented with 1% HS at 4 °C for 10 min. Cells were washed and incubated with antibodies against surface proteins in 30 μ L PBA supplemented with 1% HS for 10 min on ice. Afterwards, cells were washed with PBA followed by a wash with PBS. Cells were fixed and permeabilized with Cytotfix/Cytoperm solution (BD, 100 μ L) for 20 min at 4 °C. Next, cells were washed with Perm/Wash buffer (BD) and blocked for 10 min at 4 °C using Perm/Wash buffer supplemented with 1% HS. Subsequently, cells were incubated with antibodies against intracellular proteins in 30 μ L Perm/Wash buffer supplemented with 1% HS for 30 min at 4 °C. Cells were washed twice with Perm/Wash buffer followed by a wash with PBA and resuspended in PBA. For IRF7 staining, cells were instead fixed with 4% paraformaldehyde (Merck) in PBS for 10 min at room temperature. After incubation, PBA was added and cells were washed twice with PBA, followed by a wash with PBA supplemented with 0.1% Triton X (Sigma). Cells were blocked for

10 min at 4 °C using PBA supplemented with 0.1% Triton X and 1% HS. Subsequently, cells were incubated with antibodies against intracellular proteins in 30 µL PBA supplemented with 0.1% Triton X and 1% HS for 30 min at 4 °C. Cells were washed twice with PBA supplemented with 0.1% Triton X followed by a wash with PBA and resuspended in PBA. All cells were kept at 4 °C until acquisition on a FACS Verse flow cytometer (BD). To guarantee highest purity in experiments, we limited our analysis to viable CD14⁻CD19⁻ pDCs.

2.11 ELISA analysis

The enzyme-linked immunosorbent assay (ELISA) plates (Nunc MaxiSorp ELISA Plates for IFN α , Greiner bio-one high binding microplates for TNF α ELISA) were incubated with PBS containing anti-cytokine antibodies at the manufacturer-recommended concentration (Human IFN-alpha matched antibody pairs, Human TNF alpha ELISA Ready-SET-Go, both from eBioscience) overnight at 4 °C. Next, plates, coated with antibodies against IFN α , were washed once with PBS supplemented with 0.05% Tween-20 (Merck, subsequently referred to as ELISA wash buffer and used for all wash steps) and blocked using 250 µL ELISA wash buffer supplemented with 0.5% BSA for 2 h at room temperature. Plates were washed twice and incubated with 50 µL of sample or standard and 50 µL of horseradish peroxidase (HRP)-conjugated detection antibody at the recommended concentration for 2 h at room temperature. Plates coated with antibodies against TNF α were washed once and blocked with ELISA diluent (eBioscience) for 2 h at room temperature. Plates were washed once and incubated with 50 µL sample or standard. Next, plates were washed 4 \times and incubated with detection antibody at the recommended concentration. Subsequently, plates were washed 4 \times and incubated with Avidin-HRP at the recommended concentration for 30 min at room temperature. Finally, all plates were washed three times and incubated with 100 µL TMB Solution (eBioscience). Reaction was stopped by adding 100 µL of 1 M H₃PO₄ and absorption was measured at 450 nm using a microplate reader (Bio-Rad).

2.12 Flow cytometry and ELISA analysis

Flow cytometry data were analyzed using FlowJo X (Tree Star) and SPICE (downloaded from <http://exon.niaid.nih.gov>)[37]. Analysis and presentation of distributions was performed using PRISM for windows version 5.03 (GraphPad) and The R Project for Statistical Computing

using the ggplot2, reshape, and xlsx packages[38–41]. For statistical analysis, Student's *t*-test, Mann–Whitney test, and linear regression analysis using least square fit were performed.

2.13 Linear regression model

Two models were generated: direct interactions between two random pDCs amplify the type I IFN production ($2 \times \text{percentage of droplets with } >1 \text{ cells} / [100\% + \text{percentage of droplets with } >1 \text{ cells}] \times 100\% \sim \text{percentage of cells that produce IFN}\alpha$); interactions between early type I IFN-producing pDCs and other pDCs amplify type I IFN production ($\text{percentage of droplets } >1 \text{ cells} \cdot \text{percentage of early-responding cells} + \text{the percentage of early-responding cells} \sim \text{percentage of cells that produce IFN}\alpha$). In both models, droplets with 3 or more cells are treated as if they contained only 2 cells. To compare the fit of each model, the dataset ($n = 24$) was randomly split into training (75%) and test (25%). Model parameters were estimated based on the training dataset, and the test dataset was used to predict the fraction of type I IFN-producing cells. Predicted and measured values were compared using the root-mean-square error (RMSE). This process was repeated 100 times and the average RMSE for each model was calculated.

2.14 ScRNA-seq analysis

Paired-end reads from Illumina sequencing were aligned to the human transcriptome with BWA[42]. Read 1 was used for assigning reads to correct cells and libraries, while read 2 was mapped to gene models. Reads that mapped equally well to multiple locations were discarded. Read counts were first corrected for UMI barcode by removing duplicate reads that had identical combinations of library, cellular, and molecular barcodes and were mapped to the same gene. Transcript counts were then adjusted to the expected number of molecules based on counts, 4096 possible UMIs, and poissonian counting statistics.

Samples were normalized by down-sampling to a minimum number of 1700 transcripts. RaceID2 was used to cluster cells and to perform outlier analysis. Differentially expressed genes between two subgroups of cells were identified based on DEseq[35]. Gene ontology (GO) and KEGG (Kyoto Encyclopedia of Genes and Genomes) analysis was conducted by submitting lists of up to 50 most upregulated genes ($\log_2(\text{fold change})$ of >1.5 , adjusted p value $< 10^{-8}$) to the DAVID 6.7 online platform[43,44].

2.15 Data availability

All relevant data related to this manuscript are available on request from the authors. The accession number for the single-cell RNA-sequencing data described in this study is GEO: GSE114161. All relevant codes related to this manuscript are available from the authors or as Supplementary Information.

3. Results

3.1 Functional pDC heterogeneity arises early after stimulation

pDCs operate in complex microenvironments that influence their cellular state. To investigate the intrinsic potential of single pDCs to produce IFN α without interference of other cells, we developed a droplet microfluidic single-cell assay for the detection of cytokine secretion (Fig. 1a). In short, pDCs were coated with capture reagents for cytokine readout and encapsulated in picoliter droplet microenvironments using a microfluidic device (Fig. 1b, c). During in-droplet incubation, produced IFN α and tumor necrosis factor- α (TNF α) was captured on the cell surface by the cytokine capture reagents. After breaking the emulsion, pDCs were isolated and analyzed via multicolor flow cytometry. Each droplet served as a standardized and independent cell reactor and allowed the investigation of tens of thousands of individually stimulated cells simultaneously. This massively parallel approach facilitated the characterization of rare, truly single-cell behavior. This system greatly exceeds the throughput and possibilities when compared to conventional limited dilution experiments which require numerous replicate cultures and, crucially, cannot prohibit cellular crosstalk. Further, the low droplet volume greatly reduced reagent consumption and allowed us to work with small numbers of (primary) cells. We routinely probed rare pDCs using as few as 40,000 cells as input, showing that our technique is highly suited for the use of small biological samples. Importantly, our droplet-based cytokine capture approach enables sensitive cytokine detection and makes no use of transport inhibitors, which negatively impact cellular function and viability. This enabled us to measure cytokine secretion for extended time periods in an accumulative rather than snapshot fashion and facilitated the analysis of extremely early secretion events within the first 30 min of stimulation. Early activation events are problematic

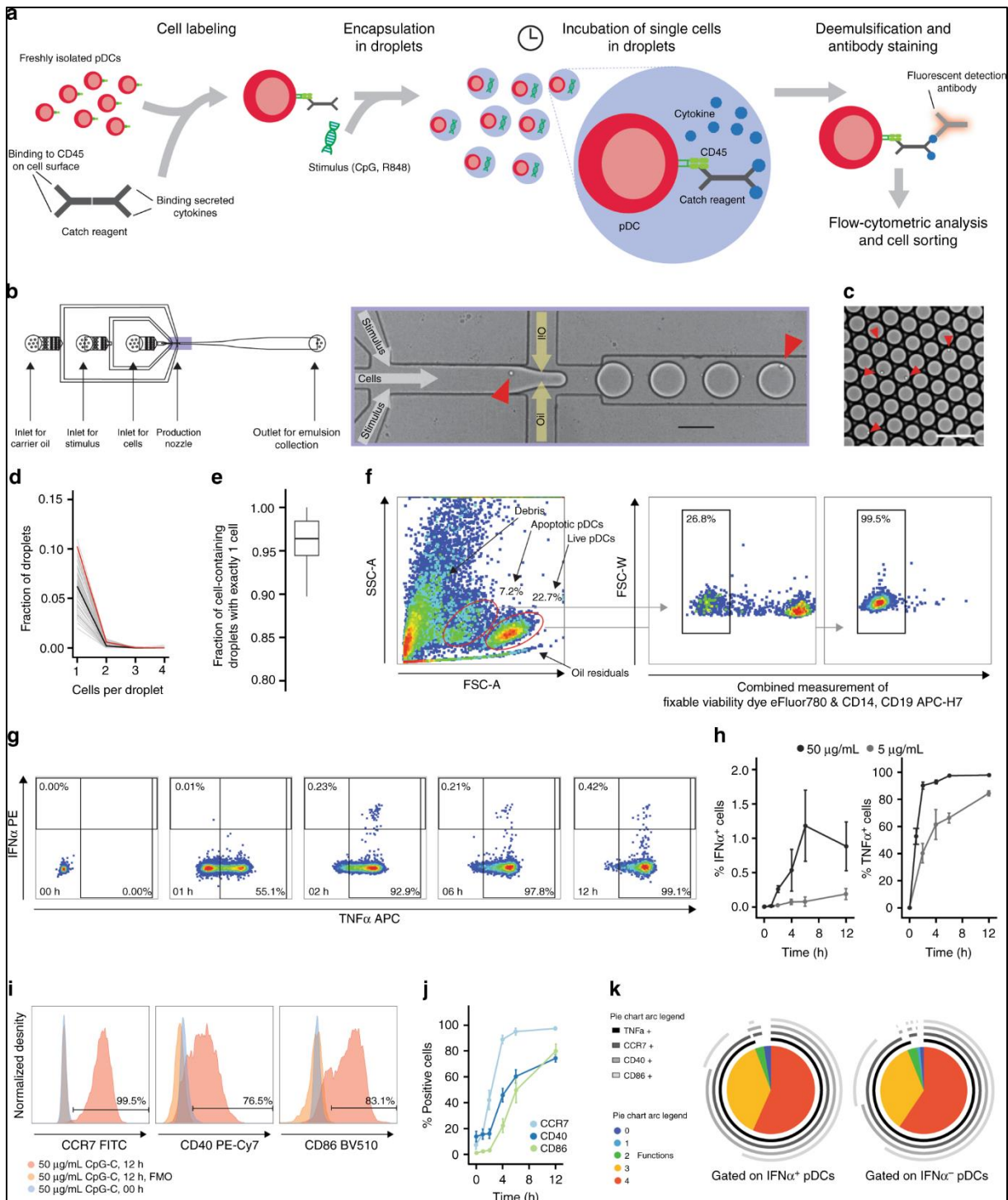


Figure 1. Single-cell analysis reveals functional heterogeneity within individually stimulated pDCs. *a.* Schematic overview of the droplet microfluidic assay. The pDCs were coated with cytokine capture reagents, encapsulated in picoliter droplets, and stimulated with TLR ligands. After incubation, cells were stained for viability, cytokine, and surface marker expression, and analyzed by flow cytometry. *b.* Schematic overview of the employed microfluidic chip with microscopic image of the flow-focusing nozzle for the encapsulation of cells in droplets. *c.* Microscopic image of emulsion after droplet production. B,C Red arrows indicate cells. Scale bars equal 100 μ m. *d.* The pDCs were

encapsulated at a concentration of 1,300,000 cells/mL in 92 pL droplets. The distribution of cells in droplets was measured by manual analysis of microscopic images showing the emulsion directly after production. Shown is the fraction of droplets plotted against the number of cells per droplet; n = 85, black line indicates median, red line indicates predicted values. e. Shown is the fraction of cell-containing droplets with exactly one cell; n = 85. Lines indicate mean, hinges mark interquartile ranges, and whiskers reach to the highest/lowest value that is within 1.5 × interquartile range. f-k The pDCs were treated as described above and stimulated with 5 μg/mL or 50 μg/mL CpG-C. f. Viable pDCs were detected by forward scatter (FSC) and side scatter (SSC) analysis and subsequent gating on CD14⁻CD19⁻ and viability dye⁻ cells. g. IFNα⁻ and TNFα-secreting cells were detected within that population. h. Shown is the fraction of cytokine-secreting cells plotted against incubation time; n (5 μg/mL) = 3, n (50 μg/mL) = 6. i. Surface marker-expressing pDCs were identified comparing the expression levels to fluorescence-minus-one controls. j. Shown is the fraction of surface marker-expressing cells plotted against the incubation time; n > = 4. k. The co-expression of CCR7, CD40, CD86, and TNFα by single IFNα⁺ and IFNα⁻ pDCs was analyzed. Shown is the relative contribution of each functional response pattern to the total pDC population. h,j Dots indicate mean, error bars indicate SEM

to investigate with transport inhibitor-based methods as they negatively impact cell signaling, thereby distorting the measurement. In contrast to microtiter-based approaches, our microfluidic setup makes use of computer-controlled syringe pumps. This allowed us to precisely control environmental factors and vary droplet volume and local cell density in a range that currently cannot be obtained with conventional cultures.

First, we encapsulated pDCs in picoliter droplets (average 92 pL, SEM 1.8 pL, n = 85) with an encapsulation efficiency of approximately 6% cell-containing drops (Fig. 1d) of which 96% contained a single cell (Fig. 1e). Cells were incubated with the synthetic nucleic acid compound CpG-C (TLR9 agonist) and analyzed by flow cytometry (Fig. 1f). Strikingly, only a minor subset of pDCs produced IFNα, which emerged as early as 2 h after stimulation and peaked after 6 h of stimulation (Fig. 1g, h). In contrast, we observed that virtually all pDCs produced TNFα during incubation in droplets (Fig. 1g, h). Similarly, the majority of pDCs was positive for the activation markers CCR7, CD40, and CD86 and most pDCs were highly multifunctional (Fig. 1i–k). Furthermore, we confirmed previous findings that a recently discovered subset of pDC-like progenitor cells, called AS DCs, was not involved in IFNα production (Supplementary Fig. 1)[15].

Next, we studied the capacity of TLR signaling to modulate the probability of pDCs to produce IFN α . We encapsulated cells with varying concentrations of CpG-C and measured the fraction of cells producing IFN α (Fig. 2a). Surprisingly, we only observed minor variations in the fraction of pDCs secreting IFN α irrespective of the concentration of CpG-C. In contrast, the production of TNF α , the expression of the activation markers CCR7, CD40, and CD86, and cell viability all positively correlated with CpG-C concentration (Fig. 2a, Supplementary Fig. 2). To exclude CpG-C-specific limitation in the TLR9 signaling pathway, we stimulated pDCs with the synthetic TLR7/8-agonist R848 (Fig. 2b) and the strong IFN α inducer TLR9 agonist CpG-A (Supplementary Fig. 3). Similar to CpG-C stimulation, only a small fraction of pDCs produced IFN α and this effect was independent of stimulus concentration. Thus far, virtually all knowledge on IFN α secretion by human pDCs is based on bulk cultures. Therefore, cells from the same donor were analyzed by microfluidics and bulk culture side-by-side. Our results demonstrate that individually stimulated cells in droplets indeed have an inferior capacity to secrete IFN α as compared to bulk stimulated cells (Supplementary Fig. 4). Finally, to rule out that the observed IFN α production was due to stimulus-independent constitutive secretion, we stimulated pDCs with either interleukin-3 (IL-3) or CpG-C. The pDCs treated with IL-3, a survival factor for pDCs, which only survive briefly *ex vivo* when left unstimulated, showed a significantly reduced probability to produce IFN α (Fig. c). To exclude that IFN α production by single pDCs is delayed compared to bulk analysis, we incubated pDCs for 12 h and 24 h but only observed small deviations (Fig. 2d).

Together, our data demonstrate that our microfluidic assay is suited for the sensitive detection of cytokine secretion and protein expression by single cells. Functional heterogeneity emerges immediately after TLR activation in pDCs, as only a small fraction of cells is able to produce IFN α . IFN α production is enhanced by TLR signaling but appears to be regulated by an additional stochastic, i.e. random, component which is not associated with strength, amplitude, or duration of cell activation.

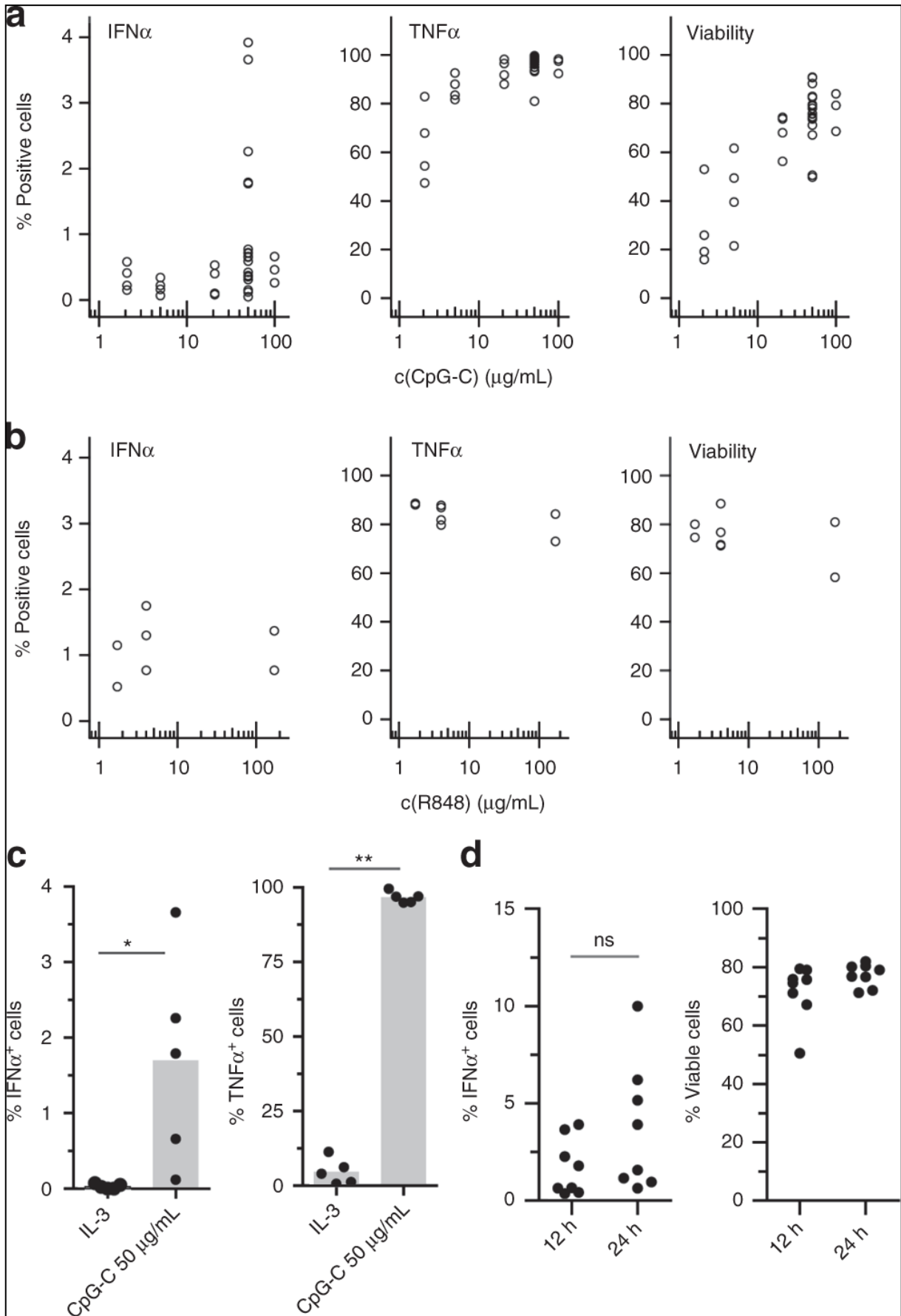


Figure 2. TLR-L concentration does not influence the fraction of IFN α -producing pDCs in droplets. a,b. The pDCs were coated with capture reagent, encapsulated in picoliter droplets, and stimulated individually with a. CpG-C or b. R848 for 12 h. After staining for viability, surface marker expression and cytokine secretion, cytokine-secreting cells, and viable cells were detected via flow cytometry. Shown is the fraction of marker-expressing cells plotted against TLR ligand concentration. Different concentrations were tested in different donors; a $n \geq 3$, b $n \geq 2$. **c.** The pDCs were treated as described above and stimulated with 0.01 $\mu\text{g}/\text{mL}$ IL-3 or 50 $\mu\text{g}/\text{mL}$ CpG-C. Shown is the fraction of cytokine-secreting cells plotted against treatment condition; $n = 5$. Bars indicate mean. **c.** The pDCs were treated as described above and stimulated with 50 $\mu\text{g}/\text{mL}$ CpG-C for 12 h or 24 h. Shown is the fraction of IFN α -secreting or viable cells plotted against treatment condition; $n = 8$ (c,d)) Mann–Whitney test * $p < 0.05$, ** $p < 0.01$.

3.2 Type I IFN is an important regulator of early pDC function

Cellular heterogeneity often emerges from random processes during gene transcription[45]. To probe whether the observed differences in IFN α production originate from such stochastic gene regulation or whether a privileged pDC subset already exists at steady state, we employed scRNA-seq to profile the onset of the type I IFN response upon perturbation with CpG-C. Freshly isolated pDCs from a healthy donor were encapsulated in droplets and individually stimulated with CpG-C using our microfluidic platform (Fig. 3a). After incubation for 0, 1, or 2 h, the emulsion was broken, cells were stained for cytokine secretion, and 384 cells at each time point were sorted into well plates for scRNA-seq (Fig. 3b). Single cells were processed using the SORT-Seq (sorting and robot-assisted transcriptome sequencing) protocol followed by sequencing of ~ 0.1 million to 0.2 million paired-end reads per cell[35]. At 2 h, when we detected the first IFN α + pDCs, we enriched for this subset by sorting 39 IFN α + pDCs before randomly filling up remaining wells with IFN α + and IFN α - cells. In total, we profiled 1152 cells with an average of 4677 transcripts per cell and 1574 unique genes detected per cell. After filtering, down-sampling, and removal of 141 DCs that clustered separately in initial analyses and expressed gene signatures of non-pDC subsets (CD1c+, CD141+), the final dataset contained 774 cells expressing 13,214 genes (Supplementary Fig. 5)[15].

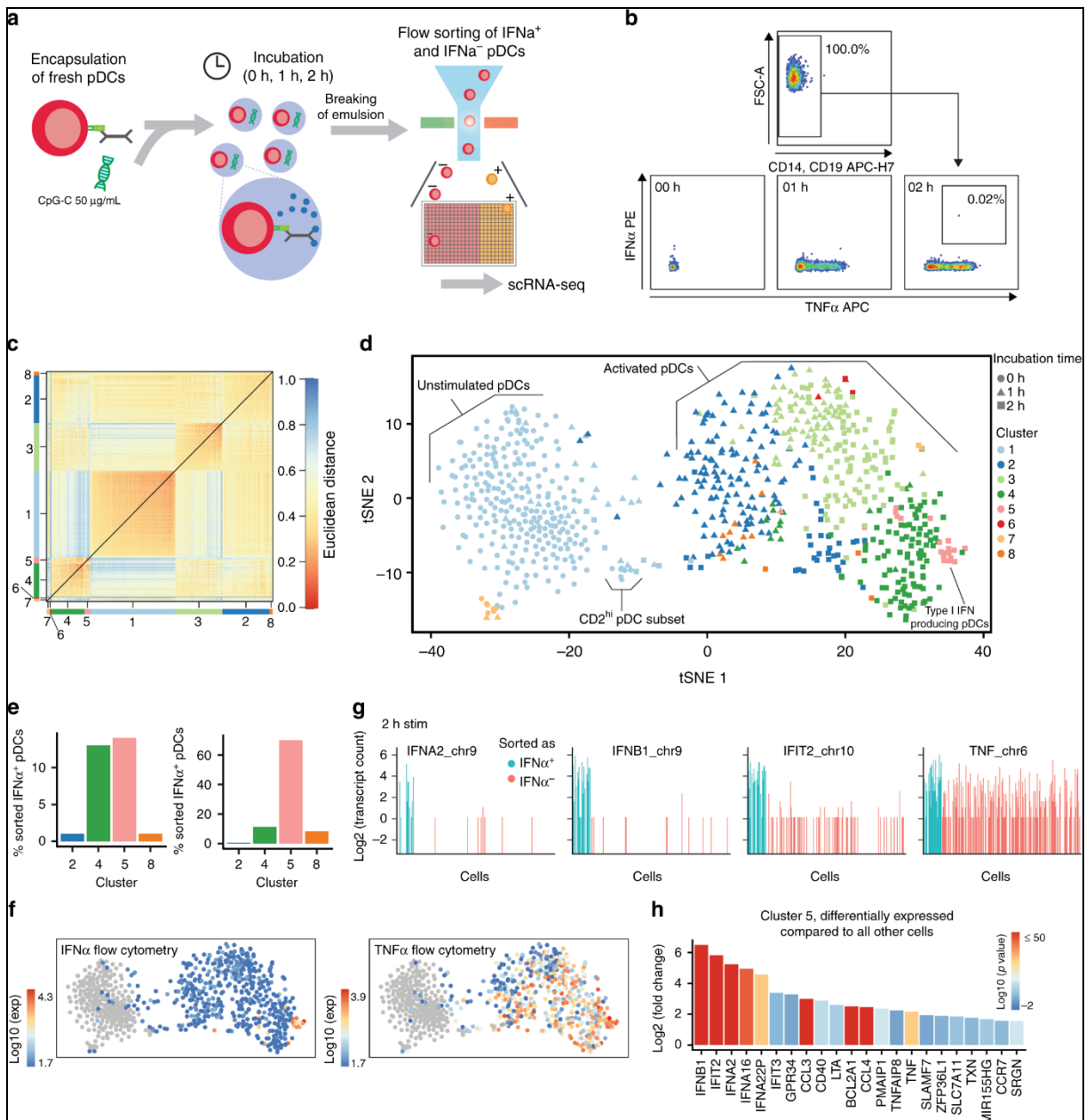


Figure 3. Single-cell RNA-sequencing identifies type I IFN-expressing cells early after activation. a. The pDCs were coated with capture reagent, encapsulated in picoliter droplets, and stimulated individually with 50 $\mu\text{g}/\text{mL}$ CpG-C for varying amounts of time. **b.** After staining for surface marker expression and cytokine secretion, different pDC subsets were collected using fluorescence-activated cell sorting (FACS) and their transcriptomes were sequenced using the SORT-Seq protocol. **c.** Heat map of the 774 cells that passed quality control filters representing transcriptome similarities as measured by Euclidean distance. The k-medoid clustering in combination with the raceID2 algorithm identified 8 distinct cell clusters. **d.** t-SNE map showing all identified clusters. Different colors indicate clusters, different shapes indicate stimulation time. **e.** The employed workflow allowed to link protein expression data acquired during FACS to the transcriptome data. The number of IFN- α^+ cells assigned to each

cluster, and the percentage of sorted IFN- α + cells in each cluster, is plotted against the cluster name. **f.** t-SNE map showing the fluorescence intensity of IFN α and TNF α as measured during FACS for each cell. **g.** Shown are transcript counts for genes of the type I IFN response and the TNF gene in single cells stimulated for 2 h with CpG-C. IFN α + cells, identified during FACS, are indicated in blue, other cells are shown in red. **h** Genes that were upregulated in cluster 5 compared to cells from all other clusters were detected ($p < 10^{-8}$). Shown is the $\log_2(\text{fold change})$ for each gene. The color scale indicates the corresponding p value.

Unsupervised k-medoid clustering of the correlation matrix combined with outlier detection using the raceID2 algorithm suggested the presence of 8 cell clusters (Supplementary Figure 6a-e) which were visualized in two dimensions using t-distributed stochastic neighbor embedding (t-SNE) (Fig. 3c, d; Supplementary Fig. 6f-h)[46]. We observed two clusters of unstimulated cells, CI1 and CI7. CI1 also contained a group of cells that expressed characteristics of the described CD2hi pDC and AS DC subsets (Supplementary Fig. 7)[12,15]. Cells stimulated for 1 h mapped into CI2 with few cells also present in CI3 and CI8. CI4, CI6, and CI5 were dominated by pDCs that were stimulated for 2 h. Cells sorted as IFN α + mapped to CI4 and CI5 at equal fractions and more than 60% of cells in CI5 were sorted as IFN α + (Fig. 3e). The pDCs mapping to CI5 produced high levels of IFN α as measured by flow cytometry (Fig. 3f) and cells sorted as IFN α + expressed high levels of type I IFN genes, such as IFNA2, and IFNB1, as well as the interferon-inducible gene IFIT2 (Fig. 3g). Differential gene expression analysis showed an enrichment of type I IFN genes or type I IFN-induced genes in CI5 as compared to all other cells (Fig. 3h). In contrast, no obvious transcriptionally distinct pDC subset that could predict type I IFN production was observed at steady state. This could either be because type I IFN production is genuinely a stochastic process, or because the nature of such a privileged cell state cannot be determined a priori by present technology. Similar results were obtained when pDCs from two additional healthy donors were profiled at steady state (Supplementary Fig. 8).

Next, we compared the gene expression of individually stimulated pDCs and unstimulated cells. We argued that the underlying mechanisms of CI5 pDCs' unique activation state might become evident when comparing the differential gene expression profiles of all stimulated pDC clusters. On average, CI5 pDCs showed 77 upregulated genes ($\log_2(\text{fold change}) > 1.5$; p value $< 10^{-8}$) and 1 downregulated gene ($\log_2(\text{fold change}) < -1.5$; p value $< 10^{-8}$) compared

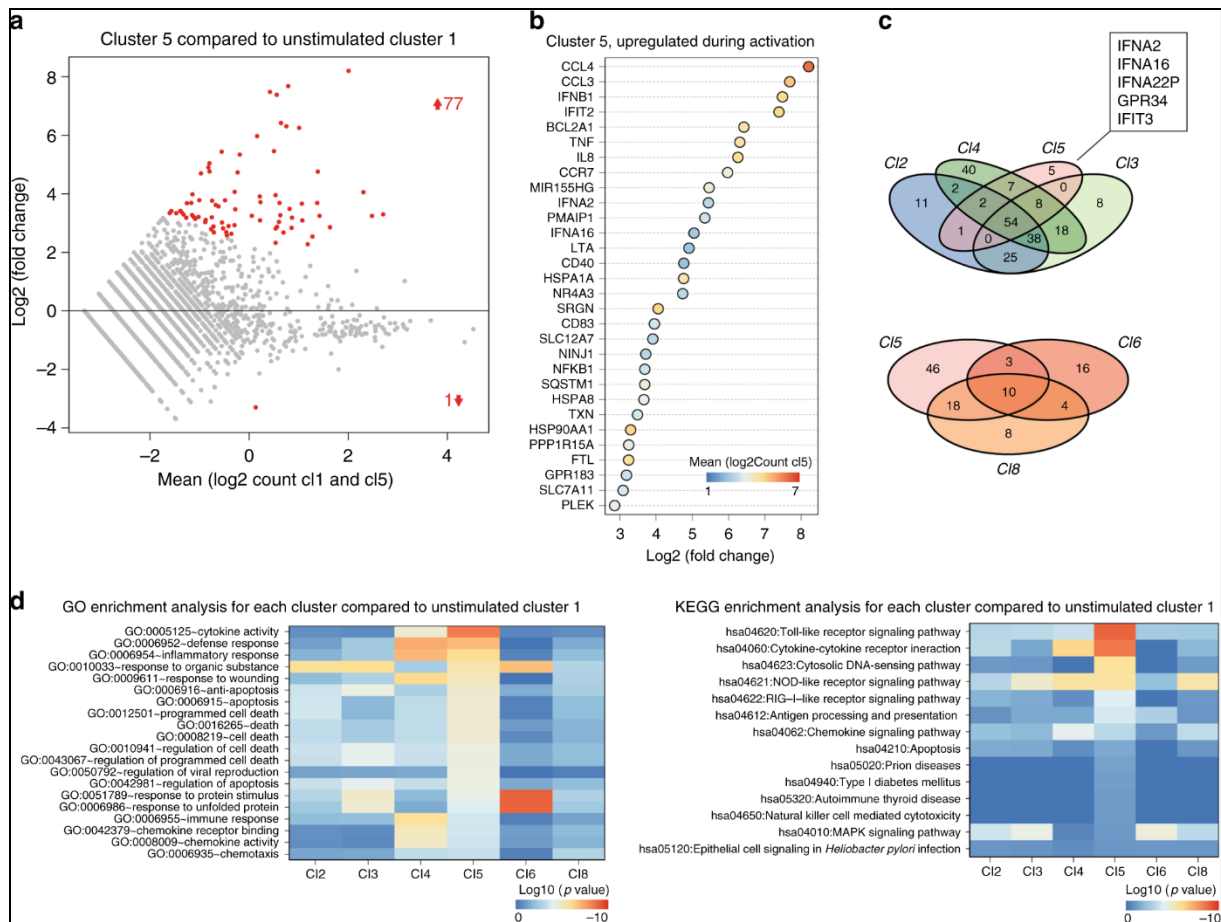


Figure 4. Type I IFN-expressing pDCs show unique gene expression patterns. a. Differentially regulated genes in cells from all activated clusters compared to cluster 1 were identified. Differentially regulated genes from cluster 5. The average $\log_2(\text{count})$ of each gene is plotted against the $\log_2(\text{fold change})$ compared to cells in C1. Red color indicates p value $< 10^{-8}$. **b.** The top 30 most upregulated genes are shown for cluster 5. Shown is the \log_2 fold change for each gene. The color scale indicates the average $\log_2(\text{Count})$ for each transcript in C15. **c.** Venn diagram of the upregulated genes ($\log_2(\text{fold change}) > 1.5$, p value $< 10^{-8}$) within different clusters. **d.** Lists of upregulated genes were submitted to DAVID for GO enrichment analysis and KEGG enrichment analysis. Heat maps show the most significantly enriched terms for the gene list from cluster 5. The color scale indicates the significance of enrichment of a particular term in all selected clusters after Benjamini–Hochberg correction for multiple testing

to unstimulated pDCs in C1 (Fig. 4a). Type I IFN and IFN response genes were among the most upregulated genes as well as several genes that support IFN α production in pDCs including MIR155HG, HSPA1A, and HSP90AA1 (Fig. 4b)[47–49]. Notably, the chemokines CCL3 and CCL4 that bind to the chemokine receptor CCR5 were upregulated. CCR5 is expressed on all pDCs and CCL3/4-CCR5 signaling might be responsible for the generation of large pDC clusters early

after activation[50,51]. Next, we checked for other clusters with similar expression patterns. Cl5 cells shared many upregulated genes with cells from other clusters, especially Cl3 and Cl4; however, they also retained a group of uniquely upregulated genes centered around type I IFN production (Fig. 4c). Gene enrichment and functional annotation analysis using DAVID (Database for Annotation, Visualization and Integrated Discovery) showed that upregulated genes in Cl5 pDCs were enriched for anti-viral responses, cytokine responses, and apoptosis (Fig. 4d and Supplementary data 1–4)[43,44]. Similarly, type I IFN-related or -induced pathways were uniquely enriched in Cl5 genes, including TLR signaling, cytosolic DNA sensing, and the RIG-I-like pathway.

These results demonstrate that our microfluidic platform is ideally suited to work in conjunction with scRNA-seq to link functional information from extremely rare cells (<0.02% IFN α -producing pDCs) to whole transcriptome profiling. Together, the data show that type I IFN-producing cells possess unique transcriptional features, many of which are associated with autocrine type I IFN signaling. ScRNA-seq data revealed no evidence for a privileged pDC subset at steady state but type I IFN appears to be an important orchestrator of early pDC activation. The question remains of how pDC populations regulate the cellular heterogeneity originating from variation in type I IFN production.

3.3 Environmental factors modulate type I IFN production

In vivo, pDCs act in a dynamic microenvironment and migrate considerably during their life cycle. To assess the impact of environmental changes on the observed heterogeneity during pDC-driven type I IFN responses, we systematically varied key droplet parameters (Fig. 5a). First, we generated droplets of varying size, covering several orders of magnitude (Fig. 5b). Single pDCs were encapsulated in droplets ranging from 31 to 1209 pL and stimulated for 12 h (Fig. 5c). No significant difference in the fraction of IFN α -secreting cells was detected (Fig. 5d, colored dots). Comparison with pDCs from additional donors, which were encapsulated in droplets of up to 3371 pL—a volume comparable to the average volume of a single pDC in a perfectly mixed microtiter plate—showed no increase in the fraction of IFN α -secreting cells (Fig. 5d, gray dots).

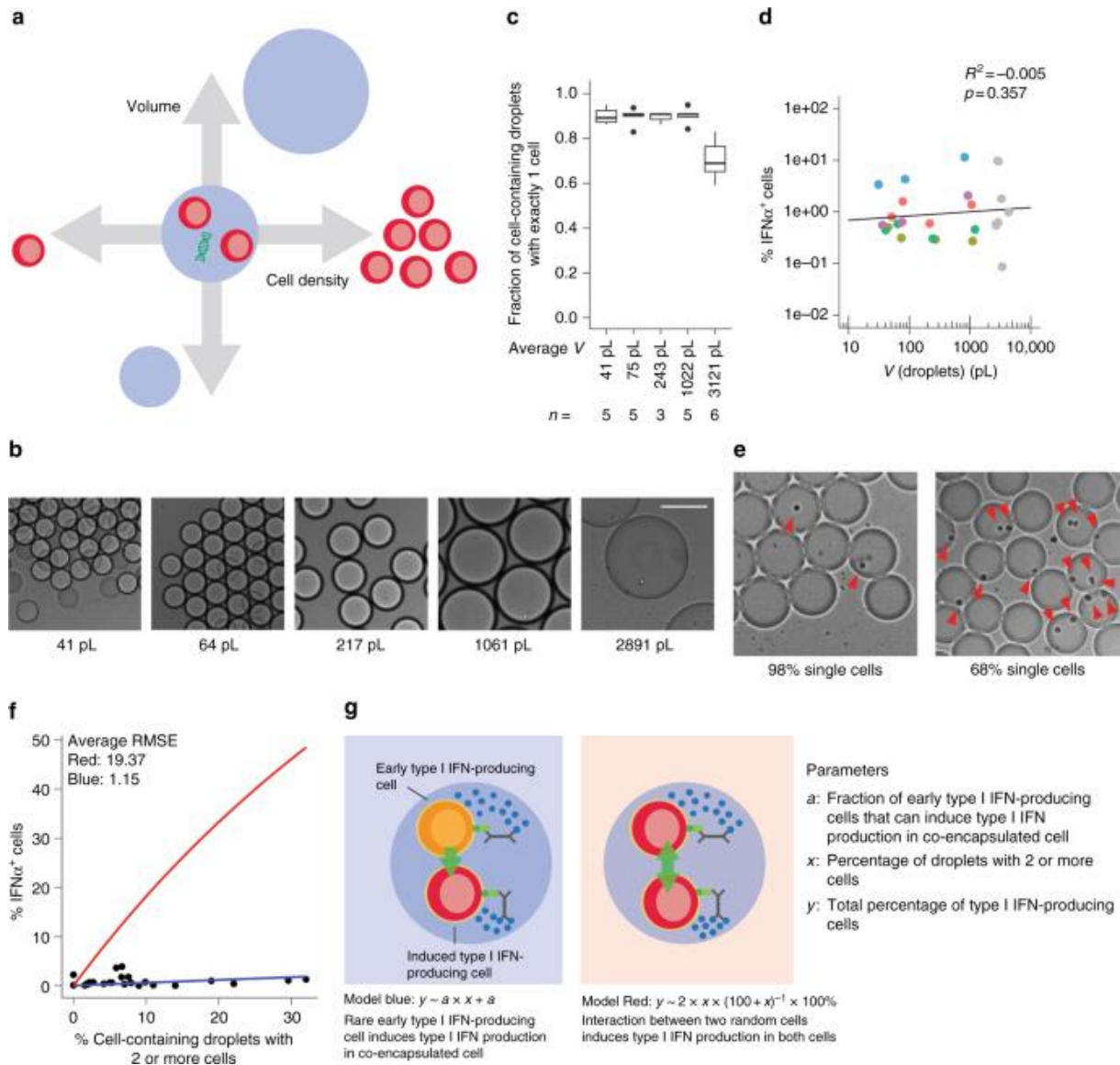


Figure 5. Microenvironmental factors influence the fraction of IFN α -producing pDCs. a,b. The pDCs were coated with cytokine capture reagents, encapsulated in droplets of varying size (b, scale bar equals 100 μ m), and stimulated individually with 50 μ g/mL CpG-C for 12 h. The distribution of cells in droplets was measured by manual analysis of microscopic images after production. After staining for viability and surface marker expression, viable cells and TNF α -positive cells were detected via flow cytometry. **c.** Shown is the fraction of cell-containing droplets with exactly one cell; $n > 3$. Lines indicate mean, hinges mark interquartile ranges, and whiskers reach to the highest/lowest value that is within $1.5 \times$ interquartile range. **d.** The fraction of IFN α -secreting pDCs was plotted against droplet volume. Dots of the same color indicate cells from the same donor. Gray dots are all originating from different donors. Linear regression was employed to calculate a trend line; $n = 24$. **e.** The pDCs were stimulated in ~ 92 pL droplets with an increasing fraction of droplets containing more than 1 cell. **f.** Shown is the fraction of IFN α -secreting cells plotted against the fraction of droplets containing more

than 1 cell. Two models were generated to explain the observed pattern: (red) two random pDCs co-encapsulated in the same droplet can induce type I IFN production in each other; (blue) rare early type I IFN-producing cells can induce type I IFN production in conventional co-encapsulated cells. The root-square-mean error (RMSE) was calculated for both models to compare the fit to the data; $n = 24$. **g.** Schematic overview of both models

Previous studies indicated that pDCs build homologous cell clusters upon stimulation, indicating that cellular crosstalk might be involved in their activation process[2,51]. To test this, we stimulated pDCs at various cell densities in microtiter plates in bulk (Supplementary Fig. 9A). Indeed, the fraction of IFN α -expressing pDCs depended on cell density (Supplementary Fig. 9B–F).

Communication between abovementioned pDCs in bulk can, thus, amplify the fraction of IFN α -producing cells. To get more insight into the nature of this communication, we tested whether crosstalk between two random interacting cells would be sufficient to enable IFN α production. We encapsulated pDCs in 90 pL droplets and gradually increased the fraction of droplets containing multiple cells (Fig. 5e). The fraction of IFN α -secreting cells increased slightly with the fraction of multiple cells per drop but did not match the predictions of a random interaction model (Fig. 5f, red). In contrast, the increase was better described by an alternative model based on the assumption that the early IFN α -producing pDCs activate co-encapsulated cells to produce IFN α as well (blue). However, in the employed system, we cannot rule out the possibility that the increase was caused by passive diffusion of cytokines or capture reagent between two co-encapsulated cells (Supplementary Fig. 10).

Together, these results show that the microenvironment—in this case represented by surrounding pDCs—has a critical impact on the probability of a pDC to produce IFN α .

3.4 Priming with type I IFN increases the chance to produce IFN- α

Communication between IFN α -producing pDCs and surrounding pDCs occurs either in a juxtacrine or paracrine fashion. To elucidate whether paracrine signaling is the driving factor, freshly isolated pDCs were primed for 2 h with conditioned medium (CM) harvested from overnight bulk pDC cultures (Fig. 6f). After priming, pDCs were thoroughly washed, coated with capture reagent, encapsulated in picoliter droplets, and stimulated individually with CpG-C. Priming cells with 10% CM significantly increased the fraction of single pDCs that produced IFN- α (Fig. 6b). In contrast, no effect was observed when cells were primed with remnant CpG-

C, fresh cell culture medium, or primed without subsequent TLR stimulation. Similar to previous experiments, IFN- α -secreting cells were highly multifunctional (Fig. 6c). Interestingly, the fraction of IFN- α -secreting pDCs depended on the concentration of the CM, but not on the concentration of CpG-C (Fig. 6d, e). These findings indicate that priming modulates the probability of a pDC to produce IFN- α but does not directly induce IFN- α production.

To identify the responsible factor for the priming effect, we tested several cytokines described to positively affect IFN- α -production by pDCs[22,27]. An initial screen revealed that only IFN- β —which acts similar to IFN- α via the IFN- α/β -receptor—increased the average per-cell IFN- α production by pDCs cultured in microtiter plates at low cell density (Supplementary Fig. 11A, B). Furthermore, blocking the IFN α/β receptor and adding neutralizing antibodies against IFN- α and - β inhibited the positive effect of CM on per-cell IFN- α production. Priming of pDCs with IFN- β also led to an increase in the fraction of low-density cultured pDCs producing IFN- α as measured by flow cytometry (Supplementary Fig. 11C). Finally, priming with IFN- β increased the fraction of IFN- α -secreting cells in droplets to a similar extent as CM (Fig. 6f).

Previous studies identified IRF7 as a limiting factor in non-pDC models of type I IFN production[18]. In our hands, all pDCs displayed high levels of IRF7 immediately after isolation which decreased, however, during ex vivo culture (Supplementary Figs. 12, 13). High levels of IRF7 were induced by priming with IFN- β or by natural production of type I IFN by pDCs and coincided with but did not precede IFN- α production (Supplementary Figs. 12, 13).

Together, these results unambiguously show that signaling via the type I IFN receptor amplifies TLR-induced IFN α production, thus modulating the patterns of heterogeneity within the pDC population. Next, we challenged our hypothesis that the bulk type I IFN response is governed by a small driver population of cells by conducting bulk experiments where type I IFN-mediated paracrine communication was abrogated by blocking the IFN- α/β receptor and by adding neutralizing antibodies against IFN- α and - β prior to bulk activation. Our experiments revealed that blocking the IFNAR in combination with neutralizing sera reduced the fraction of cells secreting IFN- α to similar numbers as observed in our droplet experiments (Supplementary Fig. 14), indicative for a pool of early responder cells.

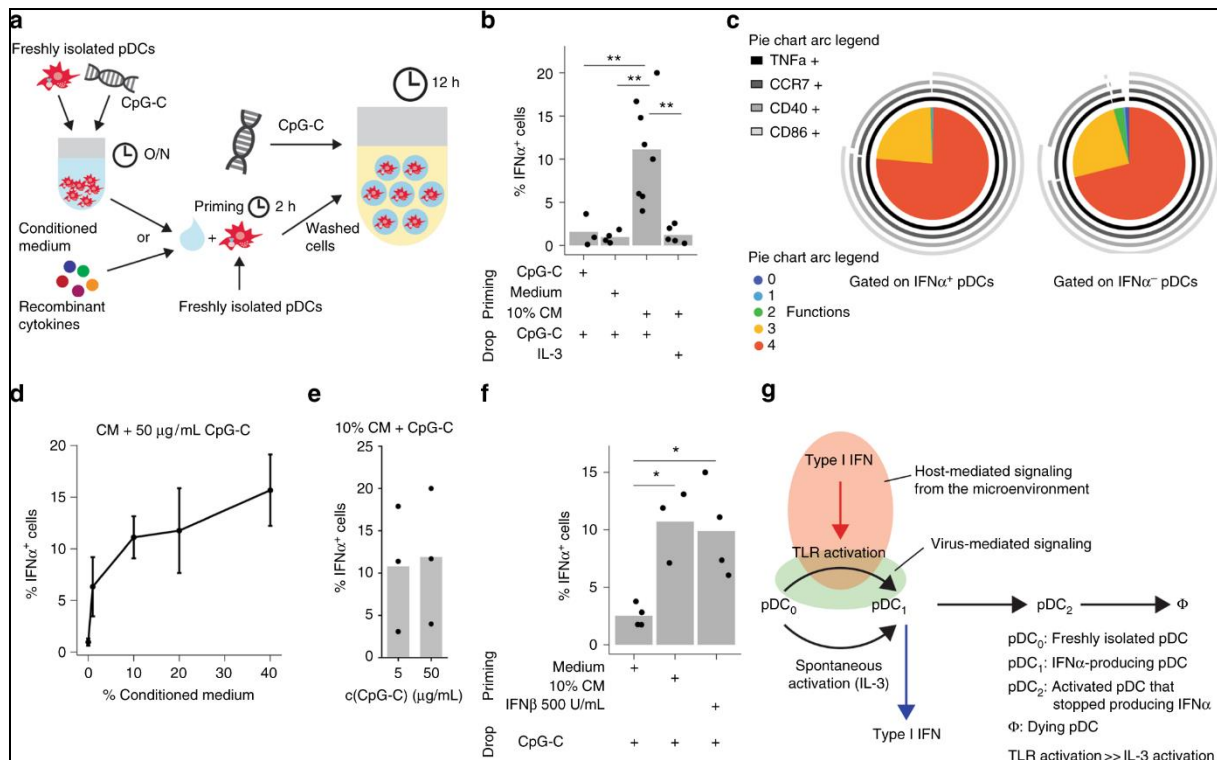


Figure 6. The pDCs primed with CM or IFN β are more likely to produce IFN α . **a.** Schematic overview of the priming experiment. The pDCs were stimulated for 2 h with conditioned medium (CM), 0.5 μ g/mL CpG-C, or control medium. Cells were washed, coated with cytokine capture reagent, encapsulated in droplets, and stimulated individually with 0.01 μ g/mL IL-3 or 50 μ g/mL CpG-C for 12 h. CM was generated from bulk pDC cultures stimulated with 5 μ g/mL CpG-C at a density of 25,000 cells/well. Cytokine-secreting cells were detected using flow cytometry. **b.** The fraction of IFN α -secreting cells is plotted against different treatment conditions. **c.** Co-expression of CCR7, CD40, CD86, and TNF- α by single IFN- α ⁺ and IFN- α ⁻ pDCs was analyzed. Shown is the relative contribution of each functional response pattern to the total pDC population. **d.** The pDCs were primed with different concentrations of CM and stimulated with 50 μ g/mL CpG-C. Shown is the fraction of IFN α -secreting cells plotted against CM concentration; $n > 3$. Dots indicate mean and whiskers indicate SEM. **e.** The pDCs were treated as described above, primed with 10% CM, and stimulated with different concentrations of CpG-C. Shown is the fraction of IFN- α -secreting cells plotted against CpG-C concentration; $n = 3$. **f.** The pDCs were primed with 10% CM, control medium, or 500 U/mL IFN- β , and stimulated with 50 μ g/mL CpG-C. The fraction of IFN α -secreting cells is plotted against different treatment conditions; $n > 3$. **g.** Schematic model illustrating stochastic IFN α -production by pDCs. Few pDCs produce IFN α constitutively without stimulation by TLR ligands, here resembled by differentiation from a freshly isolated pDC (pDC₀) to an IFN- α -secreting pDC (pDC₁). Literature indicates that this is not IRF7 dependent but NF- κ B and AP-127. Upon TLR9 triggering the IRF7-dependent pathway is activated which also allows differentiation to IFN- α -secreting pDC at a much higher rate. Despite involvement of the IRF7 pathway,

*still only very few pDCs produce IFN- α . Paracrine signaling via the type I IFN receptor can increase this rate, probably via the upregulation of IRF7 expression, leading to a large fraction of cells expressing IFN- α . After producing IFN- α , pDCs become refractory to re-stimulation (pDC2) and eventually die (Φ). b,f Welch-corrected two-sample t-test; * $p < 0.05$, ** $p < 0.01$*

Based on our results, we propose the following model of early pDC activation (Fig. 6g). The pDCs are able to produce IFN- α constitutively, but this is a rare and stochastic process that is controlled by transcription factors such as nuclear factor (NF)- κ B or activator protein 1 (AP-1), but not IRF7[27]. TLR triggering, which behaves as a sensitive and digital process, leads to the activation of the MyD88–IRF7 pathway and a 20-fold increase in stochastic IFN α expression. In many cells, this pathway is, however, limited by downstream components and by trafficking of CpG molecules to early endosomes. This leads to a still very limited pool of early responder pDCs that secrete type I IFN. Secreted type I IFN, then, primes surrounding pDCs and induces the expression of important factors for the IFN- α production. This increases the probability of IFN α expression in those cells and leads to a robust population response.

4. Discussion

We show that type I IFN production by freshly isolated human pDCs is controlled by stochastic gene regulation and amplified by environmental signals. This is supported by several observations. First, TLR signaling was necessary but insufficient for the induction of type I IFN production. Only a minor subset of cells produced IFN α , whereas all cells expressed TNF- α or CCR7, implying universal activation of the TLR signaling pathway. Second, neither TLR signaling strength nor duration influenced the fraction of IFN- α -producing cells. Third, RNA profiling of single pDCs indicated no evidence of a privileged pDC subset with superior ability to produce type I IFN. On the contrary, a type I IFN-expressing pDC subset emerged at 2 h after activation, at the same time as type I IFN secretion was first observed in droplets, indicating that heterogeneity emerges simultaneously at protein and messenger RNA (mRNA) levels. Stochastic gene regulation is one of the strongest drivers of cellular heterogeneity and can be caused by not only the inherently random nature of gene expression itself but also by limitations in the signalling pathways leading to the production of a cytokine[19,21,45]. In our system, high IRF7 expression, which represented the most important cause of stochasticity in other systems, did not guarantee type I IFN production in all pDCs[18].

In contrast, we show here that the microenvironment has a decisive impact on type I IFN responses as IFN- α production by pDCs depended directly on cell density. This effect could be mimicked by pre-treating pDCs with type I IFN leading to an increase in the fraction of IFN α -producing individually stimulated pDCs. This combination of stochastic gene regulation and environmental response amplification poses an efficient yet flexible solution for pDCs to generate robust type I IFN responses. IFN α production by rogue cells that detect host-derived nucleic acids in sterile situations is limited without type I IFN amplification, but rapid and robust responses are guaranteed when pDCs are triggered in inflamed tissue with high pDC density or type I IFN signals from infected body cells. Furthermore, controlling type I IFN production in such a population-regulated stochastic manner allows the induction of an antiviral state in all cells of a given tissue but bypasses the necessity of all cells being type I IFN producers, reducing type I IFN levels and tissue damage.

These insights have far-reaching implications: on an applied level, pDC-focused treatments, such as DC-based immunotherapy, need to reconsider vaccine parameters, such as number of injected cells, location and pre-treatment of injection site, and cell density during stimulation for better efficacy. On a more fundamental level, our insights imply that the functional behavior of pDCs is plastic and adaptable to local cues from the tissue microenvironment, similar to macrophages[52]. Therapy approaches that target pDCs inside the body should take into account that not all pDCs are the same and that pDCs might react differently to treatment depending on the tissue context of the disease.

Here, we show that well-studied human primary immune cell responses can be based on stochastic processes at the single-cell level and emphasize the importance of single-cell techniques to deconstruct immunological responses at the single-cell level.

5. Acknowledgements

The authors want to thank Johannes Textor and Mauro Muraro for supporting the statistical analysis and Michael Valente for enthusiastic discussions. F.W. was supported by a Radboudumc PhD grant. J.T. is supported by NWO-Veni grant 863.130.24 from the Netherlands Organization for Scientific Research and acknowledges generous support by the Eindhoven University of Technology.

6. Reference

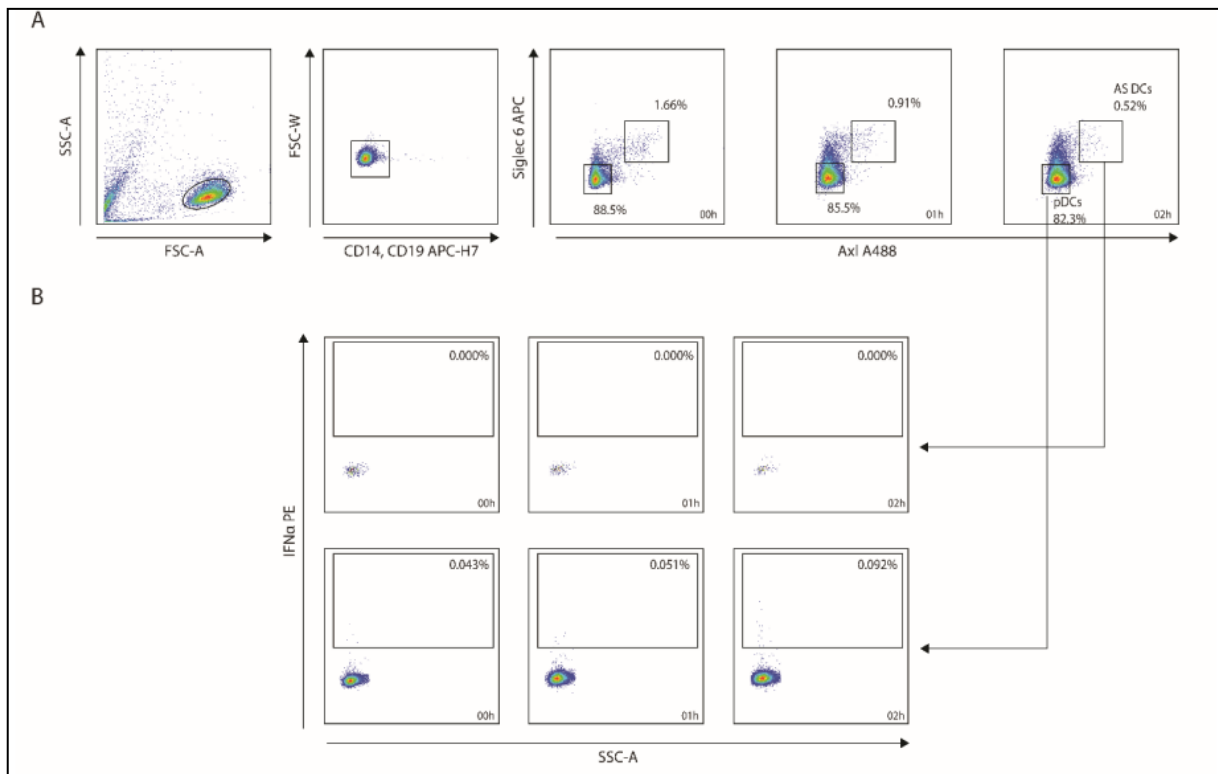
- [1] F.P. Siegal, N. Kadowaki, M. Shodell, P.A. Fitzgerald-Bocarsly, K. Shah, S. Ho, S. Antonenko, Y.J. Liu, The nature of the principal Type 1 interferon-producing cells in human blood, *Science* (80-.). (1999). <https://doi.org/10.1126/science.284.5421.1835>.
- [2] M. Cella, D. Jarrossay, F. Facchetti, O. Alebardi, H. Nakajima, A. Lanzavecchia, M. Colonna, Plasmacytoid monocytes migrate to inflamed lymph nodes and produce large amounts of type I interferon, *Nat. Med.* (1999). <https://doi.org/10.1038/11360>.
- [3] M. Swiecki, M. Colonna, The multifaceted biology of plasmacytoid dendritic cells, *Nat. Rev. Immunol.* (2015). <https://doi.org/10.1038/nri3865>.
- [4] F.J. Barrat, T. Meeker, J. Gregorio, J.H. Chan, S. Uematsu, S. Akira, B. Chang, O. Duramad, R.L. Coffman, Nucleic acids of mammalian origin can act as endogenous ligands for Toll-like receptors and may promote systemic lupus erythematosus, *J. Exp. Med.* (2005). <https://doi.org/10.1084/jem.20050914>.
- [5] T.K. Means, E. Latz, F. Hayashi, M.R. Murali, D.T. Golenbock, A.D. Luster, Human lupus autoantibody-DNA complexes activate DCs through cooperation of CD32 and TLR9, *J. Clin. Invest.* (2005). <https://doi.org/10.1172/JCI23025>.
- [6] M. Menon, P.A. Blair, D.A. Isenberg, C. Mauri, A Regulatory Feedback between Plasmacytoid Dendritic Cells and Regulatory B Cells Is Aberrant in Systemic Lupus Erythematosus, *Immunity*. (2016). <https://doi.org/10.1016/j.immuni.2016.02.012>.
- [7] L.M. Kranz, M. Diken, H. Haas, S. Kreiter, C. Loquai, K.C. Reuter, M. Meng, D. Fritz, F. Vascotto, H. Hefesha, C. Grunwitz, M. Vormehr, Y. Hüsemann, A. Selmi, A.N. Kuhn, J. Buck, E. Derhovanessian, R. Rae, S. Attig, J. Diekmann, R.A. Jabulowsky, S. Heesch, J. Hassel, P. Langguth, S. Grabbe, C. Huber, Ö. Türeci, U. Sahin, Systemic RNA delivery to dendritic cells exploits antiviral defence for cancer immunotherapy, *Nature*. (2016). <https://doi.org/10.1038/nature18300>.
- [8] J. Tel, H.J.G.A. Erik, T. Baba, G. Schreibelt, B.M. Schulte, D. Benitez-Ribas, O.C. Boerman, S. Croockewit, J.G.O. Wim, M. Van Rossum, G. Winkels, P.G. Coulie, J.A.P. Cornelis, C.G. Figdor, I.J.M. De Vries, Natural human plasmacytoid dendritic cells induce antigen-specific T-cell responses in melanoma patients, *Cancer Res.* (2013). <https://doi.org/10.1158/0008-5472.CAN-12-2583>.
- [9] N. Kadowaki, S. Antonenko, Y.-J. Liu, Distinct CpG DNA and Polyinosinic-Polycytidylic Acid Double-Stranded RNA, Respectively, Stimulate CD11c – Type 2 Dendritic Cell Precursors and CD11c + Dendritic Cells to Produce Type I IFN, *J. Immunol.* 166 (2001) 2291–2295. <https://doi.org/10.4049/jimmunol.166.4.2291>.
- [10] J.M. Lund, L. Alexopoulou, A. Sato, M. Karow, N.C. Adams, N.W. Gale, A. Iwasaki, R.A. Flavell, Recognition of single-stranded RNA viruses by Toll-like receptor 7, *Proc. Natl. Acad. Sci. U. S. A.* (2004). <https://doi.org/10.1073/pnas.0400937101>.
- [11] J. Dai, N.J. Megjugorac, S.B. Amrute, P. Fitzgerald-Bocarsly, Regulation of IFN Regulatory Factor-7 and IFN- α Production by Enveloped Virus and Lipopolysaccharide in Human Plasmacytoid Dendritic Cells, *J. Immunol.* (2004). <https://doi.org/10.4049/jimmunol.173.3.1535>.
- [12] H. Zhang, J.D. Gregorio, T. Iwahori, X. Zhang, O. Choi, L.L. Tolentino, T. Prestwood, Y. Carmi, E.G. Engleman, A distinct subset of plasmacytoid dendritic cells induces activation and differentiation of B and T lymphocytes, *Proc. Natl. Acad. Sci. U. S. A.* (2017). <https://doi.org/10.1073/pnas.1610630114>.
- [13] T. Matsui, J.E. Connolly, M. Michnevitc, D. Chaussabel, C.-I. Yu, C. Glaser, S. Tindle, M. Pypaert, H. Freitas, B. Piqueras, J. Banchereau, A.K. Palucka, CD2 Distinguishes Two Subsets of Human Plasmacytoid Dendritic Cells with Distinct Phenotype and Functions, *J. Immunol.* (2009). <https://doi.org/10.4049/jimmunol.0802008>.
- [14] X. Zhang, A. Lepelley, E. Azria, P. Lebon, G. Roguet, O. Schwartz, O. Launay, C. Leclerc, R. Lo-Man, Neonatal Plasmacytoid Dendritic Cells (pDCs) Display Subset Variation but Can Elicit Potent Anti-Viral Innate Responses, *PLoS One*. (2013). <https://doi.org/10.1371/journal.pone.0052003>.
- [15] A.C. Villani, R. Satija, G. Reynolds, S. Sarkizova, K. Shekhar, J. Fletcher, M. Griesbeck, A. Butler, S. Zheng, S. Lazo, L. Jardine, D.

- Dixon, E. Stephenson, E. Nilsson, I. Grundberg, D. McDonald, A. Filby, W. Li, P.L. De Jager, O. Rozenblatt-Rosen, A.A. Lane, M. Haniffa, A. Regev, N. Hacohen, Single-cell RNA-seq reveals new types of human blood dendritic cells, monocytes, and progenitors, *Science* (80-). (2017). <https://doi.org/10.1126/science.aah4573>.
- [16] P. See, C.A. Dutertre, J. Chen, P. Günther, N. McGovern, S.E. Irac, M. Gunawan, M. Beyer, K. Händler, K. Duan, H.R. Bin Sumatoh, N. Ruffin, M. Jouve, E. Gea-Mallorquí, R.C.M. Hennekam, T. Lim, C.C. Yip, M. Wen, B. Malleret, I. Low, N.B. Shadan, C.F.S. Fen, A. Tay, J. Lum, F. Zolezzi, A. Larbi, M. Poidinger, J.K.Y. Chan, Q. Chen, L. Rénia, M. Haniffa, P. Benaroch, A. Schlitzer, J.L. Schultze, E.W. Newell, F. Ginhoux, Mapping the human DC lineage through the integration of high-dimensional techniques, *Science* (80-). (2017). <https://doi.org/10.1126/science.aag3009>.
- [17] S. Patil, M. Fribourg, Y. Ge, M. Batish, S. Tyagi, F. Hayot, S.C. Sealfon, Single-cell analysis shows that paracrine signaling by first responder cells shapes the interferon- β response to viral infection, *Sci. Signal.* (2015). <https://doi.org/10.1126/scisignal.2005728>.
- [18] M. Zhao, J. Zhang, H. Phatnani, S. Scheu, T. Maniatis, Stochastic expression of the interferon- β gene, *PLoS Biol.* (2012). <https://doi.org/10.1371/journal.pbio.1001249>.
- [19] J. Hu, G. Nudelman, Y. Shimoni, M. Kumar, Y. Ding, C. López, F. Hayot, J.G. Wetmur, S.C. Sealfon, Role of cell-to-cell variability in activating a positive feedback antiviral response in human dendritic cells, *PLoS One.* (2011). <https://doi.org/10.1371/journal.pone.0016614>.
- [20] A.K. Shalek, R. Satija, J. Shuga, J.J. Trombetta, D. Gennert, D. Lu, P. Chen, R.S. Gertner, J.T. Gaublomme, N. Yosef, S. Schwartz, B. Fowler, S. Weaver, J. Wang, X. Wang, R. Ding, R. Raychowdhury, N. Friedman, N. Hacohen, H. Park, A.P. May, A. Regev, Single-cell RNA-seq reveals dynamic paracrine control of cellular variation, *Nature.* 510 (2014) 363–369. <https://doi.org/10.1038/nature13437>.
- [21] U. Rand, M. Rinas, J.S. Werk, G. Nöhren, M. Linnes, A. Kröger, M. Flossdorf, K. Kály-Kullai, H. Hauser, T. Höfer, M. Köster, Multi-layered stochasticity and paracrine signal propagation shape the type-I interferon response, *Mol. Syst. Biol.* (2012). <https://doi.org/10.1038/msb.2012.17>.
- [22] H. Gary-Gouy, P. Lebon, A.H. Dalloul, Type I interferon production by plasmacytoid dendritic cells and monocytes is triggered by viruses, but the level of production is controlled by distinct cytokines, *J. Interf. Cytokine Res.* (2002). <https://doi.org/10.1089/10799900260100132>.
- [23] W. Cao, S. Manicassamy, H. Tang, S.P. Kasturi, A. Pirani, N. Murthy, B. Pulendran, Toll-like receptor-mediated induction of type I interferon in plasmacytoid dendritic cells requires the rapamycin-sensitive PI(3)K-mTOR-p70S6K pathway, *Nat. Immunol.* (2008). <https://doi.org/10.1038/ni.1645>.
- [24] C. Guiducci, C. Ghirelli, M.A. Marloie-Provost, T. Matray, R.L. Coffman, Y.J. Liu, F.J. Barrat, V. Soumelis, PI3K is critical for the nuclear translocation of IRF-7 and type I IFN production by human plasmacytoid predendritic cells in response to TLR activation, *J. Exp. Med.* (2008). <https://doi.org/10.1084/jem.20070763>.
- [25] M.L. Shinohara, L. Lu, J. Bu, M.B.F. Werneck, K.S. Kobayashi, L.H. Glimcher, H. Cantor, Osteopontin expression is essential for interferon- α production by plasmacytoid dendritic cells, *Nat. Immunol.* (2006). <https://doi.org/10.1038/ni1327>.
- [26] I. Marie, Differential viral induction of distinct interferon-alpha genes by positive feedback through interferon regulatory factor-7, *EMBO J.* (1998). <https://doi.org/10.1093/emboj/17.22.6660>.
- [27] S. Kim, V. Kaiser, E. Beier, M. Bechheim, M. Guenther-Biller, A. Ablasser, M. Berger, S. Endres, G. Hartmann, V. Hornung, Self-priming determines high type I IFN production by plasmacytoid dendritic cells, *Eur. J. Immunol.* (2014). <https://doi.org/10.1002/eji.201343806>.
- [28] E.Z. Macosko, A. Basu, R. Satija, J. Nemeshe, K. Shekhar, M. Goldman, I. Tirosh, A.R. Bialas, N. Kamitaki, E.M. Mardersteck, J.J. Trombetta, D.A. Weitz, J.R. Sanes, A.K. Shalek, A. Regev, S.A. McCarroll, Highly parallel genome-wide expression profiling of individual cells using nanoliter droplets, *Cell.* 161 (2015) 1202–1214. <https://doi.org/10.1016/j.cell.2015.05.002>.

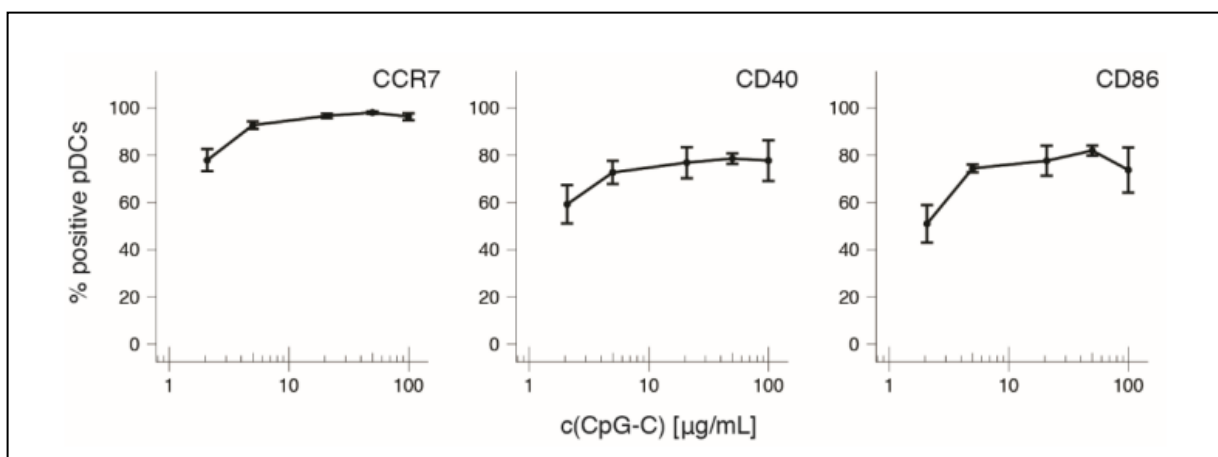
- [29] F. Lan, B. Demaree, N. Ahmed, A.R. Abate, Single-cell genome sequencing at ultra-high-throughput with microfluidic droplet barcoding, *Nat. Biotechnol.* 35 (2017) 640–646. <https://doi.org/10.1038/nbt.3880>.
- [30] V. Chokkalingam, J. Tel, F. Wimmers, X. Liu, S. Semenov, J. Thiele, C.G. Figdor, W.T.S. Huck, Probing cellular heterogeneity in cytokine-secreting immune cells using droplet-based microfluidics, *Lab Chip.* 13 (2013) 4740. <https://doi.org/10.1039/c3lc50945a>.
- [31] L. Mazutis, J. Gilbert, W.L. Ung, D.A. Weitz, A.D. Griffiths, J.A. Heyman, Single-cell analysis and sorting using droplet-based microfluidics, *Nat. Protoc.* (2013). <https://doi.org/10.1038/nprot.2013.046>.
- [32] C.A. Schneider, W.S. Rasband, K.W. Eliceiri, NIH Image to ImageJ: 25 years of image analysis, *Nat. Methods.* (2012). <https://doi.org/10.1038/nmeth.2089>.
- [33] J. Schindelin, I. Arganda-Carreras, E. Frise, V. Kaynig, M. Longair, T. Pietzsch, S. Preibisch, C. Rueden, S. Saalfeld, B. Schmid, J.Y. Tinevez, D.J. White, V. Hartenstein, K. Eliceiri, P. Tomancak, A. Cardona, Fiji: An open-source platform for biological-image analysis, *Nat. Methods.* (2012). <https://doi.org/10.1038/nmeth.2019>.
- [34] T.D. Schmittgen, K.J. Livak, Analysis of relative gene expression data using real-time quantitative PCR and the $2^{-\Delta\Delta C(T)}$ Method., *Methods.* (2001).
- [35] M.J. Muraro, G. Dharmadhikari, D. Grün, N. Groen, T. Dielen, E. Jansen, L. van Gurp, M.A. Engelse, F. Carlotti, E.J.P. de Koning, A. van Oudenaarden, A Single-Cell Transcriptome Atlas of the Human Pancreas, *Cell Syst.* (2016). <https://doi.org/10.1016/j.cels.2016.09.002>.
- [36] T. Hashimshony, N. Senderovich, G. Avital, A. Klochendler, Y. de Leeuw, L. Anavy, D. Gennert, S. Li, K.J. Livak, O. Rozenblatt-Rosen, Y. Dor, A. Regev, I. Yanai, CEL-Seq2: Sensitive highly-multiplexed single-cell RNA-Seq, *Genome Biol.* (2016). <https://doi.org/10.1186/s13059-016-0938-8>.
- [37] I. Le Mercier, D. Poujol, A. Sanlaville, V. Sisirak, M. Gobert, I. Durand, B. Dubois, I. Treilleux, J. Marvel, J. Vlach, J.Y. Blay, N.V. Bendriss, C. Caux, I. Puisieux, N. Goutagny, Tumor promotion by intratumoral plasmacytoid dendritic cells is reversed by TLR7 ligand treatment, *Cancer Res.* (2013). <https://doi.org/10.1158/0008-5472.CAN-12-3058>.
- [38] R Core Team, R: A language and environment for statistical computing., *R Found. Stat. Comput.* (2019).
- [39] H. Wickham, *ggplot2 Elegant Graphics for Data Analysis (Use R!)*, Springer. (2016).
- [40] A.A. Dragulescu, Read, write, format Excel 2007 (xlsx) files, *R Guid.* (2014).
- [41] H. Wickham, Reshaping data with the reshape package, *J. Stat. Softw.* (2007). <https://doi.org/10.18637/jss.v021.i12>.
- [42] L. H, D. R, Fast and accurate long-read alignment with Burrows-Wheeler transform ." Alignment algorithms, *Bioinformatics.* (2010).
- [43] D.W. Huang, B.T. Sherman, R.A. Lempicki, Systematic and integrative analysis of large gene lists using DAVID bioinformatics resources, *Nat. Protoc.* (2009). <https://doi.org/10.1038/nprot.2008.211>.
- [44] D.W. Huang, B.T. Sherman, R.A. Lempicki, Bioinformatics enrichment tools: Paths toward the comprehensive functional analysis of large gene lists, *Nucleic Acids Res.* (2009). <https://doi.org/10.1093/nar/gkn923>.
- [45] A. Raj, A. van Oudenaarden, Nature, Nurture, or Chance: Stochastic Gene Expression and Its Consequences, *Cell.* (2008). <https://doi.org/10.1016/j.cell.2008.09.050>.
- [46] D. Grün, A. Lyubimova, L. Kester, K. Wiebrands, O. Basak, N. Sasaki, H. Clevers, A. Van Oudenaarden, Single-cell messenger RNA sequencing reveals rare intestinal cell types, *Nature.* (2015). <https://doi.org/10.1038/nature14966>.
- [47] K. Saito, K. Kukita, G. Kutomi, K. Okuya, H. Asanuma, T. Tabeya, Y. Naishiro, M. Yamamoto, H. Takahashi, T. Torigoe, A. Nakai, Y.

- Shinomura, K. Hirata, N. Sato, Y. Tamura, Heat shock protein 90 associates with Toll-like receptors 7/9 and mediates self-nucleic acid recognition in SLE, *Eur. J. Immunol.* (2015). <https://doi.org/10.1002/eji.201445293>.
- [48] C. Jacquemin, J. Rambert, S. Guillet, D. Thiolat, N. Boukhedouni, M.S. Doutre, A.S. Darrigade, K. Ezzedine, P. Blanco, A. Taieb, K. Boniface, J. Seneschal, Heat shock protein 70 potentiates interferon alpha production by plasmacytoid dendritic cells: relevance for cutaneous lupus and vitiligo pathogenesis, *Br. J. Dermatol.* (2017). <https://doi.org/10.1111/bjd.15550>.
- [49] T.S. Elton, H. Selemon, S.M. Elton, N.L. Parinandi, Regulation of the MIR155 host gene in physiological and pathological processes, *Gene.* (2013). <https://doi.org/10.1016/j.gene.2012.12.009>.
- [50] A. Brewitz, S. Eickhoff, S. Dähling, T. Quast, S. Bedoui, R.A. Kroczek, C. Kurts, N. Garbi, W. Barchet, M. Iannacone, F. Klauschen, W. Kolanus, T. Kaisho, M. Colonna, R.N. Germain, W. Kastenmüller, CD8+ T Cells Orchestrate pDC-XCR1+ Dendritic Cell Spatial and Functional Cooperativity to Optimize Priming, Immunity. (2017). <https://doi.org/10.1016/j.immuni.2017.01.003>.
- [51] F. Facchetti, W. Vermi, D. Mason, M. Colonna, The plasmacytoid monocyte/interferon producing cells, *Virchows Arch.* (2003). <https://doi.org/10.1007/s00428-003-0918-8>.
- [52] Y. Okabe, R. Medzhitov, Tissue biology perspective on macrophages, *Nat. Immunol.* (2016). <https://doi.org/10.1038/ni.3320>.

7. Supplementary Figures

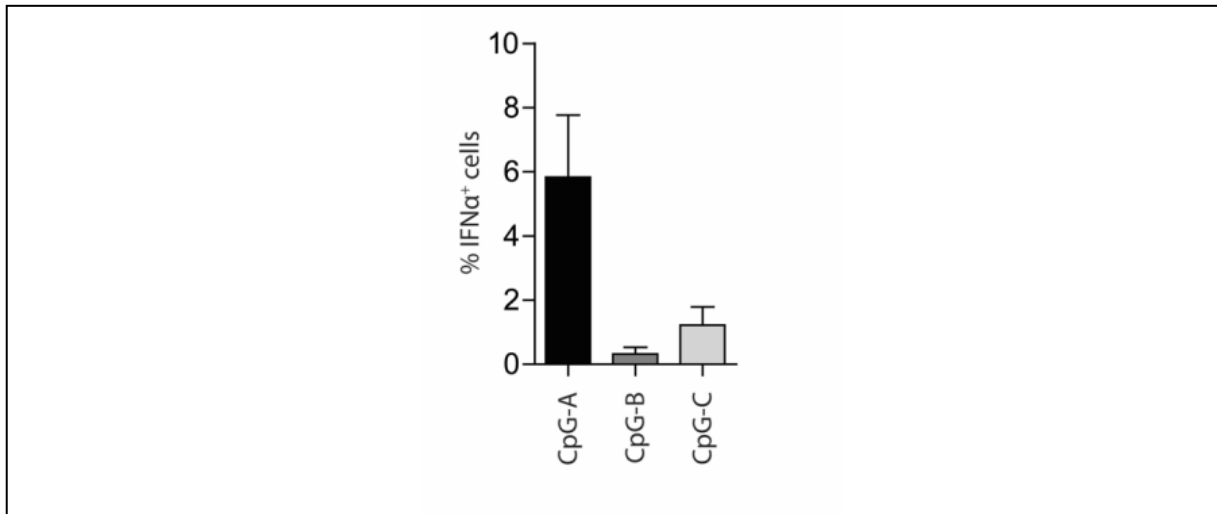


Supplementary Figure 1 – Axl expression by pDCs vanishes early after stimulation with CpG-C and AS DCs produce no IFN α . PDCs were coated with capture reagent, encapsulated in picoliter droplets, and stimulated individually with 50 $\mu\text{g}/\text{mL}$ CpG-C. **A.** After staining for viability, surface marker expression and cytokine secretion, AS DCs were detected via flow cytometry. **B.** Cytokine expression in AS DCs and traditional pDCs was analyzed.

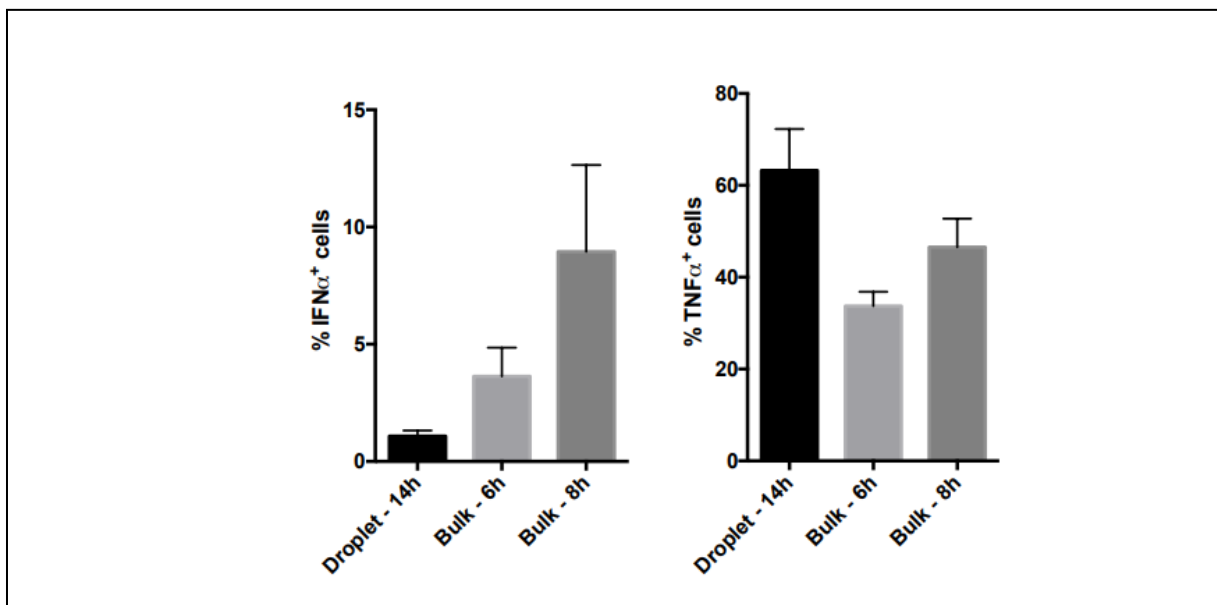


Supplementary Figure 2 – Expression of cell surface markers by individually stimulated pDCs is depending on CpG-C concentration. PDCs were coated with capture reagent, encapsulated in picoliter droplets, and stimulated individually with CpG-C for 12h. After staining for viability, surface marker expression and cytokine secretion, CCR7-, CD40- and CD86-expressing cells were detected via flow

cytometry. Shown is the fraction of surface marker-expressing cells plotted against CpG-C concentration. Different concentrations were tested in different donors. Dots indicate mean, error bars indicate SEM. $n \geq 3$

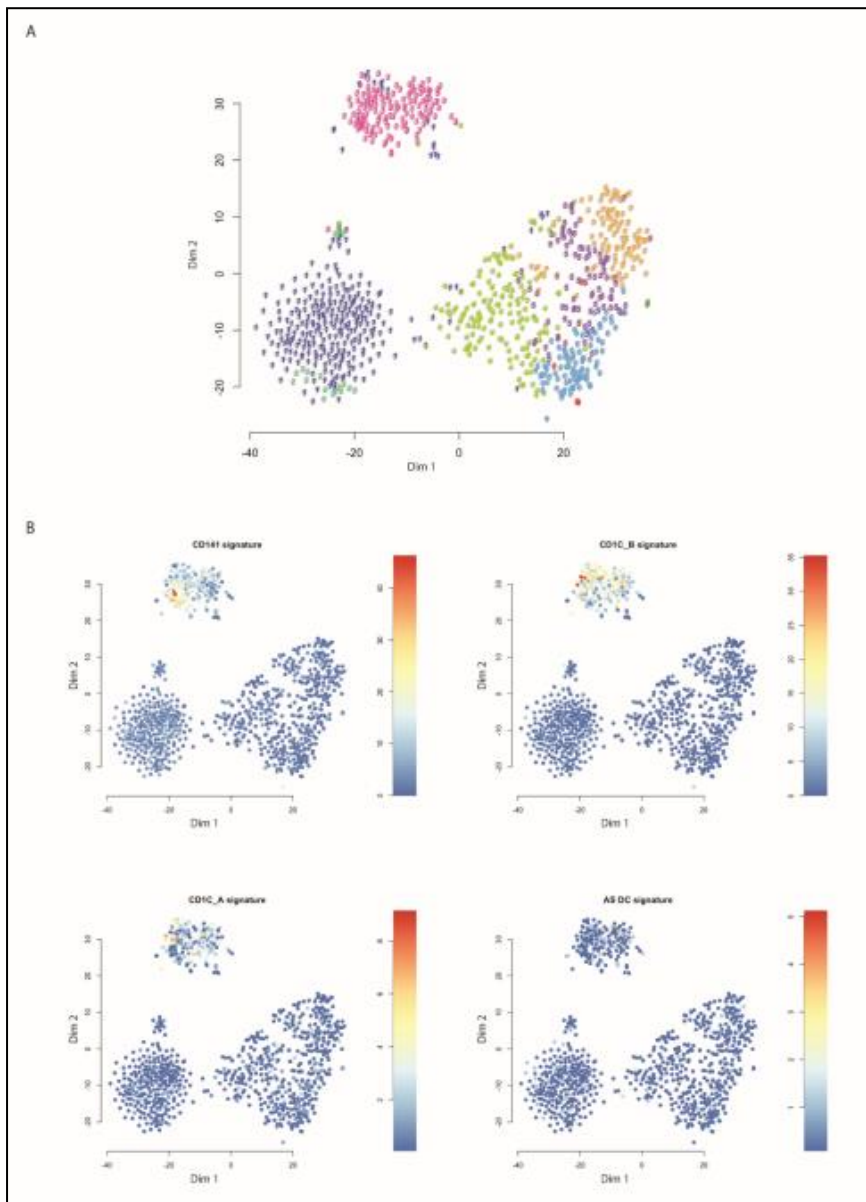


Supplementary Figure 3 – IFN α expression by pDCs stimulated with different CpG molecules. PDCs were coated with capture reagent, encapsulated in picoliter droplets, and stimulated individually with 50 μ g/mL CpG-A, -B or -C for 12h. After staining for viability and cytokine secretion, IFN α secreting cells were detected via flow cytometry. Shown is the fraction of IFN α -secreting cells plotted against treatment condition. Bars indicate mean, error bars indicate SEM. $n=2$



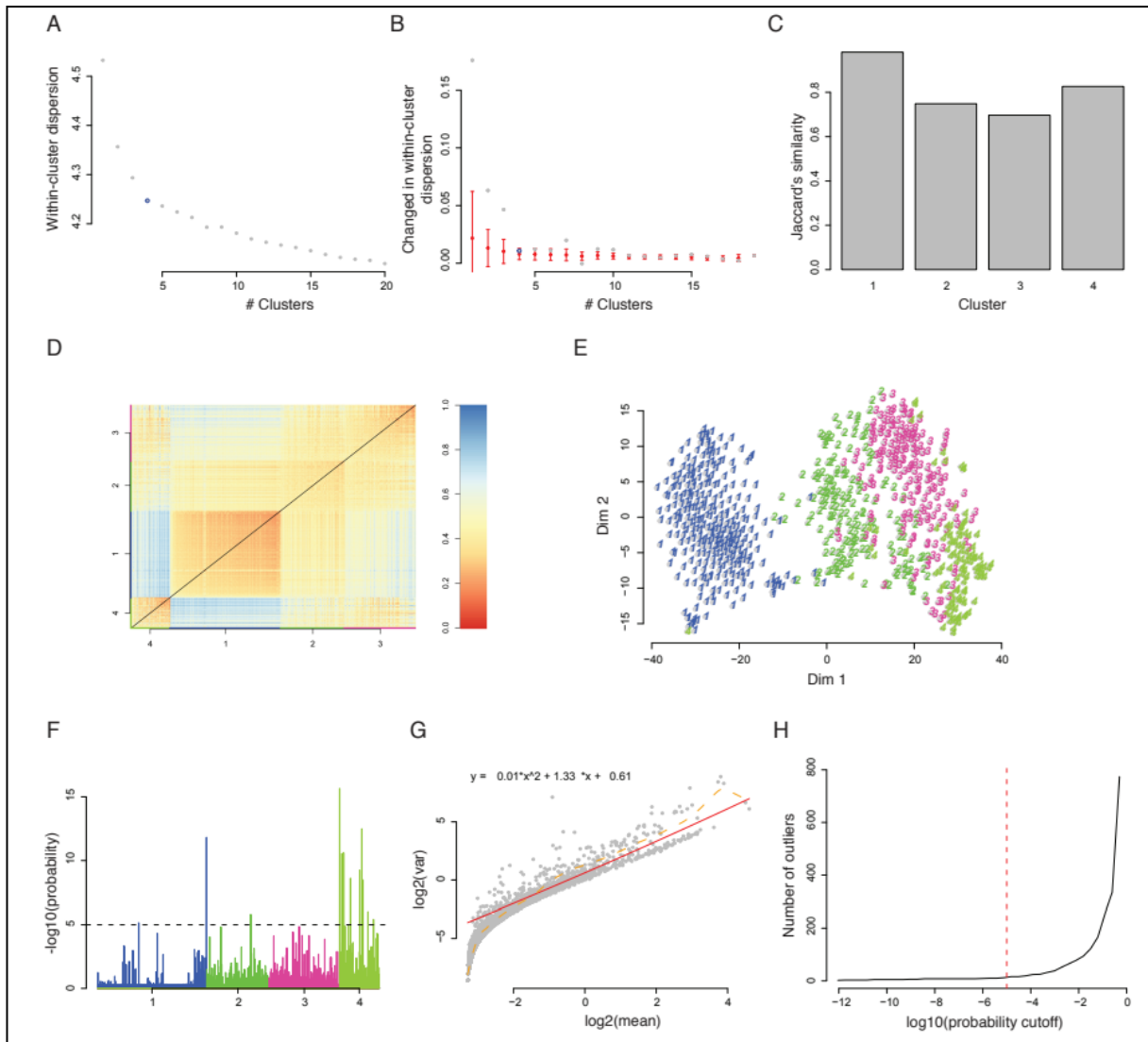
Supplementary Figure 4 – IFN α and TNF α expression by single or bulk activated pDCs from the same donor. PDCs were encapsulated in picoliter droplets and stimulated individually with 50 μ g/mL CpG-C for 14h (black bars). Alternatively, pDCs were stimulated with CpG-C in microtiter plates at a density of 25,000 cells/well. After incubation, cells were fixed, permeabilized, and stained for viability and

cytokine expression. IFN α - and TNF α -expressing cells were detected using flow cytometry. Shown is the fraction of cytokine-expressing pDCs after 6 hours (light grey bars) or 8 hours (dark grey bars) of incubation. Bars indicate mean, error bars indicate SEM. n=6

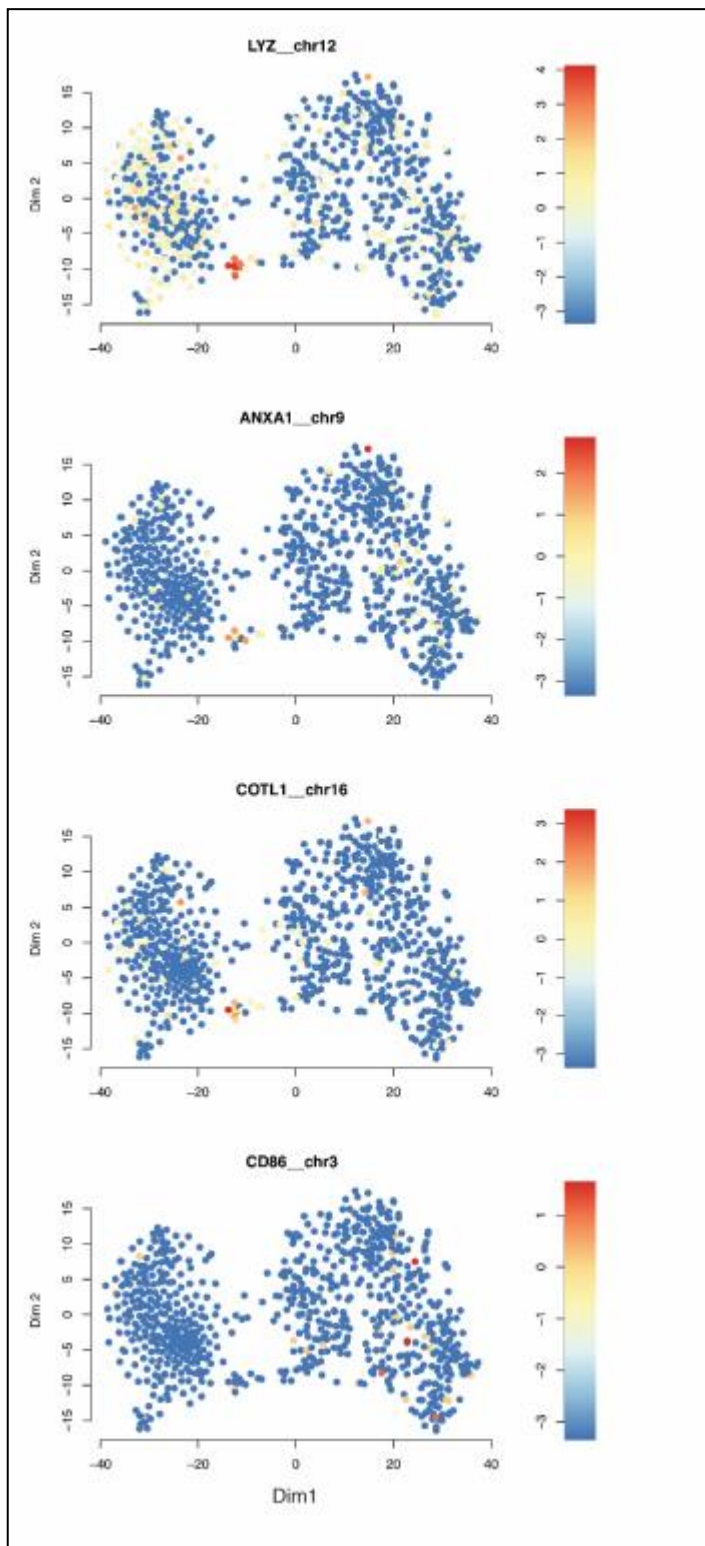


Supplementary Figure 5 – A subset of cells analyzed by scRNA-seq expressed gene signatures from DC subsets other than pDCs. A. t-SNE map showing different DC clusters after initial quality control filtering, cell clustering using k-medoids, and raceID2 (n = 915, see Methods). **B.** Expression of different gene signatures by each analyzed cell. Gene signatures are derived from Villani et al.¹ CD141: CLEC9A,

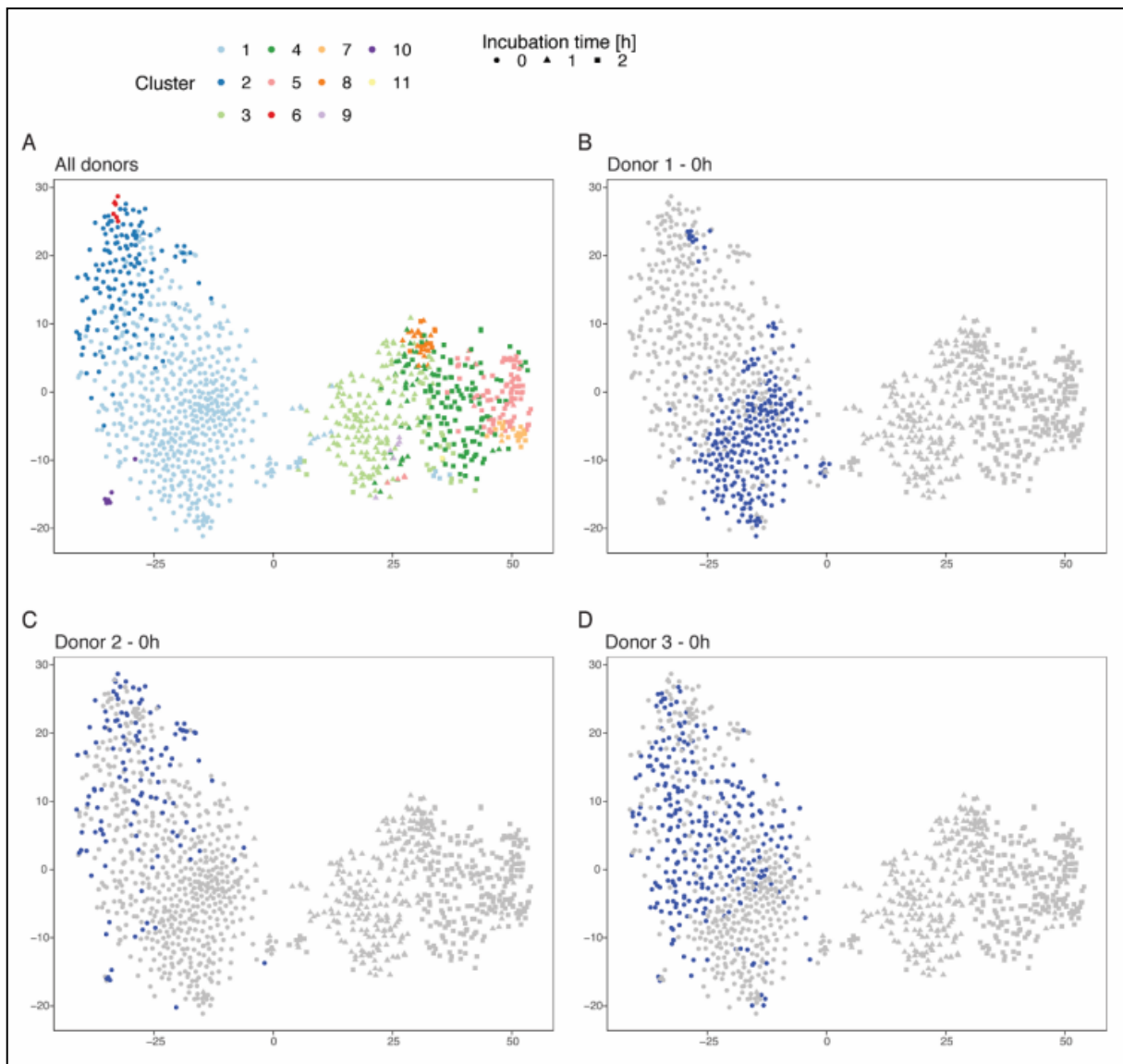
HLA-DPA1, CADM1, CAMK2D; CD1C_B: S100A9, S100A8, VCAN, LYZ, ANXA1; CD1C_A: CD1C, FCER1A, CLEC10A, ADAM8, CD1D; AS DC: AXL, SIGLEC6, PPP1R14A, CD22, DAB2.



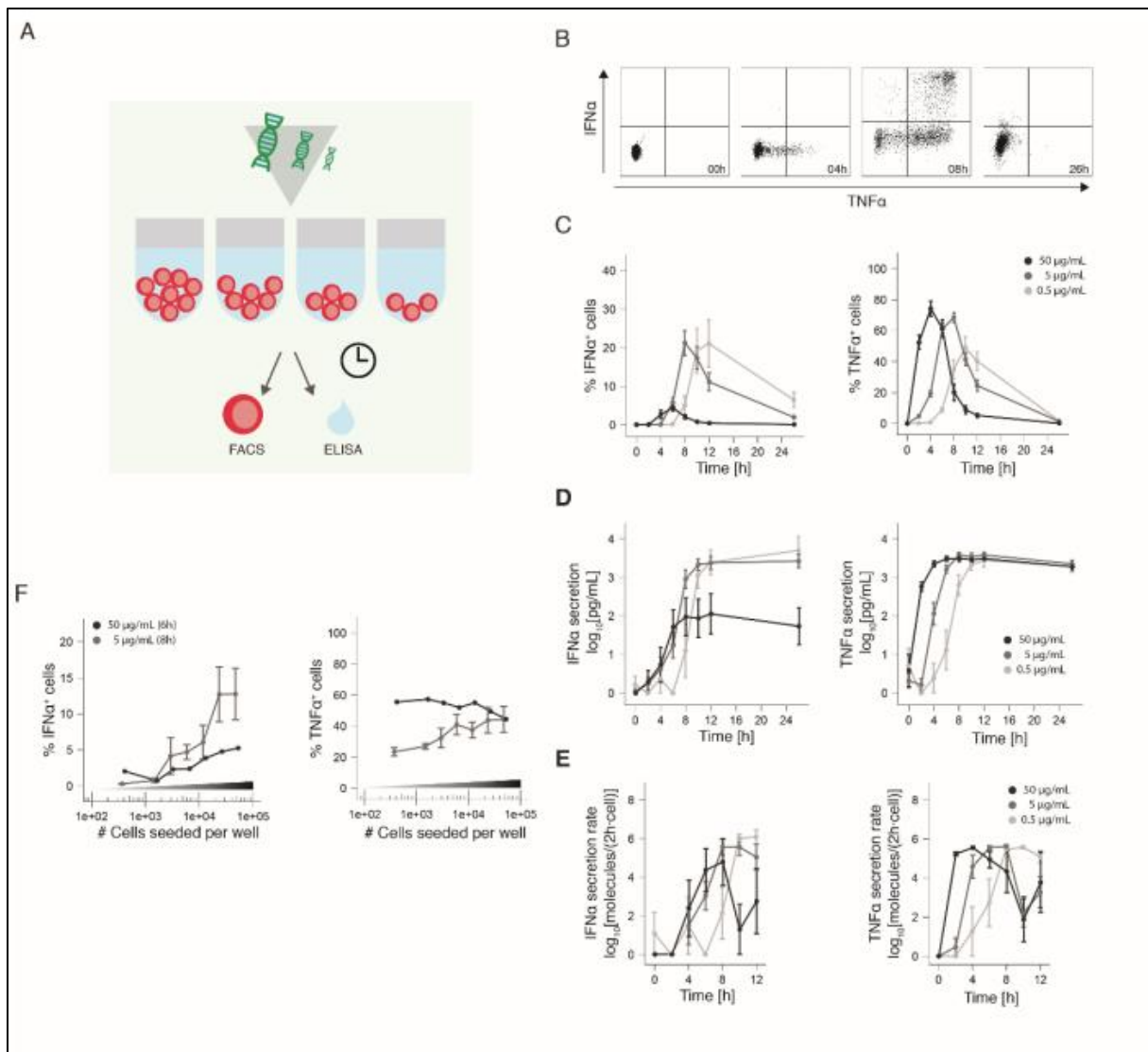
Supplementary Figure 6 – K-medoids clustering and raceID2 of unstimulated and early stimulated pDCs. A, B. Shown is the simulated within-cluster dispersion **A.** or its change **B.** for a range of seed cluster numbers in k-medoids clustering. $N(\text{bootstrapping}) = 50$. **C.** The bars indicate the Jaccard's similarity for each cluster identified by k-medoids clustering. **D.** Heat map of the 774 cells that passed quality control filters representing transcriptome similarities as measured by Euclidean distance. Kmedoids clustering characterized 4 clusters based on input from A) - C). **E.** t-SNE map of different clusters. **F.** Histogram showing the $-\log_{10}$ probability that transcript levels in a particular cell are explained by a background model **G.** accounting for the expected variability. The probability threshold for outlier identification (10^{-5}) is included (black broken line). **G)** Background model for expected variability. Shown is the \log_2 variance plotted against the \log_2 mean. **H.** The number of the potential outlier cells plotted against the \log_{10} probability threshold is indicated.



Supplementary Figure 7 – A subset of cells analyzed by scRNA-seq expressed gene signatures of the *CD2hi* pDC subset. t-SNE map showing different DC clusters after quality control filtering, cell clustering using *k*-medoids, and *raceID2* (see Methods). Color scale indicates the expression values of several genes associated with the *CD2hi* pDC subset.

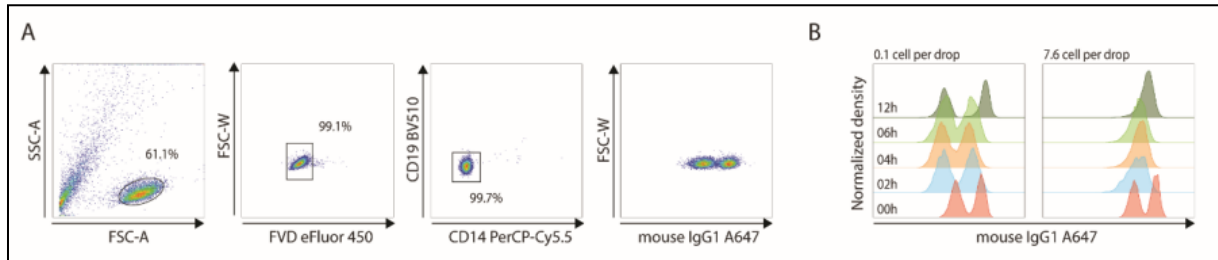


Supplementary Figure 8 – Single cell RNA-sequencing of pDCs from additional healthy donors. pDCs from two additional donors were isolated from PBMCs, collected using fluorescence activated cell sorting (FACS), and their transcriptomes were sequenced using the SORT-Seq protocol. Single cell transcripts were pooled with Figure 3, and all cells were analyzed together using the previously established filtering pipeline. In total, 1,190 cells expressing 14,979 genes were then subjected to kmedoids clustering and raceID2 analysis using the previously established clustering parameters. A) tSNE map with identified clusters. Different colors indicate clusters, different shapes indicate stimulation time. Cells in C17 show a differential gene expression profile that is similar to cells in C15 in Figure 3 (data not shown). B-D) Same t-SNE map as in A). Blue color indicates location of unstimulated pDCs from a particular donor.

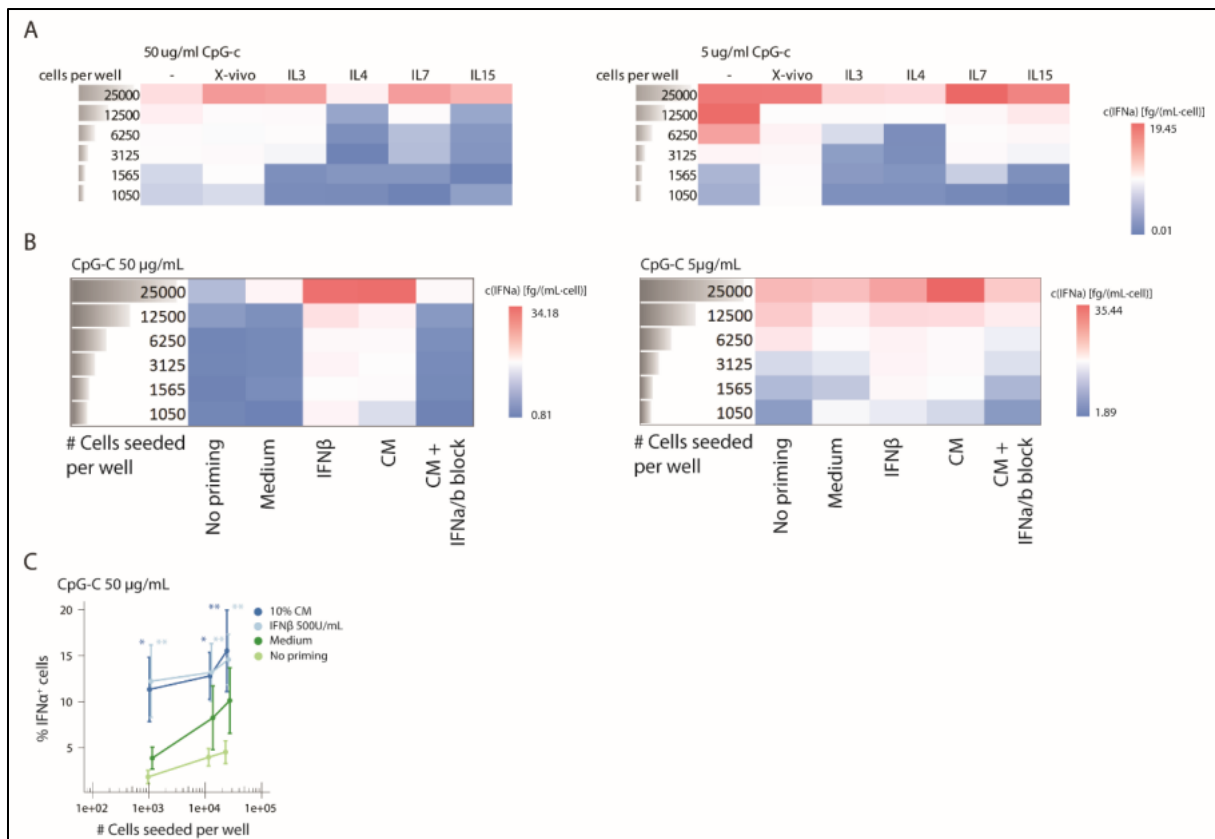


Supplementary Figure 9 – Kinetics of IFN α and TNF α secretion by pDCs in microtiter plate cultures. **A.** PDCs were stimulated with CpG-C in microtiter plates at varying cell densities or varying CpG-C concentrations. After incubation, cells were fixed, permeabilized, and stained for viability and cytokine expression. **B.** IFN α - and TNF α -expressing cells were detected using flow cytometry. **C.** PDCs were stimulated at a density of 25,000 cells/well. Shown is the fraction of cytokine-expressing pDCs plotted against incubation time. $n \geq 5$. At 50 $\mu\text{g}/\text{mL}$ CpG-C less cells produce IFN α . Previous studies showed that an initial lag-phase before the onset of IFN α secretion is crucial to prime pDCs via autocrine or paracrine mechanisms.² The early onset of IFN α production by pDCs stimulated with 50 $\mu\text{g}/\text{mL}$ CpG-C most-likely undercuts this threshold. In accordance with this, we observed robust IFN α responses when pre-treating pDCs for 2h with 500U/mL of IFN β (Supplementary Figure 10). **D.** Supernatant was analyzed using ELISA. Shown is the concentration of IFN α and TNF α plotted against the incubation time. $n \geq 5$. **E.** Cytokine concentration from D) was combined with the number of cytokine-expressing cells, as determined via flow cytometric analysis in duplicate cultures (C), to calculate the average secretion rate

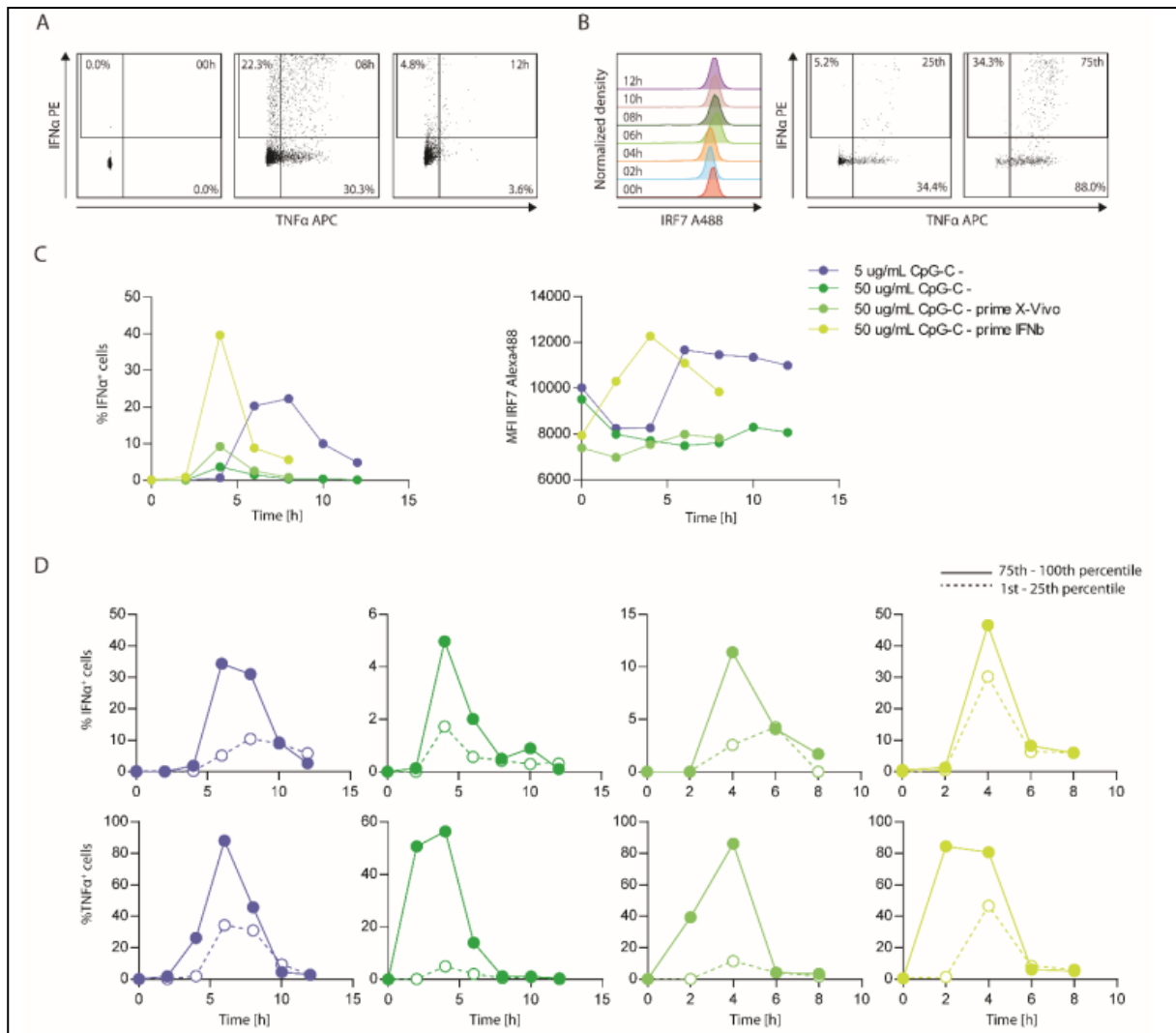
of a single cell. Shown is the number of molecules, added to the supernatant every two hours by a single cell, plotted against the incubation time. $n \geq 5$ F) PDCs were stimulated at different cell density and cytokine-expressing cells were detected using flow cytometry. $n[5 \mu\text{g/mL}] = 3$, $n[50 \mu\text{g/mL}] = 1$). B - F) Dots indicate mean, error bars indicate SEM.



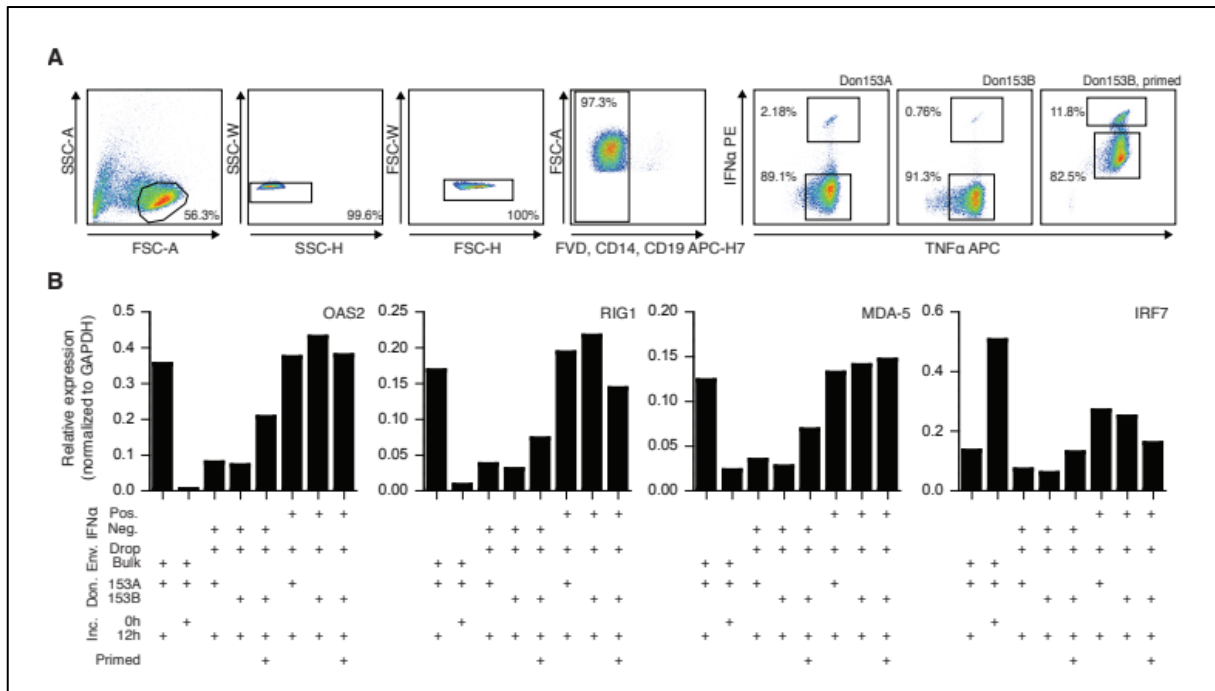
Supplementary Figure 10 – Cytokine capture-reagents can be exchanged between two cells encapsulated in the same droplet but not between two cells encapsulated in different droplets. PDCs were coated with capture reagent or left untreated and mixed at a 1:1 ratio. Subsequently, cells were encapsulated in picoliter droplets with either 0.1 or 7.6 cells per drop on average, and stimulated individually with $50 \mu\text{g/mL}$ CpG-C. **A.** Next to viability and surface marker expression, pDCs were also stained for cytokine capture reagent-coating using an antibody against mouse IgG1. **B.** Shown is the distribution of the fluorescence intensity of the capture reagent at each time point.



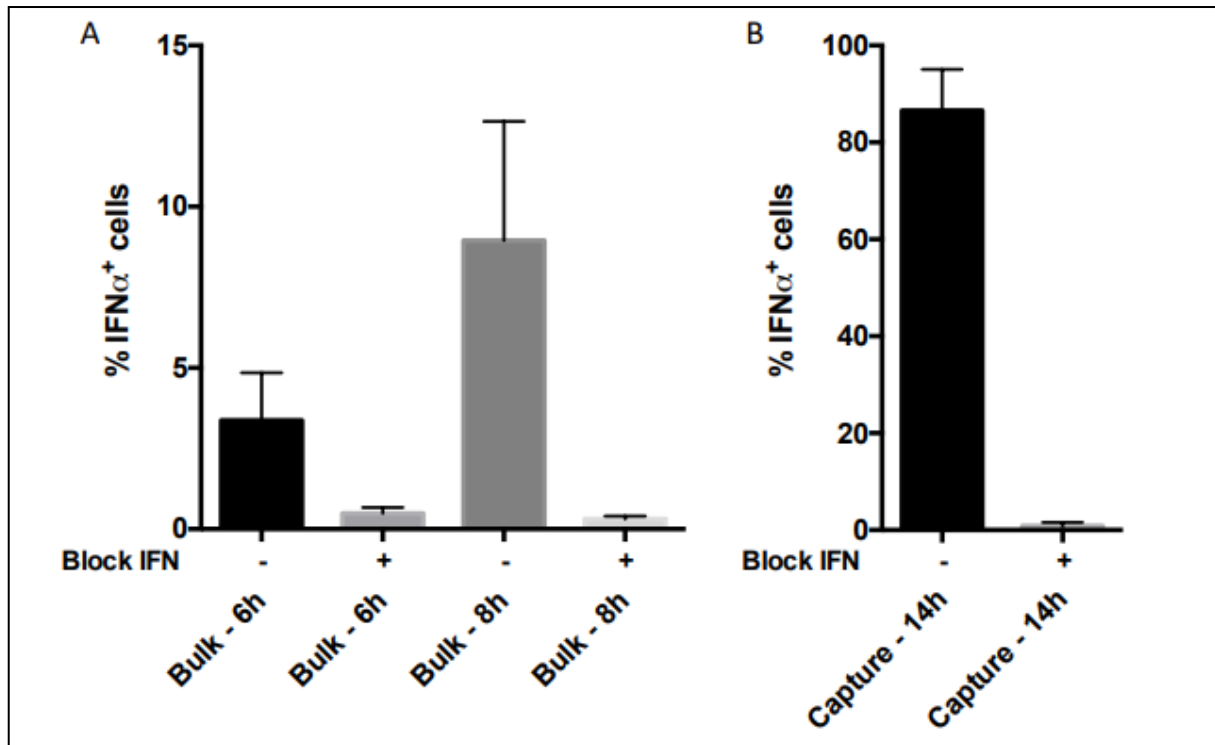
Supplementary Figure 11 – Effect of priming with different cytokines on IFN α production by pDCs. A, B) pDCs were incubated with fresh medium, conditioned medium or different cytokines (0.01 μ g/ml IL-3, 60 μ g/ml IL-4, 50 μ g/ml IL-7, 20 μ g/ml IL-15, 500 U/ml IFN β) for two hours or left untreated. In some cases, cells were pre-incubated with blocking antibodies against IFNAR2 and CM was supplemented with neutralizing serum against IFN α and IFN β (block). Subsequently, pDCs were stimulated with CpG-C in microtiter plates for 12h at varying cell densities, and cytokine concentration in supernatants was measured using ELISA. Shown is the log cytokine concentration relative to the number of seeded cells plotted against cell density and priming condition. A: n=1, B: n=3 C) pDCs were incubated with fresh medium, conditioned medium or 500 U/mL recombinant IFN β for 2h or left untreated. Subsequently, pDCs were stimulated with CpG-C for 6h in microtiter plates at varying cell densities. After incubation, cells were fixed, permeabilized, and stained for viability and cytokine expression. IFN α - and TNF α -expressing cells were detected using flow cytometry. Shown is the fraction of IFN α -expressing cells plotted against the number of seeded cells. Values were compared to non-primed pDCs using the Mann-Whitney test. * $p < 0.05$, ** $p=6$ Dots indicate mean, error bars indicate SEM.



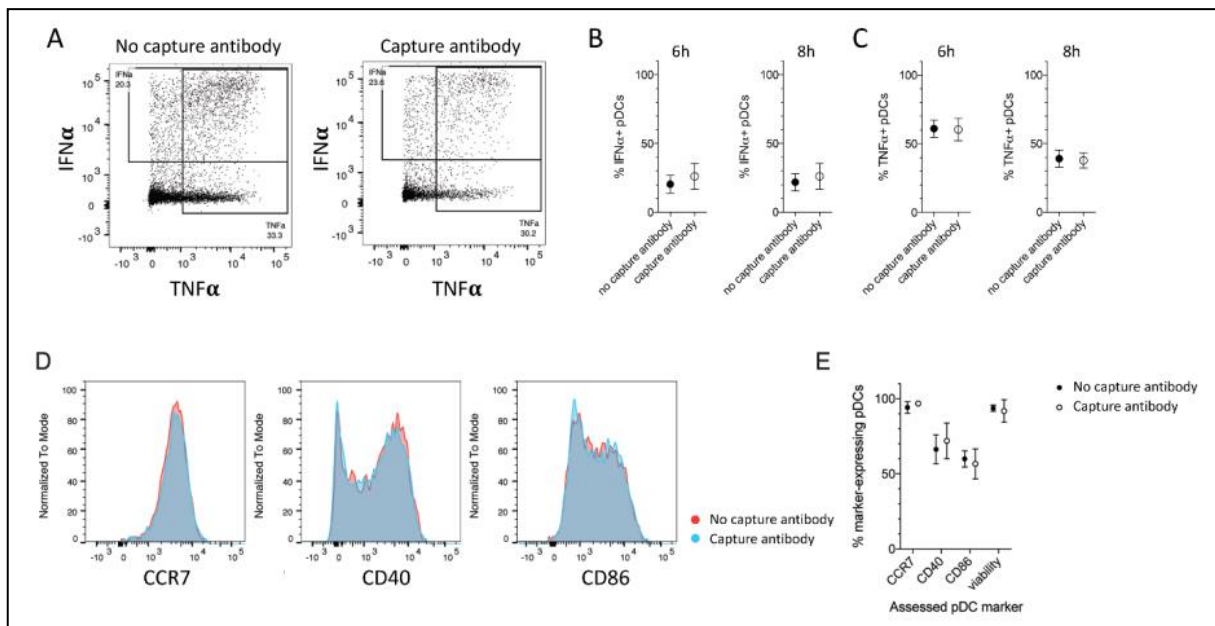
*Supplementary Figure 12 – IRF7 expression dynamics in primed and stimulated pDCs. PDCs were incubated with fresh medium or 500 U/mL recombinant IFN β for 2h or left untreated. Subsequently, pDCs were stimulated with CpG-C in microtiter plates at a density of 25.000. After incubation, cells were fixed, permeabilized, and stained for viability, cytokine expression and IRF7 expression. **A, B.** IFN α -, TNF α -, and IRF7-expressing cells were detected using flow cytometry. **C.** The fraction of cytokine producing cells or the fluorescence intensity of IRF7 was plotted against the incubation time. **D.** The 25% pDCs that had the lowest or highest expression of IRF7 were further selected and cytokine expression in those cells was analyzed separately. The fraction of cytokine producing cells for each group was plotted against the incubation time.*



Supplementary Figure 13 – Expression of interferon stimulated genes in individually activated, sorted pDCs. pDCs were incubated with 40% conditioned medium for 2h or left untreated. Subsequently, cells were coated with capture reagent, encapsulated in picoliter droplets, and stimulated individually with 50 μ g/mL CpG-C for 12h. Control cells were stimulated with 5 μ g/mL CpG-C for 12h in a microtiter plate at a density of 25,000 cells (bulk) or left at 4°C (0h). **A.** After staining for viability and cytokine secretion, IFN α ⁺ and IFN α ⁻ cells were isolated using fluorescence activated cell sorting. Sorted cells were lysed, RNA was isolated, and the expression of the interferon stimulated genes OAS2, RIG1, MDA-5, and IRF7 as well as the house keeping gene GAPDH was determined via quantitative PCR. **B.** Shown are the expression levels relative to GAPDH plotted against treatment conditions.



Supplementary Figure 14 – Effect of blocking paracrine type I IFN signaling on IFN α production by bulk cultured pDCs. **A.** PDCs were incubated with fresh medium (- block) or pre-incubated with blocking antibodies against IFNAR2 and the medium was supplemented with neutralizing serum against IFN α and IFN β (+ block). Subsequently, pDCs were stimulated with CpG-C in microtiter plates for 6h or 8h at a density of 25.000 cells/well. After incubation, cells were fixed, permeabilized, and stained for viability and cytokine expression. IFN α -expressing cells were detected using flow cytometry. $n=5$ **B.** PDCs were coated with capture reagent, were pre-incubated with blocking antibodies against IFNAR2 and medium was supplemented with neutralizing serum against IFN α and IFN β (block) prior to activation with 5 $\mu\text{g}/\text{mL}$ CpG-C in bulk (25.000 cells/well) for 14h. IFN α -secreting cells were detected via flow cytometry. Shown is the fraction of IFN α -secreting cells plotted against treatment condition. $n=5$ A – B) Bars indicate mean, error bars indicate SEM.



Supplementary Figure 15 – Effect of Cytokine Catch Reagents on cellular function and viability of bulk cultured pDCs. pDCs were coated with capture reagent or left untreated and subsequently activated with 5 $\mu\text{g}/\text{mL}$ CpG-C in microtiter plates for 6h, 8h or 12h at a density of 25.000 cells/well. **A.** IFN α - and TNF α -secreting cells were detected via intracellular cytokine staining and flow cytometry after 8 hours and the result of 1 representative donor is shown. **B, C.** Shown is the fraction of IFN α - or TNF α -secreting cells plotted against treatment condition and stimulation for either 6 hours or 8 hours. Circles indicate mean, error bars indicate SEM, $n=5$. **D.** The expression of CCR7, CD40 and CD86 by differently treated pDCs was assessed after 12 hours of activation using flow cytometry. One representative experiment is shown. **E.** Shown is the viability and the expression of CCR7, CD40 and CD86 plotted against treatment condition. Circles indicate mean, error bars indicate SD, $n=3$.

Supplementary Methods

Supplementary Table 1 – Employed stimuli and cytokines

Stimulus	Comment	Standard conc bulk [$\mu\text{g/ml}$]	Standard conc drop [$\mu\text{g/ml}$]	Manufacturer
R848	Resiquimod	4	4	Enzo
CpG-A	ODN 2216	5	50	Enzo
CpG-B	ODN 2006	5	50	Enzo
CpG-C	ODN M362	5	50	Enzo
PMA	Phorbol 12-myristate 13-acetate		0.05	Calbiochem
Iono	Ionomycine		1	Sigma
IL-3	Recombinant human interleukin-3	0.1	0.1	Cellgenix
IFN β	Recombinant human IFN- β	500 U/mL		Peptotech
IL-4	Human IL-4, premium grade	60		Miltenyi Biotec
IL-7		50		R&D
IL-15		20		Biologend

Supplementary Table 2 – Employed primers

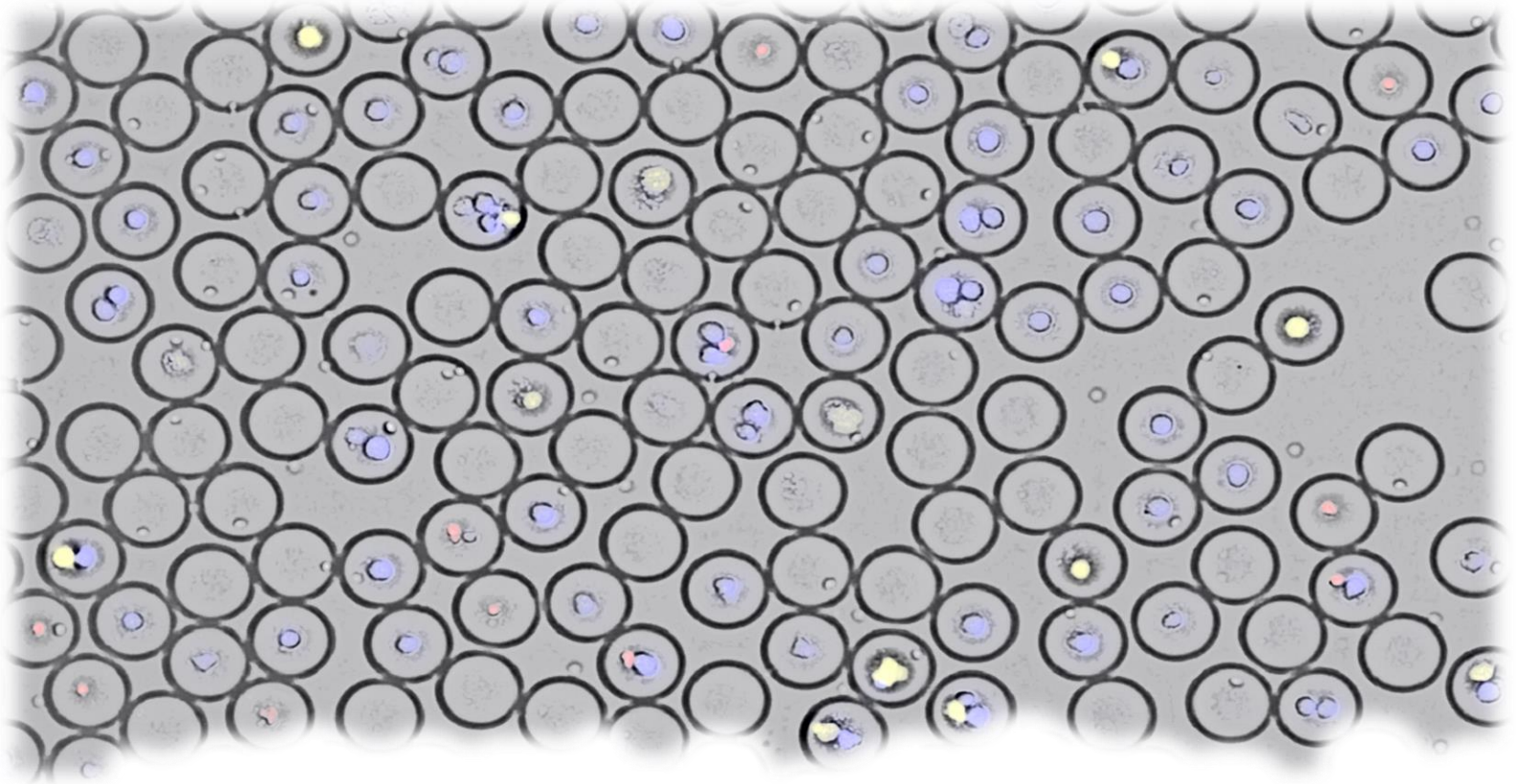
Gene	Name	Direction	Sequence (5' to 3')
GAPDH	hGAPDH FW	Forward	GAAGGTGAAGGTCGGAGT
GAPDH	hGAPDH RV	Reverse	AGATGGTGATGGGATTTTC
IRF7	IRF-7.forw	Forward	GAGCCGTACCTGTCACCCT
IRF7	IRF-7.rev	Reverse	GGGCCGTATAGGAACGTGC
MDA5	MDA-5.forw	Forward	CAACATGGGCAGTGATTCAGG
MDA5	MDA-5.rev	Reverse	TGGGCAACTTCCATTTGGTAAG
OAS2	OAS2_fwd_1	Forward	AAGCCCTACGAAGAATGT
OAS2	OAS2_rev_1	Reverse	TTGGCTTCTTCTGATCCTGG
RIG-I	RIG-I.forw	Forward	TGTGCTCCTACAGGTTGTGGA
RIG-I	RIG-I.rev	Reverse	CACTGGGATCTGATTCGCAAAA

Supplementary Table 3 – Employed antibodies and cytokine detection kits

Antigen	Clone	Label	Dilution	Manufacturer
CD303	AC144	APC	1:10	Miltenyi Biotec
Lineage Cocktail 1		FITC	1:10	BD
CD3	SK7			
CD14	MφP9			
CD16	3G8			
CD19	SJ25C1			
CD20	L27			
CD56	NCAM16.2			
CD304	AD5-17F6	PE	0.5 µL per 1M cells	Miltenyi Biotec
CD304	12C2	BV510	2 µL per 1M cells	Biolegend
HLA-DR	AC122	VioBlue, PE-Cy7	0.5 µL / 0.3 µL per 1M cells	Miltenyi Biotec
PD-L1	MIH1	BV421	1/40	BD
CD80	2D10.4	PerCp-eFluor710	1/20	eBioscience
CD86	2331	BV510	1/20	BD
CD40	5C3	PE-Cy7	1/90	BD
CCR7	150503	FITC	1/10	R&D
CD14	MφP9	APC-H7	1/75	BD
CD14	M5E2	PerCP-Cy5.5	1/100	eBioscience
CD19	SJ25C1	APC-H7	1/20	BD
CD19	SJ25C1	BV510	1/50	BD
IFNα	LT27:295	PE	1/30	Miltenyi Biotec
TNFα	cA2	APC	1/30	Miltenyi Biotec
IRF7	12G9A36	Alexa488	1/25	Biolegend
Axl	108724	Alexa488	1/30	R&D
Siglec6	767329	APC	1/10	R&D
Mouse IgG1	Polyclonal	Alexa647	1/400	Life Technologies
IL-2 Cytokine capture reagent	Not disclosed	PE	1/10	Miltenyi Biotec
IFNγ Cytokine capture reagent	Not disclosed	FITC	1/10	Miltenyi Biotec
IFNα Cytokine capture reagent	Not disclosed	PE	1/10	Miltenyi Biotec
TNFα Cytokine capture reagent	Not disclosed	APC	1/10	Miltenyi Biotec
INFAR2	MMHAR-2		10 µg/mL	PBL Assay Science
IFNβ	Sheep serum		1000 NU/mL	PBL Assay Science
IFNα	Sheep serum		1000 NU/mL	PBL Assay Science

Supplementary Table 4 – Flow rates and droplet sizes

V (droplet)	Channel height	Flow rate continuous phase	Flow rate stimuli	Flow rate cells
41 pL	25 µm	1200 µL/h	150 µL/h	150 µL/h
75 pL	25 µm	900 µL/h	200 µL/h	200 µL/h
243 pL	50 µm	900 µL/h	200 µL/h	200 µL/h
1022 pL	80 µm	1000 µL/h	1000 µL/h	1000 µL/h
3121 pL	80 µm	150 µL/h	225 µL/h	225 µL/h



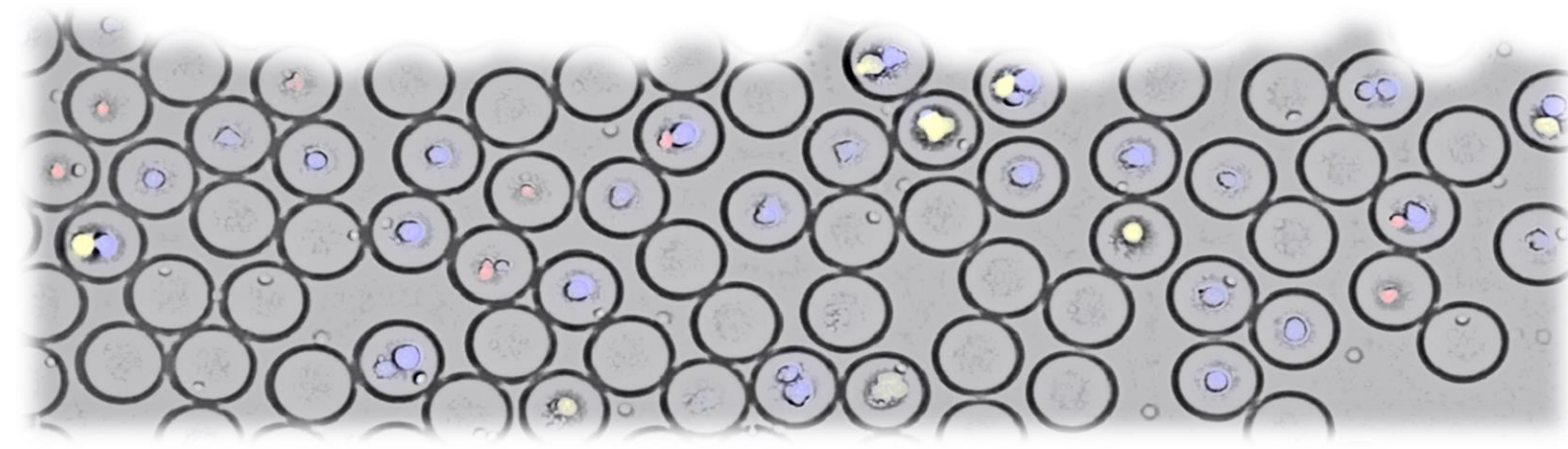
CHAPTER 6

POTENT CROSSTALK BETWEEN A SINGLE PLASMACYTOID DENDRITIC CELL AND A NATURAL KILLER CELL THROUGH IFN- α DEPENDENT MANNER

This chapter is under preparation as:

Potent crosstalk between a single Plasmacytoid Dendritic Cell and a Natural Killer Cell through IFN α dependent manner

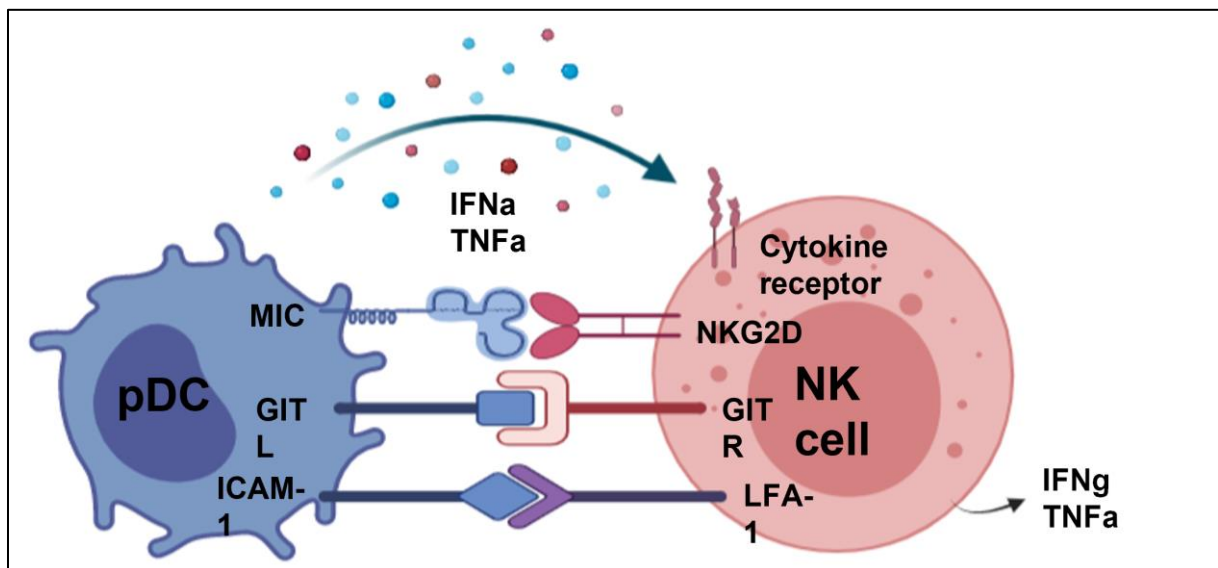
Nikita Subedi, Laura Van Eyndhoven, Jurjen Tel



Abstract

The interaction between NK cells and dendritic cells (DC) has been suggested to play a crucial role in their functional regulation, but most studies are limited to conventional DCs. Plasmacytoid dendritic cells (pDCs) represent a specialized cell population producing type I interferon (IFN-I) that acts as a natural killer (NK) cell modulator. Limited studies have shown a bidirectional talk between these immune cells, while these studies could not encompass the wide range of functional heterogeneity displayed by each of these cell types. Here, we report a microfluidic droplets-based single-cell study to investigate the consequences of the interaction upon functions of these cells. We showed CpG-C activated pDCs could induce IFN- γ secretion in NK cells and showed the implications of IFN- α on regulating the function of NK cells. To increase our understanding of cellular communication between NK cells and pDCs can provide crucial information for clinical use.

Graphical Abstract



1. Introduction

The innate immune system, with the rapid ability to mount an immune response against pathogenic threats, is crucial to modulate the response of the adaptive immune system[1]. Natural killer (NK) cells and dendritic cells (DCs) represent two distinct innate immune components that also act as liaisons between innate and adaptive responses. Several studies showed the bi-directional talk between these cell types to regulate each other's functions[2–4]. Dendritic cells, specifically Plasmacytoid DCs (pDCs) upon viral recognition, can secrete large amounts of type 1 interferon (IFN-I), which can function as a NK cell activity modulator[5]. In term, NK cells regulate the maturation of pDCs and have also been shown to assist in pDCs mediated T cell priming in vivo[6,7].

The NK/pDCs crosstalk plays an important role in tumor cell lysis and antiviral immune responses, especially during Cytomegalovirus infection[8–10]. The ability of TLR-9 stimulated pDCs to activate NK cells, enhancing the CD56^{bright} phenotypes, has been shown by Romagnani and colleagues[11]. Contact-dependent activation of NK cells via OX40-OX40L interactions has been found to promote induction of IFN- γ secretion by NK cells[6]. An important role of pDCs on enhancing the functional capability of NK cells to induce anti-tumor cytotoxicity against hematological malignancies have been shown in several studies[12,13]. Thus, the NK/pDCs crosstalk is pivotal in bridging the innate immune response with adaptive immune responses. However, the mechanisms involved in the crosstalk remains largely uncharacterized. Although some studies have attempted to study these interactions, they lack to appreciate the heterogeneity existing within both cell types. To improve the fundamental understanding of NK/pDCs interaction, a zoomed-in study at a single-cell level is required.

We designed a microfluidic droplets-based study, which on single-cell level allowed investigating the crosstalk between the cells. By utilizing microscopy and FACS-based analysis tools, we studied the percentage of NK cells and pDCs secreting IFN- γ and IFN- α as a measure of their activation. Our preliminary data suggest a potent crosstalk between the cell types however requires additional experiments to strengthen the findings.

2. Materials and methods

2.1 Cell isolation and culture

K562 cells were cultured in 1:1 (v/v) mixture of RPMI 1640 (Gibco, Catalog no. 22400089) and IMDM (Gibco, Catalog no.12440053) supplemented with 10% fetal bovine serum (FBS; Gibco) and 1% penicillin/streptomycin (PS; Gibco). Primary human NK cells and pDCs were obtained from buffy coats of healthy donors (Sanquin) after written informed consent according to the Declaration of Helsinki and all experimental protocols concur to institutional guidelines. In short, peripheral blood mononuclear cells (PBMCs) were isolated from donor blood via density gradient centrifugation using Lymphoprep Density Gradient Medium (Stem cell). The NK cells were subsequently isolated using magnet-activated cell sorting (MACS) by negative selection using the NK cell isolation kit (Miltenyi Biotec, Catalog no. 130-092-657) following the manufacturer's instructions. pDCs were isolated by positive selection using the CD304 Microbeat Kit (Miltenyi Biotec, 130-090-532). Cells were counted and purity was routinely assessed using flow cytometry by cell surface marker staining for 10 minutes at 4°C, using PE-CY7-labeled anti-CD56 (Biolegend, Catalog no. 362509), PE-labeled anti-CD16 (Biolegend, Catalog no. 302007), and PerCP-labeled anti CD3 (Biolegend, Catalog no. 300328) antibodies in 50 µL FACS buffer (2% FBS in PBS). The NK cells were identified as CD16⁺CD56⁺CD3⁻, and purity was on average 91%. Subsequently, isolated NK cells were encapsulated into droplets with K562 pair in presence of 1400 ng/mL IL-2, as stimulant (Peprotech, Catalog no. 200-02). For pDCs FITC-labeled anti-CD123 and APC-labeled anti-CD303 were used for purity. The pDCs were identified as CD123⁺CD303⁺ with an average purity of 92%.

2.2 Microfluidic chip for droplet production

The three-inlet and four-inlet microfluidic devices were developed following the protocols as described in Sinha et. al[14]. The microfluidic device was molded using an SU-8 photo resist structure on a silicon wafer and a commercially available polydimethylsiloxane silicone elastomer (Sylgard 184, Dow Corning), mixed with curing agent at the ratio 10:1 (w/w) and allowed to cure for 3 hours at 60°C. The surface of the Sylgard 184 was activated by exposure to plasma and sealed with a plasma-treated glass cover slide to yield closed micro channels. Channels were subsequently treated with a 5% (v/v) silane (1H,1H,2H,2H-

Perfluorooctyltriethoxysilane; Fluorochem, Catalog no. S13150) solution in fluorinated oil (Novec HFE7500, 3M, Catalog no. 51243) and thermally bonded for 12 hours at 60°C. The dimensions of the microfluidic channels are 40 μm \times 30 μm at the first inlet, 60 μm \times 30 μm at the remaining three inlet and the production nozzle, and 100 μm \times 30 μm at the collection channel.

2.3 Assembly of Droplet observation chamber

Glass microscopy slides (76 \times 26 \times 1 mm; Corning) were used as top and bottom covers (76 \times 26 \times 1 mm). Two access holes of 1.5 mm diameter were drilled in the top glass. Both slides were thoroughly cleaned using soap, water, and ethanol, and were exposed to air plasma (60 W) for 5 minutes. A cutout sheet of 60 μm thick double-sided tape (ORAFOL) was carefully placed above the bottom glass slide. Afterwards, the glass slides were stacked on top of each other, and the assembly was pressed using Atlas Manual 15T Hydraulic Press (Specac) for 5 minutes at 155°C at 400 kg per m² pressure load. Next, two nano ports (Idex) were attached to the holes using UV curable glue (Loctite 3221 Henkel) which was cured under UV light for 5 min. Subsequently, the surface of the 2D chamber was treated with 5% (v/v) silane solution. Lastly, the chamber was dried, filled with fluorinated oil, and sealed until use. The chamber was reused multiple times and cleaned after each experiment by flushing fluorinated oil to remove droplets and was stored filled until the next use.

2.4 Cell loading in microfluidic chip

Droplets were produced with a three-inlet microfluidic device. The protocol for loading cells in the microfluidic chips using pipette tips is described in Sinha et al. and Subedi et al.[14,15]. The droplets of \sim 102 μm diameter were generated using 3 inlet droplet devices at flow ratio of 1:2 (20 $\mu\text{L}/\text{min}$ for oil and 5 $\mu\text{L}/\text{min}$ for each sample). Droplet production using 4-inlet droplet devices was performed at the flow ratio of 1:2 (20 $\mu\text{L}/\text{min}$ for oil and 0.33 $\mu\text{L}/\text{min}$ for each sample). The droplets were produced for around 5-10 minutes, thereby generating \sim 700,000 droplets in total. For the stability of droplets, 2.5% (v/v) Pico-Surf[®] surfactant (Sphere Fluidics, Catalog no. C024) was used in fluorinated oil.

2.5 Bulk Interaction Assay

Peripheral blood pDCs were primed with IFN- β (1000IU/ml; Peprotech) for 2 hours. NK cells and pDCs were incubated in 100 μL per 1 million cells PBA containing the IFN- γ Catch

Reagent (Miltenyi Biotec, 130-092-605) and IFN α Catch Reagent (Miltenyi Biotec, 130-092-605) respectively at 4 °C for 20 minutes. Next, cells were washed and resuspended in X-vivo culture medium (Lonza) + RPMI culture medium (Gibco) (at 1:1 ratio) supplemented with 2% HS, 1% PS, at 25,000 cells per 100 μ L in U-bottom microwell plates together with CpG C (TLR9 Ligand; ODN M362; Enzo life sciences) at 1:1 NK:pDC ratio. The cells were incubated at 5% CO₂ and 37 °C temperature for 20 hours.

2.6 Single-NK/pDC Interaction Assay

Peripheral blood pDCs were primed with IFN- β (1000IU/ml; Peprotech) for 2 hours. NK cells and pDCs were incubated in 100 μ L per 1 million cells PBA containing the IFN- γ Catch Reagent (Miltenyi Biotec, 130-092-605) and IFN- α Catch Reagent (Miltenyi Biotec, 130-092-605) respectively at 4 °C for 20 minutes. The cells were then washed and resuspended in X-vivo culture medium+ RPMI culture medium (1:1) supplemented with 2% HS and 1%PS, at 2 million cells/mL for single-cell encapsulation. Next the NK cells (5 million cells/mL) were encapsulated into 1.2 nL (~130 μ m) droplets together with primed or unprimed pDCs (15 million cells/mL) loaded from another inlet. TLR9 ligand CpG C (150 μ g/ml) was mixed with NK cells. Droplet production and encapsulation rates were carefully monitored using a microscope (Nikon) at 10x magnification and a high-speed camera. The droplet emulsion was collected and covered with culture medium to protect droplets from evaporation. The encapsulated cells were incubated in Eppendorf tubes with a few punched holes to allow gas exchange, at 5% CO₂ and 37 °C temperature. After 20 hours of incubation, the droplets were de-emulsified by adding 100 μ L 20 v/v% 1H,1H,2H,2H-Perfluoro-1-octanol (Sigma Aldrich, 370533) in HFE-7500 for cell retrieval and the cells were then stained for FACS analysis.

2.7 FACS-Antibody Staining

Cells were washed once with PBS and dead cells were stained with Zombie NIR fixable viability dye (Biolegend, 423111), 1:10.000 in PBS, 50 μ L) at 4°C for 20 minutes. Subsequently, cells were washed once with PBS and incubated with anti-human antibodies against IFN γ (FITC, Miltenyi), IFN α (PE, Miltenyi) and CD303 (APC, Biolegend) at 4 °C for 30 minutes. Next the cells were washed twice with PBS buffer with 0.5% BSA and analyzed via BD FACS Arial.

2.8 Bulk cytotoxicity assay

The K562 cells were stained with CMAC, Cell tracker Blue (Invitrogen) for 30 minutes. NK cells (5×10^5 cells/mL), pDCs (5×10^5 cells/mL) and K562 (5×10^5 cells/mL) cells were loaded into the microwells at different E:T ratio (0:1:1; 1:0:1; 1:1:1; 2:2:1; 1:1:2) to make total of 0.6×10^5 cells/100 μ L and incubated for 6 hours at 37 at 5% CO₂ and 37 °C temperature. After 6 hours, 7ADD (1 μ L in 10^5 cells, Stem cell) was added to the culture as viability dye and the cells were analysed with by flow cytometry on a BD FACS Canto.

2.9 Single cytotoxicity assay

The NK cells, pDCs and K562 cells were stained with LysoTracker deep red (Invitrogen), Calcein red (ATT Bioquest) and CMAC, Cell tracker Blue (Invirtogen) for 30 minutes. The labelled cells were loaded into different inlets of a 4-inlet device at the concentration of 20 million cells/mL for all the cell types. Thus, generated droplets were collected in an observation chamber and monitored for 16 hours.

2.10 Nanoparticle functionalization

50 μ g of Paramagnetic nanoparticles (Bio-Adembeads Streptavidin Plus 300nm, Ademtech) were washed with 50 μ g PBS (Gibco) using a magnet. The supernatant was removed, and the nanoparticles were resuspended in 990 μ L PBS with biotinylated anti-IFN- γ (Biolegend) antibodies and incubated for 30 min at room temperature while mixing. 10 μ L Biotin was added with a final concentration of 1mM in the solution and incubated for 10 min at room temperature. The beads were washed again with PBS using magnets and resuspended in 5% Pluronic F-68 (Gibco) PBS solution and incubated for 30 min at room temperature. The beads were washed and resuspended in assay buffer containing RPMI 1640 (Gibco, life technologies), 5% Human Serum (HS) (Sanquin), and 25 mM HEPES (Gibco) and incubated for 10 min at room temperature. The nanoparticles were washed again and finally resuspended in the 100 μ L of assay buffer containing fluorescently labeled AF568-detection antibodies for IFN γ (Biolegend).

When performing time-lapse experiments with cells, the final nanoparticle suspension contained 700 ng/ml IL-2 stimuli (Peprotech) and 10 μ M Sytox Green (Invitrogen) additionally. For experiments concerning the calibration curve and optimization steps, IFN- γ (Peprotech) cytokine samples ranging from 0.001 - 100 nM were prepared in assay buffer. All calculations were made considering the final concentration inside the droplets.

2.11 Image acquisition and analysis

Fluorescence imaging was performed using a Nikon Eclipse Ti2 microscope, using a 10X objective and mCherry, DAPI, and FITC/YFP filters every hour. The images were viewed using NIS Element and Image J. Automated Image analysis was performed using custom-made in-built MATLAB script (Mathworks), DMALAB (available on request). The script generated droplet mask that was overlaid onto the fluorescence images, and each droplet was analyzed separately. The output received are in terms of droplet index, cell count, fluorescence intensity and dead cell count. Detailed description of image analysis script is provided in Subedi et al.[15].

2.12 Statistics and software

The Graphs were generated using GraphPad Prism 9.0.0. The results are expressed as mean \pm SEM. Significant differences between two groups were analyzed by two-tailed unpaired Student's t-test. P values < 0.05 were considered statistically significant.

3. Results

3.1 TLR-9 Activated pDCs induced IFN- γ secretion in NK cell in population-based assay

The bi-directional interaction between pDC and NK cell plays an important role in host defense[2,16]. Plasmacytoid DC promotes NK cell-mediated cytotoxicity mostly through secretion of IFN- α , whilst juxtacrine interaction via surface receptors such as OX40-OX40L enhances the IFN- γ secretion. Activated NK cells enhance the release of IFN- α by pDCs via LFA-1 mediated interaction, thus promoting pDC maturation[17] (Figure 1A).

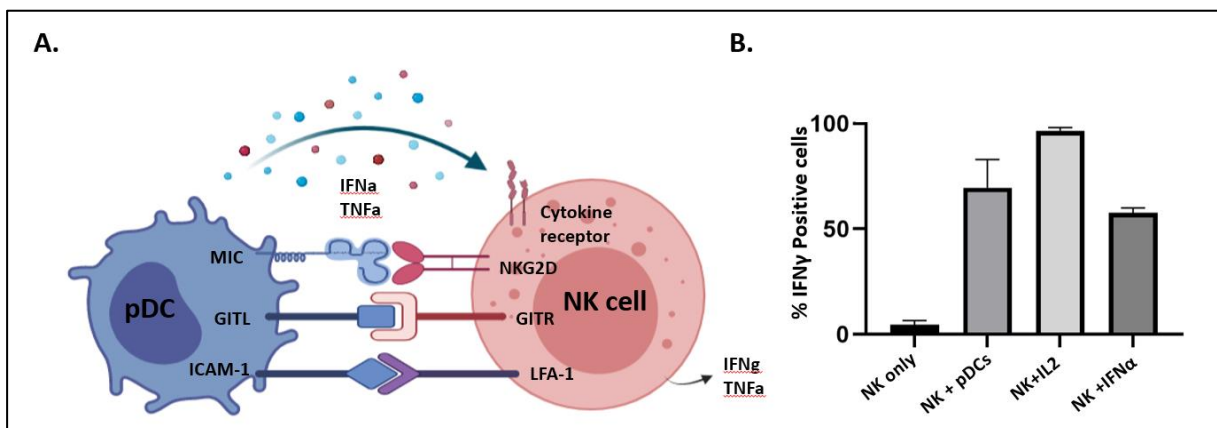


Figure 1. NK/pDCs crosstalk: A. Schematics of bi-directional interaction between pDC and NK cell. Plasmacytoid DC promotes NK cell-mediated cytotoxicity mostly through secretion of IFN- α , whilst juxtacrine interaction via surface receptors such as OX40-OX40L enhances the IFN- γ secretion. Activated NK cells enhance the release of IFN- α by pDCs via LFA-1 mediated interaction, thus promoting pDC maturation. **B.** The graph depicting IFN- γ secretion by NK cells when stimulated at different conditions (no stimulus, pDCs, IL-2 and IFN- α) in population level. Results are shown as the mean \pm SEM of 3 independent experiments with different donors.

To optimize the experimental approach for single cell pDCs/NK cell interaction, NK cells were co-cultured with pre-activated pDCs in the presence of CpG-C (TLR9 agonist) overnight. Four hours of incubation was not enough to induce IFN- γ secretion, while overnight activation led to around 60% NK cells positive for IFN- γ (Figure 1B). Even though the percent of IFN- γ positive NK cells was lower than what had been observed for IL-2 activated NK cells, a similar percentage was observed when they were activated with pDCs conditioned media or IFN- α . Taken together, we showed TLR-9 activated pDCs could induce IFN- γ secretion in NK cells.

3.2 pDCs induces IFN γ secretion in NK cells via IFN α dependent manner

Assessment of pDC/NK cell interaction in population-based assays can be affected by paracrine and juxtacrine interactions, thus hiding the actual mechanism involved. To understand the intrinsic behavior of the interaction, we used droplet-based microfluidics to facilitate the crosstalk between cells excluding the influence of the microenvironment. NK cells and pDCs were labelled with cytokine catch reagents for IFN- γ and IFN- α to allow for capturing and monitoring cytokine secretion by a single cell. We used pipette tips for loading cells in microfluidic chips to increase the probability of cellular encapsulation, and to achieve the optimal cell pairing at a ratio of 1:1 in the oil-water droplets (\sim 1.2nL)[14]. After overnight activation, the cells were retrieved from the droplets by breaking the emulsion with PFO and prepared for downstream FACS analysis (Figure 2A). Like our previous studies with other cell types, the viability of cells after culturing in droplets was warranted (Figure 2B)[15,18].

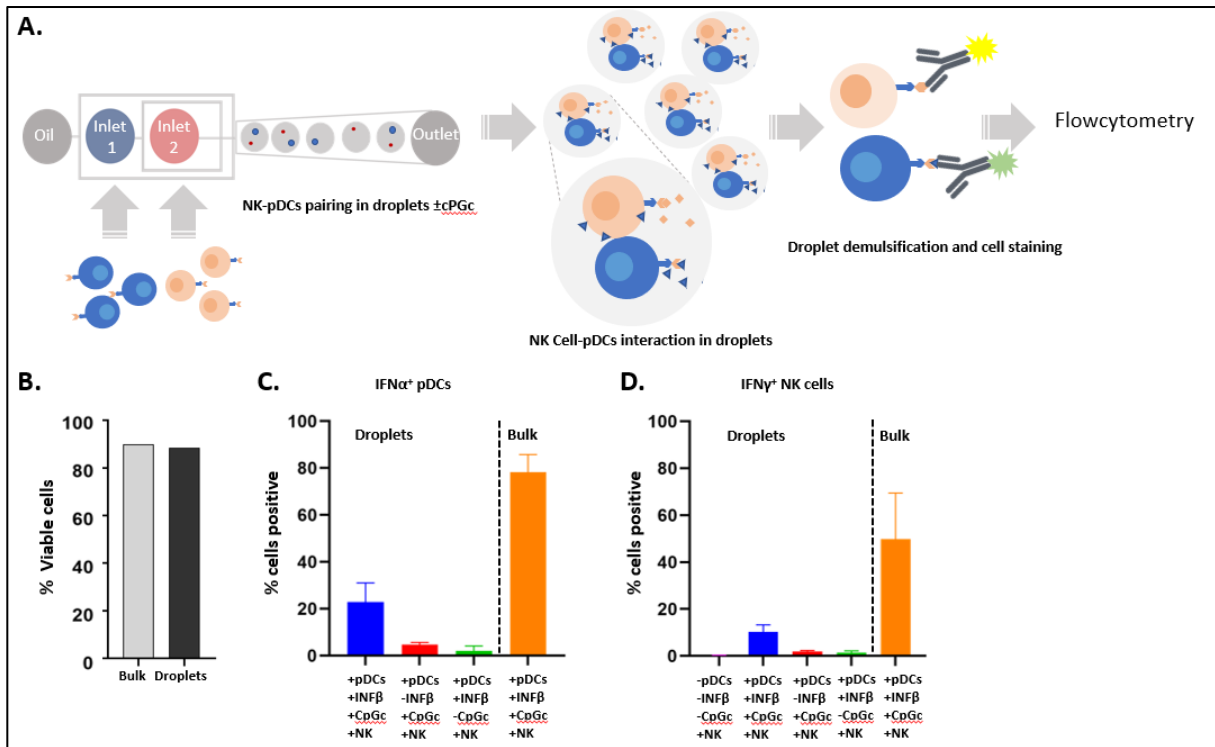


Figure 2. NK/pDCs interaction at single cell level: A. Experimental schematics of interaction between pDC and NK cell in 1.2 nL droplets. NK cell and pDCs (IFN- β primed or not primed) were labelled with IFN- γ and IFN- α catch reagent respectively and loaded into the 3-inlet droplet chip with the height 30 μ m from different inlets. After 20 hours of incubation, droplets were demulsified using PFO solution with HFE oil and the cells were stained for IFN- γ and IFN- α for FACS. **B.** The viability of cells after bulk and droplet stimulation is shown in the graph. **C.** Percentage of positive pDCs for IFN- α at different conditions (droplets-based experiments with primed and non primed pDCs in presence or absence of CpG-C. **D.** Percentage of positive NK cells for IFN- γ at different conditions (droplets-based experiments with primed and non primed pDCs in presence or absence of CpG-C. Results are shown as the mean \pm SEM of 3 independent experiments with different donors.

During encapsulation, CpG-C was mixed with NK cells and was loaded from another inlet to ensure in-droplet activation of pDCs. Priming with IFN- β 2 hours prior to encapsulation enhanced the percentage of pDCs secreting IFN α (Figure 2C). Similar effect of priming was observed with the percentage of IFN γ positive NK cells while the percentage for IFN γ positive NK cells with unprimed or unstimulated activated pDCs were observed to be minimal (Figure 2D). In summary, we showed that pDC mediated activation of NK cells at single-cell level is IFN- α dependent.

3.3 Co activation of NK cells with pDCs augments IFN γ secretion in NK cells

Previously, we presented an integrated platform for studying single cell secretion upon interaction with other cells. In this study, we used a 4-inlet device with 30 μm height to facilitate efficient cell encapsulation and pairing without overcrowding the inlets (Figure 3A). Two cell types and nanoparticles were loaded from three different inlets using tip loading method as described in Sinha et al[14]. At optimal loading concentration of 20 million cells/ml for both the cells, we achieved 7% cell pairing, of which 80% contained 1:1 pairing ratio (Figure 3B,C). Around 23% NK cell, that have been paired with primed pDCs showed positive IFN- γ secretion while only 6% unpaired NK cells was observed to be positive (Figure 3D).

In this way, our results showed that the activated single pDCs enhance IFN- γ secretion in NK cells.

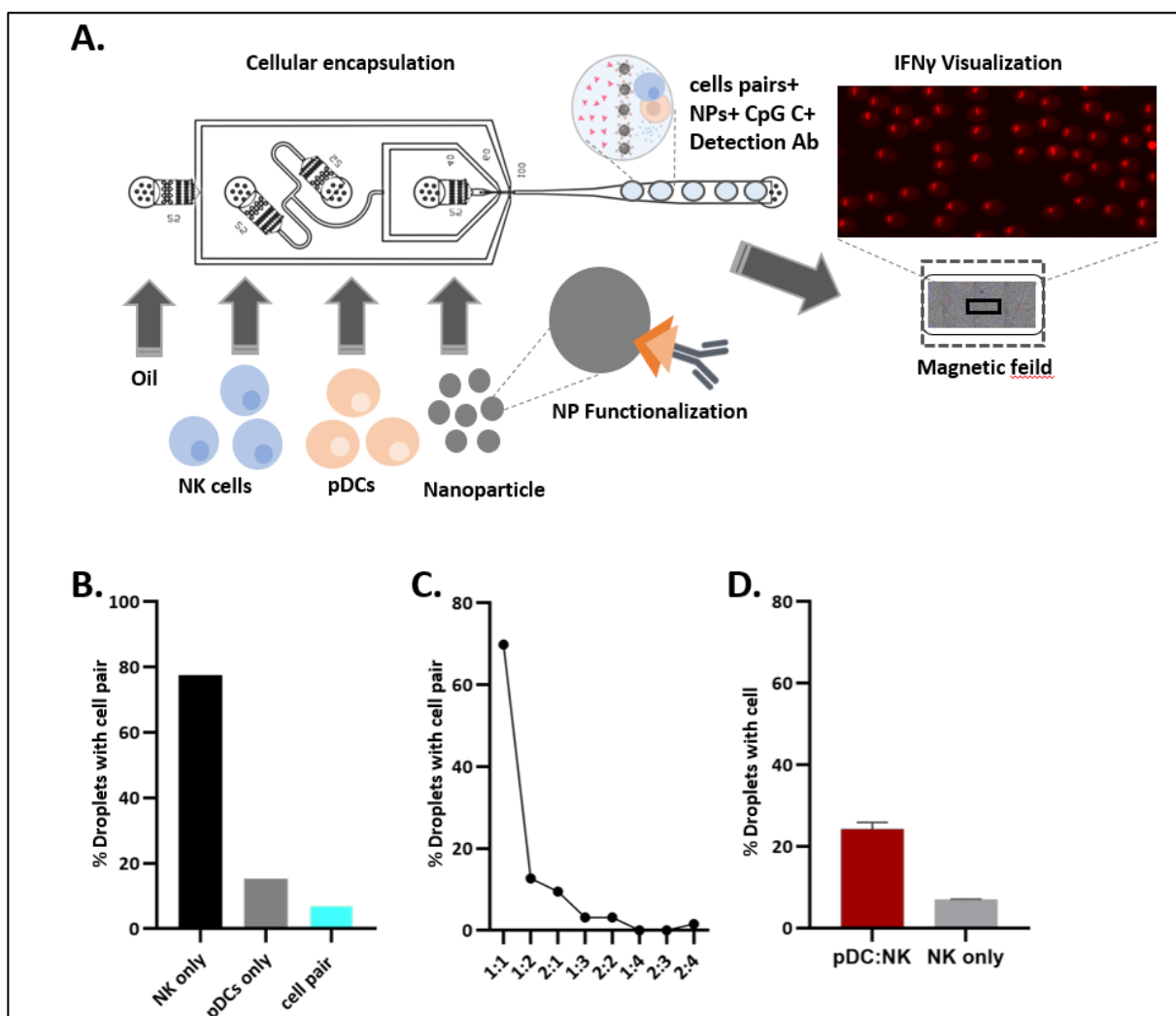


Figure 3. In-droplet IFN γ secretion assay upon NK/pDCs interaction: **A.** A 4-inlet droplet chip with 30 μm height was used to generate droplets containing functionalized nanoparticles for IFN gamma catch, NK-pDC pairs, CpGc and detection dye encapsulated within the 1.2 nL droplets. NK cells and pDCs were loaded from two different inlet while nanoparticle, CpGc and detection antibody was added from the innermost inlet. The outermost inlet was used to flow HFE oil with 2.5% Picosurf. Thus, generated droplets were immobilized in the observation chambers that was placed within the magnetic field. The droplets were monitored for 16 hours' time frame under fluorescent microscope **B.** The graph showing cell pairing efficiency within droplets **C.** The graph showing the percentage of droplets with different E:T ratio in the droplets **D.** The graph showing percentage of droplets with NK cells positive for IFN γ in presence or absence of pDCs. Results are shown as the mean \pm SEM of 2 independent experiments with different donors.

3.4 Monitoring cytotoxic function of NK cells upon interaction with pDCs

It has previously been shown that NK cells cocultured with activated pDCs showed enhanced ability to kill tumor cells[7,11]. To investigate similar behavior at single cell level, we utilized the four-inlet droplet to encapsulate the immune cell together with K562 at the optimal concentration of 20 million NK cells/ml. All the cells were loaded into the chip through different inlets and the flow rate of oil and cells were maintained at the ratio 2:1 respectively (Figure 4A). Approximately 8% of the droplets with cells contained all three cells at 1:1:1 ratio (Figure 4B,C).

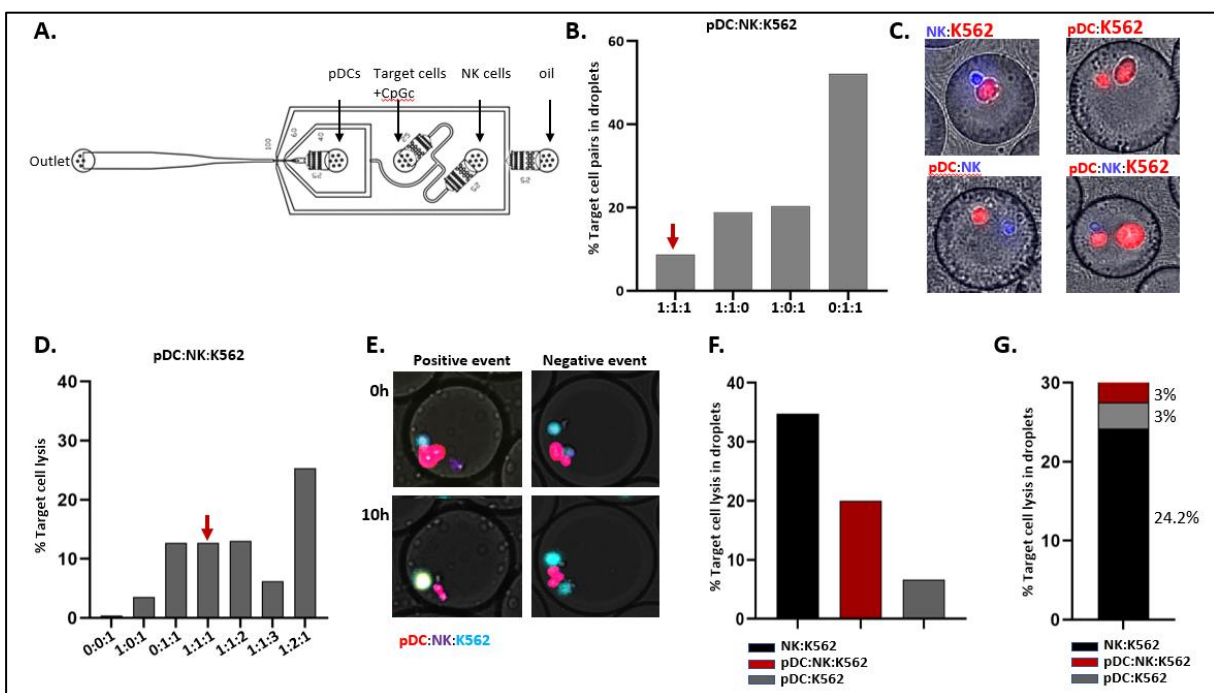


Figure 4. In-droplet cytotoxicity assay upon NK/pDCs interaction: **A.** A 4-inlet droplet chip with 30 μm height was used to pair NK cell together with pDC and K562. NK cells and pDCs and K562 were stained with lysotracker deep red, calcein red and cell tracker blue and were loaded from three different inlet at the concentration of 20 million cell/mL. The viability dye mixture (sytox green and cell event caspase 3/7) was added to the cell culture medium prior to encapsulation. The outermost inlet was used to flow HFE oil with 2.5% Picosurf. The droplets were monitored for 16 hours' time frame under fluorescent microscope. **B.** The graph showing cell pairing efficiency within droplets. **C.** The microscopic overview of NK cells (blue), pDCs (red, small) and K562 (red, big) pairing at different ratios in the droplets. **D.** The graph showing percentage of droplets with percentage of target cell lysis in population-based cytotoxicity assay. **E.** Microscopic overview of positive and negative cytotoxic event within droplets with pDCs (red), NK cells (purple) and K562 cells (blue). **F.** Graph showing the percentage of cell lysis in droplets at different condition. **G.** Graph showing the contribution of different conditions (NK:K562, pDC:NK:K562 and pDC:K562) in total observed cytotoxic events. The experiment has been performed once.

The pDCs were primed for 2 hours before the cytotoxicity assay and later were stimulated with CpG C. At population level, we did not observe any variation in the cytotoxicity with or without pDCs (Figure 4D). At a single cell level, around 20% of droplets with all three cells showed positive lysis when monitored for 10 hours. We observed total 30% positive cytotoxic events in droplets of which 24% was mediated by only NK cells while 3% was observed when NK cells were paired together with pDCs. Plasmacytoid DCs on their own also showed around 3% target cell lysis as had been observed in the bulk-based assay.

Taken together, we did not observe enhanced cytotoxic ability of NK cells upon interaction with activated pDCs in both bulk and single cell level.

4. Discussion and Conclusion

Both DCs and NK cells are effector innate immune cells that can trigger and orient the immune responses against pathogens and tumors[19,20]. Even though these cells possess an extraordinary ability to induce a response on their own, several studies showed their regulatory effect on each other's activity[7,21]. In this study, we explored the interplay between pDCs and NK cells at a single cell level to decipher the effect of underlying cellular

heterogeneity. Based on cytokine based functional output, we showed that activated pDCs could induce NK cell activation also at the single-cell level.

Similar to our earlier findings, we showed that IFN- α secretion by pDCs is highly regulated by its microenvironment. In the absence of paracrine signaling, only a few percent of cells showed IFN- α secretion, whereas upon priming with IFN- β , the IFN- α positive pDCs also increased [18,22]. By co-encapsulating NK cells with primed or unprimed pDCs we showed the association of IFN- α secretion in pDCs and IFN- γ secretion in NK cells since primed pDCs could spike the percentage of IFN- γ positive NK cell. Blocking of the IFN- α receptor in NK cells could provide a definitive information regarding the mechanism involved for future research.

Interaction of activated pDCs with NK cells have shown to boost the cytotoxic ability of NK cells in mice cells [6]. In contrast, in our preliminary experiments we were unable to find any augmented cytolytic ability with human peripheral blood NK cells. Both in our population-based assay as well as in our droplet based single cell assay, we did not observe differences in cytotoxic ability of NK cells upon interacting with pDCs. By increasing the interaction time between pDCs and NK cells and studying different E:T ratios for incubation, we could test the hypothesis more accurately in the future. Furthermore, by optimizing the setup, the regulatory effect of individually activated NK cells onto single pDCs could also be explored which had only been studied in population level [7,23].

The implication of NK/pDCs bidirectional crosstalk has been found in viral infections and autoimmune conditions [5,24]. Understanding the fundamentals of the interaction can therefore provide crucial information for clinical as well as research purposes.

5. References

- [1] C.A. Janeway, R. Medzhitov, Innate immune recognition, *Annu. Rev. Immunol.* (2002). <https://doi.org/10.1146/annurev.immunol.20.083001.084359>.
- [2] R. Wehner, K. Dietze, M. Bachmann, M. Schmitz, The bidirectional crosstalk between human dendritic cells and Natural killer cells, *J. Innate Immun.* (2011). <https://doi.org/10.1159/000323923>.
- [3] D. Mavilio, G. Lombardo, A. Kinter, M. Fogli, A. La Sala, S. Ortolano, A. Farschi, D. Follmann, R. Gregg, C. Kovacs, E. Marcenaro, D. Pende, A. Moretta, A.S. Fauci, Characterization of the defective interaction between a subset of natural killer cells and dendritic cells in HIV-1 infection, *J. Exp. Med.* (2006). <https://doi.org/10.1084/jem.20060894>.
- [4] B. Jacobs, V. Gebel, L. Heger, V. Grèze, H. Schild, D. Dudziak, E. Ullrich, Characterization and Manipulation of the Crosstalk Between Dendritic and Natural Killer Cells Within the Tumor Microenvironment, *Front. Immunol.* (2021). <https://doi.org/10.3389/fimmu.2021.670540>.
- [5] K.N. Reitano, S. Kottlilil, C.M. Gille, X. Zhang, M. Yan, M.A. O'Shea, G. Roby, C.W. Hallahan, J. Yang, R.A. Lempicki, J. Arthos, A.S. Fauci, Defective plasmacytoid dendritic cell-NK cell cross-talk in HIV infection, *AIDS Res. Hum. Retroviruses.* (2009). <https://doi.org/10.1089/aid.2008.0311>.
- [6] C. Liu, Y. Lou, G. Lizée, H. Qin, S. Liu, B. Rabinovich, G.J. Kim, Y.H. Wang, Y. Ye, A.G. Sikora, W.W. Overwijk, Y.J. Liu, G. Wang, P. Hwu, Plasmacytoid dendritic cells induce NK cell-dependent, tumor antigen-specific T cell cross-priming and tumor regression in mice, *J. Clin. Invest.* (2008). <https://doi.org/10.1172/JCI33583>.
- [7] F. Gerosa, A. Gobbi, P. Zorzi, S. Burg, F. Briere, G. Carra, G. Trinchieri, The Reciprocal Interaction of NK Cells with Plasmacytoid or Myeloid Dendritic Cells Profoundly Affects Innate Resistance Functions, *J. Immunol.* (2005). <https://doi.org/10.4049/jimmunol.174.2.727>.
- [8] F. Golsaz-Shirazi, M.M. Amiri, F. Shokri, Immune function of plasmacytoid dendritic cells, natural killer cells, and their crosstalk in HBV infection, *Rev. Med. Virol.* (2018). <https://doi.org/10.1002/rmv.2007>.
- [9] C.C. Shi, E.T.T.L. Tjwa, P.J. Biesta, A. Boonstra, Q. Xie, H.L.A. Janssen, A.M. Woltman, Hepatitis B virus suppresses the functional interaction between natural killer cells and plasmacytoid dendritic cells, *J. Viral Hepat.* (2012). <https://doi.org/10.1111/j.1365-2893.2011.01496.x>.
- [10] Y.O. Alexandre, C.D. Cocita, S. Ghilas, M. Dalod, Deciphering the role of DC subsets in MCMV infection to better understand immune protection against viral infections, *Front. Microbiol.* (2014). <https://doi.org/10.3389/fmicb.2014.00378>.
- [11] C. Romagnani, M. Della Chiesa, S. Kohler, B. Moewes, A. Radbruch, L. Moretta, A. Moretta, A. Thiel, Activation of human NK cells by plasmacytoid dendritic cells and its modulation by CD4+ T helper cells and CD4+ CD25hi T regulatory cells, *Eur. J. Immunol.* (2005). <https://doi.org/10.1002/eji.200526069>.
- [12] Y. Díaz-Rodríguez, P. Cordeiro, A. Belounis, S. Herblot, M. Duval, In vitro differentiated plasmacytoid dendritic cells as a tool to induce anti-leukemia activity of natural killer cells, *Cancer Immunol. Immunother.* (2017). <https://doi.org/10.1007/s00262-017-2022-y>.
- [13] L.M.E. Müller, M. Holmes, J.L. Michael, G.B. Scott, E.J. West, K.J. Scott, C. Parrish, K. Hall, S. Ståble, V.A. Jennings, M. Cullen, S. McConnell, C. Langton, E.L. Tidswell, D. Shafren, A. Samson, K.J. Harrington, H. Pandha, C. Ralph, R.J. Kelly, G. Cook, A.A. Melcher, F. Errington-Mais, Plasmacytoid dendritic cells orchestrate innate and adaptive anti-tumor immunity induced by oncolytic coxsackievirus A21, *J. Immunother. Cancer.* (2019). <https://doi.org/10.1186/s40425-019-0632-y>.
- [14] N. Sinha, N. Subedi, F. Wimmers, M. Soennichsen, J. Tel, A Pipette-Tip Based Method for Seeding Cells to Droplet Microfluidic Platforms., *J. Vis. Exp.* (2019) 1–10. <https://doi.org/10.3791/57848>.
- [15] N. Subedi, L.C. Van Eynhoven, A.M. Hokke, L. Houben, M.C. Van Turnhout, C.V.C. Bouten, K. Eyer, J. Tel, An automated real-time microfluidic platform to probe single NK cell heterogeneity and cytotoxicity on-chip, *Sci. Rep.* 11 (2021) 17084. <https://doi.org/10.1038/s41598-021-96609-9>.
- [16] S. Mahmood, D. Upreti, I. Sow, A. Amari, S. Nandagopal, S.K.P. Kung, Bidirectional interactions of NK cells and dendritic cells in immunotherapy: Current and future perspective, *Immunotherapy.* (2015). <https://doi.org/10.2217/imt.14.122>.
- [17] T.S.M. Mathan, C.G. Figdor, S.I. Buschow, Human plasmacytoid dendritic cells: From molecules to intercellular communication network, *Front. Immunol.* (2013). <https://doi.org/10.3389/fimmu.2013.00372>.
- [18] L.C. Van Eynhoven, E. Chouri, N. Subedi, J. Tel, Phenotypical Diversification of Early IFN α -Producing Human Plasmacytoid

Chapter 6 - Potent crosstalk between a single pDC and a NK cell

- Dendritic Cells Using Droplet-Based Microfluidics, *Front. Immunol.* (2021). <https://doi.org/10.3389/fimmu.2021.672729>.
- [19] J. Banchereau, R.M. Steinman, Dendritic cells and the control of immunity, *Nature.* (1998). <https://doi.org/10.1038/32588>.
- [20] A. Moretta, C. Bottino, M.C. Mingari, R. Biassoni, L. Moretta, What is a natural killer cell?, *Nat. Immunol.* (2002). <https://doi.org/10.1038/ni0102-6>.
- [21] N.C. Fernandez, A. Lozier, C. Flament, P. Ricciardi-Castagnoli, D. Bellet, M. Suter, M. Perricaudet, T. Tursz, E. Maraskovsky, L. Zitvogel, Dendritic cells directly trigger NK cell functions: Cross-talk relevant in innate anti-tumor immune responses in vivo, *Nat. Med.* (1999). <https://doi.org/10.1038/7403>.
- [22] F. Wimmers, N. Subedi, N. van Buuringen, D. Heister, J. Vivié, I. Beeren-Reinieren, R. Woestenenk, H. Dolstra, A. Piruska, J.F.M. Jacobs, A. van Oudenaarden, C.G. Figdor, W.T.S. Huck, I.J.M. de Vries, J. Tel, Single-cell analysis reveals that stochasticity and paracrine signaling control interferon-alpha production by plasmacytoid dendritic cells, *Nat. Commun.* (2018). <https://doi.org/10.1038/s41467-018-05784-3>.
- [23] M. Della Chiesa, C. Romagnani, A. Thiel, L. Moretta, A. Moretta, Multidirectional interactions are bridging human NK cells with plasmacytoid and monocyte-derived dendritic cells during innate immune responses, *Blood.* (2006). <https://doi.org/10.1182/blood-2006-02-004028>.
- [24] K. Hjorton, N. Hagberg, E. Israelsson, L. Jinton, O. Berggren, J.K. Sandling, K. Thörn, J. Mo, M.L. Eloranta, L. Rönnblom, Cytokine production by activated plasmacytoid dendritic cells and natural killer cells is suppressed by an IRAK4 inhibitor, *Arthritis Res. Ther.* (2018). <https://doi.org/10.1186/s13075-018-1702-0>.

CHAPTER 7

DISCUSSION: NEW AVENUES TOWARDS CELLULAR IMMUNOTHERAPY



As Plato had rightly said, “Necessity is the mother of invention”. The necessity to understand variation in cellular responses and minute functional nuances missed by population-based assays led to advancement in single cell technologies. Innovation in microsystems and microfluidics facilitated the integration of numerous complex functions on-chip that were earlier not feasible. At the same time, the ability of these platforms to dynamically acquire information from immune cells and monitor immune cell activities in real time made them popular among researchers[1]. These high-throughput analysis platforms allow both real-time and end-point measurements and can facilitate one to one cell pairing for decoding communication between immune cells, e.g., for monitoring cytotoxic cellular function[2,3]. Droplet-based microfluidics facilitates compartmentalization of immune cells in a closed environment to understand cellular behavior with high sensitivity and high throughput[4]. Cellular heterogeneity is speculated to be a fundamental property of the immune system enabling it to recognize myriads of antigens. This is achieved in various ways. Immune cells leverage wide diversity either by rearranging their receptors or maintain it during their development and maturation. Understanding cellular heterogeneity in immune cell populations aid in development of superior cell-based immunotherapies to treat infection, inflammation, and cancer[5].

The objective of this thesis was to successfully integrate different adaptations of droplet-based microfluidic technology to investigate the underlying heterogeneity in human plasmacytoid dendritic cells (pDCs) and natural killer (NK) cells, ultimately aimed at improving cell-based immunotherapeutic strategies. In the following sections, I provide an overview of the technological innovations presented in this thesis and the results that enhance the understanding of functional cellular heterogeneity.

1. Technological developments, challenges, and limitations:

One of the major challenges of adopting micro-systems/microfluidics technology with interaction-based immunoassays is efficient cell pairing to facilitate cellular communication. The hydrodynamic trap-based system could meet this challenge by delivering the highest cell pairing efficiency; however, they were limited by the possibility of paracrine signaling between neighboring cells[2,6]. Cell pairing in isolated setups was made possible by implementing micro and nano wells-based platforms, but these were not very efficient in terms of cell

loading and cellular distribution into the wells[3,7,8]. Alternatively, droplet-based microfluidics provided the ability to tune the cellular encapsulation and the adaptation of tip loading technique (**Chapter 2**). Thereby it allowed encapsulating a desired number of cells enabling different effector:target cell ratios in a droplet. Droplets with only either effector or target cells served as an internal negative control for viability, while droplets with multiple effector cells were used to examine the effect of intercellular interactions and paracrine stimulation. The tip loading technique provided an elegant solution to cellular sedimentation and cell clumping problems; however, a limitation was observed while encapsulating cells from a larger suspension. An example could be, encapsulating pDCs directly from PBMCs since it may take a relatively long time, ultimately affecting the functional state of the cells. Engineering a parallel droplet device that allows cellular encapsulation from multiple inlets could solve this problem. Despite droplets-based microfluidic platforms being well known for their high throughput ability, the studies involving real-time immunoassays could not fully exploit this characteristic. In the lack of proper droplets docking system, only a few hundred droplets were being monitored while over 100,000 droplets with cells could be produced within a few minutes[9,10]. Application of a glass immobilization chamber was therefore useful in enhancing the number of droplets visualized under the microscope and allowing incorporation of different in-droplet immunoassays (cytotoxicity and ELISA) (**Chapter 3 and 4**). Since droplets constitute a lower volume than micro/nano wells, they could detect a small number of proteins secreted by a single cell. Currently, the platform detects up to 1nM of IFN γ secreted by a single NK cell upon stimulation. Even though the sensitivity is higher compared to other existing studies[11,12], it could further be enhanced by optimizing the microscopy settings and the thickness of the observation chamber, allowing uniform focus all over the chamber[4]. Controlled labeling of catch (with biotin) and detection (with fluorescent dye) antibodies, respectively, would also help enhance the sensitivity of the assay[4].

In this way, the droplet-based real-time platforms have enhanced the functionality of the single-cell immunoassays by incorporating the temporal aspect in the overall assay. However, it lacks in terms of further downstream analysis. Application of sortable hydrogel-based droplets together with real-time immunoassays could, therefore, provide an exciting opportunity to identify and characterize the cells based on their functional responses.

2. Harnessing the power of single immune cells: Paving the way to superior immunotherapy

Decades of technological advancements have facilitated studying immune cells in a segregated environment with minimal noise. However, it still seems that the major achievement of single cell immunology has still not surpassed the level of technological developments and subsets identification, while bigger promises were made. Extending the field of single cell immunology requires a multi-parametric approach by integrating proteomics, secretion dynamics, nucleic acid analysis, cell-cell interactions, and functional attributes (such as migration, lysis, apoptosis) at a single cell level. Only then it will be possible to decipher the relevance of heterogeneity within the immune cell population. Combining the “omics-based” approach with single cell stimulation and interaction would therefore be an important “next step” for the research presented in this thesis.

Since the immune response is a cumulative output of well-balanced coordination between multitudes of cells, understanding the functional heterogeneity also requires an in-depth analysis of this intracellular interaction[13]. While there are multiple instances where immune cells talk with each other, only a few single cell-based studies are available that have voyaged into this futuristic investigation[6]. One limitation is the inability to monitor the functional output and relate them to specific cell types. Although as a preliminary study, I have initiated an approach towards implementation of single cell tools into fundamental understanding of cellular coordination in the immune system. Cellular crosstalk, such as NK/macrophages interaction during inflammation and tissue regeneration; NK/DCs crosstalk while viral infections; NK/T cells or DC/T cells interaction against cancer could provide an excellent way to understand immune coordination while also generating interesting therapeutic strategies that have potential to work in vivo[14–16]. By pairing NK cells with pDCs, I investigated their cross talk, showing that interaction with activated pDCs is enough to induce IFN γ secretion in NK cells (**Chapter 6**). The preliminary findings presented in this chapter aligned with the earlier findings regarding cross talk mediated secretion by NK cells, however, was not able to provide many insights regarding the cytotoxic abilities of NK cells. It was only possible to assess NK cells, while more optimization is required for measuring the functional parameters (IFN- α ; cytotoxicity; T cells priming markers) for studying how this crosstalk influences activation of

pDCs. Since the cross talk has also been observed to play an important role in enhancing the priming of T cells via pDCs, it would also be an interesting aspect to investigate. The results obtained from these studies can develop a combinatorial approach involving these cells to enhance the cytotoxic ability of immune cells. For example, TLR 9 activated pDCs could enhance tumor infiltration and activation of NK cells, which could also be a strategy to investigate in the future.

The insights gained from studying single immune cells have a broad implication, especially in immunotherapy. NK cells provide a promising alternative to T cell-based therapy because of their fierce ability to lyse tumor cells. Different strategies have been developed that aimed at increasing the lytic ability of NK cells against tumor cells, such as the use of cytokines; adoptive transfer of allogeneic NK cells; monoclonal antibodies targeted against cancer cells to exploit the antibody-dependent cytotoxic ability of NK cells, and antibodies against inhibitory receptors of NK cells[17]. Adaptation of these different strategies has improved disease-free survival and lowered cancer relapse rates, especially for leukemic patients[18]. Several companies like Kiadis Pharmaceuticals and Gycostems in the Netherlands, XNK Therapeutics in Sweden, Cellectis in France, US-based Cytovia, etc. have realized this potential and are investing heavily towards the development. One of the main bottlenecks in NK cell therapies remains the varied interactions between the NK cell and the target cancer cell since it determines the effectiveness of the treatment. It also provides information on potential undesired effects, such as life-threatening levels of inflammation. The cytotoxicity and secretion platforms presented in this thesis could provide an innovative approach for understanding the interaction and treatment prognosis for NK cell-based therapy.

The vast heterogeneity of immune cells at a steady state in individuals has become clear using single cell technologies that can be used for enhancing immunotherapy[19–21]. The allogeneic infusion of NK cells derived from different sources is a popular mode of NK cell-based therapy with an optimistic outlook. However, the clinical outcomes showed that this approach could not deliver in coherence with what was promised. By monitoring thousands of droplets with NK cell paired together with different cancer cells in real time, I showed that NK cell population is composed of cells with different cytotoxic strength and efficacy (**Chapter 4**). Along with their binary killing behavior (either kill or not kill), I also showed that the NK cell cytotoxicity dynamics also varies within different target cells. Therefore, the biggest shortcoming of this

approach is the use of the whole NK cell component without understanding the distribution of different functional subsets. This approach could benefit by using functionally superior cells, for example, serial killers. By increasing the droplet size and the cell concentration, I increased the number of target cells inside the droplets thus allowing identification of the serial killers NK cells (**Chapter 4**). Characterizing the phenotypical markers and surface regulation of these serial killers could further guide in engineering "serial-killer CAR NK cells" thus enhancing the potential of NK-based products. I also showed that NK cell in a confined space (as inside the droplets), operate independently to mediate the lysis of a single target cell and do not show cumulative cytolytic effect by cooperating with neighboring NK cell as in bulk-based co-culture. Using the information related to how NK cells are functionally shaped by their microenvironment in both healthy and diseased states will allow harnessing the full potential of tissue-resident NK cells and peripheral blood NK cells.

The temporal function of the assay suggested that NK cells can kill their target cell in fast or slow manner. However, this study could not identify the exact mechanism (Perforin-granzyme B based or TRAIL based) involved that could be associated with variation in cytotoxic dynamics. An easiest approach for studying NK cell lytic pathways could be in-droplet proteolytic degradation of perforin to prevent granzyme-mediated killing or blocking the TRAIL-Death receptors on the target cells to identify the pathways involved[22]. Other approaches like using a reporter NK cell lines, confocal microscopy have also been applied to study the synaptic factors and exocytosis of lytic granules, however, they might not be applicable for real time study using primary NK cells[22]. On a larger perspective, transcriptomic profiling of NK cells with varying killing abilities will also provide a wider information on the relevance of the NK cell heterogeneity.

Similarly, the results shown in this thesis are also beneficial for optimizing the parameters for effective pDC-based vaccination. One of the key features of pDCs is to produce large amounts of type I interferons (IFNs) upon TLR7 or TLR9 ligation[21]. By activating pDCs at single cell level in droplets, I showed that stimulation induces functional diversification of pDCs. The IFN-I pathway is controlled by stochastic gene regulation and amplified by environmental signals in pDCs rather than subsets-based division of labor (**Chapter 5**). The knowledge regarding paracrine signaling of IFN-I and its regulatory effect on pDCs could enhance the functional output of the vaccination, for example, an extra dose of IFN- α together with the vaccine to

ensure the response from maximum cells. Understanding the dynamics of pDCs activation could guide on optimizing the parameters for pDCs vaccination such as an optimal number of pDCs that could deliver the effective response in vivo, stimulation time before injection, and the optimal stimulating agent for activation. To this date, only two studies have tested peripheral blood pDCs as cell-based cancer therapy[19,20]. Both the trials yielded positive outcomes however, a differential ability of pDCs to prime T cells was observed in melanoma and prostate cancer. Since pDCs comprise highly diverse cells that could perform ranges of functions, it would be beneficial to exploit this diversity cleverly rather than just hoping for optimal performance. My research could provide the ability to study the interaction between pDCs and T cells on a single cell level to identify the ability of each pDCs in T cell priming. Moreover, this study could be expanded to pDCs/T cells infiltrating different cancer microenvironments to test the efficacy of vaccination in clinic.

One of the most common drawbacks of using primary immune cells for cell-based therapies is its availability. While it is difficult to harvest the adequate number of cells of interest from patients, it is also painstaking to prepare them for therapy every single time. Hence, the prospects of CD34+ hematopoietic stem cells for developing more “off-the shelves” products are becoming popular. Several groups have successfully differentiated these cells into the immune cells of interest; however, the optimal potential of individual cells remains elusive. This study and several other microfluidic-based approaches have evaluated the potential of CD34+ derived immune cells of interest[23]. Proper characterization of these cells could therefore open ways to enhance the prospects of cell-based therapy immensely.

In conclusion, the results presented in this thesis showed that by deconstructing the immunological responses of a single immune cell, we could build an effective toolbox for designing and developing effective treatment strategies to enhance the pre-existing natural potential of immune cells.

3. References

- [1] A. Yalçın, Y.J. Yamanaka, J.C. Love, Analytical technologies for integrated single-cell analysis of human immune responses., *Methods Mol. Biol.* 853 (2012) 211–35. https://doi.org/10.1007/978-1-61779-567-1_16.
- [2] B. Dura, M.M. Servos, R.M. Barry, H.L. Ploegh, S.K. Dougan, J. Voldman, Longitudinal multiparameter assay of lymphocyte interactions from onset by microfluidic cell pairing and culture, *Proc. Natl. Acad. Sci.* 113 (2016) E3599–E3608. <https://doi.org/10.1073/pnas.1515364113>.
- [3] Y.J. Yamanaka, C.T. Berger, M. Sips, P.C. Cheney, G. Alter, J.C. Love, Single-cell analysis of the dynamics and functional outcomes of interactions between human natural killer cells and target cells, *Integr. Biol. (United Kingdom)*. 4 (2012) 1175–1184. <https://doi.org/10.1039/c2ib20167d>.
- [4] Y. Bounab, K. Eyer, S. Dixneuf, M. Rybczynska, C. Chauvel, M. Mistretta, T. Tran, N. Aymerich, G. Chenon, J.F. Llitjos, F. Venet, G. Monneret, I.A. Gillespie, P. Cortez, V. Moucadet, A. Pachot, A. Troesch, P. Leissner, J. Textoris, J. Bibette, C. Guyard, J. Baudry, A.D. Griffiths, C. Védrine, Dynamic single-cell phenotyping of immune cells using the microfluidic platform DropMap, *Nat. Protoc.* 15 (2020) 2920–2955. <https://doi.org/10.1038/s41596-020-0354-0>.
- [5] V.Y.S. Oei, M. Siernicka, A. Graczyk-Jarzynka, H.J. Hoel, W. Yang, D. Palacios, H.A. Sbak, M. Bajor, D. Clement, L. Brandt, B. Onfelt, J. Goodridge, M. Winiarska, R. Zagodzón, J. Olweus, J.A. Kyte, K.J. Malmberg, Intrinsic functional potential of NK-Cell subsets constrains retargeting driven by chimeric antigen receptors, *Cancer Immunol. Res.* (2018). <https://doi.org/10.1158/2326-6066.CIR-17-0207>.
- [6] B. Dura, S.K. Dougan, M. Barisa, M.M. Hoehl, C.T. Lo, H.L. Ploegh, J. Voldman, Profiling lymphocyte interactions at the single-cell level by microfluidic cell pairing, *Nat. Commun.* (2015). <https://doi.org/10.1038/ncomms6940>.
- [7] E. Forslund, K. Guldevall, P.E. Olofsson, T. Frisk, A.E. Christakou, M. Wiklund, B. Önfelt, Novel microchip-based tools facilitating live cell imaging and assessment of functional heterogeneity within NK cell populations, *Front. Immunol.* (2012). <https://doi.org/10.3389/fimmu.2012.00300>.
- [8] B. Vanherberghen, P.E. Olofsson, E. Forslund, M. Sternberg-Simon, M.A. Khorshidi, S. Pacouret, K. Guldevall, M. Enqvist, K.J. Malmberg, R. Mehr, B. Önfelt, Classification of human natural killer cells based on migration behavior and cytotoxic response, *Blood*. 121 (2013) 1326–1334. <https://doi.org/10.1182/blood-2012-06-439851>.
- [9] S. Sarkar, P. Sabhachandani, D. Ravi, S. Potdar, S. Purvey, A. Beheshti, A.M. Evens, T. Konry, Dynamic analysis of human natural killer cell response at single-cell resolution in B-Cell Non-Hodgkin Lymphoma, *Front. Immunol.* 8 (2017) 1–13. <https://doi.org/10.3389/fimmu.2017.01736>.
- [10] S. Antona, I. Platzman, J.P. Spatz, Droplet-Based Cytotoxicity Assay: Implementation of Time-Efficient Screening of Antitumor Activity of Natural Killer Cells, *ACS Omega*. 5 (2020) 24674–24683. <https://doi.org/10.1021/acsomega.0c03264>.
- [11] S. Antona, T. Abele, K. Jahnke, Y. Dreher, K. Göpfrich, I. Platzman, J.P. Spatz, Droplet-Based Combinatorial Assay for Cell Cytotoxicity and Cytokine Release Evaluation, *Adv. Funct. Mater.* (2020). <https://doi.org/10.1002/adfm.202003479>.
- [12] S.C. Hsiao, H. Liu, T.A. Holstlaw, C. Liu, C.Y. Francis, M.B. Francis, Real Time Assays for Quantifying Cytotoxicity with Single Cell Resolution, *PLoS One*. (2013). <https://doi.org/10.1371/journal.pone.0066739>.
- [13] R. Satija, A.K. Shalek, Heterogeneity in immune responses: From populations to single cells, *Trends Immunol.* 35 (2014) 219–229. <https://doi.org/10.1016/j.it.2014.03.004>.
- [14] N. Lapaque, T. Walzer, S. Méresse, E. Vivier, J. Trowsdale, Interactions between Human NK Cells and Macrophages in Response to Salmonella Infection , *J. Immunol.* (2009). <https://doi.org/10.4049/jimmunol.0803329>.
- [15] I. Pedroza-Pacheco, A. Madrigal, A. Saudemont, Interaction between natural killer cells and regulatory T cells: Perspectives for immunotherapy, *Cell. Mol. Immunol.* (2013). <https://doi.org/10.1038/cmi.2013.2>.
- [16] T.D. Holmes, E.B. Wilson, E.V.I. Black, A. V. Benest, C. Vaz, B. Tan, V.M. Tanavde, G.P. Cook, Licensed human natural killer cells aid dendritic cell maturation via TNFSF14/LIGHT, *Proc. Natl. Acad. Sci. U. S. A.* (2014). <https://doi.org/10.1073/pnas.1411072112>.
- [17] R. Tarazona, N. Lopez-Sejas, B. Guerrero, F. Hassouneh, I. Valhondo, A. Pera, B. Sanchez-Correa, N. Pastor, E. Duran, C. Alonso, R. Solana, Current progress in NK cell biology and NK cell-based cancer immunotherapy, *Cancer Immunol. Immunother.* (2020). <https://doi.org/10.1007/s00262-020-02532-9>.
- [18] J.E. Rubnitz, H. Inaba, R.C. Ribeiro, S. Pounds, B. Rooney, T. Bell, C.H. Pui, W. Leung, NKAML: A pilot study to determine the safety and feasibility of haploidentical natural killer cell transplantation in childhood acute myeloid leukemia, *J. Clin. Oncol.* (2010).

- <https://doi.org/10.1200/JCO.2009.24.4590>.
- [19] D. Brownlie, M. Scharenberg, J.E. Mold, J. Hard, E. Kekalainen, M. Buggert, S. Nguyen, J.N. Wilson, M. Al-Ameri, H.G. Ljunggren, N. Marquardt, J. Michaelsson, Expansions of adaptive-like NK cells with a tissue-resident phenotype in human lung and blood, *Proc. Natl. Acad. Sci. U. S. A.* (2021). <https://doi.org/10.1073/pnas.2016580118>.
- [20] M.C. Costanzo, D. Kim, M. Creegan, K.G. Lal, J.A. Ake, J.R. Currier, H. Streeck, M.L. Robb, N.L. Michael, D.L. Bolton, N.J. Steers, M.A. Eller, Transcriptomic signatures of NK cells suggest impaired responsiveness in HIV-1 infection and increased activity post-vaccination, *Nat. Commun.* (2018). <https://doi.org/10.1038/s41467-018-03618-w>.
- [21] A.R. Schuurman, T.D. Reijnders, A. Saris, I. Ramirez Moral, M. Schinkel, J. de Brabander, C. van Linge, L. Vermeulen, B.P. Scicluna, W.J. Wiersinga, F.A. Vieira Braga, T. van der Poll, Integrated single-cell analysis unveils diverging immune features of COVID-19, influenza, and other community-acquired pneumonia, *Elife.* (2021). <https://doi.org/10.7554/elife.69661>.
- [22] I. Prager, C. Liesche, H. Van Ooijen, D. Urlaub, Q. Verron, N. Sandström, F. Fasbender, M. Claus, R. Eils, J. Beaudouin, B. Önfelt, C. Watzl, NK cells switch from granzyme B to death receptor-mediated cytotoxicity during serial killing, *J. Exp. Med.* (2019). <https://doi.org/10.1084/jem.20181454>.
- [23] J.M.R. Van der Meer, R.J.A. Maas, K. Guldevall, K. Klarenaar, P.K.J.D. de Jonge, J.S.H. van Evert, A.B. van der Waart, J. Cany, J.T. Safrit, J.H. Lee, E. Wagena, P. Friedl, B. Önfelt, L.F. Massuger, N.P.M. Schaap, J.H. Jansen, W. Hobo, H. Dolstra, IL-15 superagonist N-803 improves IFN γ production and killing of leukemia and ovarian cancer cells by CD34+ progenitor-derived NK cells, *Cancer Immunol. Immunother.* (2021). <https://doi.org/10.1007/s00262-020-02749-8>.

Publication list (based on author's contribution)

- A Pipette-Tip Based Method for Seeding Cells to Droplet Microfluidic Platforms. **J Vis Exp.** **2019**; 144, 10 p., e57848.
Nidhi Sinha*, [Nikita Subedi](#)*, Florian Wimmers*, Melf Soennichsen, Jurjen Tel
*Authors contributed equally
- An automated real-time microfluidic platform to probe single NK cell heterogeneity and cytotoxicity on-chip. **Sci Rep.** **2021**; 11, 1, 11 p., 17084.
[Nikita Subedi](#), Laura C. Van Eyndhoven, Ayla M. Hokke, Lars Houben, Mark C. Van Turnhout, Carlijn V.C. Bouten, Klaus Eyer, Jurjen Tel
- Understanding Natural killer cell biology from a single cell perspective. **Cellular Immunology.** **2022**; 373, 12 p., 104497.
[Nikita Subedi](#), Liesbeth Petronella Verhagen, Esmée Michelle Bosman, Ilse van Roessel, Jurjen Tel
- Probing functional heterogeneity and serial killing in single human peripheral and ex vivo-generated CD34+ progenitor derived Natural Killer cells. **Submitted**
[Nikita Subedi](#), Liesbeth Petronella Verhagen, Paul de Jonge, Laura Van Eyndhoven, Mark C. van Turnhout, Vera Koomen, Jean Baudry, Klaus Eyer, Harry Dolstra, Jurjen Tel
- Single-cell analysis reveals that stochasticity and paracrine signaling control interferon-alpha production by plasmacytoid dendritic cells. **Nat Commun.** **2018**; 9, 1, 12 p., 3317.
Florian Wimmers, [Nikita Subedi](#), Nicole van Buuringen, Daan Heister, Judith Vivié, Inge Beeren-Reinieren, Rob Woestenenk, Harry Dolstra, Aigars Piruska, Joannes F. M. Jacobs, Alexander van Oudenaarden, Carl G. Figdor, Wilhelm T. S. Huck, I. Jolanda M. de Vries, Jurjen Tel
- Integrating Immunology and Microfluidics for Single Immune Cell Analysis. **Frontiers Immunol.** **2018**; 9, 16 p., 2373.
Nidhi Sinha, [Nikita Subedi](#), Jurjen Tel
- Phenotypical Diversification of Early IFN α -Producing Human Plasmacytoid Dendritic Cells Using Droplet-Based Microfluidics. **Front Immunol.** **2021**; 12, 12 p., 672729.
Laura C. Van Eyndhoven, Eleni Chouri, [Nikita Subedi](#), Jurjen Tel
- Programmable Bivalent Peptide-DNA Locks for pH-Based Control of Antibody Activity. **ACS Cent Sci.** **2020**; 6, 1, p. 22-31 10 p.
Wouter Engelen, Kwankwan Zhu, [Nikita Subedi](#), Andrea Idili, Francesco Ricci, Jurjen Tel, Maarten Merckx
- T cell-targeting nanoparticles focus delivery of immunotherapy to improve antitumor immunity. **Nat Commun.** **2017**; 8, 17 p., 1747.
Daniela Schmid, Chun Gwon Park, Christina A. Hartl, [Nikita Subedi](#), Adam N. Cartwright, Regina Bou Puerto, Yiran Zheng, James Maiarana, Gordon J. Freeman, Kai W. Wucherpfennig, Darrell J. Irvine, Michael S. Goldberg

CURRICULUM VITAE

Nikita Subedi was born on 24 September 1990 at Lalitpur, Nepal. She completed her B.Tech. in Biotechnology in 2012 from Kathmandu University, Dhulikhel, Nepal. After working for a short time in a tissue culture laboratory as a culture specialist, she moved to the Netherlands. She finished her MSc in Molecular Mechanism of Diseases at Radboud University, Nijmegen, the Netherlands. She was selected for Radboud Scholarship Program and MMD study fund for the Master program. During her study, she specialized in single-cell immunology with an internship with Dr. Jurjen Tel at the Tumor Immunology Lab at RIMLS, Nijmegen, the Netherlands. Later, she joined the group of Dr. Michael Goldberg at Dana Farber Cancer, Harvard Medical School, Boston, USA, where she developed T cells targeted nanoparticles. In 2017, she joined the group of Dr. Jurjen Tel to pursue a Ph.D. in immunoengineering at the Eindhoven University of Technology, Eindhoven, the Netherlands. She investigated the functional heterogeneity in Natural killer cells and plasmacytoid dendritic cells by integrating real-time droplet-based microfluidics, the result of which is presented in this thesis. She received a travel grant in 2019 to present the findings of her work at the Synthims symposium, Ascona, Switzerland.

ACKNOWLEDGEMENTS

How does our body function? Why do we get sick? How does the medicine work? These were some questions that motivated me to choose the career path of a scientist. Now, I realize, being a scientist is not only about finding answers to your curiosities but also to be able to understand the entire process of researching, challenging your own belief, and most of the time accepting the failure. As a scientist, you are answerable to society and at the same time maintain the great responsibility of preserving its integrity. The past five years for me have therefore become a process of continuous learning, understanding, criticism, and numerous failures. In the end, however, I have emerged as a proud scientist who now understands the value of the science and the process. This journey would have not been successful without support from my mentors, colleagues, friends, and family.

Jurjen, you have been my mentor for more than seven years now. I first met you as an enthusiastic scientist whose energy and positivity inspired me to get into this field. You have always pushed me to get the best out of me, rather be convincing me to go to Harvard or do a Ph.D. The best part of working with you is your approachability and the amicable atmosphere you have maintained within the group. Thank you very much for trusting me as one of your first students and challenging me, in many ways, to reach this finish line. I wish all the best for your future, and I hope the immunoengineering group will always keep shining.

Carlijn, you have set an example to all of us with what can be achieved as an excellent scientist. Your humility and intellect speak all and thank you very much for your support in every step.

Klaus, most of my projects would not have been possible without the collaboration with you. Thank you very much for the continuous support and discussions to guide me throughout the journey.

I also want to express my gratitude towards my Committee Members, **Maarten Merkx**, **Cecilia Sahlgren**, **Tom de Greef**, **Stefan Snierken**, and **Harry Dolstra** for their time to review my thesis.

Nidhi, we started this journey together, and together we have shared all the ups and downs. All those times we spent created beautiful memories to cherish (movie dates, countless conferences, food haunts, inspiring experimental plans), funny anecdotes to laugh at (drunk

Nidhi and so many more), and some salty moments (break up stories) that will always keep us bonded. Our “bichoo hatela jokes”, typical Bollywood moments, love for extremely spicy food, excellent “business” ideas (we had so many), passionate scientific discussion, and never-ending gossip are some of the highlights that we both will never forget. Thank you for being there for me as my soul sister and my Ph.D. buddy with whom I could always rant, complain, express my annoyance and insecurities. You have been very strong support and encouragement for me to finish this Ph.D. with such dignity. You have always been the first person to know when my experiments fail (or when it surprisingly works). You are my personal trainer, reviewer, editor, and the one and only baker onto whom I can trust without any doubt. I was looking for a good friend in this foreign country, but I got a sister instead. Thank you for being there for me in every hard and happy step of my life.

Bart, I have known you as my student and now very happily as my colleague. You have been an amazing friend who is smart and also funny. I know I give you quite a hard time, but finally, I accept that you are a sweet and amazing person. And with no doubt, your “ewerteen soup (in my funny accent)” recipe is amazing (you keep on bragging with no reference until now). You are a passionate scientist and your innovative approach towards problem-solving is quite inspiring. Keep it up, Barty.

Laura, you have become a wonderful friend within a short time. Until now, I had never met a person so compassionate, smart, and yet so much helpful and understanding. Thank you for showing me that it is possible to fulfill your dream but also be equally passionate about others. I will miss our spar breaks, fancy dinners, and critical work discussions. Always remain as motivated as you are.

Haowen, we did not get to work directly on a project, but we did share some wonderful times as a group. I know you as a passionate scientist and quite a helpful person who is always ready to help. I wish you all the best and hope you will achieve your dream quite nicely.

Annelies, we met in our first years and were quite connected even though we did not share the same building. I will miss our dinners and sweet conversations both on a personal and professional level. You are a good scientist and am so happy that you got to do what you had desired.

Lucie, even though we have only met few times, I could see that you are an amazing person. I wish we could have known each other more. I wish you all the best for your project and hope that you achieve what you are aiming for.

Liesbeth, thank you for everything you have done for our project and team. You have been a great support for me, and I wish you all the best for the future.

Florian, I learnt everything about research from you. You were also a struggling PhD when I first met you and now you have fulfilled your aim so gracefully and have always been my inspiration. Thank you very much for your support and I wish you the very best for your future.

Dina, I still remember the first day I had met you. We connected instantly and until now, I know you have become a good friend to me. Even though you doubt sometimes, I believe that you are an excellent scientist and you have achieved so much. I know how difficult it is to start your life and career in a new country, but you have managed it so beautifully. Keep it up and you will definitely achieve the best. I will always remember our chats, lunch, and trips together.

Winne and Nayeli, you have been dear friends with whom we share our beautiful birthday moments. I am so happy to have you as a friend and wish you all the best for the completion of your Ph.D. and life goals.

Lars, Ayla, Vera you have become an important part of my thesis and without your hard work and compassion, most of the chapters would have remained incomplete. I want to thank you all for your hard work, amazing discussions, and creative ideas for achieving our scientific goal. I hope that you are proud of your accomplishments and good luck with your future.

Yuana, Moneik, Marloes, Serena, Mark, Catarina, thank you very much for providing the amazing environment to work in the cell lab and facilitating our every need so graciously.

My cell lab colleagues, **Sultan, Phani, Aref, Cas, Suzzane, Bente, Tamar, Jelle, Andreas, Tanveer**, thank you for all your help and enthusiasm to achieve the ultimate scientific goal. You all are doing amazing work, keep it up.

Swornima and Saida, girls you are my non-TU/e buddies who have become an extremely important support system. You have provided a space for me to vent my insecurities and anxieties. Saida, as you know, you take all the credits for my life in the Netherlands. And

Swornima, you have been my biggest strength without whom I can't imagine my life here. I am so glad to have you, girls, in my life. With you I got amazing friends **Deep Raj** and **Milan** and three cute kids. Deep, I am always looking forward to our beyond the scope discussions. **Arati**, your enthusiasm and happiness are quite infectious. I can never feel down when with you.

Nisha B, Nisha G, Deepti, and Shraddha, my girls, my power. I can't imagine my scientific life without you. Decades ago, we started our journey together and I am so proud that each of us has made our own niches. Love you girls, keep it up.

Baba, Mummy, Umesh, and Anisha, thank you very much for your support and blessing to complete this journey with immense strength.

Aayush, bhai we used to discuss our dreams and passion and how we want to achieve them successfully. You have always been my best friend, my counsellor, my pillar, and my inspiration. Love you a lot.

Maya, my mayalu, you know how much you mean to me. There have been days when I was relentlessly working, (you don't know how much guilt I feel), but I hope this work will someday become an inspiration and pride for you. You can achieve anything you set your heart upon, and I will always be there to pick you up when you fall. Love you very much my darling.

Rajesh, finally it is done!! It feels like we have been doing this Ph.D. together. I can't even imagine if I would have finished it without you standing by my side. You took care of me, my life, and our Maya so well that I could focus on my work without any worry and guilt. More importantly you have always motivated me to realize my strength and I feel very lucky to have you. Love you so much for this. Congratulation Mr, you are now a "डाक्टर साहब".

Nana, baba, you have given up so much to get us into this phase. You have been a wonderful parent who always trusted me and accepted all my decisions wholeheartedly. I would not be doing this if you were not there to show me my capabilities and taught me to believe in myself. You never gave up on me and so neither did I. This is more of your moment than it is mine. Love you both very much and I hope I will keep on making you prouder every single day.

